CELLULAR AND MOLECULAR BASIS OF THORIUM-INDUCED CYTOTOXICITY AND CARCINOGENESIS

By

RAKHEE YADAV

LIFE01201304007

Bhabha Atomic Research Centre, Mumbai

A thesis submitted to the

Board of Studies in Life Sciences

In partial fulfillment of requirements

for the Degree of

DOCTOR OF PHILOSOPHY

of

HOMI BHABHA NATIONAL INSTITUTE

May 2021

Homi Bhabha National Institute

Recommendations of the Viva Voce Committee

As members of the Viva Voce Committee, we certify that we have read the dissertation prepared by **Ms. Rakhee Yadav** entitled "**Cellular and Molecular Basis of Thorium-induced Cytotoxicity and Carcinogenesis**" and recommend that it may be accepted as fulfilling the thesis requirement for the award of Degree of Doctor of Philosophy.

Chairman – Dr. S Gautam	Signature with date	21/05/2021
Guide / Convener – Dr. Badri N. Pandey	Signature with date	14.5.2021
Co-guide - Dr. Amit Kumar	Signature with date	25.5.2021
Examiner - Prof. C K Panda	Signature with date	14/5/2021
Member 1- Dr. Bhavani Shankar	Signature with date	24/5/21
Member 2- Dr. Anand Ballal	Signature with date	25/05/21
Member 3- Dr. Sanjay Gupta	Signature with date	21/5

Final approval and acceptance of this thesis is contingent upon the candidate's submission of the final copies of the thesis to HBNI.

I/We hereby certify that I/we have read this thesis prepared under my/our direction and recommend that it may be accepted as fulfilling the thesis requirement.

Date: 25.5.2021 14.5.2021

Place:

Signature
Co-guide

Signature
Guide

STATEMENT BY AUTHOR

This dissertation has been submitted in partial fulfillment of requirements for an advanced degree at Homi Bhabha National Institute (HBNI) and is deposited in the Library to be made available to borrowers under rules of the HBNI.

Brief quotations from this dissertation are allowable without special permission, provided that accurate acknowledgement of source is made. Requests for permission for extended quotation from or reproduction of this manuscript in whole or in part may be granted by the Competent Authority of HBNI when in his or her judgment the proposed use of the material is in the interests of scholarship. In all other instances, however, permission must be obtained from the author.

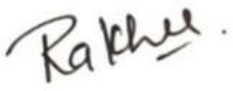

Rakhee Yadav

DECLARATION

I, hereby declare that the investigation presented in the thesis has been carried out by me. The work is original and has not been submitted earlier as a whole or in part for a degree / diploma at this or any other Institution / University.

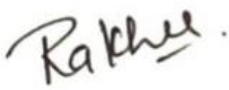

Rakhee Yadav

List of Publications arising from the thesis

PUBLICATIONS IN REFEREED JOURNAL

1. **Rakhee Yadav**, A.K. Agrawal, Manjoor Ali, Amit Kumar, B. Singh, Y. Kashyap, A. Sinha, S.C. Gadkari, B.N. Pandey. Thorium-induced Anatomical and Histopathological Changes in Liver of Swiss Mice, *Toxicology and Environmental Health Sciences, 2018,* 10, 1-10.
2. **Rakhee Yadav**, Amit Kumar and B. N. Pandey. Estimation and in-situ detection of thorium in human liver cell culture by arsenazo-III based colorimetric assay. *BioMetals*, 2020, 33,75–85.
3. **Rakhee Yadav,** Manjoor Ali, Amit Kumar, Badri N Pandey. Mechanism of carcinogenesis after Exposure of Actinide Radionuclides: Emerging Concepts and Missing Links. *Journal of Radiation and Cancer Research* (2017); (8): 20-34 (*review article)*.
4. **Rakhee Yadav**, Sourav K Das, Manjoor Ali, Badri N Pandey, Amit Kumar. Role of Calcium Ion Channels and Cytoskeletal Proteins in Thorium-232 induced Toxicity in Normal Human Liver Cells (WRL 68) and Its Validation in Swiss mice, (*Journal of Hazardous Material*, Submitted)
5. A.K. Agarwal, **Rakhee Yadav**, J. Bahadur, B. Singh, M. Ali, P. Singhai, A Kumar, Y Kashyap, B N Pandey. SRμCT and SAXS studies on micro & Nano scale structural changes in mice femoral bone due to thorium administration *(Journal of Physics, Under revision).*
6. **Rakhee Yadav,** S. Das, Amit Kumar, Badri N Pandey. Alterations in hepato-carcinogenic genes in WRL 68 cells after treatment with thorium and alpha particles. *(Under submission)*

ABSTRACTS PRESENTED IN CONFERENCES

1. **Rakhee Yadav**, Manjoor Ali, Sangita Dhara, N.L. Misra, B.N. Pandey, Development of a colorimetric protocol for thorium estimation and localization in liver cells/tissues, *ICRR-HHE-2016*, Feb.11-13, 2016, BARC, India. **(Poster presentation)**
2. **Rakhee Yadav**, Amit Kumar, B. N. Pandey, Studies on intracellular targets of thorium in normal human liver cells, *ICRR-HHE 2018*, University of Hyderabad, India Feb. 1-4, 2018. **(Best Poster Presentation Award)**

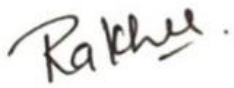

Rakhee Yadav

DEDICATIONS

Dedicated to my Parents and my family

ACKNOWLEDGEMENTS

I would like to express my heartfelt gratitude to my Ph.D. guide, Dr. B.N. Pandey, and my co-guide and mentor, Dr. Amit Kumar for their continuous help and support from the beginning to conclusion of my research journey. Their continuous support, encouragement and various scientific discussions helped me immensely to develop a rational and scientific temperament. A very special thanks is also due to Dr. Sathees Raghavan who provided me with a research platform and gave me the opportunity to learn work on scientific problems which ultimately developed a renewed interest for science in me.

I would like to thank all the members of my Doctoral Committee Dr. K. Indira Priyadarshini, Dr. S Gautam, Dr. Anand Ballal, Dr. Bhavani S Shankar and Dr. Sanjay Gupta for providing me with timely scientific input during doctoral committee meetings. A special thanks is due to Dr. Tapan Ghanty (Division Head, Radiation Biology & Health Sciences Division and Associate Director, Bioscience Group) for his support and encouragement. I would also like to extent my gratitude to Dr. J Bandekar and Dr. Vinay Kumar (Ex- Division Heads of Radiation Biology & Health Sciences division and to Dr. S Chattopadhyay, Dr. Venugopalan and Dr. SK Ghosh (Ex- Group Directors, Bioscience Group) for providing me with various opportunities and platforms for my research work which ultimately led to the fulfillment of my doctoral degree. A heartfelt thank you goes to Dr. Hema Rajaram (Dean, Life sciences HBNI) for always being supportive towards my PhD. A note of Thank You also goes to Dr. Ashish Agrawal and Mr. Balwant Singh of RRCAT, Indore and Dr. Amar Sinha and Dr. S.C. Gadkari from BARC, for providing me the access to Synchrotron imaging facility and offering me their expertise in the data analysis. I would also like to thank TEM imaging facility of ACTREC, Mumbai and AIIMS, Delhi for their help in acquiring high quality TEM images for my research work. The list would not be complete without acknowledging the extensive support provided by Dr. HD Sarma and Mr. B Swami of Animal House facility, Dr. Sanjukta and Mr. Kiran Kumar of Analytical Chemistry Division for their help in performing ICP-MS and Dr. NL Misra and Dr. Sangeeta Dhara of Fuel Chemistry Division for their help in TXRF.

I would also like to thank Mr. Manjoor Ali, Mrs. Deepika, Bhange, Mrs. Neena Shetake and Mrs. Pooja Melwani from my lab for all their help during the entire duration of my work. They are the ones I shared my ideas and doubts on ground level and discussions with them helped me immensely towards my understanding of various scientific concepts and increased my hunger to know more various concepts in depth. A special thanks is also due to all other lab members Mr. Saurav Das, Mrs. Vasumathy, Dr. Sagar Balla, Mr. Sanjay Shinde, Mrs. Hansa Yadav and Project Trainee Ms. Sushmita for all their help during the entire duration.

I would also like to thank Bhabha Atomic Research Centre for allowing me the access to its various facilities and instruments for conducting my experiments and Department of Atomic Energy (DAE) for providing me with the financial help in form of both funding for my project and HBNI PhD fellowship to help me sustain during the entire duration.

I would also like to thank my parents (Mr. Ram Charitra Yadav and Mrs. Sangeeta Yadav), my sisters (Rashmi, Pushpa and Sapna) and my nephew Master Mudit Kumar for their continuous believe and support in me during the long and arduous process leading to the fulfillment of my Ph.D. degree. A special thanks is also due to my parents-in-law (Mr. Basudeo Roy and Mrs. Urmila Kumari), my brother-in-law (Mr. Prabhat Kumar), his wife (Mrs. Ratna Kumari) for their unwavering support.

This entire acknowledgement would not be complete without thanking my husband (Mr. Prakash Kumar) for his unwavering support and his guidance during all the times. His support was of absolute necessary towards the conclusion of my entire hard work. At last, but not the least, I would also like to thank almighty for gifting me the joy of my life (my son, Viwaan Kumar Roy) whose arrival has given a new meaning to our lives and made everything worthwhile.

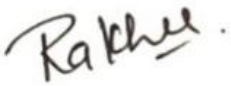

Rakhee Yadav

Contents

LIST OF FIGURES

LIST OF TABLES

CHAPTER 5:
CONCLUSIONS AND FUTURE DIRECTIONS

Even if thorium is being seen as an attractive replacement of uranium for the nuclear energy production and in many industrial applications, the cellular and molecular targets of thorium are still not well established. Moreover, the effect of thorium on intracellular organelles and the molecular pathways through which may exert its carcinogenic effect is also required to be studied. To address the unanswered questions in the literature, in the present study a range of *in vitro* and *in vivo* studies were carried using cellular and molecular techniques. Based on these experiments, the major conclusions of the thesis are as following:

a. Commonly used methods (ICP-MS, ICP-AES, TXRF) for thorium estimation are limited for their day-to-day use for biological samples due to costly instrumentation and requirement of extensive sample preparation, large sample volume and technical expertise for acquisition/analysis. To overcome these limitations, in the preset thesis for the first time a colorimetric method based on arsenazo dye was established to estimate thorium in biological samples.

b. The arsenazo based method was found to an easy, high throughput and convenient spectrophotometry-based arsenazo assay for routine thorium estimation in biological samples. The technique was also found to be specific to thorium, and not to monazite's common contaminants [La (III), Ce (IV) and U(VI)] and other biologically relevant metals (such as Ca, Fe, Mn, Zn, Cu).

c. Thorium uptake in human normal liver cells was found to be unaffected by transferrin but partially governed by endocytosis.

d. Out of different ion channels studied, thorium uptake was significantly inhibited in the presence of thapsigargin (ER Ca^{2+} mobilizer), while other calcium ion channel

inhibitors increased the thorium uptake. Based on the inhibitor study, it is hypothesized that cellular uptake of thorium is being governed by the level of cytoplasmic calcium.

e. The order of thorium binding to different sub-cellular protein fractions was found to be cytoskeletal > cytoplasmic > extracellular > chromatin > nuclear > membrane. TEM studies showed that thorium internalization leads to a significant increase in the number of extracellular membranous vesicle-like extensions, nucleus distortion and nucleolus disintegration, altered mitochondrial structure from oval to flat disc-shaped.

f. Expression a panel of 84 genes involved in hepatocarcinogenesis studied after thorium treatment and without alpha particle irradiation showed pronounced magnitude of alteration in their expression for the late passage (P15) than the cells obtained at the early passage (P5). At P5, genes such as *ADAM17, ANGPT2, BAX, BCL2, BID, BIRC2, CASP8, CCL5, CCND1, CCND2, CDKN1A, CDKN1B, CFLAR, E2F1, EGFR, EP300, FADD, FAS, FHIT, FZD7, GSTP1, HRAS, IGF2, IGFBP1, IRS1, MET, MTDH, PTEN, PTGS2, PTK2, RASSF1, RB1, RELN, RHOA, SMAD4, SMAD7, STAT3, TCF4, TGFA, TGFB1, TGFBR2, TLR4, TNFRSF10B, TNFSF10, TP53, XIAP* were over-expressed whereas genes such as *KDR, PYCARD, SOCS3, PDGFRA, MYC* were downregulated in all the treatment groups. Whereas at P15, genes such as *BAX, MYC, CDKN1A, TNFRSF10B, PTEN, MSH2, CCND1, MET, BIRC5, BIRC2, HHIP, CXCR4, SMAD7, EGF, SFRP2, TGFBR2, ADAM17, CCL5, DLC1, AKT1, KDR, TERT* were over-expressed whereas genes such as *CDH1, OPCML, NFKB1, CDKN1B, STAT3, RAC1, RASSF1, TP53, NRAS, SMAD4, E2F1, CTNNB1, GADD45B, CFLAR, PTGS2* are downregulated in all the treatment groups.

f. Thorium bio-distribution studies in male Swiss mice intravenously injected with thorium showed total thorium highest in the liver followed by spleen > skeleton > kidney

> lungs whereas thorium concentration per gram of tissue was highest in spleen followed by liver > skeleton > kidney > lungs.

g. Synchrotron imaging performed to study the anatomical changes of liver of mice treated with thorium showed shortening of the blood vessels in a dose-dependent manner while thorium seems to be accumulated along the blood vessel of the spleen.

h. Histopathological studies performed after six and twelve months of thorium treatment showed normal liver histopathology at 4 and 10 mg/Kg dose, whereas protein deposition was observed in the hepatocytes at 20 mg/Kg. Spleen at 10 mg/Kg showed an increased extramedullary hematopoiesis at the red pulp. Thorium at high concentration (20 mg/Kg) showed amyloid deposition at 6 months and increased megakaryocytosis at 12 months.

i. Histopathology of bone and brain showed normal tissue architecture with no visible abnormality. Histopathology of lungs did not show any abnormality in the tissue architecture at 6 months. Interestingly at 12 months, the highest dose of thorium (20 mg/Kg) caused papillary adenoma neoplasia in lungs.

j. An increase in the level of glucose in the blood was observed at 1 month, 6 and 12 months.

k. Analysis of serum cytokine and chemokine profiles showed an increase in the levels of proliferative, inflammatory cytokines/chemokines after 12 months of thorium treatment.

l. Gene expression studies in liver tissue showed that at low dose (i.e., at 4 mg/Kg) the number of genes with altered expression was decreased at higher time point i.e., 12 months compared to 6 months. However, at higher dose i.e., at 20 mg/Kg, the number

of genes with altered expression showed a marked increase at 12 months as compared to 6 months.

M. After 6 months, *Hhip, Tgfbr2, Rassf1, Msh2, Bcl2, Tert, Cdkn2a, Ptgs2, Myc* are some of the oncogenes which showed an increase while genes like *Opcml,* showed downregulation. Similarly, after 12 months, *Pdgfra, Stat3, Tgfb1, Ptk2, Birc5, Hgf, Nras, Flt1, Pin1, Msh2, Nfkb1, Hhip, Xiap, Tlr4, Rassf1, Cxcr4, Wt1, Fzd7, Ctnnb1* were the common genes with increased expression and tumor suppressor gene *Trp53* was downregulated in thorium treated groups.

At one hand, the thesis provides deeper mechanistic insights about cellular and molecular effects of thorium-induced toxicity and carcinogenesis. On the other hand, it opens many new avenues for research in thorium biology. Some of the future directions of the thesis are as following:

a. Thesis showed that cellular uptake of thorium to be governed by the level of cytoplasmic calcium. Further studies are needed to understand the role of calcium ion/store-operated channels and associated proteins in thorium uptake.

b. Spleen was found to be one of the major target organs. Moreover, the histopathological studies of spleen showed an increased extramedullary hematopoiesis at the red pulp, amyloid deposition and megakaryocytosis after thorium treatment. Spleen plays major role in immune system and hence in the process of toxicity as well as in carcinogenesis. Hence, it would be interesting to study the effect of thorium on immune parameters and its contribution in toxicity/carcinogenesis.

c. Incidence of thorium induced liver and bone cancer has been established. In the thesis, for the first-time lung cancer incidence after intravenous injection of thorium was observed. However, detail mechanism of lung carcinogenesis caused by thorium treatment is further warranted.

d. In the present thesis effect of thorium nitrate after intravenous administration was studied. Effects of other chemical forms of thorium with other routes of administration (inhalation, wound) should also be studied. It would be interesting to study different dust sizes of chemical forms of thorium after different routes of administration especially after inhalation.

e. The magnitude of health effects of thorium may get affected by many confounding factors associated with thorium workers as well as to the public. Hence, role of factors (like smoking, hepatitis virus infection) in the process of thorium-induced lung/liver carcinogenesis can be envisaged.

SUMMARY

The work presented in this thesis is performed towards understanding the mechanism through which thorium exerts its toxic effects under both in-vitro and in-vivo conditions. To achieve this, first a technique has been standardized to estimate thorium in biological samples in a rapid, easy, high throughput manner. The colorimetric method developed using arsenazo dye has been standardized in such a manner that it detects only thorium specifically and sensitively within the range of 2.5 to 40 µM. To further validate the technique, its results have been compared with that of a standard estimation technique i.e., TXRF.

Thorium uptake in human liver cells (WRL 68) has been studied and it was found that thorium uptake occurs independent of transferrin receptor mediated endocytosis. To an extent, uptake occurs through receptor-mediated active pathway, but majority of thorium is internalized in a passive way involving ion channels. Screening of different ion channels in order to understand the role of different ion channels established that calcium ion channels play a role in thorium uptake. Further studies involving inhibitors for different types of calcium ion channels showed that thorium uptake is governed by cytoplasmic calcium ion concentration. Thorium uptake and concentration of calcium ions is inversely proportional. Studies involving intracellular targets of thorium showed that thorium mainly binds to cytoskeletal proteins, both soluble and chromatin-bound nuclear extract, cytoplasmic proteins, and membrane contents as well. Cellular imaging after thorium treatment using TEM showed various alterations in cellular architecture including nucleus shrinkage, distortion of mitochondria, increase in the number of vesicles, rearrangement of intracellular organelles around nucleus and formation of numerous extracellular vesicular aggregates upon thorium treatment. Thorium injected in mice intravenously for different time points (1, 6 and 12 months) were studied for their distribution among different body organs and it was

found that thorium accumulates mainly in liver, spleen, and bone. The highest amount of thorium is found in liver however, the highest concentration of thorium was found in spleen suggesting high affinity binding of thorium in spleen. X-ray phase contrast images obtained using Synchrotron showed thorium to be mainly accumulated in and around blood vessels in liver and spleen. Further histopathological studies carried out using H&E staining showed that thorium treatment causes megakaryocytosis in spleen and amyloid deposition in liver and spleen. Development of lung cancer following intravenous injection of thorium is being reported for the first time. Biochemical studies of serum parameters showed an increase in the level of glucose in thorium treated mice even at low doses. Level of urea and creatinine showed a dose-dependent decrease in their level in serum. Study of cytokine and chemokine profile showed an increase in the level of proliferative and inflammatory cytokines and chemokine in serum.

Alterations in gene expression upon thorium treatment was carried out under both in-vitro and in-vivo conditions. Upregulation and downregulation of many genes showed the involvement of two primary pathways in the process of hepatocarcinogenesis i.e., PI3k-Akt and Wnt/β-catenin pathway. Further studies are required to be performed to establish their role in thorium induced hepatotoxicity and carcinogenesis concretely.

CHAPTER 1:

INTRODUCTION

1. Heavy metal radionuclides toxicity research

Heavy metal radionuclides (HMRs) mostly occur naturally in our environment and contribute mainly to natural background radiation. Living beings are continuously exposed to natural background radiation in different forms. Natural radiation sources include cosmic radiation, terrestrial radiation and intake of naturally occurring radionuclides through inhalation and/or ingestion. Earth is being hit by cosmic radiation coming from galactic, solar and Earth belt radiation particles (protons, electrons, heavy ions charged particles etc.), which however, only fraction could reach to Earth due to its magnetic field. Cosmic radiation also includes non-ionizing UV-rays which penetrates the Earth's protective layer and is readily absorbed by human skin. Terrestrial radiation is mainly caused by the huge deposits of naturally occurring radionuclides such as potassium, uranium, thorium and their decay products. Radon and thoron gases are the most common radionuclides to which humans are exposed mainly thorough inhalation. Radon is the decay product of uranium-238 and thoron is the decay product of thorium. These gases occur naturally in the atmosphere and sometimes get concentrated inside the houses which poses a significant health risk to the occupants. Ingestion of radionuclides mainly occurs when they get dissolved in water or incorporated in food/vegetables cultivated in soil containing radionuclides. Intake/ingestion of these water and food/vegetables leads to their incorporation in humans.

1.1. Definition and classification of heavy metal radionuclides

'Heavy Metals Radionuclides' are radioactive chemical elements with a specific gravity that is at least 5 times the specific gravity of water. Plutonium, uranium and thorium are some well-known radioactive heavy metallic elements with a specific gravity that is 5 or more times that of water. Radioactive nuclides have an unstable nucleus in order to achieve

stability, dissipates its excess energy by emitting ionizing radiation such as alpha-particles, beta or gamma rays spontaneously. The overall effects of radionuclides exposure to humans are expressed in the form of chemical toxicity as well as radiological toxicity. The radionuclides with long half-life, lower specific activity, and long biological retention time (e.g., thorium) exert their major short-term effects in the form of chemical toxicity. Over longer duration, the toxicity exhibited by such radionuclides involve both chemical as well as radiological toxicity. Similarly, radionuclides with short half-life, high specific activity and short biological retention time (e.g., uranium) exert their short-term effects mostly in the form of radiological toxicity and to a lesser extent, in the form of chemical toxicity. The radionuclides are divided into four main categories (Group A, B, C and D) depending on the level of radiotoxicity varying from very high to low and minimum as shown below in Table 1.1 (1).

Group	**Radionuclides**
Group A (particularly high level of radiotoxicity)	^{210}Pb, ^{210}Po, ^{226}Ra, ^{230}Th,^{232}Th (including natural), ^{232}U, ^{238}Pu, ^{237}Np, ^{241}Am and others.
Group B (high radiotoxicity)	^{224}Ra,^{106}Ru, ^{130}I, ^{131}I, ^{152}Eu, ^{144}Ce, ^{210}Bi, ^{230}Th, ^{235}U, ^{238}U, ^{234}U, ^{241}Pu, ^{90}Sr and others.
Group C (average radiotoxicity)	^{22}Na, ^{32}P, ^{35}S, ^{36}Cl, ^{59}Fe, ^{60}Co, ^{89}Sr, ^{90}Y, 93Mo, ^{125}Sn, ^{140}Ba, ^{234}Th and others.
Group D (low and minimal radiotoxicity)	^{7}Be, ^{14}C, ^{18}F, ^{40}K, ^{51}Cr,^{55}Fe, ^{64}Cu, ^{129}Te, ^{131}Cs, ^{197}Pt, ^{197}Hg, ^{200}Tl, ^{210}Pb and others.

	This group also includes tritium (^{3}H) and its chemical compounds (oxides of tritium and heavy water).

Table 1.1: *Classification of radionuclides based on radiotoxicity ranging from very high to low to miminum level of radiotoxicity.* ***Source:*** *Iryna P. Toxicity of Radionuclides in Determining Harmful Effects on Humans and Environment. J Environ Sci Public Heal. 2017;01(02):115–9*

1.2. Major Heavy Metal Radionuclides and their major Industrial Applications

Among the radionuclides, plutonium, uranium and thorium are the major radionuclides used for nuclear-industry applications. They are mainly used as nuclear fuel material for the generation of electricity and production of nuclear weapons.

1.2.1. Plutonium

Plutonium is a radionuclide with atomic number 94. It was first discovered in the year 1940 by scientists J.W. Kennedy, G.T. Seaborg, E.M. McMillan and A.C. Wohl at the University of California, Berkley. It is produced when uranium-238 is bombarded with cyclotron accelerated deuteron. U-238 splits into neptunium-238 and two free neutrons. The neptunium-238 then undergoes beta-decay and forms plutonium-238 (2).

1.2.1.1. Plutonium (brief introduction with Chemical/Physical Properties, Decay series)

Plutonium is bright silvery in color when freshly prepared and slowly gets oxidized in air to become dull gray, yellow or olive-green tarnish colored metal. Nearly all plutonium is man-made and undergoes decay predominantly by emitting alpha particles. Apart from alpha

particles, it also emits beta particles, neutrons, and gamma rays. There are five common isotopes of plutonium with different half-lives and decay product. They are:

Pu-238–half-life is 88 years and undergoes alpha decay to form U-234

Pu-239 – half-life is 24,000 years and undergoes alpha decay to U-235

Pu-240 – half-life is 6,560 years and undergoes alpha decay to U-236

Pu-241 – half-life is 14.4 years and undergoes beta decay to Am-241

Pu-242 – half-life is 374,000 years and undergoes alpha decay to U-238.

Pu-239 and Pu-241 are fissile in nature whereas Pu-240 is fertile material.

Plutonium is readily soluble in concentrated mineral acids and mainly undergoes decay by emitting alpha particles. A large piece of plutonium feels warm to touch due to alpha emitting and is hard and brittle at room temperature. Plutonium is a bad conductor of heat and electricity unlike other metals. It melts at 640˚C while the boiling point (that is 3228˚C) is unusually high (2).

Plutonium undergoes decay to form the more stable product Pb and the decay series of Pu-239 is known as "A parent of the Actinide Series". The decay series is shown below in Figure 1.1.

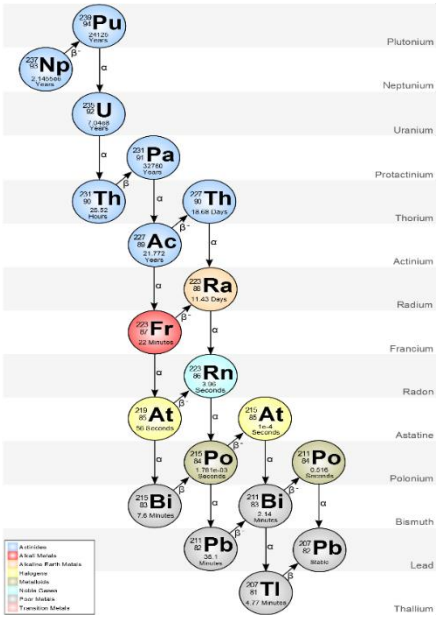

Figure 1.1: *Decay series of Pu-238, also called as "A parent of the Actinide Series".* ***Source:*** *https://metadata.berkeley.edu/nuclear-forensics/Decay%20Chains.html.*

1.2.1.2. Uses of plutonium

Out of the five isotopes of plutonium, only Pu-238 and Pu-239 are being used for various purposes. Pu-238 is used to generate electricity in space probes using radioisotope thermoelectric generators. These probes are used to generate electricity when the spaceship has travelled far away from sun and solar power is no longer available to make electricity. Examples of some probes that uses Pu-238 are Cassini, Voyager, Galileo, and New Horizons etc.

Due to its high feasibility and availability, Pu-239 is used for production of energy and nuclear weapons. It is the main fuel in fast neutron reactors. Plutonium was the nuclear material used in the bombing of Hiroshima and Nagasaki during World War II in 1945.

Plutonium is also present in the spent fuel of light water reactors. Different isotopes of plutonium such as Pu-242, Pu-240, Pu-239 and Pu-238 are present in the spent fuel which can be enriched and used as mixed oxide fuel in light water reactors (3).

1.2.1.3. Plutonium as energy source in reactor

Pu-239 and Pu-241are fissile isotopes and therefore, can sustain nuclear chain reaction. Because of this, these isotopes are mainly utilized in nuclear reactors for the production of nuclear weapons and electricity (3). The most common isotope of plutonium i.e., Pu-239 is produced in nuclear reactors by the absorption of a neutron by the most common isotope of uranium i.e., U-238. Plutonium-239 used in reactors is categorized based on its usage and are of two types i.e., reactor-grade plutonium and weapon-grade plutonium. Weapon-grade plutonium typically contains plutonium-239 between 80 to 93% while reactor-grade plutonium contains less than 80 percent Pu-239.

In order to obtain weapon-grade plutonium, the fuel rods are removed, and plutonium is separated after relatively brief irradiation. The resulting plutonium typically contains 93 percent plutonium-239. Similarly, in power reactors, the fuel rod is left in the reactor for a longer time resulting in a mix that includes more of higher isotopes of plutonium such as Pu-241, Pu-238 etc. apart from Pu-239.

The presence of higher isotopes, i.e., Pu-238 and Pu-241 in fuel mix presents certain limitations which makes them not suitable to be used in the production of nuclear weapons.

However, with the advent of new technologies, it is possible to use reactor-grade plutonium in the making of nuclear weapons as well (4).

1.2.1.4. Plutonium based reactor

Plutonium is used in the reactors for energy production by converting uranium-238 into plutonium-239. In order to generate Pu-239, the composition of fuel rod is maintained such that it contains around 95 to 98 percent of U-238, which acts as the fertile material, and U-235 makes up the rest as fissile material. The fissile uranium undergoes nuclear fission upon absorption of a neutron. The uranium nucleus upon absorption of neutron undergoes fission to produce two nuclei of nearly equal mass and releases tremendous amount of energy. The energy is mainly in the form of heat which can be absorbed by coolant, mainly water, that flows through the heat-exchanger unit of the reactor. The heated water gets converted into steam which drives a turbine connected to an electric generator (5).

On an average, around 2.5 neutrons are released upon fission of U-235. Only one neutron is required to sustain the fission of U-235 reaction while the rest of the neutrons are absorbed by the fertile U-238, which then trans-mutates into Pu-239. Pu-239 is a fissile fuel which can then be used to generate electricity. The reactors which generate plutonium from uranium upon absorption of neutrons are called breeder reactors and the neutrons absorbed in plutonium plant are fast moving neutrons. Therefore, such reactors are called as fast breeder reactors (FBRs) (5).

1.2.1.5. Advantages and disadvantages of plutonium-based reactors

One of the major advantages of plutonium-based reactors is their ability to generate electricity. The reactors in today's world generate electricity having billions of watts of capacity making them up to one-third of world's total power generation capacity (5). The spent

fuel containing unburned plutonium and uranium is chemically separated from other fission products. The reprocessed plutonium is then mixed with uranium to form mixed-oxide fuel (MOX) which can then again be used as nuclear fuel for power generation.

Plutonium based reactors i.e., breeder reactors are far more difficult to control and are quite expensive to build as compared to normal thermal reactors. Also, the plutonium generated in breeder's reactor after one fuel cycle is separated from uranium-238 and can be used in the production of nuclear weapons (5).

1.2.2. Uranium

Uranium is a radioactive heavy element of the actinide series with atomic number 92. It was discovered in 1789 by German chemist Martin Heinrich Klaproth in mineral pitchblende and named after the newly discovered planet Uranus. However, it was only in 1841 when uranium metal was isolated by French chemist Eugène Peligot by heating uranium tetrachloride with potassium. Its radioactive properties were discovered by Henri Becquerel in 1896 (6). Apart from pitchblende, other mineral ores of uranium include uraninite, carnotite, autunite and torbernite (7).

1.2.2.1. Uranium (brief introduction with Chemical/Physical Properties, Decay series)

Uranium is a dense, hard, metallic element with silvery white color. Like metals, uranium is ductile and malleable. The metal gets tarnished when exposed to air and can catch flames when divided into fine pieces. Uranium is a relatively poor conductor of electricity (6).

Uranium is a strongly electropositive metal which reacts with water. It is soluble in acids but insoluble in alkalis. +4 is its most important oxidation state. It also exhibits +3 and +5 oxidation states, however, the respective ions are unstable. Uranium, whose all isotopes are

radioactive in nature, occurs naturally in earth and consists of U-238 (99.27%), U-235 (0.72%) and U-234 (0.006%). The half-life values of each of these isotopes are as follows:

Uranium – 238: 4.46 billion years

Uranium – 235: 704 billion years

Uranium – 234: 245,000 years

Since uranium occurs naturally in rocks and have long half-lives, these are used for determining the age of Earth by measuring the amount of lead, the ultimate decay product of uranium, in uranium-containing rocks. Both U-238 and U-235 undergoes decay and ultimately forms lead where the decay series of both isotopes ends (6). The U-238 decay series is called as uranium series and/or radium series. The U-235 decay series is called as actinide series. Both the series are shown in the Figure 1.2 below:

(A) Uranium series **(B)Actinide series**

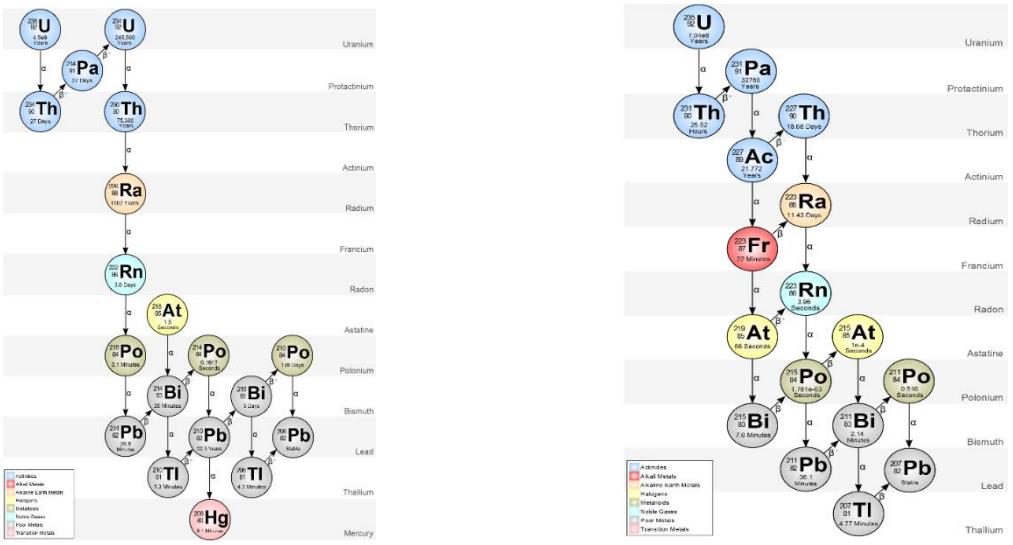

Figure 1.2: *Decay series of U-238, also called as "Uranium Series" and U-235, also called as "Actinide Series".* ***Source:*** *https://metadata.berkeley.edu/nuclear-forensics/Decay%20Chains.html*

1.2.2.2. Uses of Uranium

Uranium compounds have been used as coloring agents in ceramics. UF_6 has been widely used in the gas-diffusion and gas-centrifuge methods of separating uranium-235 from uranium-238 (6). Uranium-235, being naturally radioactive and fissile, is a suitable material for nuclear fuel in the production of nuclear energy and nuclear weapons. Depleted uranium is used as shielding to protect tanks and also in missiles and bullets. Uranium-238 is used to estimate the age of Earth and other radiometric dating techniques (8).

Uranium-238 is a fertile material and can be readily converted into fissile plutonium-239 upon absorption of neutron. It is used in breeder reactors to produce Pu-239 and generate nuclear electricity (8).

1.2.2.3. Uranium as energy source in reactor

Uranium-235 is used as a fuel in nuclear reactor to generate electricity and also as the fissile explosive in nuclear weapons. To be used as nuclear fuel, uranium dioxide (UO_2) is first converted into fuel pellets which are then placed inside thin metal rods, known as fuel rods. The fuel rods are then assembled to form the core of the reactor. A typical large sized nuclear reactor may contain up to 51,000 fuel rods with up to 18 million fuel pellets. The uranium fuel is removed from the reactor after being used for about three year and the spent fuel is then removed, stored and then depending on the amount of fissile and fertile material left in the fuel, it is either reprocessed or discarded by burying them underground (9).

Uranium is also used in breeder reactors to generated electricity by converting U-238 into Pu-239. U-238 is a fertile material which gets converted into Pu-239 after absorbing a neutron. Pu-239 is fissile in nature which undergoes fission and releases tremendous amount

of energy in doing so, which can then be utilized in the production of electricity using electric generators.

1.2.2.4. Uranium based reactor

Uranium based reactors are used to produce both nuclear energy and nuclear weapons. Uranium-235 is a naturally fissile material and can be readily used in reactors. Uranium-238 is a fertile material which when absorbs a neutron undergoes transmutation into Pu-239. The Pu-239 can then be used for both energy generation and production of nuclear weapons (8).

Uranium in nuclear reactors is used to generate about 10% of world's electricity. As per a survey by world's nuclear association, about 30 countries are currently utilizing uranium in about 440 nuclear reactors to generate electricity with total output capacity of about 390,000 megawatts. (9).

1.2.2.5. Advantages and disadvantages of Uranium -based reactor

Both U-235 and U-238 can be used as nuclear fuel to generate electricity. In addition to their peaceful applications, both isotopes of uranium i.e. U-235 and U-238 can be also used to produce nuclear weapons as well (8).

1.2.3. Thorium

Thorium is a weak radioactive metallic element with atomic number 90 in actinide series. Thorium was discovered by an amateur Norwegian mineralogist Has Morten Thrane Esmark in the year 1828 in the form of a rock who sent it to Swedish chemist Jons Jacob Berzelius working in Royal Karolinska Institute for identification. Jon Jacob Berzelius extracted the element from the mineral block and identified the new element and named it Thorium, after Thor, the Scandinavian god of war (10). Thorium is found abundantly in the

Earth's crust and occurs naturally as the minerals thorite, uranothorite, thorianite (11). Thorium is the main component of monazite and is also found in minerals such as zircon, titanite, gadolinite and betafite in significant amount (10,11).

1.2.3.1. Thorium (brief introduction with Chemical/Physical Properties, Decay series)

Thorium is a silvery white metal in its pure form when slowly gets oxidized in air to form thorium oxide. It changes its color from silvery white to grey and finally black. Thorium oxide (ThO_2), also known as thoria, has one of the highest melting points of 3300˚C of all known oxides. It is found in most rocks and soils and is three times more abundant than uranium. It is insoluble in water due to which thorium is plentiful in sands but negligible in seawater. Thorium dioxide (ThO_2) is quite inert and does not undergo further oxidization. It has high thermal conductivity and lower thermal expansion as compared to UO_2 as well as a much higher melting point (12). Thorium is moderately soft, ductile, and paramagnetic in nature. Its density is half of that of uranium and plutonium and is harder than both. Below 1.4 K temperature, thorium exhibits superconductive behavior. Thorium is electropositive in nature and mostly exists in +4 oxidation state.

^{232}Th is the most stable isotope of thorium with a half-life of 14.05 billion years. It undergoes radioactive decay slowly by emitting alpha particles and the decay series is known as "Thorium decay series" (13) which is shown below in Figure 1.3.

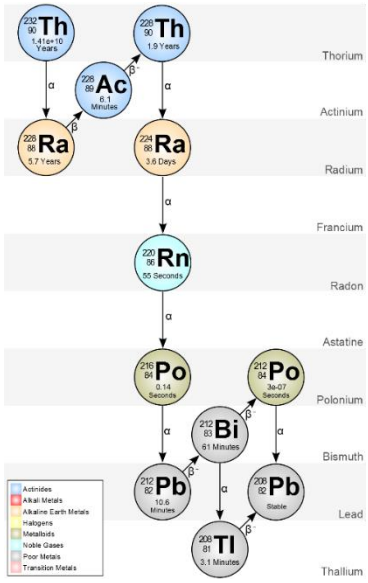

Figure 1.3: *Decay series of Th-232, also called as "Thorium Series".* ***Source: https://metadata.berkeley.edu/nuclear-forensics/Decay%20Chains.html***

1.2.3.2. Uses of Thorium

Thorium finds many uses in day-to-day activity of mankind. Apart from being used as a nuclear fuel for generation of nuclear power, it is also used as an alloying agent in Tungsten Inert Gas (TIG) welding electrodes and to strength magnesium. It is also used in the production of high-end optics and scientific instruments with precision. Thorium when burned produces white light, because of which it has been used in the making of gas mantles. Thorium is also used to make tungsten coated wires in electrical equipment. Thorium is also used in making high-temperature crucibles, heat-resistant ceramics and aircraft engines (13).

1.2.3.3. Thorium as energy source in reactor

Thorium, like uranium-238, is a fertile material which can readily be converted into uranium-233. Uranium-233 is fissile on its own like uranium-235 and can be used in nuclear

reactors to generate electricity. The thorium fuel cycle which generates fertile U-233 is shown below in Figure 1.4.

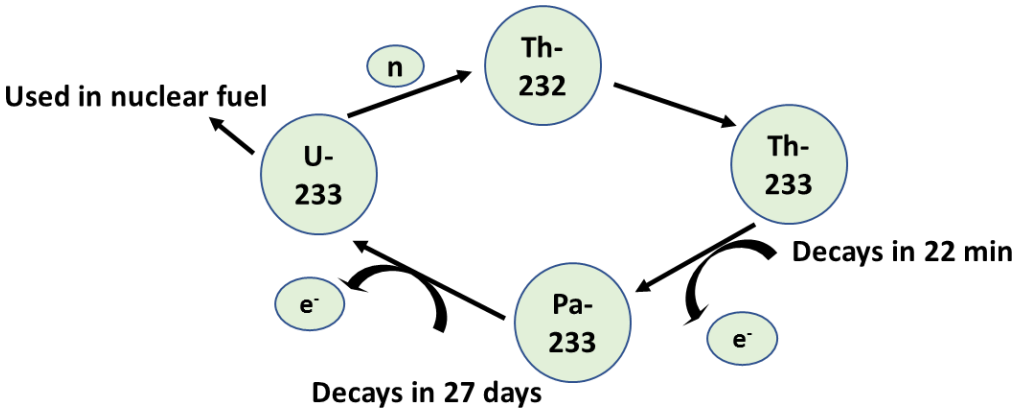

Figure 1.4: *Thorium fuel cycle through which fertile Th-232 is converted into fissile U-233.*

Fertile thorium-232 transmutates into fissile uranium-233 in nuclear reactor using thorium fuel cycle. Throium-232 is bombarded with neutrons in nuclear reactors which it absorbs and gets converted into thorium-233. It is an unstable isotope and undergoes immediate decay by emitting an electron and an antineutrino by beta decay and gets converted into protactinium. Protactinium-233 is a short-lived isotope and gets converted into fissile uranium-233 by undergoing another beta decay in 27 days.

1.2.3.4. Thorium based reactor

Thorium is used in nuclear reactors for power generation. Thorium is used to fuel different types of reactors such as light water reactors, heavy water reactors, high temperature gas reactors, sodium-cooled fast reactors, and molten salt reactor. Depending on the design of the reactor and fuel cycle, uranium-233 thus generated, is then used either in-situ or is chemically separated from other nuclear fuels and is formed into a new nuclear fuel (13).Thorium based reactors are still not in full-fledged use by different countries as the reactor design and technology are still in the development stage and many challenges still remains to

be addressed before thorium could be used as a fuel in nuclear reactors especially as solid fuel. Different countries such as India, China are in various stages of developing a fully functional thorium based nuclear reactors for power generation.

1.2.3.5. Advantages and disadvantages of Thorium -based reactor

There are many advantages of thorium-based reactors over uranium-based reactors. The main benefits include thorium makes it possible for a thorium-based breeder reactor to run on thermal i.e., slow-moving neutrons. These reactors are simpler than fast-breeder reactors. Thorium is three times abundant as compared to uranium and all but a trace of naturally occurring thorium is Th-232, thereby reducing the steps involved in fuel enrichment. This is much better as compared to uranium ore which contains only 3-5% of uranium-235. Also, unlike uranium, thorium is not fissile which means that a lot of thorium nuclei can be packed together without worrying about nuclear reaction starting on its own. Uranium-233, the fissile material generated in thorium-based breeder reactors has a relative longer life, making it possible to separate uranium-233 from thorium-232 and use it as a fuel in separate nuclear reactor to generate electricity. The probability of U-233 to undergo fission upon neutron absorption is much higher as compared to the chances of it getting trans-mutated into U-234. This process ensures that most of the fuel is used in generation of electricity rather than in the production of nuclear waste. The radioactive waste generated by thorium reactors is much less harmful as compared to uranium-based reactors and loses their radioactivity in 500 years as compared to 10,000 years for which nuclear waste generated by uranium-based reactors stays radioactive. Also, the amount of radioactive waste generated by thorium-based reactors is around 1000 to 10,000 times less as to start with (13).

Probably the most advantageous purpose of thorium-based reactors is its use for peaceful generation of electricity as the nuclear waste generated in thorium-based reactors does

not contain plutonium-239 which is used for making nuclear weapons. This is also the reason thorium-based reactors are not as much developed as uranium reactors as the primary purpose of using the nuclear reactors was to be generated nuclear weapons during world war and the cold war that followed rather than using it to for peaceful purposes.

When it comes to the application of thorium based nuclear reactors, there are several challenges faced by nuclear community, mainly when thorium is used in the form of solid fuel material. Naturally occurring thorium is largely mononuclidic which means that it contains only thorium-232 which is not fissile on its own and other fissile material, such as U-233, U-235 or plutonium should be added to it to achieve criticality.

Sintering is a process of compacting a material by applying heat or pressure to form a solid mass without melting it to the point of liquefaction. The sintering temperature of thorium dioxide fuel is quite high. Combining the sintering of thorium dioxide in order to convert it into solid nuclear fuel along-with the addition of fissile material to make it achieve criticality makes the process of fuel fabrication quite tougher for thorium-based reactors. The comparatively longer interval of thorium fuel cycle also poses certain challenges in the usage of solid thorium fuel rods. Pa-233, an intermediate product in thorium cycle has a half-life of 27 days. As a result of which, significant amount of Pa-233 accumulates in the reactor. Pa-233 is an efficient neutron absorber and sometimes absorbs two neutrons and forms U-235, thereby degrading the neutron economy in the reactor. Moreover, formation of U-235 also increases the likelihood of generation of more transuranic products in the reactor. Unlike PUREX, which is the highly developed uranium fuel recycling process to separate uranium and plutonium, thorium fuel recycling technology e.g. THOREX is still under development (13).

1.2.3.6. Fast breeder reactor program of India with thorium as its fuel

Homi J Bhabha envisioned a three-stage reactor program to secure country's energy demand over longer run by using thorium, which is found in huge abundance in India, as the nuclear fuel. In order to convert thorium from fertile to fissile, this three-stage breeder reactor program was formulated which holds its validity even in today's scenario (14). The three stages envisioned for Indian Nuclear Power Generation program are:

Stage I: Pressurized Heavy Water Reactors

Stage II: Fast Breeder Reactors

Stage III: Thorium Based Reactors

Stage I: Pressurized Heavy Water Reactor

In the first stage of the program, natural uranium is used to produce electricity while also generating fissile plutonium-239 as its by-product. Natural uranium contains 0.7% uranium-235 which is the fissile isotope while most of the remaining 99.3% contains uranium-238, which is not fissile on its own but can be converted into fissile plutonium-239 in a reactor. Heavy water (deuterium oxide, D_2O) is used as a coolant and moderator in this reactor.

Stage II: Fast Breeder Reactor

The second stage of the nuclear power program consists of fast breeder reactors which uses mixed oxide (MOX) fuel made up of plutonium-239 generated in the first stage and uranium-238 to produce electricity. Plutonium-239 generated in stage I is isolated by reprocessing the spent fuel from stage I. The energy produced by the fission of Pu-239 in stage II is used to generate electricity and to transmutate U-238 into more of Pu-239. The FBRs, thus, breed more fuel than they can consume. Once sufficient inventory of Pu-239 is generated

in stage II, thorium-232 is added as a blanket material to the reactor which gets transmutated into uranium-233 which serves as fuel in stage III.

Stage III: Thorium based reactors

The stage III of the nuclear power program uses thorium-232-uranium-233 as its fuel in a self-sustaining advanced power reactor. These types of reactors would be thermal breeder reactors which, after initial fuel recharge, would be refueled using only naturally occurring thorium-232. U-233 generated in stage II would be used as reactor core to fuel the reactor and a blanket of thorium-232 would be added around U-233 core which will produce more of U-233, resulting in the production of more U-233 enabling the reactor in its fuel requirement for long-term power generation (13).

The different stages of the nuclear power program with the project amount of electricity generated at each stage is shown below in detail in Figure 1.5.

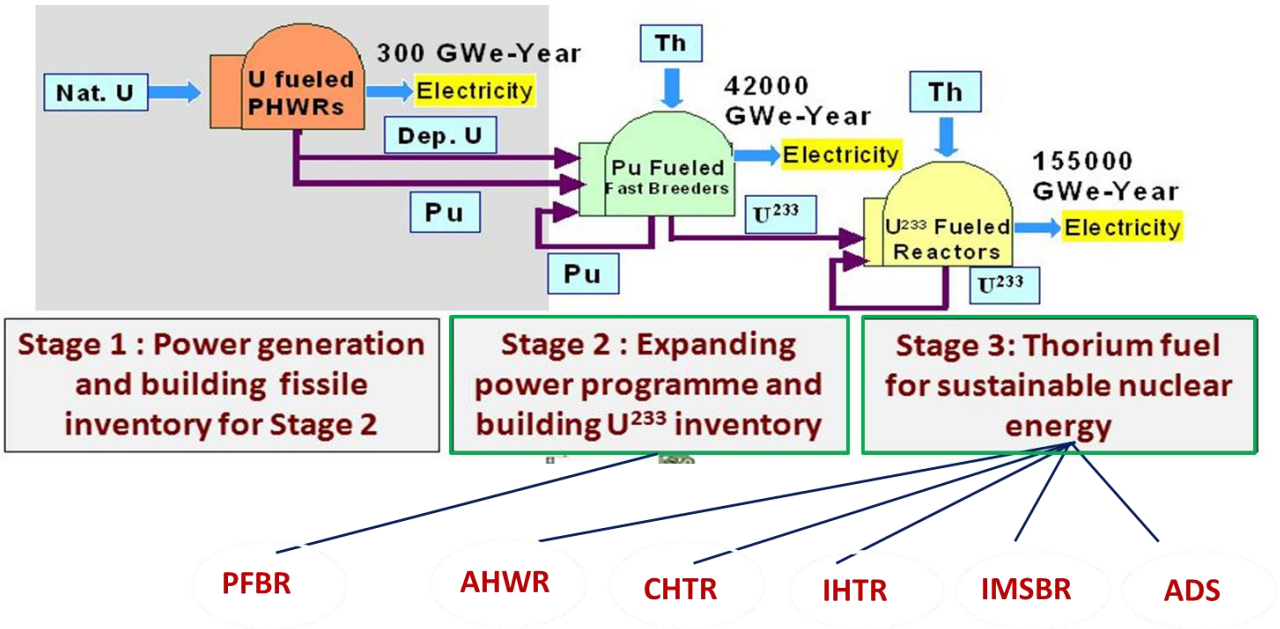

Figure 1.5: *Pictorial representation of the three stages of the nuclear power program envisioned for power generation in India using thorium as nuclear fuel. PHWR: Pressurized*

Heavy Water Reactor; PFBR: Prototype Fast Breeder Reactor; AHWR: Advanced Heavy Water Reactor; CHTR: Compact High Temperature Reactor; IHTR: Innovative High Temperature Reactor; IMSBR: Indian Molten Salt Breeder Reactor; ADS: Accelerator Driven System. Picture courtesy: Dr. Amit Kumar, Radiation Biology & Health Sciences Division, Bhabha Atomic Research Centre, Mumbai.

Thorium with its vast reserves on earth and its promise to be used only for peaceful purposes offers an important fuel for nuclear reactors. Its various advantages over the conventional nuclear fuel i.e., uranium such as easy availability, long half-life, availability of useful isotope of thorium (Th-232) in abundance, no generation of nuclear weapon material i.e., plutonium-239 as by-product and generation of less radioactive material as nuclear waste makes it an essential and attractive option as nuclear fuel. The reactors which could utilize thorium as nuclear fuel for generation of electricity are still under development with India leading the world in this technology followed by China. Although thorium is more attractive as nuclear fuel, it is still difficult to be used compared to uranium because thorium requires breeding into uranium-233 before it could be used as fuel and global uranium prices remain low enough that breeding thorium is not cost effective (13).

There are several benefits of using thorium as fuel material. The advantages mostly include wide availability of useful isotope of thorium reserves, its inability to produce plutonium as by-product, less radioactive waste generation etc. These advantages are discussed in detail above in Section 1.2.3.5.

Thorium is mostly found in small amounts in rocks and soils where is it three times more abundant as compared to uranium. On an average, ~6 ppm of thorium is found in soils. Naturally occurring thorium usually occurs in only one isotopic form i.e., Th-232. Decay series

of thorium and uranium gives rise of other isotopes of thorium such as Th-228, Th-230 and Th-234 which are negligible in terms of mass as compared to Th-232. The total reserves of thorium in different countries of the world is shown below in Figure 1.6.

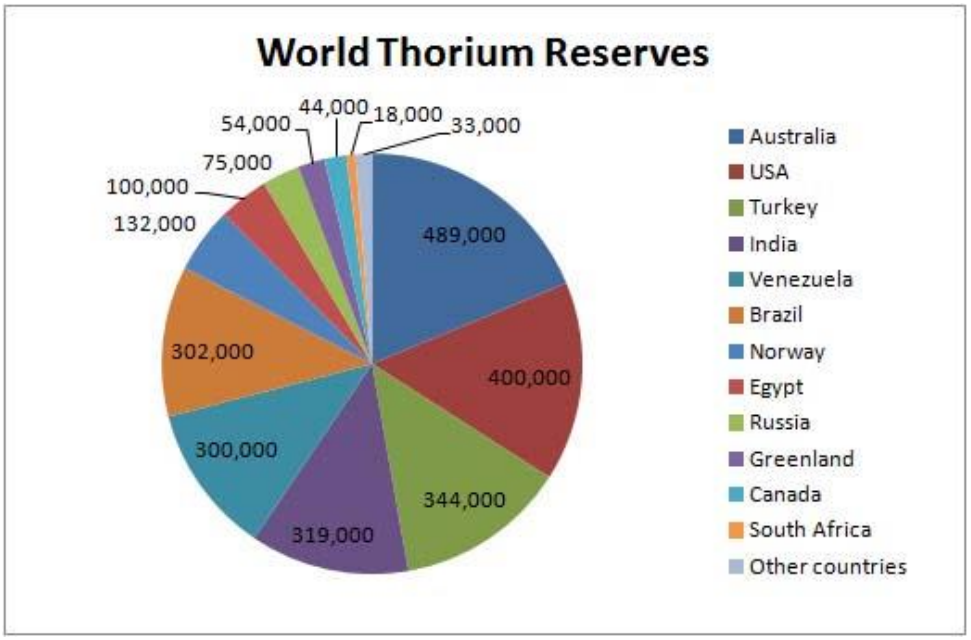

Figure 1.6: *Estimated reserves of Th in different countries of the world as published in International Atomic Energy Agency, (IAEA) 2005. India has fourth highest thorium reserves in the world having 319,000 tons of thorium after Australia, USA, and Turkey.* ***Source:*** *https://web.mit.edu/12.000/www/m2016/finalwebsite/solutions/deposits.html*.

As per International Atomic Energy Agency (IAEA) 2005 estimates, India has approximately 319,000 tons of thorium reserves which is ~12% of the total thorium reserves worldwide. However, an American estimate puts the amount of thorium reserves in India in the range of 290,000 to 650,000 tons. A survey performed by Atomic Minerals Directorate for Exploration and Research (AMD, DAE) in the year 2018 puts the thorium estimate in India around 980,000 tons. Apart from India, huge reserves of thorium is also found in countries such as United States (440,000 tons), Australia (300,000), Canada (100,000), Malaysia (4,500) and South Africa (35,000) (15).

In India, most of the thorium reserves are found in Andhra Pradesh (31%), Tamil Nadu (21%), Odisha (20%), Kerala (16%), West Bengal (10%) and Jharkhand (2%). The thorium in almost all these places are found in the form of monazite ore in the sand beaches along the coastal region of these states (15). As per an estimate by Department of Atomic Energy, the amount of thorium ore, monazite, present in different states of India is shown below in Table 1.2 (16).

State	Established Monazite resources (in Lakh tons)
Kerala	15.1
Tamil Nadu	21.6
Andhra Pradesh	37.4
Odisha	18.5
West Bengal	12.2
Jharkhand	02.2
Total	**107**

Table 1.2: *Estimate of monazite ore (in lakh tons) found in different states of India*.

1.3. Steps involved in processing of thorium ore

Thorium ore is mostly extracted from monazite, an anhydrous rare earth phosphate ore, which is present in sand reserves along the sea and riverbeds. The chemical formula of monazite is (Ce,La,Nd,Th).PO_4. Monazite typically contains 3-5% of thorium in the form on thorium dioxide (ThO_2). Thorium is extracted from monazite ore along with other rare earth elements (REEs). The steps involved in the separation of thorium from monazite include

mining and concentration, extraction and refining (acid and alkali digestion), solvent extraction and reduction to the metal (17). These steps are described below in brief

1) Mining and concentration

Monazite sand is mined with conventional mining equipment and techniques and is present as a mixture of variety of other minerals as well, mainly including silica, magnetite, ilmenite, zircon and garnet. Monazite is concentrated by washing out lighter minerals using shaking tables and treating the resulting fraction with a series of electromagnetic separators using different kinds of magnets. This process separates monazite from other minerals based on their magnetic properties.

2) Extraction and refining

The monazite ore, though, chemically stable undergoes attack by both strong mineral acids (such as sulphuric acid, H_2SO_4) and alkalis (such as sodium hydroxide, NaOH). Extraction and refining of thorium can be done via both acid digestion as well as alkaline digestion. Both the processes are discussed in brief below:

a) Acid digestion: Finely grounded monazite sand is digested with highly pure sulphuric acid by heating it at 155 to 230˚C. This process converts the phosphate and metal content of monazite into water-soluble entities. The resulting solution is then mixed with aqueous ammonia which separates hydrated thorium phosphate by precipitating it as gelatinous mass and then metathesizes it to thorium hydroxide. The resulting solution is finally converted into thorium nitrate by treating it with nitric acid. The thorium nitrate thus obtained is crude in nature and is further purified by solvent extraction.

b) Alkali digestion: In alkali digestion, finely grounded monazite sand is treated with a highly concentrated sodium hydroxide solution (NaOH) at 138˚C. This process generates solidified

thorium hydroxide, which is then dissolved in mineral acid, generally, hydrochloride acid to yield a solution of thorium chloride. This crude solution contains rare earth elements also in chloride form. Thorium chloride is separated from them by addition of NaOH. The crude thorium chloride thus obtained is finally dissolved in nitric acid to form thorium nitrate which is further purified using solvent extraction method.

3) Solvent extraction

In order to purify thorium from impurities consisting of rare earth metal species and uranium also to an extent, the crude thorium solution obtained after acid or alkali digestion is subjected to treatment with a solution of tributyl phosphate diluted by a suitable hydrocarbon. An organic extract results which contains thorium (uranium may also be present) whereas the other impurities are removed by treating it with small amount of nitric acid. The thorium present in tributyl phosphate solution is then removed by treating it with aqueous nitric acid solution. Thorium is separated in the aqueous solution while uranium is retained in the organic phase. The purified thorium thus obtained, is then concentrated by heating the thorium nitrate solution. Thorium nitrate is also calcined to thorium dioxide (ThO_2) which is incorporated into ceramic fuel elements to be used in nuclear reactors or converted into metallic thorium.

4) Reduction to metallic thorium

Thorium metal is finally obtained by treating ThO_2 with hydrogen fluoride (HF_4) which yield thorium tetrafluoride (ThF_4). Thorium metal is finally obtained by Spedding process in which powered ThF_4 is mixed with finely powdered calcium and a zinc halide (either zinc chloride or zinc fluoride) and heated up to 650˚C in a sealed, refractory-lined “bomb”. Thorium and zinc metal are produced in an exothermic reaction while also producing a slag of calcium chloride or calcium fluoride.

Upon solidification, thorium-zinc alloy is heated at a temperature which is above the boiling point of zinc (907˚C) but below the melting point of thorium. Thus, zinc is evaporated leaving highly purified thorium metal.

1.4. Exposure conditions of thorium

Considering the vision to use thorium to secure the long-term energy needs of people using three stage nuclear program, it is inevitable that the activities such as thorium ore mining, milling, fuel fabrication, reprocessing and deploying of thorium-232 would increase human exposure to thorium significantly. This increase in the usage of thorium would result in a higher thorium exposure mainly to workers engaged in mining, milling, fuel processing and nuclear workers involved in thorium plant operations as well as to general public (18). The accidental/occupational exposure to thorium causes an increased probability of thorium entering human body either through inhalation, ingestion and open wound/skin absorption (19). The conditions under which exposure occurs through these different routes and the major retention organs are discussed below.

1) Inhalation

Thorium exposure through inhalation of fine thorium dust is one of the most common routes of thorium exposure in both occupational and accidental scenarios. Fine thorium dust particles, once inhaled, gets accumulated in the lungs and are slowly absorbed by blood which transports it to other organs of thorium deposition such as liver, spleen, and bone. Toxicity of thorium to lungs and other organs is different when exposed by inhalation. Generally, when a soluble compound is inhaled, it gets readily absorbed by blood and will be more toxic to blood and distal organs as compared to lungs whereas if an insoluble compound is inhaled, it is much toxic to lungs on the account of its retention in lungs for longer duration (20).

2) Ingestion

In addition to inhalation, living beings are also exposed to thorium through ingestion of contaminated food and water. Depending upon the differences in the solubility of different forms of thorium, the absorption rate of various forms in gastrointestinal tract varies. Generally, the absorption rate ranges from 0.1 to 1% in the gastrointestinal tract. Thorium nitrate absorption is 4 times higher than thorium dioxide whereas absorption of thorium chloride is 10 to 20 times higher than thorium dioxide, depending on its concentration (19).

3) Wound/dermal absorption

Thorium exposure via wound or skin absorption is also another route of exposure which is more prevalent in case of exposure via thorium dust. The toxicity studies involving thorium exposure via wound/skin absorption route has not been well investigated (19).

The exposure to heavy metal radionuclides such as uranium, plutonium, thorium generally occurs during their mining, reprocessing and disposal. Different radionuclide has different sources depending upon their availability in nature. Uranium being quite available through natural rocks and soils is commonly found in nature. Since, it is soluble in water, a significant portion of uranium is also found in water bodies. U-235 is present in a limited extent in nature while most of the naturally available uranium is U-238. U-239 is generated in nuclear reactors for production of plutonium. Food crops growing underground in soils rich in uranium are also a source of uranium intake by humans via ingestion.

Plutonium is a man-made heavy metal radionuclide which is generated in nuclear reactors. Pu-239 is the most commonly generated product of uranium reactors which can be used for both generation of electricity and making of nuclear weapons.

Thorium is another heavy metal radionuclide which is three times more abundant as compared to uranium in natural soils and rocks. Because it is insoluble in water, negligible amount of it is found in the water bodies.

1.5. Routes of exposure for the other major Heavy Metal Radionuclides

Heavy metal radionuclides can be exposed to living beings through different routes. The main routes through which the exposure occurs includes inhalation, ingestion, and wound/dermal absorption. Exposure through inhalation mainly occurs during mining and milling operations where there is a very high concentration of dust particles containing these heavy metals. These heavy metal radionuclides also occur in higher amounts in the air surrounding the rocks where these metals are occurring naturally. In case of uranium and thorium, people who live near their mining, processing, and manufacturing facility are exposed to their higher amounts as compared to general population. In case of uranium, areas where depleted uranium weapons are used also have higher concentration of uranium. Plutonium, mostly being man-made, is released into the environment during nuclear weapon testing, from research facilities, waste disposal, nuclear fuel reprocessing facilities, nuclear weapon production facilities, accidents at plutonium handling facilities etc.(21). Plutonium usually gets attached to particles in air and gets transported along. The concentration of plutonium in air is generally low and usually ranges between 0.01 to 0.1 picocuries (pCi) per gram of soil (21). Inhaling these heavy metal radionuclide laden dust results in their deposition of lung initially from where they are absorbed by blood and transported to different organs depending upon their solubility and affinity to different organs.

Ingestion of these radionuclides occurs mainly through intake of food and water contaminated with them. Uranium being water-soluble, can be found in drinking water. It tends

to be at higher levels from wells drilled in uranium-rich rocks and soils. Uranium present in soil can stick to plant roots and can lead to root crops such as potatoes, parsnips, turnips and sweet potatoes contributing to uranium ingestion through diet. The amount of uranium in these crops is directly proportional to the amount of uranium in the soil in which they are grown. Daily human intake of uranium by human is estimated to be in the range of 0.9 to 1.5 µg/day. Phosphate fertilizer industry is also said to generate uranium and people working in these plants are exposed to higher levels of uranium as compared to general population (22).

Improper handling of these radionuclides by nuclear workers using either naked hands or torn gloves or touching different surfaces using contaminated gloves also increases the chances of exposure to these radionuclides' thorough ingestion and/or wound/dermal absorption. Settling of fine dust particles onto skin and/or open wounds also leads to their absorption into the body through skin.

1.6. Health Effects of Heavy Metal Radionuclides

Exposure to these heavy metal radionuclides results in their accumulation in different organs. Once deposited in the body, the heavy metal radionuclides exert their adverse effects by virtue of their chemical toxicity and radiological toxicity as they can bind to various biomolecules and also emit alpha particles (4-5 MeV) (23). The extent of their adverse health effects due to radiological toxicity depend on the organs these metals are deposited and also on their biological half-lives.

Uranium toxicity has been found to be mainly due to its chemical toxicity rather than radiological toxicity. According to the well-accepted theory, uranium exerts its toxicity on kidneys by releasing itself from serum bicarbonate complex in the kidney and binding to available phosphates and proteins. Overexposure to uranium causes irritation which leads to

extensive tissue damage. Proximal convoluted tubule is the most damages part of kidney upon uranium exposure followed by glomerulus (24,25). Kidney is the main target of uranium induced damage and has been consistently found to have damages in humans after inhaling or ingesting uranium. However, soldiers who have had uranium metal fragments in their bodies for several years did not show any damage to their kidney suggesting that the damages caused by uranium exposure is mainly due to its chemical toxicity and not through radiological toxicity (22).

Similarly, plutonium when internalized either through inhalation and/or ingestion causes cancer in the long run. Cancer of bone, liver and lungs has most commonly been reported in individuals exposed to plutonium. Studies involving animals have shown that a large amount of plutonium deposited in lungs will eventually move to growing bones suggesting that bones of children, if exposed to plutonium, would be most severely affected. Animal studies have also showed that a large portion of plutonium present in gut upon ingestion is absorbed (21).

Thorium internalization is known to cause cancer in long term. The organs mainly affected by thorium accumulation are liver, spleen, bone and lungs (26,27).When thorium enters into body through inhalation via thorium dust, it is retained in the lungs for a longer duration. Inhalation of insoluble form of thorium such as thorium dioxide dust particle causes it to be retained in lungs for a considerably longer time as compared to thorium nitrate which slowly gets absorbed in blood and transported to different organs in body. Inhalation of thorium dust in thorium workers was also found to have caused alterations in the genetic material of their body cells (28).

2. Carcinogenic effects of Heavy Metal Radionuclides

Exposure to heavy metal radionuclides and their internalization leads to development of cancer in the long run. Different heavy metal radionuclides accumulate in target organs and depending on type/dose of radionuclide it may also lead to cancer. The radionuclides over these years continue to may exert chemical and/or radiological toxicity depending on type/dose of radionuclides. Most of the uranium which gets absorbed in the blood is filtered by kidneys and, the rest of it is found in kidneys and bones after a few days of exposure. However, bones are the major site of uranium accumulation over long duration (24,29) where it causes bone sarcoma (30). Soft tissue targets include liver and kidney whereas pulmonary lymph nodes are the main target site for accumulation of inhaled uranium dust (24). Studies on plutonium has shown that majority of plutonium gains entry in the body via inhalation and only 1% of plutonium which enters the body through gastrointestinal routes are absorbed in blood. 90% of soluble plutonium from lungs is absorbed by blood and 80% of it is released into liver and bone. Only 10% of soluble plutonium is deposited in other body organs. Insoluble plutonium is mostly retained by lungs and deposited mainly in pulmonary lymph nodes. Plutonium exposure over longer duration has been known to cause cancers of bone, liver and lungs (31,32). Thorium accumulates mostly in liver, bone, spleen and lungs (27,33) and causes hepatocellular carcinoma, bone sarcoma after years of exposure. Besides these organs, lungs are also the main target of thorium toxicity when they enter body through inhalation. Thorium dioxide, being insoluble in water, is retained by lungs and causes its toxicity mainly to lung tissue. Other forms such are thorium nitrate, being readily water-soluble, is absorbed by blood from which it is deposited in liver, spleen and bones (33).

2.1. Radiation Carcinogenesis

Exposure to radiation, both external and internal, have been known to cause carcinogenesis. Radiation carcinogenesis, unlike chemical carcinogenesis is a stochastic process, where the probability of developing cancer depends directly on the dose of the radiation received. Most of these HMRs are alpha emitters which undergo decay while emitting alpha particles. Therefore, these HMRs cannot really cause much damage unless they have been internalized in the body. Once internalized, they get deposited slowly in different organs. Upon accumulation, these HMRs provide a continuous source of radiation to the organ until their radioactive decay. These HMRs, being heavy metals also cause chemical toxicity which add/synergize the radiological toxicity to cause carcinogenesis (20). A comparative view highlighting the various events which take place during both external-radiation and internal-radionuclide-exposure induced carcinogenesis is listed below in Figure 1.7 (20)

Both external and internal exposure to radiation, above a certain level, is carcinogenic in nature (20). Cancer incidence due to external radiation exposure (mostly gamma-rays) has been reported on people exposed to it. The first reported incidence of adverse health effects of external radiation have been reported in an ulcerated region of skin (34,35) followed by leukemia incidence in a few radiation workers (34,36). Marie Curie and her daughter Irene have also been thought to have died due to radiation-induced leukemia.(34) However, the adverse health effects of radiation and it's carcinogenic property have mainly been studied in detail after the bombing of Hiroshima and Nagasaki in 1945 and other subsequent nuclear accidents which exposed the nuclear workers to significantly higher doses of radiation. Nuclear accidents such as Chernobyl in 1986 and Fukushima in 2011 have provided risk of health effects of radiation and its carcinogenicity (23,37). Different types of cancers associated with various types of radiation and exposure conditions viz., atomic bombs, occupational, medical

have been studied and reviewed (34,38). Carcinogenic effect of radiation has been studied in both *in-vitro* and *in-vivo* models (34) in addition to epidemiological studies in human population exposed to a range of higher doses of radiation (39) in order to understand its mechanistic aspect. The mechanism of carcinogenesis due to external radiation is well investigated whereas mechanistic details of carcinogenesis because of internal exposure due to radionuclides have not been studied in depth (20).

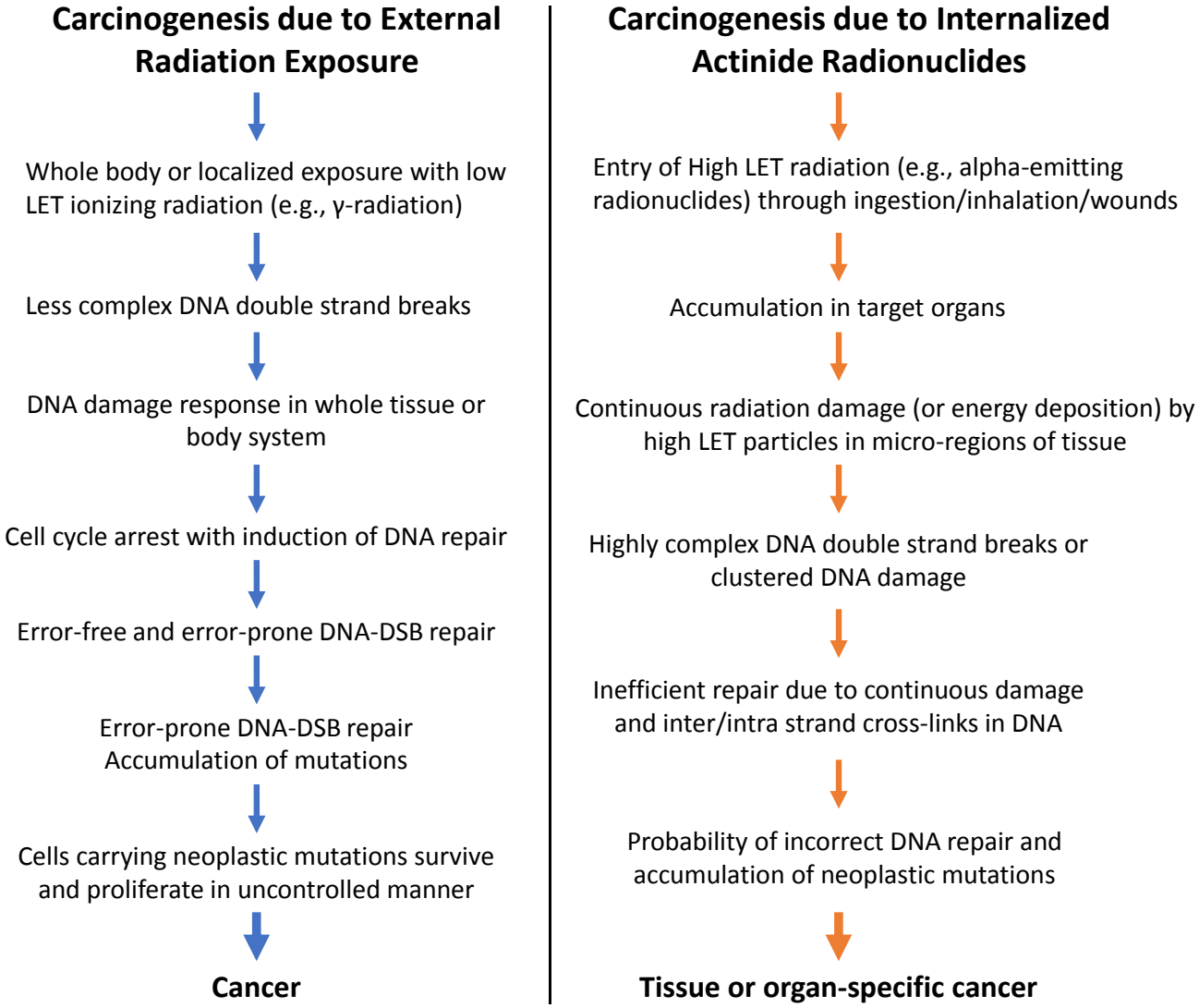

Figure 1.7: *A comparative view of the steps involved in carcinogenesis due to external-radiation exposure and internal radionuclide exposure*.

2.2. Mechanism of Radiation Carcinogenesis

Radiation carcinogenesis, unlike chemical and viral carcinogenesis, is different as radiation has the ability to penetrate the cell/tissues and deposit its energy randomly and non-specifically to its target tissues and organs whereas most of the chemical carcinogens are tissue specific and have to cross many barriers in order to cause its toxic effects. Most of the chemicals also require a promoting agent in order to initiate a carcinogenic effect. Radiation, however, does not require a promoting agent in order to initiate carcinogenesis (20). The ability of radiation to penetrate its target cell/tissue to be a "universal carcinogen" i.e., it has the ability to cause cancer in most tissues of most species at all ages including fetus (40).

Studies on malignant transformation in cellular systems showed that radiation is both a weak carcinogen as well as a mutagen which causes a broad spectrum of DNA lesions in cells including damage to nucleotide bases, cross-linking and DNA single- and double-strand breaks (DSBs). DNA-DSBs were originally thought to be the most cytotoxic of radiation effects while thymine glycols were implicated in mutagenesis. It is now known that mis-repaired DSBs are the principal lesions important for the induction of mutagenesis and carcinogenesis (41,42). Molecular evidence obtained from mutant cell lines lacking/defective in the repair of radiation-induced damage also suggest the importance of DSBs in biological effects of radiation (43). Although most of the DSBs can be repaired by homologous recombination which is an error-free process, this mechanism is fairly uncommon in mammalian cells (44). Most of the DSBs in mammalian cells are repaired by an illegitimate process of non-homologous end joining (NHEJ) which is highly error-prone (45) and thus, likely accounts for most of the mutagenic DNA lesions found in radiation-induced DSBs.

The most predominant molecular-structural changes leading to radiation-induced mutations are events such as loss of heterozygosity (LOH) (46). Other large-scale changes

include events such as deletions, chromosomal rearrangements or recombinational processes. These processes generally take place after DSBs (47,48). These observations, therefore, suggests that the initiating event leading to radiation-induced carcinogenesis is most likely to be inactivation of a tumor-suppressor gene by LOH rather than activation of protooncogene such as RAS (40).

Radiation carcinogenesis caused by actinide radionuclides upon internalization includes damages caused by both chemical as well as radiation toxicity. Most of the effects of these radionuclides inside body is manifested through the formation of DSBs, either through direct deposition of energy on DNA or indirectly through free radicals or reactive oxygen species (ROS) generated during ionization process. As per a study, 1 Gy of low LET γ-radiation induces around 850 pyrimidine lesions, 450 purine lesions, 1000 single strand breaks (SSBs) and 20-40 DSBs (49,50). Another study used plasmid DNA (pEC) and irradiated it with both gamma radiation and alpha particles. Post-irradiation, the plasmid DNA was incubated with endonuclease III and the number of SSBs and DSBs generated were quantified. The number of SSBs were found to be 5.98 x $10^{-8}$$Gy^{-1}$$Da^{-1}$ in case of γ-radiation with LET approx. 0.3 keV $\mu m^{-1}$and 8.66 x 10^{-8} Gy^{-1} Da^{-1} in case of alpha radiation with LET of 97 keV μm^{-1}. Similarly, the number of DSBs were found to be 1.45 x 10^{-9} Gy^{-1} Da^{-1} in case of γ-radiation and 1.07 x 10^{-19} Gy^{-1} Da^{-1} in case of alpha particle irradiation (51). Another study showed that when ratios of non-DSBs and DSBs were calculated for different types of radiations, it was found to be in the range of 5-10 for -rays and 3-5 for high LET radiations such as alpha particles (52). As discussed above, it is the mis repaired DSBs that initiate neoplastic changes and increase cancer risk. However, cells/tissues exposed to lethal doses of radiation would be eliminated through apoptosis, thereby, reducing the risk of cancer. Although the fate of individual cells is decided by the extent of DNA damage, there are other

non-targeted radiation effects such as abscopal effect, communication between bystander/distant organs, clastogenic factors etc. which also contribute to the development of radiation-induced carcinogenesis (20).

2.3. Carcinogenesis by heavy metal radionuclides

A. Plutonium

As discussed above in Section 1.4 and 1.6, plutonium enters into the body through inhalation, ingestion and through dermal absorption. Since gastrointestinal absorption of plutonium is very low (<0.001%), most of the plutonium which enters through food or water is excreted out through feces (53). Plutonium dust particles which enter the lungs through inhalation is either retained in the lungs for a long-time or is absorbed by blood eventually depending upon the chemical form and size of plutonium dust particles. Lungs, bone and liver are the main organs of plutonium deposition (54–56). Plutonium deposited in these organs remains in the body organs for a long duration and continues to expose the surrounding tissues with radiation, thereby, increasing the risk of cancer in these organs. Macrophages have been found to play an essential role in the retention and clearance of inhaled compounds. However, the extent to which these phagocytic cells are involved in these processes is highly dependent upon the solubility properties of the plutonium particles deposited in lungs (57).

B. Uranium

Unlike plutonium, uranium occurs naturally in a weakly radioactive form. Approximately around 2-5 µg/g in soil, 0.03 pCi/L in water and 4-10 ng/m^3 in air is found naturally which contributes to low level of natural background radiation (22). Uranium causes inhibition of mitochondrial ATPase activity and sodium transport mechanisms which can in

turn reduce the repair capacity of the epithelial cells and also causes them to reduce their functionality (24,25). The mechanism of lung toxicity has been cited as deep lung irritation which later results in fibrosis and/or emphysema. This state is associated with oxidative stress, changes in gene expression and inhibition of sodium-dependent phosphate and also glucose transport systems (24,25)

C. Thorium

Like uranium and plutonium, the most common pathway for thorium to enter human body is either through inhalation, ingestion or through dermal absorption. Over time, it has been found that thorium accumulates in liver, spleen, bone and lungs, depending upon the route of exposure and chemical form of thorium, and slowly causes cancer. Liver cancer and its mechanistic aspect have been studied in a few cases. In case of liver cancer developed in thorotrast patients, it was found that there was an induction of point mutation in exons 5-8 of p53 gene. Also, the frequency of large deletions such as loss of heterozygosity was found in only 27% of the cases of liver tumor (58) whereas mutations such as single-base deletions, transition and transversion was found in 47% cases of liver tumor. However, the mechanism thorough which thorium exposure leads to mutations in oncogenic pathways and causes development of liver cancer still needs to be investigated further.

3. Current Status of Thorium Toxicity Research

The huge reserves of thorium found in monazite sand all over the world and the decision to develop thorium based nuclear reactors to generate electricity increases the likelihood of thorium exposure manifold to the public as well as occupational workers. However, much need to be studied in order to understand the basic thorium biology inside

living systems. Current literature survey of the toxicity of thorium was carried out and divided into three main groups:

In-vitro: studies of primary cell lines and normal cell lines

In-vivo: studies on animal models such as mice, rat, *Chironomus* larvae

Human: studies involving human exposure to thorium due to occupational, medical, accidental etc. reasons.

A detailed account of the literature survey in all the three above mentioned groups is listed below:

A. In vitro

Studies detailing the effect of thorium on cells are rare in literature (59). Few studies have been performed in this regard and the main findings are as follows. Kumar et. al., (2010) studied the effect of thorium on human erythrocytes and found that thorium treatment causes aggregation and/or lysis of erythrocytes depending on thorium concentration. Low concentration causes aggregation and high concentration (> 40 µM) induced erythrocytes to undergo lysis. The underlying mechanism of this behavior of cells was found to the interaction of thorium with membrane sialic acid (aggregation) and hemolytic effect was observed due to the colloid osmotic mechanism (60). Ali et al (2014) studied the effect of thorium on human liver cells (HepG2) and found that low concentration of thorium (0.1-10 µM) exerts cyto-proliferative effect on cells which is mediated by insulin-like growth factor 1 receptor and its downstream signaling (61). Kumar et al., (2016) studied the effect of thorium along with other lanthanide and actinides on hemoglobin molecule and validated the same using *Chironomus* larvae. The study reported that thorium interacts with the carbonyl and amide group of

hemoglobin and causes structural alterations by distorting the alpha-helix conformation. Beyond 75 µM, thorium was found to interact with heme moiety and this interaction affected the oxygen-binding capacity of hemoglobin (62). Another study by Ali et al, (2019) studied the efficacy of different bio-compatible decorporating agents under in vitro conditions using erythrocytes and WRL 68, human liver cells. It was found that out of the ten decorporating agents selected for the study, tiron, silibin, phytic acid and L52 showed enhanced thorium decorporation abilities (63).

Olivera et al studied the effect of thorium, cerium and lanthanum toxicity on lymphocytes and found that thorium and cerium did not exert any toxic effects on lymphocytes individually. However, thorium in combination with lanthanum increases its toxic effect and therefore, reduces the viability of lymphocytes at low concentrations of metals in the mixture (64). Iwahara et al studied the effect of three main constituents of monazite sand i.e., thorium, cerium and lanthanum on human osteoblasts and report the metal combinations (Th-Ce, Th-La, Th-Ce-La) in association with radiation can cause combined effects on osteoblasts. The study indicates that there is an increased possibility of occupational risks to workers involved in handling monazite ore at nuclear facilities. The ore mixtures and their cytotoxic and radiotoxic effects needs to be properly highlighted (65).

B. In vivo:

Thorium accumulation in long-tailed ducks residing in Gdansk Bay water was estimated by Szefer et. al., (1983) and it was found that the stomach accumulated highest amount of thorium while the lowest concentration was in breast muscle (66). A similar study estimated the concentration of thorium in soft muscles of mussels in coastal areas of North sea and Baltic region and reported the values to range from 11–26 µg/Kg dry weight (67). The

effect of chronic exposure to thorium in water bodies was studied by Kochhann et. al., (2009) in silver Catfish (*Rhamdia quelen*). Juvenile silver catfish were exposed to different concentrations of thorium and their accumulation and oxidative stress was measured. It was found that maximum amount of thorium was accumulated in gills, skin and kidney. Alterations in oxidative parameters were also observed at highest dose of thorium (68). Jadon et al (1983) studied the effect of thorium nitrate on mice testes and showed thorium caused reduction in the diameter of seminiferous tubule and also caused a decrease in the gametogenic count (69).

Likhachev et al.(1975) reported that rats exposed to different concentrations of thorium dioxide for 6-9 months developed lung cancer (70). Easton et. al., (1952) studied the role of movement of macrophages in the transport and elimination of thorium from mice after intravenous injection of thorium dioxide. Their study reported that thorium-laden macrophages move into the liver and are held there temporarily before going into the lungs (71). Peter et. al. (1981) studied the interaction of thorium with blood serum components of adult female Heiligenberg rats and reported that thorium mainly binds to iron-carrying protein, transferrin, found in the blood serum. The binding site of thorium is more likely the same as the binding site of iron on transferrin (72).

Various groups are also engaged in studying the strategies to decorporate thorium after its exposure using different animal models. Peter-Witt et al., (1985) undertook a comparative analysis of the abilities of calcium diethylenetriamine pentaacetate (Ca-DTPA) and Zn-DTPA to decorporate thorium from rats as a function of dose, number of doses and time of administration. It was found that at early time of administration, Ca-DTPA was much effective in removing thorium as compared to Zn-DTPA. The ability of Ca-DTPA to remove thorium was decreased with an increase in the time of their administration. At delayed administration, both Zn-DTPA and Ca-DTPA were found to be equally effective in thorium decorporation

(73). Kumar et al (2007) studied the effect of thorium on mice in terms of thorium-induced oxidative stress and abrogation of this stress using DTPA. They reported that intraperitoneal administration of subtoxic concentration of thorium to Swiss mice significantly altered liver function and induced oxidative stress in liver, femur, and spleen. It was further reported that administration of Ca-DTPA showed a protective effect against the toxic effects of thorium (33). Similar study was also carried out by Kumar et. al., (2011) where they studied the efficacy of DTPA in decorporating thorium from Wistar rats in free and in a liposomal encapsulated form. It was found that neutral liposomal DTPA was much more effective in removing and thereby mitigating the toxic effect of thorium as compared to free DTPA (74).

Kumar et. al. (2009) also studied the effect of intraperitoneally injected thorium on the brain of Swiss mice and reported that maximum amount of thorium was accumulated in cerebellum of brain followed by cortex, hippocampus and striatum. Alterations in oxidative parameters were also observed which probably led to the changes in neurobehavior and neurochemicals of Swiss mice (75).Similar studies were also performed by Rezk et al., (2018) (76) and Abdel-Rehman et al.,(2020) (77) to study the effect of thorium on rat brains and reported thorium accumulation in different parts of the brain the same order as reported by Kumar et al(75). Additionally, Rezek et al reported a thorium-induced increase in the content of malondialdehyde and Na^{+}, Ca^{2+}, Fe^{3+} ions and a decrease in the levels of glutathione and K^{+} levels. Administration of alginate mitigated these adverse effects on brain (76). Abdel-Rehman also found that in addition to thorium accumulation in different parts of the brain, thorium administration also interrupted the balance of free radicals and antioxidants in brain. Additionally, the level of TSH was also found to have increased upon thorium treatment (77). Another study by Rezk et. al., (2018) showed thorium induced hematological, hepatic and lipid dysfunction in rats apart from their distribution and accumulation in different organs (78).

C. Humans:

Goto et al. (2002) studied the tissues from thorotrast treated patients and found that radioactive thorium deposited in organs always migrated with the help of macrophages and that the organ was evenly exposed to alpha particles (79). Another group namely Muramatsu et. al. (1999) studied the amount of thorium deposited in different organs of thorotrast patients using inductively coupled plasma mass spectrometry (ICP-MS). Thorium was estimated in a total of 27 different organs from 98 different samples. They reported that highest thorium level in spleen (16,000 µg/g wet weight) followed by liver (2100 µg/g) and bone marrow (600 µg/g). Other organs where thorium deposition was reported by them are as follows in the decreasing order: lymph node, gall bladder, testis, lung, small intestine, adrenal gland, pancreas, dura, esophagus, muscle, thyroid, large intestine, stomach, fat, kidney, urinary bladder, main artery, prostate, diaphragm, trachea, heart, cerebellum, cerebrum and intervertebral disk (80). Stehney et.al. (1999) studied the distribution of thorium in various organs of thorium refinery workers during autopsy. Thorium activity were determined in different organs [mBq per gram of wet tissue lungs (0.17-94), pulmonary lymph nodes (3.9-1210), bones (0.14-1.19), liver (0.015-0.68), spleen (0.97-3.8) and kidneys (0.009-0.068)] (81,82). The high level of thorium in lungs and lymph nodes were probably due to the insolubility of the material inhaled by the workers. Warnakulasuriya et.al. (2017) studied the frequency of micronuclei (MN) in the peripheral blood lymphocytes of the employees of Lanka Mineral Sands Ltd (LMS) and the nearby population in Sri Lanka. The plant has been involved in the mining of minerals including monazite since 1957. They reported that the frequency of micronuclei among the employees of LMS and the population residing within 5 km radius of LMS was significantly higher as compared to those residing 20-25 Km and 50 km away from LMS indicating the higher risk of developing MN as a consequence of high background radiation in these areas (83). Another

study by Dang et. al. (1986) estimated thorium intake in the population of Mumbai through food, water, and air. It was found that the daily intake of through was highest through food (2 µg) followed by water (0.02 µg) and air (0.02 µg) (84). Ludwig et al. (1999) studied the intake of thorium during TIG wielding by workers using thoriated tungsten electrodes and found that in the absence of a suction system, considerable intake of thorium occurred during both alternating-current wielding and electrode grinding. The amount of thorium intake by workers was estimated to range between 0.1 to 144 Bq per year during wielding and 0.02 to 30 Bq per year during grinding (85). Chen et. al. (2005) studied the thorium lung burden in Chinese miners and found that average measured thorium was significantly higher in high-dust exposure miners compared to low-dust exposure miners leading to increased incidences of severe breathlessness and pneumoconiosis in the previous group. Also, the rate of lung cancer mortality was much higher in exposed group relative to general population (86). Valiathan et. al. (1989) studied the possible link between tropical endomyocardial fibrosis in Kerala and major elements present in laterite and monazite soil and found that the endomyocardial fibrosis tissue samples contained an excess of thorium, sodium and calcium with a deficiency of magnesium. They speculated that the occurrence of tropical endomyocardial fibrosis is associated with an excess of thorium and deficiency of magnesium (87). Iyengar et. al. studied the internal radiation dose in Asian population due to daily dietary intake of thorium. They reported 4 mBq to be the median intake of thorium in Asian population which is found to be comparable with global intake value of 4.6 mBq. 0.34 µSv was the annual committed effective dose of ^{232}Th in Asian population (88).

4. Gap in Knowledge in Thorium Toxicity Research

In view of the increased usage of thorium in both nuclear and non-nuclear process, the risk of thorium exposure has also increased greatly. However, studies involving interaction of thorium with biological systems which causes its adverse health effects are still in nascent stages. A lot of research is needed to understand the mechanism of its uptake in different target organs and its movement among organs upon internalization. The effect of thorium on intracellular organelles and the signaling pathways through which thorium exerts its carcinogenic effect is also required to be studied in detail. The carcinogenic model which thorium follows and the genes playing a key role in carcinogenesis are also unknown.

5. Scope of the Thesis

The objectives of this thesis have been framed keeping in mind the above gaps in our knowledge of thorium toxicity. Since liver has been shown to be the main target of thorium accumulation leading to hepatocellular carcinoma, the focus of the present work has been on the mechanism of toxicity of thorium on liver both *in-vitro* and *in-vivo*. With this thesis, an attempt has been made to understand the mechanism through which thorium is internalized by liver cells. Also, the intracellular targets of thorium, its effect of various intracellular organelles and the mechanism through which it exerts its toxic effects would also be addressed. The process of carcinogenicity would also be validated using *in-vivo* Swiss mice model. An attempt has also been made to understand the adverse effects caused by chemical as well as radiological toxicity of thorium under *in-vitro* conditions.

6. Objectives and relevance of the Thesis

With these challenges of thorium toxicity in mind, the following objectives were framed for this thesis:

Objective I: To develop a colorimetric method for thorium estimation in biological samples.

Objective II: To determine the mechanism of thorium uptake, its sub-cellular distribution, intra-cellular targets, and alterations in major oncogenes/tumor suppressor genes.

Objective III: To study thorium bio-distribution, anatomical, histopathological, biochemical, and carcinogenic changes in mice.

With an answer to the above questions, an attempt has been made to understand thorium biology in deeper detail. The knowledge gained from this work would be helpful in framing strategies to mitigate the toxic effects of thorium and design better therapeutics to deal with thorium exposure and accidental incidents of thorium internalization.

CHAPTER 2: MATERIALS AND METHODS

2.1. Materials

2.1.1. Chemicals

Thorium nitrate [^{232}Th $(NO_3)_4.4H_2O$] salt was obtained from SRL labs (Mumbai, India). Analytical grade ^{238}U salts were obtained from the Radiochemistry Division, BARC, Mumbai, India. Nitrates of Ce (IV) and La (III) were obtained from Sigma, USA. Manganese (II) chloride tetrahydrate ($Mncl_2.4H_2O$), ACS reagent, ≥ 98% (Cat. No. 221279) and Iron (III) chloride ($FeCl_3$) salts, reagent grade, 97% (Cat. No. 157740) were obtained from Sigma, USA. Calcium chloride ($CaCl_2$), 98% (Cat. No. 13200) was obtained from Molychem, Mumbai, India. Salts of Copper (II) chloride ($CuCl_2.2H_2O$) (Cat. No. 10088) was procured from Sevron Safety Solutions, UK and Zinc chloride ($ZnCl_2$) 97% (Cat. No. 87288) was obtained from SRL labs, India. Arsenazo-III (Cat. No. 11090) salt was obtained from Sigma Aldrich, USA.

2.1.2. Preparation of solutions

Stock solutions of thorium, uranium and lanthanum salts ranging in concentration from 1 to 100 mM were prepared by dissolving them in 0.01 N HNO_3 and stored at room temperature. Ce (IV) stock solution was prepared as described (89,90). Briefly, Ce (IV) salt was dissolved in concentrated sulfuric acid. The acid is then evaporated by heating the solution and the slurry left is dissolved in 0.01 N HNO_3 to obtain the stock solution. Stock solutions of manganese chloride, iron chloride, calcium chloride, copper chloride and zinc chloride salts were prepared in concentrations ranging from 10-50 mM by dissolving them in ddH_2O. All these stock solutions were stored at room temperature. Thorium, uranium, lanthanum, and cerium salt solutions were used for 1 year and solutions for manganese chloride, iron chloride, calcium chloride, copper chloride and zinc chloride were used within 1 month. Arsenazo-III

solution was made by dissolving the arsenazo-III salt in ddH_2O, covered with foil and stored at 4˚C for a week. Fresh arsenazo-III solution was prepared every week before use.

2.2. Techniques/Experiments

2.2.1. UV-Visible spectrophotometry

UV-Visible spectrophotometric studies using wavelengths ranging from 400-700 nm at different concentrations of arsenazo-III (25–100 µM) were conducted using UV-Visible multiwell microplate reader (Tecan infinite M200PRO, Austria). Spectrophotometric studies were also performed to study the absorbance of the complex formed by arsenazo-III with different concentrations (0-100 µM) of different metal ions (thorium, lanthanum, uranium, cerium) in the range of 400-700 nm.

2.2.2. Binding constant and molar extinction coefficient calculation

Binding constant and molar extinction coefficient for thorium-arsenazo complex was calculated using Benesi-Hildebrand equation (91). The binding stoichiometry was calculated using Job's plot by plotting mole fraction of Th ions against their absorbance at 660 nm. The peak of the Job's plot corresponds to the mole fraction of ligand bound to a molecule. The peak was found to be 0.5 or 1/2 which corresponded to the mole fraction of thorium bound to arsenazo and calculated as follows: $\frac{[Th]}{[Th+ASN]} = \frac{1}{2}$. By cross multiplying and solving the equation, the ratio between [Th] and [Asn] was found to be 1:1. Therefore, to calculate binding constant and molar extinction coefficient, Benesi-Hildebrand equation was used which is as follows:

$$\frac{1}{\Delta A} = \frac{1}{K\Delta\in [dye]}\left(\frac{1}{[M]}\right) + \frac{1}{\Delta\in [dye]}$$

where ΔA is change in absorbance of dye i.e., arsenazo at wavelength 660 nm, K is binding constant, Δε is change in molar extinction coefficient at 660 nm, [dye] is concentration of arsenazo used (50 x 10^{-6} M), and [M] is the concentration of thorium. To calculate the binding constant (K), the equation was simplified and slope and intercept for thorium was calculated by plotting 1/[ΔA] vs 1/[M]. The formula 1/ (intercept x [dye]) was obtained by the above equation and was used for the calculation of molar extinction coefficient (Δε) at 660 nm and binding constant (K) was obtained by the formula intercept/slope.

2.2.3. TXRF

Total reflection X-ray fluorescence (TXRF; TX2000, Ital Structures, Italy) using Mo K_α radiation as excitation source (at 40 kV and 30 mA) was used to measure Th in the samples as described previously (92). The sample (10 µL aliquot) was deposited on quartz support and dried under an IR lamp to make a thin film. The X-rays were detected with a Si (Li) detector having a resolution of 139 eV (FWHM) at 5.9 keV (Mn K_α) and data were processed by computer programs TXRFACQ-32 and EDXRF32 (93).

2.2.4. Methods used for thorium estimation

2.2.4.1. Spectrophotometry using arsenazo-III

A: Preparation of standard graph: Known concentrations of thorium samples were prepared by serial dilution. Using a 24-well plate, thorium samples were first added to HCl followed by addition of arsenazo. The solution mixture was made up to 1 ml using HCl and absorbance was measured immediately using a plate reader set at 660 nm. The final concentration of

arsenazo and HCl in reaction mixture was adjusted at 50 µM and 2.3 N, respectively. The readings were obtained in triplicates and the final absorbance was obtained by averaging all three absorbance readings. Thorium concentration was then plotted against absorbance at 660 nm. The graph was linear fitted and correlation coefficient was calculated using Origin 8.0 software. The values for slope and interference were obtained from the linear fit using straight line equation and used to calculate thorium in unknown samples.

B: Estimation of thorium in biological samples: Biological samples were first digested by adding cHNO_3 followed by heating them at 95˚C for 4-5 h. The samples were then concentrated to obtain a clear, transparent solution. To estimate thorium in these samples using arsenazo method, the samples were first converted from their nitrate form to chloride form i.e., from thorium nitrate to thorium chloride by dissolving them in hydrochloric acid. The sample was mixed with 2.9 N HCl and arsenazo solution to make 1 ml of reaction mixture. The amount of arsenazo and HCl added was adjusted in such a way that the final concentration of arsenazo and HCl in reaction mixture was found to 50 µM and 2.33 N, respectively. The absorbance of the reaction mixture was measured immediately at 660 nm and thorium concentration in each sample was calculated using standard graph plotted earlier. A schematic diagram detailing the steps involved in thorium estimation using arsenazo is shown in Scheme 1 in Section 2.2.9.

2.2.4.2. ICP-MS

A. Preparation of standard graph: Known concentration of thorium standards were prepared by serial dilution and their counts per second (CPS) were measured by ICP-MS.

B: Estimation of thorium in biological samples: Biological samples digested and concentrated using cHNO_3 were diluted to a final concentration of 2% nitric acid and subjected

to thorium estimation by ICP-MS. The cps obtained were then converted to concentration using the standards used earlier.

2.2.5. Cell lines and cell culture

Human liver carcinoma (HepG2) and human normal liver (WRL 68) cell lines were obtained from National Centre for Cell Sciences (NCCS), Pune, India. The cells were cultured in Dulbecco's Modified Eagle's Medium (DMEM; GIBCO, Invitrogen, CA, USA) supplemented with 10% fetal calf serum (FCS; Himedia Laboratories, Mumbai, India) and antibiotics (100 U/ml penicillin and 100 µg/ml streptomycin) in a humidified incubator maintained at 37˚C supplied with 5% CO_2.

2.2.6. Cellular localization studies of thorium using arsenazo

3 x 10^4 HepG2 and WRL 68 cells were seeded onto sterile coverslips and incubated overnight under culture conditions. The cells were then washed with serum-free medium (SFM) and incubated with 10 and 50 µM thorium in serum-free medium for 1 h at 37˚C. The coverslips were then rinsed with 0.1 N HCl and incubated with 50 µM arsenazo for 5 min followed by washing to remove excess arsenazo dye. They coverslips were then mounted onto glass slides using mounting medium and observed under bright field microscope using 40 X objective lens (Eclipse-Ti, Nikon, Japan).

2.2.7. Bright field microscopy for morphological changes

1 x 10^6 cells were seeded onto sterile 60 mm dishes and incubated overnight under cell culture conditions. The cells were washed with SFM and incubated with SFM containing 10 and 50 µM thorium for 6 h. Cellular images were obtained using bright field microscope at 20

and 40 X and observed for morphological alterations caused by thorium treatment to cells as compared to control.

2.2.8. Viability assay

Thorium toxicity to cells at different time points was determined using trypan-blue assay. A solution of 0.4% trypan-blue dye was prepared by dissolving it in phosphate buffered saline (PBS), pH 7.2. 0.5, 1 and 2 million cells were seeded onto 60 mm plates and incubated overnight. Cells were washed with SFM and treated with different concentrations of thorium and incubated for 1, 6, 24 and 48 h time points. Cells were harvested at different time points. 1 part of suitably diluted cell suspension was mixed with 1 part of 0.4% trypan blue dye and incubated for ~3 minutes. 10 µl of this suspension was taken on hemocytometer and transparent (live) and blue stained (dead) cells were counted under bright field microscope. Percent viability was then calculated and plotted against different time points to determine the time at which incubated thorium is least toxic to cells for *in-vitro* studies.

2.2.9. Thorium uptake study

1 x 10^6 WRL 68 cells were seeded onto sterile 60 mm plates and incubated overnight. The cells were washed with serum free medium (SFM) followed by treatment with thorium containing SFM and incubating them for 6 and 24 h. The cells were then trypsinized using trypsin-EDTA and different fractions of cell culture i.e., medium, trypsin-EDTA and cells were harvested in different sterile tubes. Thorium was estimated in medium and trypsin-EDTA fraction without any further processing using arsenazo method. In case of cells, the organic matter of cells was digested by dissolving them in conc. HNO_3 and heating them at ~90°C for 5-6 h until a clear, transparent solution was obtained. The total volume in cellular fraction was

maintained at 100 µl before estimating thorium by arsenazo method. A schematic for thorium estimation in different fractions of cell culture is given below in Scheme 1.

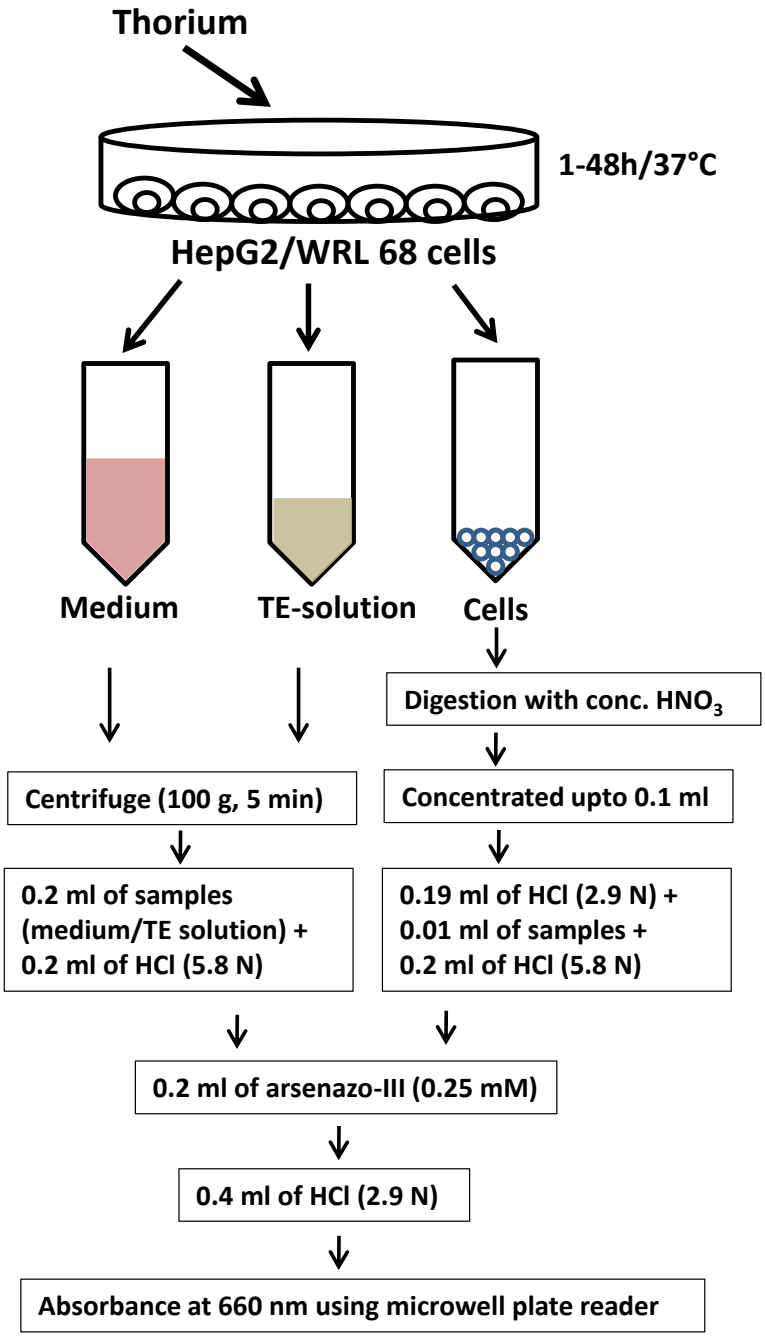

Scheme 1: *Schematic representation of the protocol developed for estimation of thorium in human cells (HepG2 and WRL 68 cells) using arsenazo dye.*

2.2.10. Thorium uptake studies at different treatment conditions

The mechanism of cellular uptake of was studied under different conditions such as presence and absence of transferrin in the medium, at different temperature and in the presence of various ion channel inhibitors. The protocol used for these studies are described as following:

2.2.10.1. In presence and absence of transferrin

1 x 10^6 cells were seeded into sterile 60 mm dishes and incubated overnight. The cells were then washed with SFM followed by addition of SFM with/without 2 mg/ml transferrin. Human serum transferrin salt was obtained from Sigma, USA (Cat. No. T8158) and stock solution was prepared by dissolving the salt in DMEM. The cells were incubated with/without transferrin for 2 h before washing them with SFM and adding SFM containing 10 µM thorium to the cells. The cells were then incubated again for 6 h followed by harvesting by trypsinization. Cells were collected in centrifuge tubes. These cells digested and thorium was estimated using the protocol as described in thorium uptake studies (Section 2.2.9).

2.2.10.2. At different incubation temperature

Thorium uptake was also studied at different incubation temperatures in order to determine the role of receptor and non-receptor mediated uptake of thorium by cells. For this, 1 x 10^6 cells were seeded into sterile 60 mm plates and incubated overnight. Out of two sets of cultures, one set of cells were washed with SFM at 4˚C and another set of cells were washed with SFM at 37˚C. In these cultures, thorium was added (thorium solution prepared in SFM and maintained these respective temperature) such that the final concentration of thorium is 10 µM. These cultures were incubated for 6 h at 4 and 37˚C under sterile culture conditions. Cells

were trypsinized, digested and thorium was estimated in cells fraction using the arsenazo method as mentioned in Section 2.2.9.

2.2.10.3. Thorium uptake in the presence of different inhibitors

Different ion channels inhibitors [such as nifedipine (voltage gated calcium ion channel inhibitor), mercury (II) chloride (aquaporin inhibitor), tetra ethyl ammonium (potassium channel inhibitor), verapamil (calcium ion channel inhibitor), thapsigargin (endoplasmic reticulum calcium ion mobilizer), bipyridyl hydrochloride (voltage independent calcium ion channel inhibitor), SN-6 (sodium-calcium ion exchanger inhibitor) and BTP-2 (calcium release-activated channel inhibitor)] purchased from Sigma, USA were used for the study. For this study, 1 x 10^6 cells were seeded into sterile 60 mm dishes and incubated overnight. The cells were washed with SFM and incubated for 2 h with 10 µM of different inhibitors (stock prepared in SFM). Following 2 h incubation, the inhibitor was removed, and cells were gently washed once with SFM and incubated with 10 µM thorium for 6 h. After incubation, cells were trypsinized, digested and thorium was estimated in cells fraction using ICP-MS method as mentioned in Section 2.2.4.2.

2.2.11. Determination of thorium in different sub-cellular protein fractions

In addition to studying the intracellular targets of thorium by determining thorium bound to different sub-cellular fractions, thorium bound to different sub-cellular protein fractions of human liver cell was also studied. For this, sub-cellular protein fractions were obtained using sub-cellular protein fractionation kit (Thermo Scientific Pierce MA, USA) and estimating the amount of thorium bound to each protein fraction. The protocol provided with the kit was followed to obtain proteins from different sub-cellular organelles. Briefly, 1 x 10^6 cells were seeded into sterile 60 mm dishes and incubated overnight. The cells were washed

with SFM and treated with SFM containing 10 µM thorium. The corresponding control set was treated with vehicle control i.e., 0.01 N HNO_3. The cells with thorium containing SFM were incubated under culture conditions for 24 h following which the cells were harvested by trypsinization. Cells from three different plates were pooled together to obtain a single sample tube. 3 such different samples were processed separately to obtain same set of samples in triplicates. Ice-cold cytoplasmic extraction buffer (CEB) containing protease inhibitor was added to the cell pellet and incubated at 4˚C for 10 minutes with gentle mixing. CEB selectively permeabilizes the cell membrane causing release of soluble cytoplasmic contents which is present in the form of supernatant when the CEB cell suspension is subjected to centrifugation at 500 x g for 5 minutes at 4˚C. This soluble cytoplasmic protein content is then transferred into new, sterile, and pre-chilled centrifuge tubes and pellet is subjected to ice-cold membrane extraction buffer (MEB) containing protease inhibitor. The suspension is then vortexed at highest setting for 5 s for pellet dissolution and incubated for 10 minutes at 4˚C with gentle mixing. MEB solubilizes plasma, ER/Golgi bodies and mitochondrial membrane and their protein content is then separated in the supernatant upon centrifugation. The buffer does not solubilize nuclear membrane and thus, intact nuclei are obtained in the pellet. After incubation of 10 minutes, the MEB containing cell suspension is centrifuged at 3000 x g for 5 minutes. The membrane protein containing fraction is separated in a clean, pre-chilled tube as the supernatant and the pellet is processed further for nuclear proteins. Chromatin-extraction buffer was then prepared by adding 5 µl of 100 mM $CaCl_2$ and 3 µl of micrococcal nuclease per 100 µl of nuclear extraction buffer (NEB) maintained at room temperature. This freshly prepared chromatin-extraction buffer was then added to the pellet and vortexed at highest setting for 15 s for pellet dissolution. The buffer suspension was then incubated in water bath at 37˚C for 5 minutes. After incubation, the suspension was again vortexed at the highest

setting for 15 s followed by centrifugation at 16000 x g for 5 minutes. The chromatin-bound protein fraction was separated out in the supernatant which was collected in a fresh, clean, and pre-chilled tube. The pellet was dissolved in protease inhibitor containing pellet extraction buffer (PEB) maintained at room temperature and vortexed on highest setting for 15 s followed by incubation at room temperature for 10 minutes. The PEB suspension was then centrifuged at 16000 x g for 5 minutes. The supernatant containing the cytoskeletal protein extract was transferred into a new, clean, pre-chilled tube. All these protein fractions are immediately stored at -80˚C for downstream processing and analysis. A diagrammatic representation of all the steps involved in separation of each fraction is shown in detail in Scheme 2.

To estimate thorium bound to different protein extracts, conc. HNO_3 was added to each fraction and heated at 90˚C till a clear, transparent solution is obtained. The volume in each fraction was carefully recorded and thorium was estimated using ICP-MS as mentioned in Section 2.2.4.2.

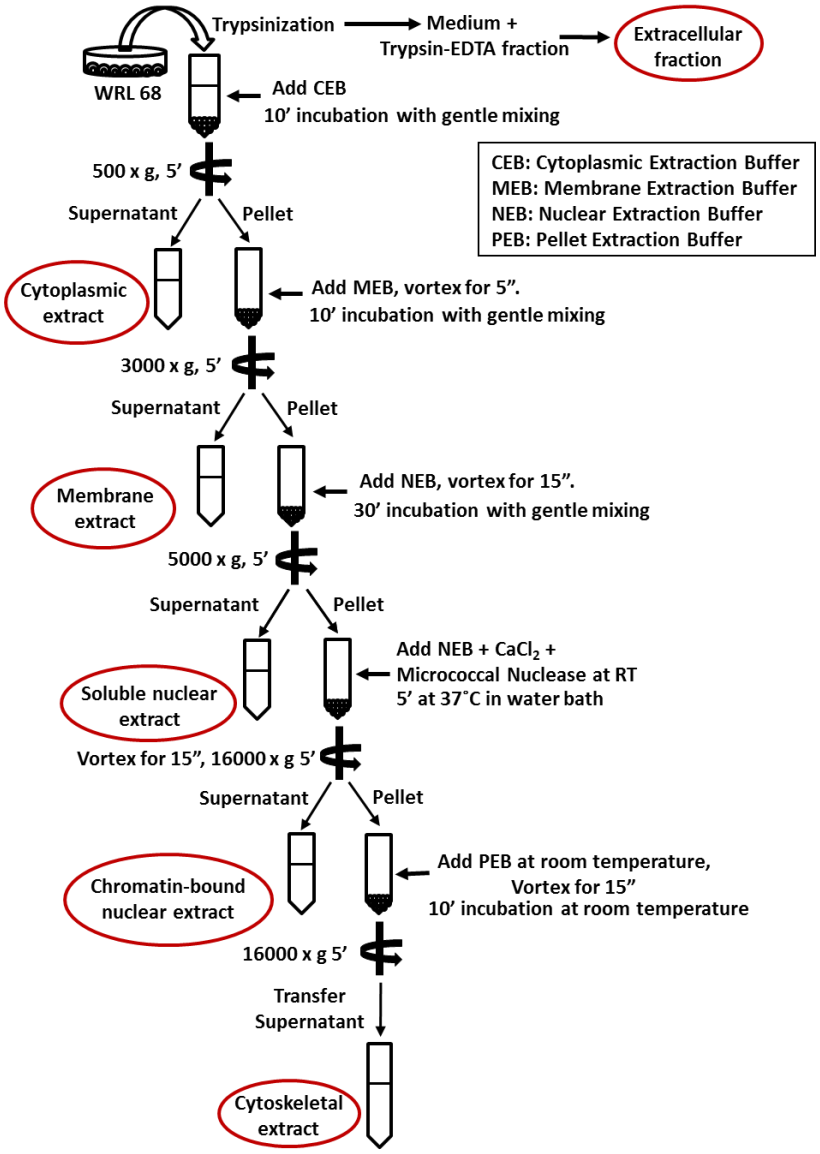

Scheme 2: *Stepwise diagrammatic representation of the method followed for the separation of various sub-cellular protein fractions using sub-cellular protein fractionation kit. All steps were performed at 4˚C unless mentioned otherwise. Protease inhibitor was added to all buffers just before the experiment.*

2.2.12. Transmission Electron microscopy

a. **For *in-vitro* samples:** 5 x 10^6 WRL 68 cells were seeded onto 100 mm sterile Petri dishes and incubated overnight for attachment. The cells were washed with SFM and

incubated with 10 µM thorium for 24 h. After 24 h, cells were trypsinized and harvested in suspension form. The cells were washed three times to remove any dead cells, cellular debris and precipitates. The culture medium is then replaced by glutaraldehyde fixative. The cells were immersed completely in glutaraldehyde for at least 1 h followed by multiple washes in cacodylate buffer (pH 7.4). The cells were stored in cacodylate buffer at 4˚C and processed further for TEM. TEM studies were performed at ACTREC, Navi Mumbai.

b. **For *in-vivo* samples:** Structural alterations in liver caused by highest dose of thorium i.e., 20 mg/kg for one year were studied using transmission electron microscopy. The liver sample obtained by sacrificing mice after one year of thorium treatment were preserved in 10% formalin. The samples were then cut into small pieces and primary fixing was carried out by keeping the sample in 2.5% glutaraldehyde in 0.1 M sodium phosphate buffer (pH 7.4) at 4˚C for 2-3 h. Post primary fixation, the sample was washed thoroughly in 0.1 M phosphate buffer to remove excess of primary fixative and secondary fixation was carried out by using 1% osmium tetroxide and washed thoroughly once again and processed for TEM at AIIMS, New Delhi.

2.2.13. Thorium uptake in presence of fetal calf serum (FCS)

To study the carcinogenic changes, a long-term exposure of thorium (about 15 passages of cells) with intermittent alpha exposure is required. Before starting this experiment, a few optimization experiments were performed.

2.2.13.1. Optimization of FCS percentage for cell growth: For thorium uptake and other related studies, serum free medium was used. However, for long term treatment of thorium, cells are required to be cultured in the presence of serum. To standardize serum percentage for optimum cell growth, cells were grown using different concentrations of serum and cellular

viability was estimated using two different approaches a) MTT assay and b) Cell counting as described below:

a. ***MTT assay:*** 10,000 cells were seeded into each well of 96-well plate and incubated overnight for attachment in serum-containing media. The cells were washed with SFM, replaced media containing different percentage of serum i.e. 0, 2, 4, 6, 8 and 10% and incubated for 72 h. The media with thorium was removed, replaced by 0.5 mg/ml MTT containing medium and incubated for 3 h. The MTT containing medium was removed and the blue colored formazan cellular crystals formed by MTT were dissolved using 100 µl of dimethyl sulfoxide (DMSO) to each well. Absorbance was measured at 550 nm using multiwell plate reader (Tecan infinite 200 Pro, Germany).

b. ***Cell counting:*** 2 x 10^6 cells were seeded into 60 mm sterile dishes and incubated overnight with serum containing medium for attachment. The dishes were washed with SFM and media containing different concentrations of serum i.e., 0, 2, 4, 6, 8 and 10% were added into the plates and cells were incubated under sterile culture conditions for 72 h. Following incubation, cells were harvested and counted using hemocytometer under bright field microscope with appropriate dilutions of cell suspension.

2.2.13.2. Thorium uptake at different FCS concentration*:* 2 x 10^6 WRL 68 cells were seeded into sterile 60 mm dishes and incubated overnight for attachment. The cells were washed with SFM and incubated with media containing 0, 6 and 10% concentrations of serum for 2 h. After 2 h, 10 µM thorium was added and incubated for 6 h under sterile culture conditions. The cells were harvested, and their organic content was digested using cHNO_3

followed by heating at 90˚C for 4-5 h. Thorium was estimated in each fraction of all groups using arsenazo method.

After these experiments, WRL 68 cells were treated with thorium and alpha + thorium for 15 passages to simulate the conditions of real-life thorium exposure and hence, to study the changes caused by thorium internalization under actual life conditions over a longer period. The rationale for the experiment is described in detail in Section 3.2.3 in Chapter 3 - Results and discussion.

2.2.14. Alpha irradiation of WRL 68 cells

The alpha-particle irradiation was carried out with alpha irradiator (BARC-BioAlpha) designed and developed at Bhabha Atomic Research Centre ,Mumbai with ^{241}Am source (energy 5.48 MeV) for *in vitro* radio-biological experiemnts (94,95). Dosimetry was carried out by CR-39 track dosimetry (94,95). The flux of the source and dose rate was found to be 2000/cm^2/s and 1.36 cGy/min, respectively. The energy of alpha particles irradiating the cells was ~4.0 MeV. For α-irradiation, WRL 68 cells (1×10^6) were cultured overnight at 37ºC in specially designed irradiation dish (Figure 2.1 B) bottomed with 2.5 µm thick mylar membrane (Goodfellow, UK), which was pre-coated with fibronectin (95). The upper part of the irradiation dish has removable screwcap while the bottom part of the dish is fitted with a holder with 'O' rings to hold mylar membranes onto which cells were grown. For fibronectin coating of dishes, the irradiation dish was layered with fibronectin solution [(Sigma, stock: 0.1 mg/ml), diluted in culture medium (1:10 in DMEM supplemented with FCS and antibiotics)] and, incubated at 37°C (5% CO_2 in a humidified incubator for 1 h) followed by removal of fibronectin solution and washing the dish with PBS.

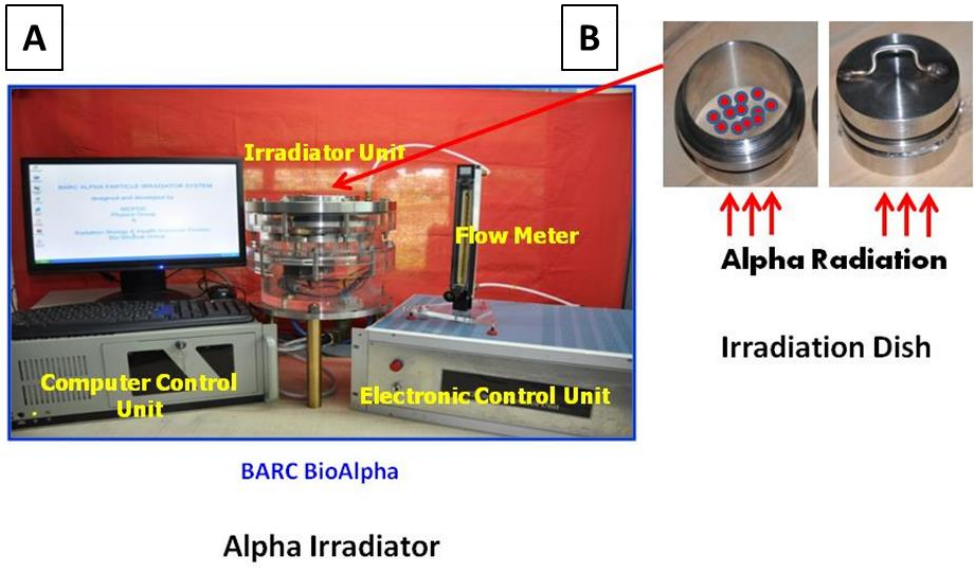

***Figure 2.1 A**: Schematic outline of different components of BARC BioAlpha. **B**. Irradiation dish. (**Source:** Babu et. al., Dosimetry and radiobiological studies of automated alpha-particle irradiator. J Environ Pathol Toxicol Oncol. 2013;32(3):263–73.)*

2.2.15 Dose optimization of alpha particle irradiation using surviving fraction

To obtain the optimum dose for alpha particle irradiation, the alpha particle dosage was first optimized on WRL 68 cells using surviving fraction. For this, protocol provided by Franken et. al., were followed (96). Briefly, 1 x 10^6 million WRL 68 cells were seeded onto sterile and fibronectin-coated mylar membrane in specially designed alpha irradiation dishes as shown in Figure 2.1 B above. The cells were incubated overnight and following attachment to mylar membrane were irradiated with different doses of alpha particles using alpha-particle irradiator. Post irradiation, cells were harvested, counted and 100 cells were plated onto 60 mm sterile dishes and allowed to form colonies under sterile cell culture conditions. After colony formation, the medium was discarded, and cells were washed with PBS followed by addition of a mixture of 6.0% glutaraldehyde and 0.5% crystal violet. The cells were stained in this

solution for 30 minutes. The plates were then rinsed under tap water carefully so as not to detach the colonies. The plates were then allowed to air dry at room temperature and colonies were counted using a dissection microscope. Plating efficiency (PE) and surviving fraction (SF) was then calculated using the formulas given below:

$$Plating\ Efficiency\ (PE) = \frac{No.of\ colonies\ formed}{No.of\ cells\ seeded} \times 100\%$$

$$Surviving\ Fraction\ (SF) = \frac{No.of\ colonies\ formed\ after\ treatment}{No.of\ cells\ seeded\ \times PE}$$

Surviving fraction at different doses was then plotted against alpha radiation dose in Gy in a semi-logarithmic graph and the optimum dose of alpha particle was then decided. 0.1 Gy of alpha particle dose was found to be suitable for the long-term studies of effect of thorium in combination with alpha particle radiation experiment as described in Section 3.2.3.3.part A in chapter 3.

2.2.16. Protocol for long term studies of effect of thorium in combination of alpha radiation on WRL 68 cells

Following groups were used to study long-term effects of thorium under *in-vitro* conditions.

1. Control: WRL 68 cells grown under normal culture condition in 10% serum containing medium (SCM).

2. Thorium: WRL 68 cells grown in presence of 10 µM thorium continuously in 10% SCM.

3. Alpha irradiation: WRL 68 cells grown under standard growth condition and irradiated with alpha particles at passage 5, 10 and 15

4. Thorium + Alpha-particle irradiation: WRL 68 cells grown continuously in presence of 10 µM thorium in 10% SCM and irradiated with alpha particles at passage 5, 10 and 15.

For this experiment, unless specified, 1 x 10^6 WRL 68 cells were cultured in 10% SCM under sterile culture conditions in P-60 Petri dishes. The cells were passaged every alternate day. For group 2 and 4, cells were continuously cultured with 10 µM thorium added in the medium. For group 1 and 3, cells were cultured in the medium without thorium. At passage numbers 5 (early), 10 and 15 (late), cells in group 3 and 4 were irradiated with alpha particles for 10 min (0.1 Gy) using alpha particle irradiator as mentioned in Section 2.2.14. One day before alpha irradiation, cells from all groups were trypsinized and seeded (1 x 10^6 cells) in alpha-particle irradiation dishes (3 dishes for each groups) coated with fibronectin as mentioned in Section 2.2.14. For groups 2 and 4, thorium containing medium was added, however, in groups 1 and 3 media without thorium was used. After irradiation, the cells were trypsinized and seeded on a 60 mm sterile dish and cultured under sterile culture conditions for rest of the passages. One set of cells were collected after each irradiation (passage 5 and 15) and stored at -80˚C for further studies of gene alterations using PCR array. Cell were also studied for any morphological alterations at passage 5, 10 and 15 using 20 X and 40 X of objective lens using bright field microscope. A pictorial scheme detailing all these steps is shown below in Scheme 3.

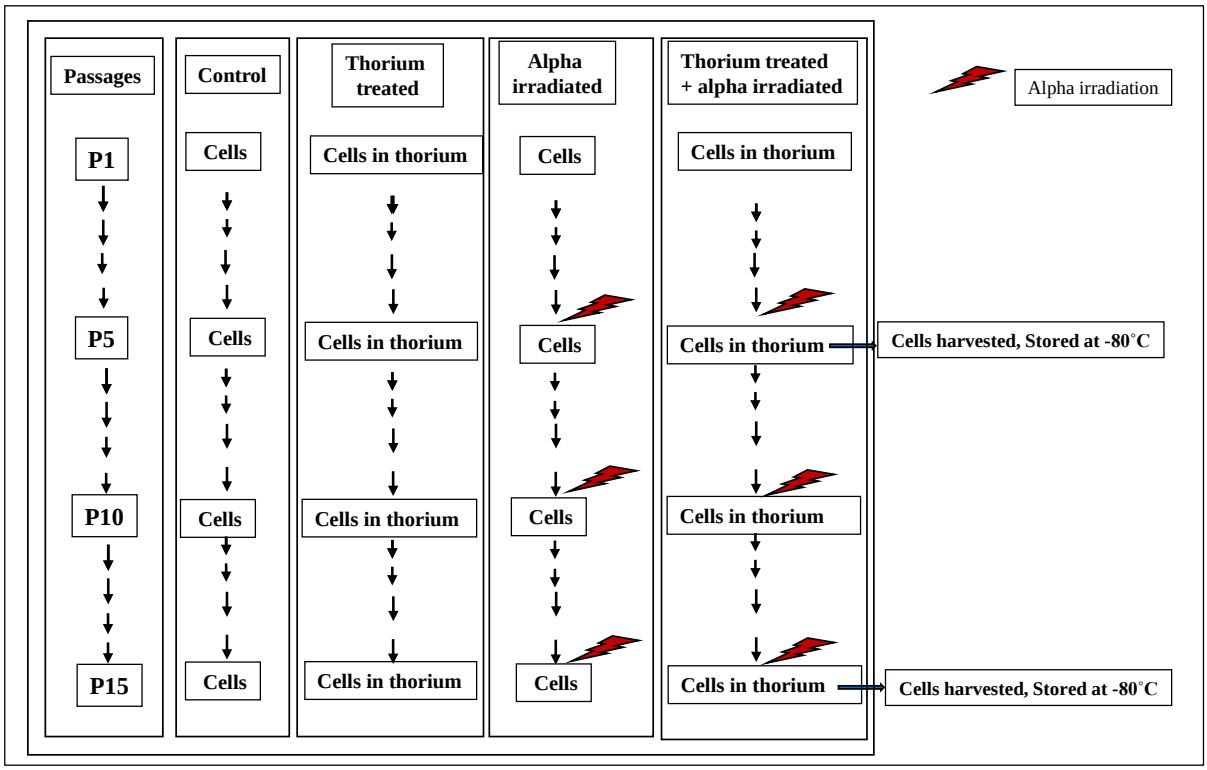

Scheme 3*: Details of steps followed for thorium and alpha particle irradiation of WRL 68 for long-term study of effects of thorium on WRL 68 cells.*

2.2.17. Thorium bio-distribution

Thorium bio-distribution under in vivo conditions were studied using Swiss albino male mice. 4-6 weeks old mice weighing around 20-25 g were injected with different concentrations of thorium for different time intervals. All animal experiments were performed after approval of Institutional Ethical Committee and adhering its guidelines. The mice were kept at hygienic conditions in mice cages in a group of five where cage, feeding bottle and bedding material were changed weekly once. Proper day and night cycle were maintained using light and dark cycle of 12 h each and temperature was maintained at 22 ± 4˚C. Food and water were given *ad libitum*.

For short term thorium bio-distribution studies, mice were divided into three groups based on the dose of thorium injected intravenously and are described as follows:

Group I: Control

Group II: 4 mg/Kg of thorium

Group III: 40 mg/Kg of thorium

For long-term bio-distribution studies, mice were divided into four different groups based on thorium dosage injected intravenously. The groups were as follows:

Group I: Control

Group II: 4 mg/Kg

Group III: 10 mg/Kg

Group IV: 20 mg/Kg

The stock solution of different concentration of thorium nitrate was prepared in 0.01 N HNO_3 such that the desired concentration was present in 100 µl of the solution. 100 µl of solution from each dosage was injected to mice once intravenously. The mice were monitored closely for any phenotypic alterations and the same were carefully recorded. For short-term studies, mice were sacrificed after one month and organs such as liver, spleen and femur bone were obtained. For long-term studies, organs such as liver, spleen, femur bone, kidney, lungs, brain, and blood were obtained. These organs were acid digested using cHNO_3 in tissue digestor (model, make and country) and concentrated to make volume up to 1 ml. This was then diluted to HNO_3 concentration up to 2% and thorium was estimated in each organ using ICP-MS.

A scheme of all experiments planned for long duration (6 and 12 months) is shown below in detail in Scheme 4.

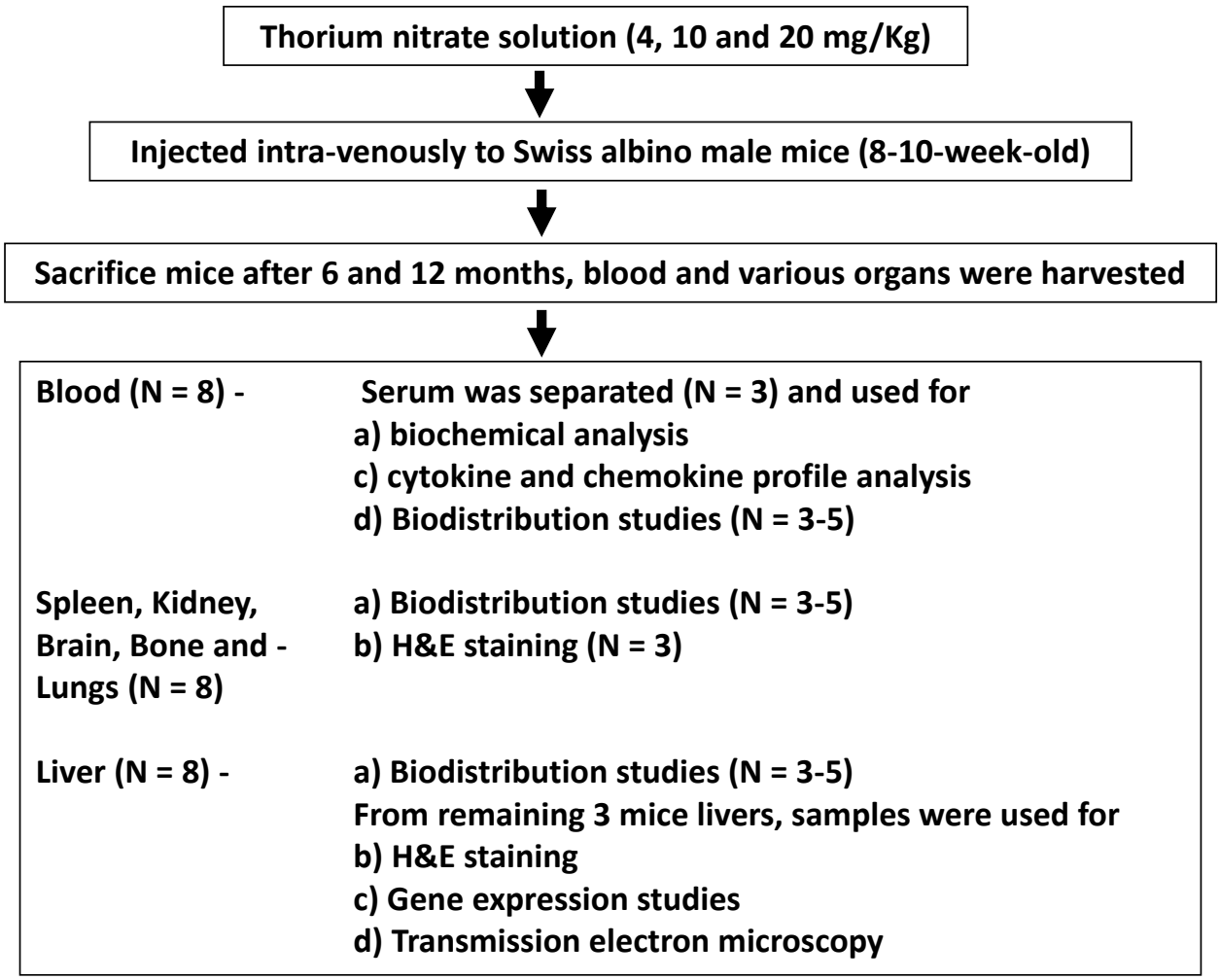

Scheme 4: *Various sets of experiments planned for treatment of Swiss albino male mice with different doses of thorium for long duration (6 and 12 months).*

2.2.18. Synchrotron imaging

Mice liver, spleen and femur bone obtained after one month of thorium treatment were subject to X-ray synchrotron imaging to study the anatomical alterations caused by thorium in these organs using different images and three-dimensional image modelling. The changes in the parameters were also calculated using appropriate software. The experiments were carried

out at Imaging Beamline (BL-4), Indus-2, Synchrotron Radiation (SR) source, Raja Ramanna Centre for Advanced Technology, Indore, India (97). The bending magnet beamline is operated in white as well as monochromatic beam modes. Si (111) type double crystal monochromator is used to choose suitable energy in the range of 8-35 keV. Shape and size of the beam is tuned using slit system installed after the monochromator. The experimental setup for Phase contrast X-ray micro-computed tomography consists of motorized precision translation x, y and z stages, rotation stage and imaging camera (98–100). The sample holder has centrally fitted chuck for holding the samples. The imaging detector is a high-resolution CCD camera with an active area of 4 k ×2.6 k pixels (each pixel is of 4.5 μm) with Gadox scintillators at its input face coupled to the CCD via fibre-optic taper of 2:1 magnification. The effective smallest pixel size thus offered by this camera is 2.25 μm. Figure 2.2 shows the experimental arrangement at imaging beamline used for 3D SR-μCT imaging of liver samples of mice treated with thorium.

Figure 2.2. *Experimental set up of SR-μCT at Indus-2. Dotted circle shows the chuck where samples are placed in the set up. Inset: vial with Kapton window where samples were placed*

for imaging. Position of vial is aligned in such a way that Kapton window (positioned with tissue imaging region) falls in the X-ray path. ***Source:*** *Yadav R, et al. Thorium-induced Anatomical and Histopathological Changes in Liver of Swiss Mice. Toxicol Environ Health Sci. 2018;10(2):97–106.*

Formalin fixed liver tissue samples of mice were used for acquisition of experimental images in SR- μCT system. The samples were placed in specially designed X-ray transparent screw capped holders. The sample holder consists of an airtight polymer vial with a Kapton window (inset, Figure 2.3). This design ensures maximum X-ray interaction/transmission and minimizes dehydration of tissue samples during the tomography experiments. The dehydration of sample during experiments may cause shrinkage of tissue, which may result in motion artefacts in the tomographic slices. SR-μCT imaging experiments of liver samples were performed by acquiring 900 projections while rotating it in 0-180° angular range with step size of 0.2°. Each projection images of liver samples were acquired at 12 keV beam energy and 0.8 s for data collection. The projection images for all the samples were pre-processed using flat field correction and normalization to remove artefacts due to beam nonuniformity and background noise. Corrected images were used to make sonogram. Cross sectional slice images of the sample were then reconstructed using filtered back projection algorithm of tomographic reconstruction for parallel beam (101). These slice images show local distribution of density and structures in the sample. In order to visualize the overall 3D variations caused by thorium deposition in the micro-structure and density of the samples, these reconstructed slice images were stacked together in the open source software Drishti (102). Quantitative 3D analysis methods based on feature segmentation and morphological operation were employed to measure these structural variations (103).

2.2.19. H & E staining

Liver, spleen, and bone samples treated with thorium and preserved in 10% formalin were stained with hematoxylin and eosin stain. The stained slides were observed under bright field microscope under different objective lens magnification.

2.2.20. Immunohistochemistry

Thin section of liver tissue mounted on glass slide were subjected to immunohistochemistry of angiogenesis and blood vasculature antigen, CD 31. The protocol was followed in three different steps viz., deparaffinization, antigen-retrieval and immunohistochemical staining (104).

a. Deparaffinization

The slides containing tissue sections were placed in slide racks and submerged in fresh xylene solution thrice for 5 minutes each followed by incubation with 100%, 95%, 70% and 50% ethanol for 10 minutes each. The sections were then washed twice in PBS for 5 minutes.

b. Antigen-retrieval

Antigen-retrieval is performed by heating method to unmask the antigen before staining. The rehydrated slides were submerged in a heating vessel containing 0.5 M Tris buffer solution, pH 10 and brought to boil. Thereafter, the buffer is maintained at sub-boiling temperature for 15 minutes. The slides were allowed to cool at room temperature on bench top for 2-5 minutes.

c. Immunohistochemical staining

The slides were washed in PBS followed by washing in wash buffer i.e., 1X TBST for 5 minutes. The sections were then blocked by using 5% goat serum for 1 h at room temperature.

The section was then stained with anti CD31 (mouse, CST) antibody diluted 1:50 times using normal goat serum and incubated overnight at 4˚C. The antibody solution was then removed, and sections were washed using wash buffer 3 times for 5 minutes each. The sections were then stained with secondary antibody conjugated with AlexaFluor 488 (mouse anti-Rabbit IgG, Invitrogen) diluted up to 1:50 times using normal goat serum and incubated for 30 minutes at room temperature. The secondary antibody was then removed, and sections were washed in wash buffer 3 times for 5 minutes each. Antifade DAPI was placed onto the sections and coverslips were mounted onto them and images were acquired using fluorescence microscope (Eclipse Ti, Nikon).

2.2.21. Periodic Acid-Schiff staining

Periodic Acid-Schiff (PAS) staining was performed to determine the glycogen content in tissues. To perform PAS staining, the liver tissues sample, both control and thorium treated ones obtained after one month, were first mounted on slides in the form of thin sections embedded in paraffin. The paraffin was first dissolved by incubating the sections in xylene solution 3 times for 5 minutes each. The section was then rehydrated by incubating them with decreasing gradient of ethanol i.e., 100%, 95%, 70%, 50% and then 30% followed by washings in PBS. The sections were then oxidized in 0.5% periodic acid solution for 5 minutes followed by rinsing with distill water. The sections were then placed in Schiff reagent for 15 minutes. The excess of the stain was removed, and color was developed by washing the sections in lukewarm water for 5 minutes. The section was incubated with Mayer's hematoxylin for 1 minute for counter-staining followed by washing in distill water for 5 minutes to remove off excess stain. The section was finally dehydrated by incubating them with increasing ethanol

gradient and sealed with coverslip using mounting medium. The sections were then observed using bright field microscope (Eclipse Ti, Nikon).

2.2.22. Biochemical studies of serum samples

Serum samples obtained from mice treated with thorium after 1, 6 and 12 months were subjected to biochemical analysis to determine the level of various metabolites and analytes after thorium treatment. Levels of serum metabolites such as creatinine, urea, cholesterol, glucose, total protein, total bilirubin were determined using automated serum biochemical analyzer (Randox, Kearneysville, WV, USA).

2.2.23. Cytokine and chemokine array profiling

Serum samples from mice treated with thorium 4, 10 and 20 mg/kg for one year were subjected to cytokine and chemokine profile using a commercially available multiplex bead-based cytokine array kit (MILLIPLEX MAP Human cytokine/chemokine Magnetic Bead Panel-Immunology Multiplex Assay, Merck Millipore, MA, USA). A total of 32 cytokines and 13 chemokines were tested using the array. The cytokines and chemokines tested were as follows: G-CSF, Eotaxin, GM-CSF, IFN-Gamma, IL-1alpha, IL-1beta, IL-2, IL-4, IL-3, IL-5, IL-6, IL-7, IL-9, IL-10, IL-12p40, IL-12p70, LIF, IL-13, LIX, IL-15, IL-17, IP-10, KC, MCP-1, MIP-1alpha, MIP-1beta, MCSF, MIP-2, MIG, RANTES, VEGF, TNF-alpha, Scd30, SGP130, sIL-1R1, sIL-1RII, sIL-2Ralpha, sIL-4R, sIL-6R, sRAGE, sTNFR1, sTNFRII, sVEGFR1, sVEGFR2, sVEGFR3. The protocol followed was as described in the kit provided. Briefly, 25 µl of serum sample was added to 96-well plate followed by addition of 25 µl of beads in each well. The plate was incubated at room temperature for 2 h with constant shaking. The contents of the well were removed and washed with 2X wash buffer before adding 25 µl

of detection antibody in each well and incubated for 1 h at room temperature. 25 µl of streptavidin-phycoerythrin was then added to each well and incubated for 30 minutes at room temperature. The contents were then removed and washed with 2X wash buffer twice. The beads were resuspended in 150 µl sheath fluid for 5 minutes in plate shaker and the plate was read on Luminex® 200™ platform.

2.2.24. PCR array for genetic alteration

To study alterations in gene expression upon thorium exposure at longer durations, PCR array was performed using RT^2 PCR array (Catalogue No. 330231, GeneGlobe ID: PAHS-133Z (human panel) and PAMM-133Z (mice panel), Qiagen, Hilden, Germany) for hepatocarcinogenesis. In this array, 84 genes, enlisted in Table 2.1, which are already known to play a role in hepatocarcinogenesis were used as pre-fixed primers and amplified of its corresponding cDNA during PCR. For this, RNA was isolated from cells/tissues and converted to cDNA followed by real time PCR and data analysis.

The genes which were studied are given the in Table below. Table A shows the list of genes studied using WRL 68 cells (human studies) and Table B lists the genes studied using mice (murine studies).

A: List of human genes

Symbol	Description
ADAM17	*ADAM metallopeptidase domain 17*
AKT1	*V-akt murine thymoma viral oncogene homolog 1*
ANGPT2	*Angiopoietin 2*
BAX	*BCL2-associated X protein*
BCL2	*B-cell CLL/lymphoma 2*
BCL2L1	*BCL2-like 1*
BID	*BH3 interacting domain death agonist*
BIRC2	*Baculoviral IAP repeat containing 2*
BIRC5	*Baculoviral IAP repeat containing 5*
CASP8	*Caspase 8, apoptosis-related cysteine peptidase*
CCL5	*Chemokine (C-C motif) ligand 5*

CCND1	*Cyclin D1*
CCND2	*Cyclin D2*
CDH1	*Cadherin 1, type 1, E-cadherin (epithelial)*
CDH13	*Cadherin 13, H-cadherin (heart)*
CDKN1A	*Cyclin-dependent kinase inhibitor 1A (p21, Cip1)*
CDKN1B	*Cyclin-dependent kinase inhibitor 1B (p27, Kip1)*
CDKN2A	*Cyclin-dependent kinase inhibitor 2A (melanoma, p16, inhibits CDK4)*
CFLAR	*CASP8 and FADD-like apoptosis regulator*
CTNNB1	*Catenin (cadherin-associated protein), beta 1, 88kDa*
CXCR4	*Chemokine (C-X-C motif) receptor 4*
DAB2IP	*DAB2 interacting protein*
DLC1	*Deleted in liver cancer 1*
E2F1	*E2F transcription factor 1*
EGF	*Epidermal growth factor*

EGFR	*Epidermal growth factor receptor*
EP300	*E1A binding protein p300*
FADD	*Fas (TNFRSF6)-associated via death domain*
FAS	*Fas (TNF receptor superfamily, member 6)*
FHIT	*Fragile histidine triad gene*
FLT1	*Fms-related tyrosine kinase 1 (vascular endothelial growth factor/vascular permeability factor receptor)*
FZD7	*Frizzled family receptor 7*
GADD45B	*Growth arrest and DNA-damage-inducible, beta*
GSTP1	*Glutathione S-transferase pi 1*
HGF	*Hepatocyte growth factor (hepapoietin A; scatter factor)*
HHIP	*Hedgehog interacting protein*
HRAS	*V-Ha-ras Harvey rat sarcoma viral oncogene homolog*
IGF2	*Insulin-like growth factor 2 (somatomedin A)*

IGFBP1	*Insulin-like growth factor binding protein 1*
IGFBP3	*Insulin-like growth factor binding protein 3*
IRS1	*Insulin receptor substrate 1*
ITGB1	*Integrin, beta 1 (fibronectin receptor, beta polypeptide, antigen CD29 includes MDF2, MSK12)*
KDR	*Kinase insert domain receptor (a type III receptor tyrosine kinase)*
LEF1	*Lymphoid enhancer-binding factor 1*
MCL1	*Myeloid cell leukemia sequence 1 (BCL2-related)*
MET	*Met proto-oncogene (hepatocyte growth factor receptor)*
MSH2	*MutS homolog 2, colon cancer, nonpolyposis type 1 (E. coli)*
MSH3	*MutS homolog 3 (E. coli)*
MTDH	*Metadherin*
MYC	*V-myc myelocytomatosis viral oncogene homolog (avian)*
NFKB1	*Nuclear factor of kappa light polypeptide gene enhancer in B-cells 1*

NRAS	*Neuroblastoma RAS viral (v-ras) oncogene homolog*
OPCML	*Opioid binding protein/cell adhesion molecule-like*
PDGFRA	*Platelet-derived growth factor receptor, alpha polypeptide*
PIN1	*Peptidylprolyl cis/trans isomerase, NIMA-interacting 1*
PTEN	*Phosphatase and tensin homolog*
PTGS2	*Prostaglandin-endoperoxide synthase 2 (prostaglandin G/H synthase and cyclooxygenase)*
PTK2	*PTK2 protein tyrosine kinase 2*
PYCARD	*PYD and CARD domain containing*
RAC1	*Ras-related C3 botulinum toxin substrate 1 (rho family, small GTP binding protein Rac1)*
RASSF1	*Ras association (RalGDS/AF-6) domain family member 1*
RB1	*Retinoblastoma 1*
RELN	*Reelin*
RHOA	*Ras homolog gene family, member A*

RUNX3	*Runt-related transcription factor 3*
SFRP2	*Secreted frizzled-related protein 2*
SMAD4	*SMAD family member 4*
SMAD7	*SMAD family member 7*
SOCS1	*Suppressor of cytokine signaling 1*
SOCS3	*Suppressor of cytokine signaling 3*
STAT3	*Signal transducer and activator of transcription 3 (acute-phase response factor)*
TCF4	*Transcription factor 4*
TERT	*Telomerase reverse transcriptase*
TGFA	*Transforming growth factor, alpha*
TGFB1	*Transforming growth factor, beta 1*
TGFBR2	*Transforming growth factor, beta receptor II (70/80kDa)*
TLR4	*Toll-like receptor 4*

TNFRSF10B	*Tumor necrosis factor receptor superfamily, member 10b*
TNFSF10	*Tumor necrosis factor (ligand) superfamily, member 10*
TP53	*Tumor protein p53*
VEGFA	*Vascular endothelial growth factor A*
WT1	*Wilms tumor 1*
XIAP	*X-linked inhibitor of apoptosis*
YAP1	*Yes-associated protein 1*
ACTB	*Actin, beta*
B2M	*Beta-2-microglobulin*
GAPDH	*Glyceraldehyde-3-phosphate dehydrogenase*
HPRT1	*Hypoxanthine phosphoribosyltransferase 1*
RPLP0	*Ribosomal protein, large, P0*
HGDC	*Human Genomic DNA Contamination*
RTC	*Reverse Transcription Control*

RTC	*Reverse Transcription Control*
RTC	*Reverse Transcription Control*
PPC	*Positive PCR Control*
PPC	*Positive PCR Control*
PPC	*Positive PCR Control*

B: List of Mice genes

Symbol	*Description*
Adam17	*A disintegrin and metallopeptidase domain 17*
Akt1	*Thymoma viral proto-oncogene 1*
Angpt2	*Angiopoietin 2*
Bax	*Bcl2-associated X protein*
Bcl2	*B-cell leukemia/lymphoma 2*
Bcl2l1	*Bcl2-like 1*

Bid	*BH3 interacting domain death agonist*
Birc2	*Baculoviral IAP repeat-containing 2*
Birc5	*Baculoviral IAP repeat-containing 5*
Casp8	*Caspase 8*
Ccl5	*Chemokine (C-C motif) ligand 5*
Ccnd1	*Cyclin D1*
Ccnd2	*Cyclin D2*
Cdh1	*Cadherin 1*
Cdh13	*Cadherin 13*
Cdkn1a	*Cyclin-dependent kinase inhibitor 1A (P21)*
Cdkn1b	*Cyclin-dependent kinase inhibitor 1B*
Cdkn2a	*Cyclin-dependent kinase inhibitor 2A*
Cflar	*CASP8 and FADD-like apoptosis regulator*
Ctnnb1	*Catenin (cadherin associated protein), beta 1*

Cxcr4	*Chemokine (C-X-C motif) receptor 4*
Dab2ip	*Disabled homolog 2 (Drosophila) interacting protein*
Dlc1	*Deleted in liver cancer 1*
E2f1	*E2F transcription factor 1*
Egf	*Epidermal growth factor*
Egfr	*Epidermal growth factor receptor*
Ep300	*E1A binding protein p300*
Fadd	*Fas (TNFRSF6)-associated via death domain*
Fas	*Fas (TNF receptor superfamily member 6)*
Fhit	*Fragile histidine triad gene*
Flt1	*FMS-like tyrosine kinase 1*
Fzd7	*Frizzled homolog 7 (Drosophila)*
Gadd45b	*Growth arrest and DNA-damage-inducible 45 beta*
Gstp1	*Glutathione S-transferase, pi 1*

Hgf	*Hepatocyte growth factor*
Hhip	*Hedgehog-interacting protein*
Hras	*Harvey rat sarcoma virus oncogene 1*
Igf2	*Insulin-like growth factor 2*
Igfbp1	*Insulin-like growth factor binding protein 1*
Igfbp3	*Insulin-like growth factor binding protein 3*
Irs1	*Insulin receptor substrate 1*
Itgb1	*Integrin beta 1 (fibronectin receptor beta)*
Kdr	*Kinase insert domain protein receptor*
Lef1	*Lymphoid enhancer binding factor 1*
Mcl1	*Myeloid cell leukemia sequence 1*
Met	*Met proto-oncogene*
Msh2	*MutS homolog 2 (E. coli)*
Msh3	*MutS homolog 3 (E. coli)*

Mtdh	*Metadherin*
Myc	*Myelocytomatosis oncogene*
Nfkb1	*Nuclear factor of kappa light polypeptide gene enhancer in B-cells 1, p105*
Nras	*Neuroblastoma ras oncogene*
Opcml	*Opioid binding protein/cell adhesion molecule-like*
Pdgfra	*Platelet derived growth factor receptor, alpha polypeptide*
Pin1	*Protein (peptidyl-prolyl cis/trans isomerase) NIMA-interacting 1*
Pten	*Phosphatase and tensin homolog*
Ptgs2	*Prostaglandin-endoperoxide synthase 2*
Ptk2	*PTK2 protein tyrosine kinase 2*
Pycard	*PYD and CARD domain containing*
Rac1	*RAS-related C3 botulinum substrate 1*
Rassf1	*Ras association (RalGDS/AF-6) domain family member 1*

Rb1	*Retinoblastoma 1*
Reln	*Reelin*
Rhoa	*Ras homolog gene family, member A*
Runx3	*Runt related transcription factor 3*
Sfrp2	*Secreted frizzled-related protein 2*
Smad4	*MAD homolog 4 (Drosophila)*
Smad7	*MAD homolog 7 (Drosophila)*
Socs1	*Suppressor of cytokine signaling 1*
Socs3	*Suppressor of cytokine signaling 3*
Stat3	*Signal transducer and activator of transcription 3*
Tcf4	*Transcription factor 4*
Tert	*Telomerase reverse transcriptase*
Tgfa	*Transforming growth factor alpha*
Tgfb1	*Transforming growth factor, beta 1*

Tgfbr2	*Transforming growth factor, beta receptor II*
Tlr4	*Toll-like receptor 4*
Tnfrsf10b	*Tumor necrosis factor receptor superfamily, member 10b*
Tnfsf10	*Tumor necrosis factor (ligand) superfamily, member 10*
Trp53	*Transformation related protein 53*
Vegfa	*Vascular endothelial growth factor A*
Wt1	*Wilms tumor 1 homolog*
Xiap	*X-linked inhibitor of apoptosis*
Yap1	*Yes-associated protein 1*
Actb	*Actin, beta*
B2m	*Beta-2 microglobulin*
Gapdh	*Glyceraldehyde-3-phosphate dehydrogenase*
Gusb	*Glucuronidase, beta*
Hsp90ab1	*Heat shock protein 90 alpha (cytosolic), class B member 1*

MGDC	*Mouse Genomic DNA Contamination*
RTC	*Reverse Transcription Control*
RTC	*Reverse Transcription Control*
RTC	*Reverse Transcription Control*
PPC	*Positive PCR Control*
PPC	*Positive PCR Control*
PPC	*Positive PCR Control*

Table 2.1 (A-B): *List of 84 genes and their description studied for their role in hepatocarcinogenesis using RT-PCR in* ***(A)*** *WRL 68 cells-human genes and* ***(B)*** *mice genes. In addition to the 84 genes, the panel also included probes for 5 housekeeping genes (HKG), 1 genomic DNA contamination (GDC), 3 reverse transcription control (RTC) and 3 positive PCR control (PPC). In case of* ***(A)*** *WRL 68 cells – human genes: Beta Actin, Beta 2-Microglobulin, Glyceraldehyde 3-Phosphate Dehydrogenase, Hypoxanthine Phosphoribosyl Transferase 1, Large Ribosomal Protein P0 were the HKGs whereas in* ***(B)*** *Swiss mice: Beta actin, Beta-2 microglobulin, Glyceraldehyde 3-phosphate dehydrogenase, Beta glucuronidase, Heat shock protein 90 alpha, class B member 1 genes were used as HKGs.*

A) RNA isolation:

a. ***For in-vitro culture (WRL 68 cells):*** Cells were collected at passage 5 and 15 and mRNA was isolated from them using Qiagen RNA isolation kit RNeasy® Plus Mini Kit. The standard protocol provided by the kit was followed for mRNA isolation. One million cells from each group at P5 and P15 were lysed using 350 µl of RLT Plus buffer containing β-mercaptoethanol. The suspension was vortexed for 30 s to homogenize. The homogenized lysate was then placed in a gDNA Eliminator spin column placed in a 2 ml collection tube supplied in the kit and centrifuged for 30 s at 11000 x g. Discard the column and add 350 µl of 70 % ethanol to the flow-through and mix by pipetting. Transfer the contents to a RNeasy spin column placed in a 2 ml collection tube supplied with the kit. Centrifuge it after closing the lid for 15 s at 11000 x g. Discard the flow-through and add 700 µl of buffer RW1 to RNeasy Mini spin column and centrifuge for 15 s at 11000 x g. Discard the flow-through and add 500 µl of buffer RPE to the RNeasy spin column. Centrifuge for 15 s at 11000 x g. Discard the flow-through. Add 500 µl of RPE buffer to the column and centrifuge for 2 min. at 11000 x g. Discard the flow-through along with the 2 ml collection tube. Place the column in new, sterile 1.5 ml collection tube supplied with the kit and add 30 µl of RNase free water directly onto the spin column membrane. Elute the RNA by centrifuging it for 1 min at 11000 x g and quantify the RNA yield and its purity using nano-drop RNA quantification method.

b. ***For in-vivo samples (mice liver):*** 50 µg of liver tissue was cut and placed in a tube containing 1 ml of Trizol solution. The tissue was homogenized in a tissue-lyzer and incubated for 5 minutes at room temperature. 200 µl of chloroform was added to the tube and mixed vigorously without vertexing followed by incubation at room temperature for 15 minutes. The tube was then centrifuged at 12,000 x g for 20 minutes

at 4˚C. The RNA gets concentrated in the upper aqueous layer which is then transferred into a fresh tube. 500 µl of isopropanol was then added to it and incubated at room temperature for 15 minutes after mixing the contents. The contents were then centrifuged again at 12000 x g for 10 minutes at 4˚C. RNA gets pelleted down which is then collected by discarding the supernatant and dissolving the RNA in 1 ml of 75% alcohol. Mix well by vertexing and transfer the contents into the column provided along-with Qiagen's RNA isolation kit. The column was then centrifuged at 11000 x g for 15 s. Discard the flow-through and add 750 µl of RW1 buffer provided in the kit. Centrifuge the column again at 11000 x g for 15 s and add 500 µl of RPE buffer after discarding the flow-through. Centrifuge at 11000 x g for 15 s and repeat the step once again followed by centrifugation at 11000 x g for 2 minutes. The column was then placed in a fresh 2 ml tube provided with the kit and centrifuge at 25000 x g for 1 minute. The RNA was finally eluted using 20 µl of RNase-free water and centrifuging the tube at 11000 x g for 1 minute. The RNA yield and its purity were then quantified using nanodrop method.

B) cDNA synthesis: Approximately 2 µg of RNA was used for cDNA synthesis which was performed in two steps, elimination of genomic DNA followed by reverse transcription using RT^2 first strand synthesis kit by Qiagen. Genomic DNA elimination mix was prepared by adding 2 µg RNA to 2 µl of buffer GE provided with the kit. The volume of the sample was made up to 10 µl using RNase-free water also provided with the kit. The solution was gently mixed by using sterile, RNA-free pipette and micro-centrifuged briefly. The genomic DNA mix was then incubated at 42˚C for 5 minutes and then placed immediately on ice for at least

1 minute. For reverse transcription, reverse-transcription mix was prepared using the components provided with the kit as given below:

Component	**Volume**
5x Buffer BC3	4 µl
Control P2	1 µl
RE3 Reverse Transcriptase Mix	2 µl
RNase-free water	3 µl
Total	**10 µl**

This 10 µl of reverse transcriptase mix was added to 10 µl of genomic DNA mix prepared earlier and mixed gently by pipetting. Incubate them at 42˚C for 15 minutes and stop the reaction immediately by increasing the temperature to 95˚C and incubating the mixture at this temperature for 5 minutes. Add 91 µl RNase-free water and place them on ice to cool. Store them at -20˚C and perform real time PCR on each sample.

C) Real time PCR: RT^2 SYBR® Green ROX FAST Master mix containing HotStart DNA Taq Polymerase, nuclease-free water provided with the kit and cDNA synthesized in the previous step were allowed to thaw on ice and briefly centrifuged for 10-15 s to bring the contents to the bottom of the tube. The PCR reaction mixture is prepared in a sterile 5 ml centrifuge tube by mixing the components as described below:

Array format	**Rotor-Disc 100**
2x RT^2 SYBR® Green ROX FAST Master mix	1150 µl
cDNA synthesis reaction	102 µl
RNase-free water	1048 µl
Total	**2300 µl**

Carefully remove RT^2 Profiler PCR Array from its sealed bag and place it into the Rotor-Disc 100 loading block under sterile conditions. The tab at position A1 should hold the tube labelled correspondingly on the array and rest of the array is fitted accordingly. 20 µl of PCR components is added into each well and mixed properly by pipetting. Seal the array with Rotor-Disc Heat-Sealing film using Rotor-Disc Heat Sealer.

Set the program for real-time cycler as described below and insert the array into Rotor-Disc 100 Rotor and secure it with securing ring before starting the run.

Cycles	**Duration**	**Temperature**
1	10 min	95˚CΔ
40	15 s	95˚C
	30 s	60˚C

Threshold cycle (C_T) of each tube in the array was calculated using real-time cycler software and the data is exported onto excel sheet and analysis was done. The relative gene expression data analysis was performed using $2^{-\Delta\Delta Ct}$ method as suggested by Livak et. al. (105). This method assumes that both target gene i.e., the gene of interest and the reference gene i.e., the housekeeping genes (internal control) are amplified with nearly 100% efficiencies in both

test sample i.e., the thorium treated sample and the calibrator sample i.e., the untreated control group. The analysis is performed in the steps given below:

1. Normalize the C_t value of gene of interest with that of housekeeping gene for both thorium treated group and untreated control group.

$$\Delta Ct_{\text{(treated group)}}: Ct_{\text{(gene of interest in treated group)}} - Ct_{\text{(HKG in treated group)}}$$

$$\Delta Ct_{\text{(untreated control)}}: Ct_{\text{(gene of interest in untreated control group)}} - Ct_{\text{(HKG in untreated control group)}}$$

2. Normalize the ΔC_t of treated group with the ΔC_t of untreated control for a given gene.

$$\Delta\Delta Ct = \Delta Ct_{\text{(treated group)}} - \Delta Ct_{\text{(untreated control)}}$$

3. Calculate the expression ratio:

$2^{-\Delta\Delta Ct}$ = normalized expression ratio.

Out of the five housekeeping genes used in the real time PCR in each set, the HKG which showed the most constant C_t values in three independent triplicates was used for calculating the ΔC_t values. For each group, the HKG used was different and is shown below along-with their C_t values.

(A) In vitro studies: WRL 68 cells:

For studies at passage 5, Beta 2 microglobulin (B2M) was used as the housekeeping gene (HKG) as its expression remained constant in both control and treated group in all three independent triplicates. The values of (B2M) obtained in each group in shown in Table 2.2.

Beta 2 microglobulin	Ct	SD
Control	12.91	0.04
Thorium	12.85	0.17
Alpha	12.89	0.04
Th + alpha	12.45	0.10
Average Ct	**12.77**	

Table 2.2: C_t values of Beta-2 microglobulin gene across all groups with its standard deviation (SD). The average of all these C_t values was used as the C_t of HKG for calculation of ΔC_t at passage 5.

Similarly, for studies at passage 15, Beta-actin was used as HKG. The C_t value of Beta-actin across all groups is shown below in Table 2.3.

Beta-actin	Ct	SD
Control	13.21	0.40
Thorium	13.42	0.29
Alpha	13.36	0.51
Th + alpha	13.21	0.47
Average Ct	**13.30**	

Table 2.3: C_t values of Beta-actin gene across all groups with its standard deviation (SD). The average of all these C_t values was used as the C_t of HKG for calculation of ΔC_t at passage 15.

(B) In vivo studies: mice studies:

For *in-vivo* studies involving Swiss mice, Heat shock protein 90 alpha, class B member 1 (Hsp90ab1) was used as HKG. The C_t values of this genes across different treatment groups is shown below in Table 2.4. Like in-vitro studies, the average of all these C_t values was used in the calculation of ΔC_t.

Hsp90ab1	Ct	SD
Control	22.79	0.86
4 mg/Kg	23.14	0.43
20 mg/Kg	22	0.51
Average Ct	22.64	

Table 2.4: C_t values of Heat shock protein 90 alpha, class B member 1 (Hsp90ab1) gene across all groups with its standard deviation (SD). The average of all these C_t values was used as the C_t of HKG for calculation of ΔC_t at 6 months' time point.

Similarly, for twelve months' time points, Beta glucuronidase (Gusb) was used as HKG. Table 2.5 below shows the C_t values of the genes across all groups along with their standard deviation.

Gusb	Ct	SD
Control	26.23	1.63
4 mg/Kg	25.77	0.97
10 mg/Kg	24.30	0.26
20 mg/Kg	25.29	0.82
Average Ct	25.39	

Table 2.5: C_t values of Beta glucuronidase (Gusb) gene across all groups with its standard deviation (SD). The average of all these C_t values was used as the C_t of HKG for calculation of ΔC_t at 12 months' time point.

The fold change values obtained by the above method started from "0". The values in the range of 0-1 showed downregulation of genes and values above 1 expressed upregulation of the respective genes. In order to obtain data in a biologically more relevant way, fold regulation was calculated where negative inverse of values ranging from 0-1 (downregulated genes) were obtained and the values from 1 above (upregulated genes) were used as it is.

The genes which showed upregulation and downregulation of 2 or more than 2 folds were plotted against their levels of expression using Origin software, version 8.0. Further, those genes were also analyzed for the interaction between the proteins encoded by them using STRING: functional protein association networks database, version 11. Also, the pathways altered by their expression were determined using KEGG Mapper-Search Pathway software provided by Kyoto Encyclopedia of Genes and Genomes (KEGG). The data was also analyzed in terms of the genes commonly upregulated and downregulated across all treatment groups using Venn diagram.

2.2.25. Statistical analysis

Graphs were plotted using Origin 8.0 software. Significance of correlation between parameters were determined by paired t-test correlation and linear fit analysis was performed using origin 8.0.

CHAPTER 3: RESULTS AND DISCUSSION

Section 3.1: Optimization of Arsenazo-III based colorimetric method for Thorium estimation in biological samples

Thorium, being the most abundant nuclear fuel available in India, has increasingly been used in nuclear industry. The extensive usage of thorium increases the risk of its exposure to personnel working in its mining, extraction, processing and enrichment facilities. Therefore, it becomes imperative to study the level of thorium in different biological systems. There are various techniques [such as inductively coupled plasma mass spectrometry/atomic emission spectrometry (ICP-MS/AES) (106), chromatography (106–108), neutron-activation analysis, gamma-ray spectrometry and total reflection X-ray fluorescence (TXRF) (109)] are available for thorium estimation in different types of samples. These techniques are specific and sensitive up to ppb levels of thorium in the samples (93). However, majority of these techniques are expensive, time-consuming, require multiple steps of sample processing, require large of sample volume and low throughput. Most of these techniques are not easily accessible/available for routine estimation of thorium required for most of the biological experiments. Because of these limitations, there is a need to optimize an alternative technique for thorium estimation for routine biological experiments. For this, arsenazo dye was used, which can estimate thorium through colorimetric based spectrophotometric technique. Arsenazo-III (3,6-bis[(2-arsonophenyl)hydrazinylidene]-4,5-dioxonaphthalene-2,7-disulfonic acid (Figure 3.1) is bis-diazo chromogenic dye which has been used to detect thorium in non-biological samples (110,111). The dye can also estimate other metals based on pH conditions (112). Under specific acidic conditions, arsenazo can be used to determine thorium (112). However, its usage for thorium estimation in biological samples has not yet been reported. In the present study, for the estimation of thorium in biological samples the conditions

(concentration of dye and pH condition) have been optimized. Under these conditions, it has also been shown to be specific for thorium and sensitive for the concentration ranges used in biological experiments conducted in the thesis. Moreover, the binding constant/ratio and molar extinction coefficient values have also been calculated. For the same concentrations of thorium, the technique was also compared with TXRF. The technique was able to estimate thorium in different fractions of cell culture. More, the dye could stain thorium, in cells maintained in culture conditions and treated with thorium. Thus, arsenazo based colorimetric technique was found to be easy, specific, sensitive, faster, cost-effective, and high throughput with additional advantage of low sample volume requirement. The technique can detect thorium both quantitatively and qualitatively in biological samples.

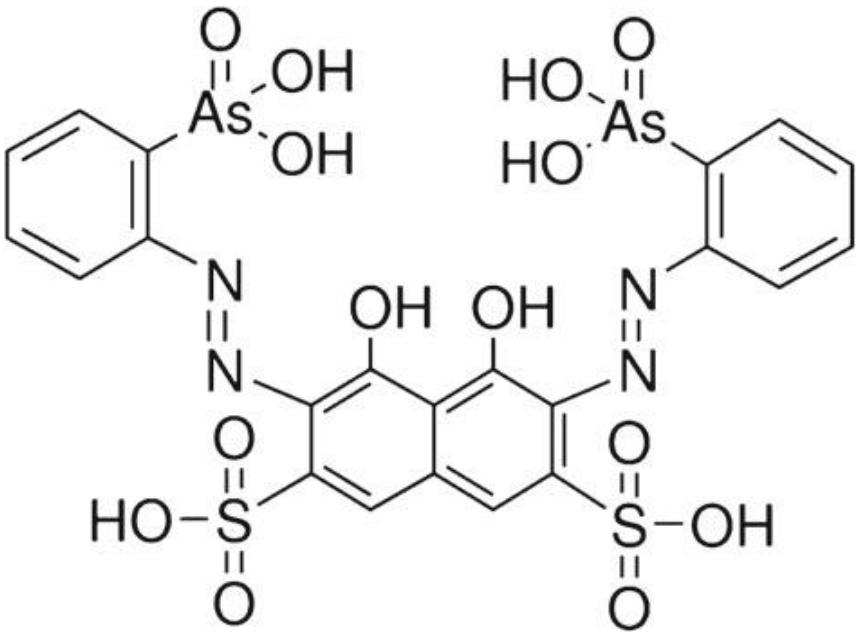

Figure 3.1: *Chemical structure of arsenazo-III dye*

3.1.1. Optimization of arsenazo concentration for Th (IV) estimation and calculation of molar extinction coefficient

In order to estimate Th (IV) using arsenazo dye, first the concentration of arsenazo dye was optimized. Based on literature (112), 50 µM and two other concentrations (one lower 25 µM and one higher 100 µM) were used for optimization. Arsenazo solutions (25, 50 and 100 µM) were prepared and their spectra from 450 to 700 nm were obtained in the presence and absence of different concentrations of thorium (Fig. 3.2). The inset (Fig. 3.2 A-C) shows the absorption spectra of free arsenazo from 450 to 700 nm. For better clarity of spectra, separate figure panels have been prepared for three concentrations of arsenazo [25 µM (Fig. 3.3A), 50 µM (Fig. 3.3B) and 100 µM (Fig. 3.3C)] along with short range spectra 450-575 nm and 575-700 nm for these concentrations of arsenazo.

When thorium was added, the peak at 570 nm reduced with concomitant appearance of two peaks at 612 and 660 nm which increased in their intensity with the corresponding increase in thorium concentration (1-60 µM). In the absence of thorium, un-complexed arsenazo showed an absorbance peak at ~570 nm (spectra in insets Fig. 3.2 A-C).

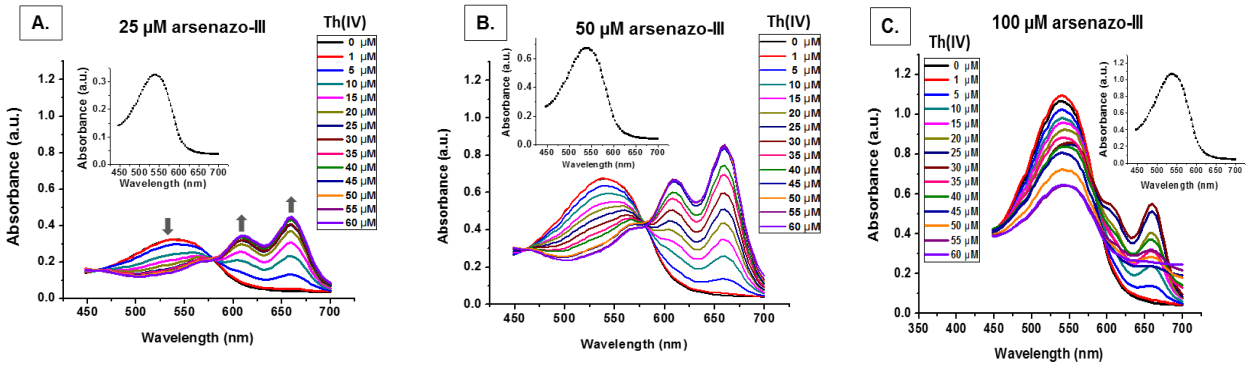

Figure 3.2. *UV-Vis spectra at* ***(A)*** *25 µM,* ***(B)*** *50 µM and* ***(C)*** *100 µM of arsenazo in the absence or presence of Th (1-60 µM). Insets show the spectra of free arsenazo. Downward*

arrow indicates decrease in absorbance at 540 nm; upward arrows show increase in absorbance at 612 and 660 nm.

For 25 µM of arsenazo, as the concentration of thorium increased from 1 to 20 µM, there was a corresponding increase in the absorbance at 612 and 660 nm. However, at the higher concentrations of thorium, the absorbance did not increase suggesting saturation of thorium-arsenazo complex formation (Fig. 3.2 A and Fig. 3.3 A). Fig. 3.3 A shows the complete spectrum of thorium-arsenazo-complex from 450 to 700 nm whereas Fig. 3.3 A-i shows the spectra from 450 nm to 575 nm and Fig. 3.3 A-ii shows the absorption spectrum from 575 nm to 700 nm.

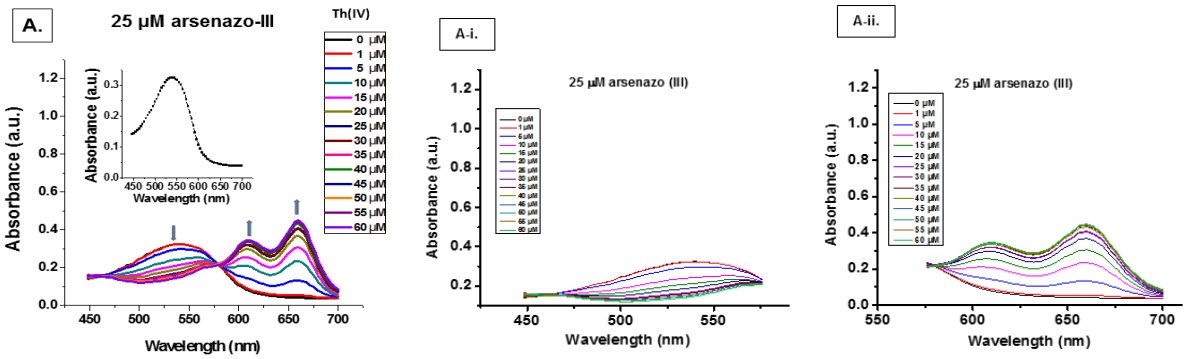

Fig. 3.3 A. *UV-Vis spectra of 25 µM arsenazo concentration in the absence or presence of Th (IV) from 1 to 60 µM. (A) 450 -700 nm (A-i) 450 – 575 nm and (A-ii) 575-700 nm.*

When 50 µM arsenazo was used, a similar pattern of absorption spectrum was observed (Fig. 3.2 B and Fig. 3.3 B). However, in this case, the absorbance peaks were much sharper and better resolved. The intensities of absorbance peaks were also much higher in case of 50 µM of arsenazo as compared to 25 µM. A sharp and well resolved isosbestic point was observed at ~575 nm at both concentrations of arsenazo (25 and 50 µM) indicating formation of thorium-arsenazo complex.

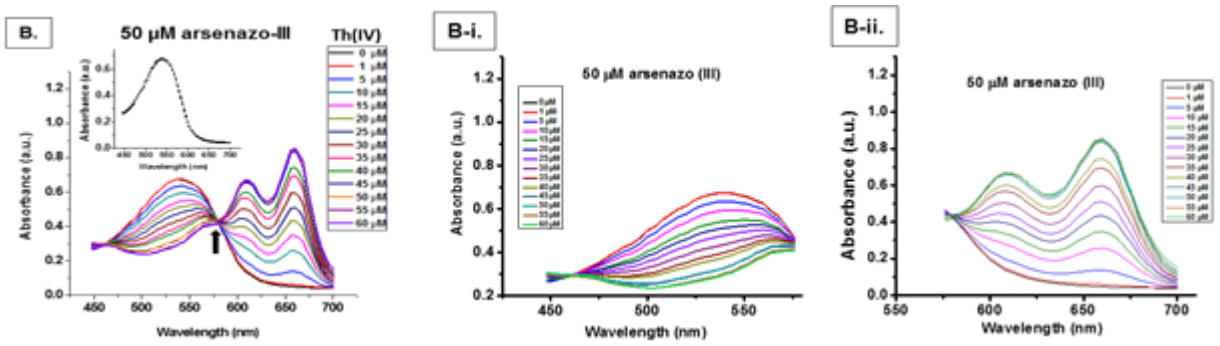

Fig. 3.3 B. *UV-Vis spectra of 50 µM arsenazo concentration in the absence or presence of Th (1-60 µM) (B) 450 -700 nm (B-i) 450 – 575 nm and (B-ii) 575-700 nm. Arrow at 575 nm indicates an isosbestic point.*

At 100 µM arsenazo, the peaks at 612 and 660 nm did not follow the same pattern as earlier concentrations. The peak at 660 nm showed a gradual increase in intensity corresponding with increasing concentrations of thorium until 25 µM and after that the peaks didn't follow any specific pattern (Fig. 3.2 C and Fig. 3.3 C).

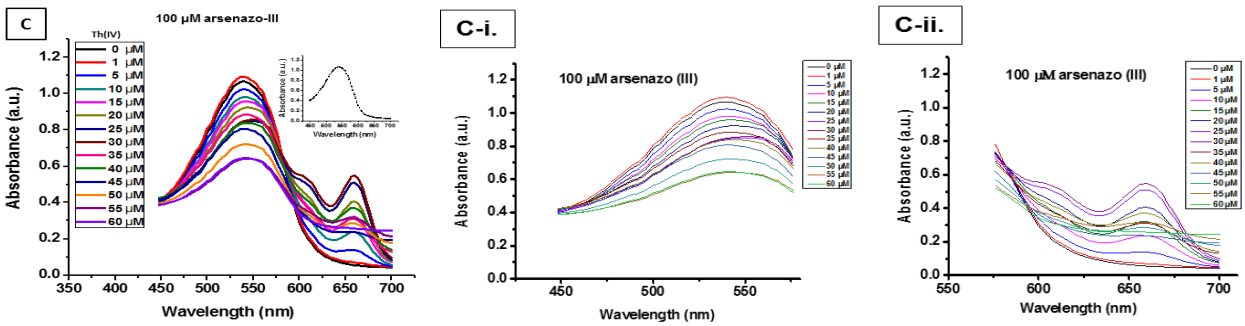

Fig. 3.3 C. *UV-Vis spectra of 100 µM arsenazo concentration in the absence or presence of Th (1-60 µM) (C) 450 -700 nm (C-i) 450 – 575 nm and (C-ii) 575-700 nm.*

Absence of a specific pattern in absorption spectra and loss of isosbestic point at 100 µM of thorium indicate formation of multiple complexes between thorium and arsenazo.

Higher intensity of peak at 575 nm suggests presence of excess of free, un-bound arsenazo in the solution.

To understand the pattern of complex formation with different concentrations of arsenazo, absorbance at 660 nm was plotted for different concentrations of thorium. Figure 3.4 A shows a comparison of absorption spectra of different concentrations of arsenazo with increasing concentrations of thorium at 660 nm. 25 µM arsenazo showed a linear increase in absorption with increasing concentrations of thorium up to 20 µM. Beyond 20 µM thorium, the absorption spectra become parallel to the x axis indicating saturation in complex formation. In case of 50 µM, the absorption spectra increased linearly with increasing concentrations of thorium up to 40 µM. Similarly, 100 µM arsenazo followed linear absorption with increasing concentrations of thorium up to 25 µM. The linear regression analysis of the increase in absorption at different arsenazo concentrations is shown in the inset table, which was found to be highest 0.99 for 50 µM.

A stoichiometry of 1.25 was observed at low and intermediate concentrations of arsenazo i.e., 25 and 50 µM (the ratio of arsenazo to thorium i.e., 25 µM/20 µM = 1.25 or 50 µM/40 µM = 1.25 20 µM and 40 µM are the range of linearity of the respective plots). It is clear that 50 µM arsenazo with highest R^2 value (0.99) is the most appropriate concentration of the arsenazo dye for thorium estimation (as low as 2.5 µM and as high as 40 µM).

Based on the above observations, the molar extinction coefficient and the binding constant of thorium-arsenazo complex was calculated at 660 nm wavelength using Benesi-Hildebrand equation (91). This equation is applicable to complexes which follow 1:1 stoichiometric binding ratio. Thorium-arsenazo complex have been reported to form 1:1 and 1:2 complex depending on the acidic conditions (110,113). In order to determine the

stoichiometric ratio of thorium-arsenazo complex in the conditions standardized for biological samples, Job's plot (Fig. 3.4 B) was used. Mole fraction of Th (IV) ions was plotted against absorbance at 660 nm. The absorbance peak was found to be at ~0.5 mole fraction suggesting 1:1 binding ratio between thorium and arsenazo as described in Section 2.2.2.

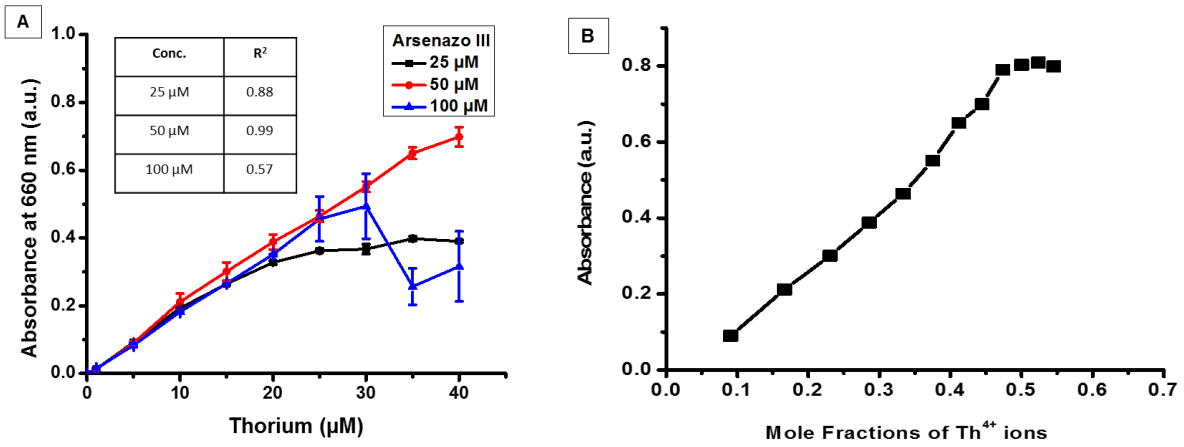

Figure 3.4.(A) *Comparison of absorbance of arsenazo at 660 nm as a function of Th (IV) concentration; Inset table showed the linear regression analysis.* ***(B)*** *Job's plot for determining the stoichiometry between thorium and arsenazo complex. Mole fraction of thorium was plotted against their absorbance at 660 nm. Peak at 0.5 indicates 1:1 binding ratio between thorium and arsenazo.*

Reciprocal values of absorbance were plotted against their corresponding thorium concentration (Figure 3.5), and slope and intercept of its linear fit was determined (inset table). Using the equation, molar extinction coefficient and binding constant were found to be 1.25 x 10^4 $M^{-1}cm^{-1}$ and 7.1 x 10^3 M^{-1}, respectively.

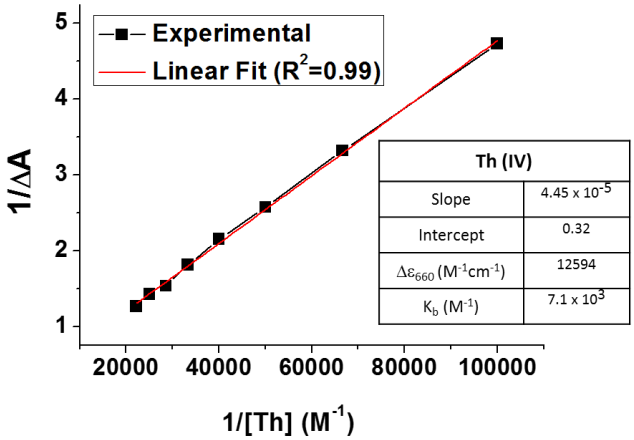

Figure 3.5: *Plot between reciprocal values of absorbance and their respective thorium concentrations for calculation of binding constant and molar extinction coefficient. Inset table shows the slope and intercept of linear fit to the experimental plot and calculated value of molar extinction coefficient and binding constant.*

3.1.2. Arsenazo specifically estimates thorium

After optimizing concentration of arsenazo, it was evaluated whether the conditions developed for thorium estimation (i.e., 2.3 N HCl and 50 µM arsenazo) is specific for its detection compared to other relevant metals such as La (III), Ce (IV), U(VI), Fe (III), Zn (II), Ca (II), Cu (II) and Mn (II). La (III), Ce (IV) and U (VI) are chemically similar to Th (IV) and are also found in monazite ore, the main ore of thorium (114,115). Different concentrations of La (III), Ce (IV) and U (VI) (1 to 100 µM) were tested for their possible detection under the conditions standardized for Th (IV) as shown in Figure 3.6. La (III) and Ce (IV) showed no change in their absorption spectra when complexed with arsenazo in the entire UV-Visible spectral range of 400 to 700 nm. The absorption pattern remained the same as in the case of free, un-bound arsenazo indicating no complex formation between La (III) and Ce (IV) with arsenazo (Fig. 3.6 A and B). In case of U (VI), no absorption was observed up to 25 µM.

Beyond that, there was a slight increase in absorption, but this increase was insignificant as compared to the absorption in case of Th (IV) as shown in Figure 3.6 C. Figure 3.6 D shows the absorbance of all three metals as compared to thorium at 660 nm when complexed with arsenazo. It is clearly shown that only thorium caused an increase in absorbance at 660 nm when complexed with arsenazo as compared to La (III), Ce (IV) and U(VI).

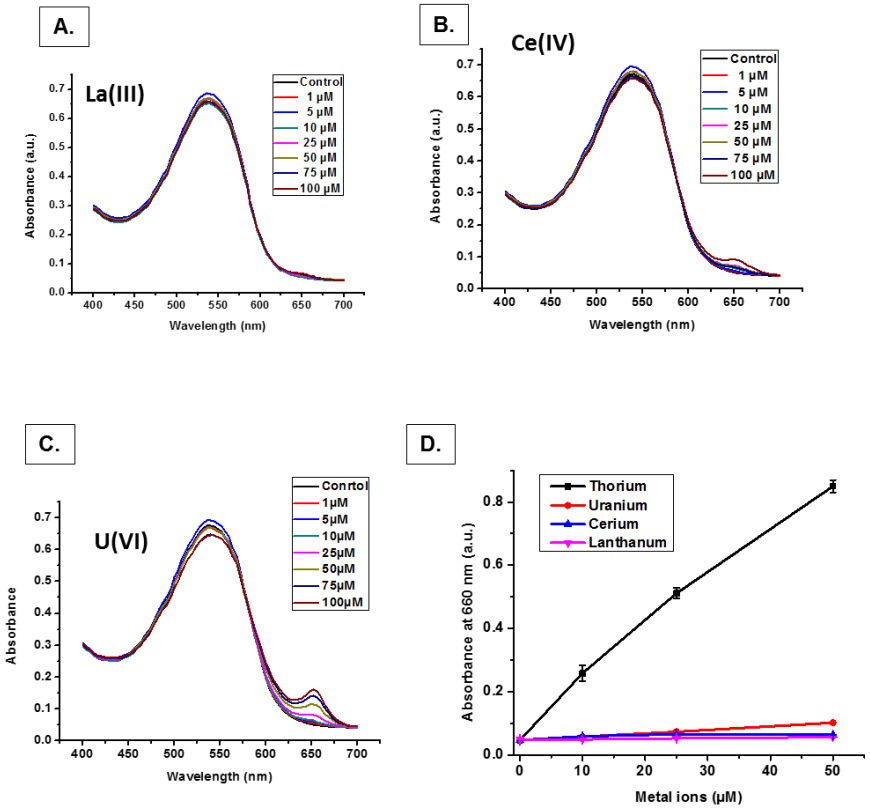

Figure 3.6: *Effect of different metal ions* ***(A)*** *La (III),* ***(B)*** *Ce (IV) and* ***(C)*** *U (VI) on UV-Vis spectra of arsenazo at 50 µM.* ***(D)*** *Absorbance of arsenazo at 660 nm as a function of concentrations of these metal ions in addition to thorium.*

Ca (II), Fe (III), Zn (II), Mn (II) and Cu (II) are other metals are commonly found in biological systems and may bind to arsenazo to form a colored complex and/or interfere in the binding of thorium with arsenazo in biological system. Binding of arsenazo to thorium

produces a colorimetric product and depending on the concentration of thorium, the color of the complex varies from pink to purple to green (Figure 3.7 A and B).

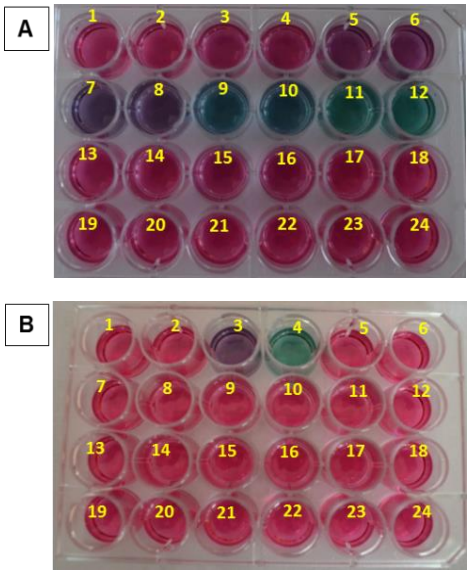

Well no.	Plate A	Plate B
1-2	Control	Control
3-4	Th (IV) – 1 µM	3) Th (IV) – 5 µM 4) Th (IV) – 25 µM
5-6	Th (IV) – 2.5 µM	Ca (II) – 10 µM
7-8	Th (IV) – 5 µM	Ca (II) – 50 µM
9-10	Th (IV) – 10 µM	Fe (III) – 10 µM
11-12	Th (IV) – 25 µM	Fe (III) – 50 µM
13-14	U (VI) – 10 µM	Zn (II) – 10 µM
15-16	U (VI) – 50 µM	Zn (II) – 50 µM
17-18	La (III) – 10 µM	Mn (II) – 10 µM
19-20	La (III) – 50 µM	Mn (II) – 50 µM
21-22	Ce (IV) – 10 µM	Cu (II) – 10 µM
23-24	Ce (IV) – 50 µM	Cu (II) – 50 µM

Figure 3.7 (A & B): *Reaction of arsenazo with different metal ions in microwell plate and change in its colour depending on the metal ions.* ***Table 3.1:*** *Summarizes the details of each well in plate A and B of Fig. 3.7*

A visual comparison of formation of colored-complex by different concentrations of Th (IV), La (III), Ce (IV), U (VI), Ca (II), Fe (III), Zn (II), Mn (II) and Cu (II) with arsenazo dye was also studied. Addition of thorium causes color change starting from 2.5 µM (pink to purple) to 25 µM (purple to green) Fig. 3.7 A (well no. 3-12). No change in coloration was observed after adding U (VI), La (III) and Ce (IV). Similarly, Ca (II), Fe (III), Zn (II), Mn (II) and Cu (II) also did not show any colored product after addition of 50 µM arsenazo even at higher concentration (50 µM) (Figure 3.7 B). Table 3.1 describes the details of each well of 24-well-plate shown in Figure 3.7 A and B.

In all these experiments to study the specificity of arsenazo assay for thorium estimation, different relevant metals were individually allowed to form complex with arsenazo. However, in living systems, different types of metal ions are present, which might interfere in thorium detection. In such a scenario, it is important to know if any of these metals commonly found inside living systems may cause any interference in detection and estimation of thorium. In order to check for the specificity of the reaction system, a fixed concentration of thorium i.e., 10 µM was added in the presence of two different concentrations (one low and one high) i.e., 10 and 50 µM of these metal ions (Figure 3.8). It was found that no metal ion other than iron interfered in the detection of thorium. The absence of interference from any of these environmentally and biologically relevant metals (except Fe) even up to 50 µM of their concentration proves the suitability of the technique for thorium detection/estimation in real scenario.

Well No.	Sample	Well No.	Sample	Well No.	Sample
1	Control	9	Th 10 µM + Ce 10 µM	17	Th 10 µM + Zn 10 µM
2	Control	10	Th 10 µM + Ce 50 µM	18	Th 10 µM + Zn 50 µM
3	Th 5 µM	11	Th 10 µM + La 10 µM	19	Th 10 µM + Mn 10 µM
4	Th 5 µM	12	Th 10 µM + La 50 µM	20	Th 10 µM + Mn 50 µM
5	Th 10 µM	13	Th 10 µM + Ca 10 µM	21	Th 10 µM + Cu 10 µM
6	Th 10 µM	14	Th 10 µM + Ca 50 µM	22	Th 10 µM + Cu 50 µM
7	Th 10 µM + U 10 µM	15	Th 10 µM + Fe 10 µM	23	Empty wells
8	Th 10 µM + U 50 µM	16	Th 10 µM + Fe 50 µM	24	Empty wells

Fig. 3.8: *The reaction plate showed that the presence of 10 and 50 µM of metal ions (U, Ce, La, Ca, Zn, Mn, and Cu), except Fe (III) did not interfere with the formation of green colour complex of arsenazo with 10 µM thorium.* ***Table 3.2:*** *Summarizes the details of each well in Figure 3.8.*

The reason for observed specificity of arsenazo for thorium could be that thorium hydrolyzes under strong acidic conditions to form thorium ions which then reacts with arsenazo

to form a colored complex having absorption maxima at 660 nm. The conditions developed in the current assay uses 2.3 N HCl and a pH of ~-0.4 providing an appropriate condition for thorium hydrolysis (116,117). Other metal ions are known to be hydrolyzed under mild acidic or neutral conditions. Because of this, they could not combine with arsenazo to give a colored complex thus, making the assay thorium specific (116). La (III), UO_2^{2+}, Ce (IV), Ca (II), Fe (III) and Cu (II) have already been reported in literature to undergo hydrolysis and form colored complex with arsenazo at higher pH (pH > 2-3) (116).

3.1.3. Validation of arsenazo method of thorium estimation by TXRF

To establish the assay developed for thorium estimation in biological samples, it is required to validate its results by comparing it with a standard technique for thorium detection/estimation. Total X-Ray Fluorescence (TXRF) is one of the standard techniques used for thorium detection (92,118). Unlike other techniques, it requires very small sample volume and is not affected by sample matrix. These are the two critical limitations faced while detecting trace elements in biological samples (low sample volume and presence of organic matrix). Hence, TXRF was used to validate the arsenazo assay developed to detect/estimate thorium. Thorium estimated by both methods showed highly significant correlation with the amount of thorium detected theoretically (Figure 3.9).

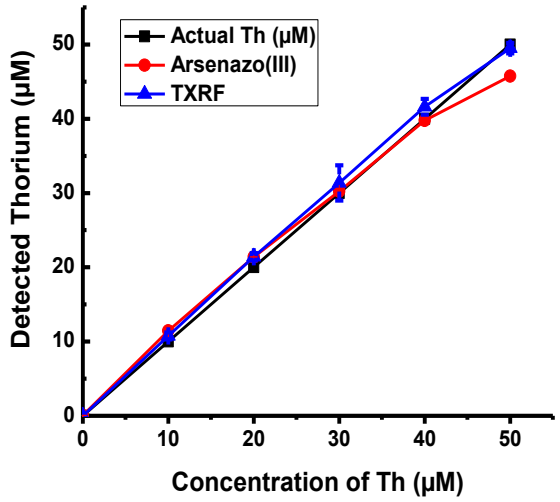

Analysis between assays	Correlation coefficient
Actual *vs.* Arsenazo assay	0.996
Actual *vs.* TXRF	0.998
Arsenazo assay *vs.* TXRF	0.999

Figure 3.9: *Graph plotted between Th concentration measured by arsenazo and TXRF methods, and its comparison with theoretical thorium concentration.* ***Table 3.3.*** *Statistical correlation between measured Th concentration and actual Th (theoretically calculated).*

Linear correlation coefficient was determined between the thorium measured by the two methods and the actual theoretically calculated thorium. It was found that actual theoretical thorium and thorium determined by arsenazo assay showed a correlation coefficient of 0.996 whereas between TXRF and actual thorium, it was 0.998. The correlation coefficient between arsenazo assay and TXRF was also found to be 0.999 (Table 3.3). These results showed the accuracy along with the specificity and sensitivity of the method for thorium estimation.

3.1.4. Thorium estimation in human liver cells using arsenazo method

Human liver has been shown to be the main target organ of thorium deposition by various studies (33) and therefore, estimation of thorium in human liver cell culture is required for such studies. Hence, human liver cell lines (HepG2 and WRL 68) were used to establish whether arsenazo technique can detect thorium at cellular level in culture conditions. Before determination of thorium uptake/binding in treated liver cells in culture conditions, thorium

levels in different culture fractions (medium, trypsin-EDTA and cells) was established using arsenazo method. This helped to validate the techniques in biological media/cells obtained from culture condition. The protocol and scheme for the thorium treatment and its estimation in various cell culture fractions has been provided in Section 2.2.9 in Materials and Methods.

The results suggest that using the technique thorium can be estimated in cell culture fractions (Figure 3.10 A-B). Approximately 50% of total incubated thorium (10 µM; 6 h) was detected in cellular fraction (internalized/bound) in HepG2 cells. In case of WRL 68, the cellular fraction showed more than 80% of total incubated thorium after 6 h of incubation. Such differences may be associated with difference in cellular receptors or content of extracellular proteins, which may contribute to uptake/binding of thorium with cells.

Since ~50% of the total incubated thorium (10-50 µM) is internalized inside the cells, the actual concentration of thorium in medium and trypsin-EDTA fractions also got reduced. This led to possibility of thorium estimation in medium, trypsin-EDTA and cellular fractions, which fell within the upper limit of detection range of arsenazo assay. Of the total incubated thorium, arsenazo assay could account for 60-70% of total thorium. The loss of rest of thorium may be attributed to adherence of thorium to the plastic surface of the culture dish, which could not get recovered. Partially thorium may be lost while culture, washing, estimation etc. steps. Since, most of the *in-vitro* experiments are conducted within this range (10–50 µM) (60,61,64,103), the optimized arsenazo assay could be used for thorium determination in these experiments of the thesis.

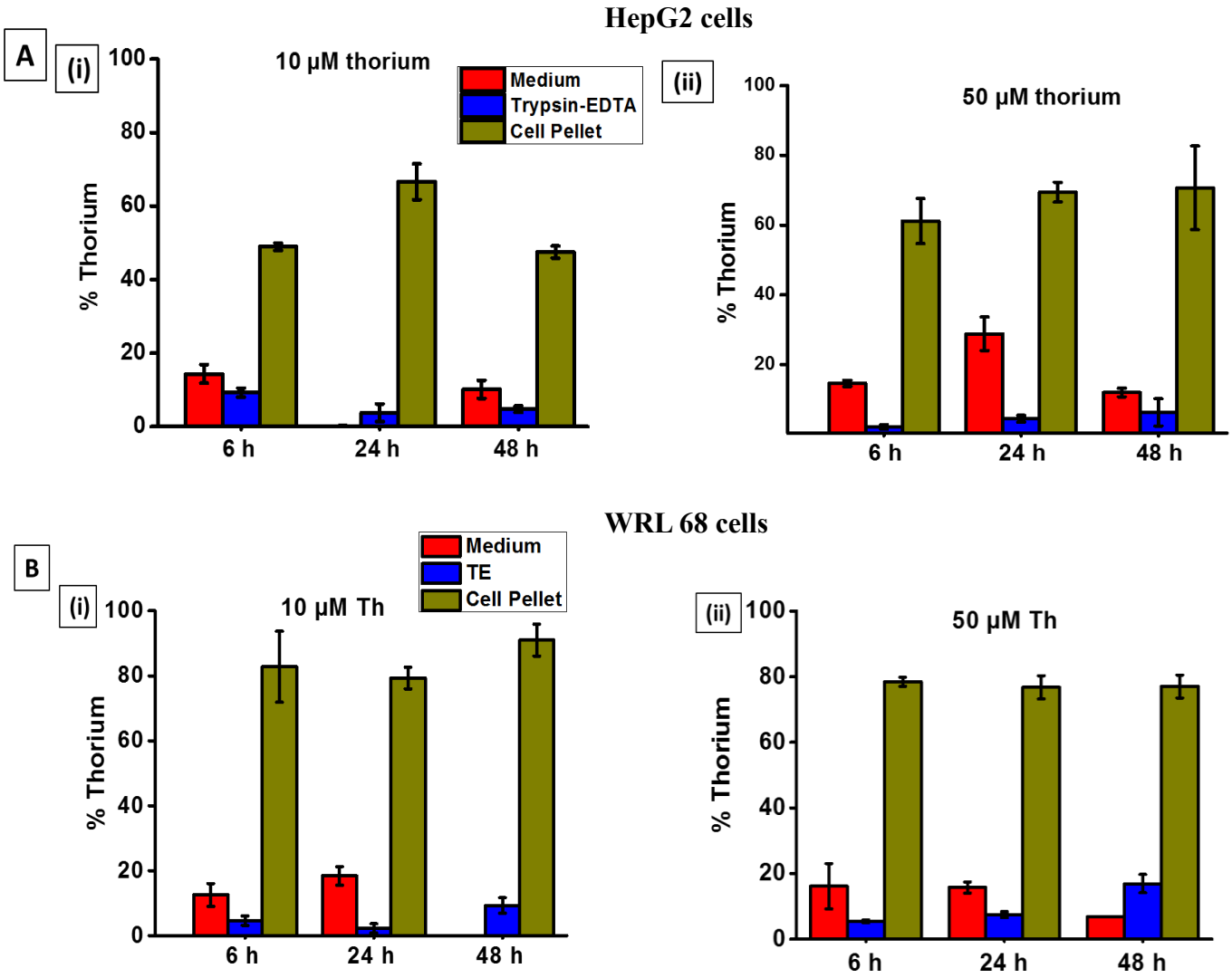

Figure 3.10: *Arsenazo assay was used to determine thorium content in different fractions of cell culture (medium, trypsin-EDTA, cell pellet) using human liver cells* ***(A)*** *HepG2 cells and* ***(B)*** *WRL 68 cells. Two different concentrations i.e., 10 and 50 µM were used to determine thorium in different fractions at 3 different time points (6, 24 and 48 h).*

In addition to detecting thorium in biological samples quantitatively, this dye could also be used to study thorium uptake qualitatively *in situ* (Figure 3.11). HepG2 cells were stained with arsenazo following thorium treatment and observed under bright field microscopy. They showed change in coloration after thorium treatment and staining with arsenazo.

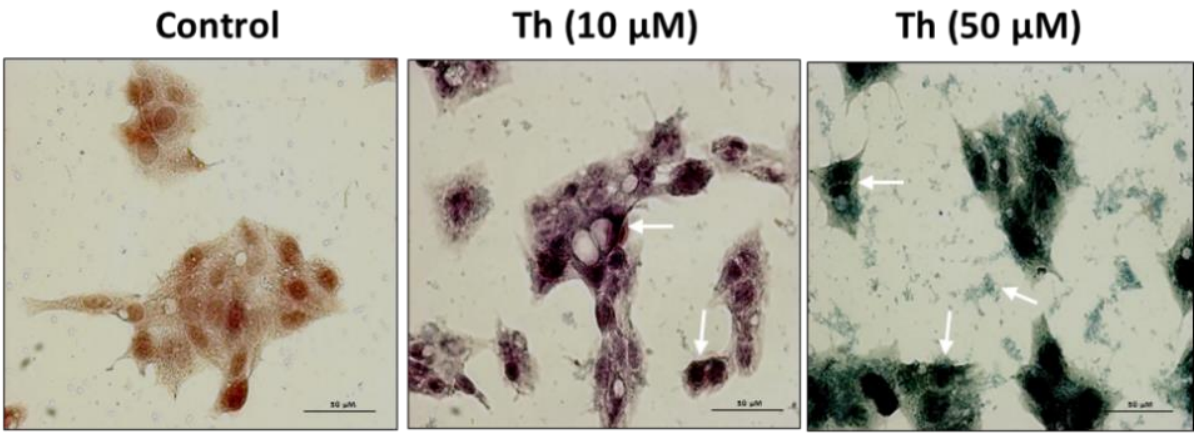

Figure 3.11. *Bright field microscopic images of untreated and Th-treated HepG2 cells after staining with arsenazo. Objective 40X.*

The color formed was in accordance with the color formation observed in 24-well plate system. Since only approximately 50% thorium is internalized by cells, in case of 10 µM and 50 µM thorium treated cells, the actual amount of thorium present in these cells would be around ~5 µM and 25 µM, respectively. The color corresponding to 5 µM is purple and 25 µM is green (Figure 3.7 A, well nos. 7-8 and 11-12), HepG2 cells treated with 10 and 50 µM thorium showed the same respective coloration *in situ* representing 50% thorium uptake qualitatively.

These results obtained for arsenazo technique optimized for biological samples showed suitability of the technique for thorium detection and estimation in biological samples. The assay is easy to be performed, less time consuming, high throughput and specific for thorium and has sensitivity in the range relevant for most of the biological experiments. Therefore, instead of other standard methods (such as ICP-MS/AES, Neutron-activation analysis, gamma-ray spectrometry and TXRF, chromatography etc.) of thorium estimation, this assay could be used for routine biological experiments. Although the standard techniques are more sensitive and specific for thorium detection/estimation as compared with the optimized arsenazo assay,

they are presented with several drawbacks such as being tedious, time-consuming, requiring extensive sample preparation steps and expensive/sophisticated instrumentation. Technique like such as ICP-MS/AES often presents the problem of blockage during nebulization with high content of organic matter present in biological samples (119). The arsenazo assay standardized overcomes these limitations and detects thorium in ranges relevant for biological studies making it handier and more useful for biologists studying thorium interaction with biological systems.

Section 3.2: Determination of mechanism of thorium uptake, its sub-cellular distribution, intra-cellular targets, and alterations in major oncogenes/tumor suppressor genes

In previous chapter, it was observed that ~70-80 % thorium is cell bound/internalized by WRL 68 cells, however, details of thorium internalization in cells are not known. Hence, in the present chapter, mechanism of thorium uptake, its sub-cellular distribution and targets were studied in human liver normal cells (WRL68). Moreover, the molecular effects of thorium treatment in terms of expression of oncogene/tumor suppressor genes were also studied.

3.2.1. Determination of mechanism of thorium uptake

As liver is the main target organ of thorium accumulation and deposition (61,103), human liver normal cell line (WRL 68) was used to study the mechanism of thorium uptake. Arsenazo-III protocol for thorium estimation, which was developed and standardized as described (93), was employed for thorium estimation, wherever possible.

3.2.1.1. Morphological changes after thorium treatment

Before studying the effects of cellular internalization of thorium, morphological changes, and alterations (if any) in thorium treated cells were studied. For this, one million WRL 68 cells were seeded onto sterile 60 mm dishes and incubated overnight for attachment. The cells were washed with serum-free media (SFM) and incubated with two concentrations of thorium i.e., 10 and 50 µM for 6 h following which bright field microscopy images were acquired as shown in (Figure 3.12) using 20X and 40X objective lenses. Morphological

alterations and changes caused by thorium on WRL 68 cells were studied by comparing them with control cells and marked accordingly using arrows.

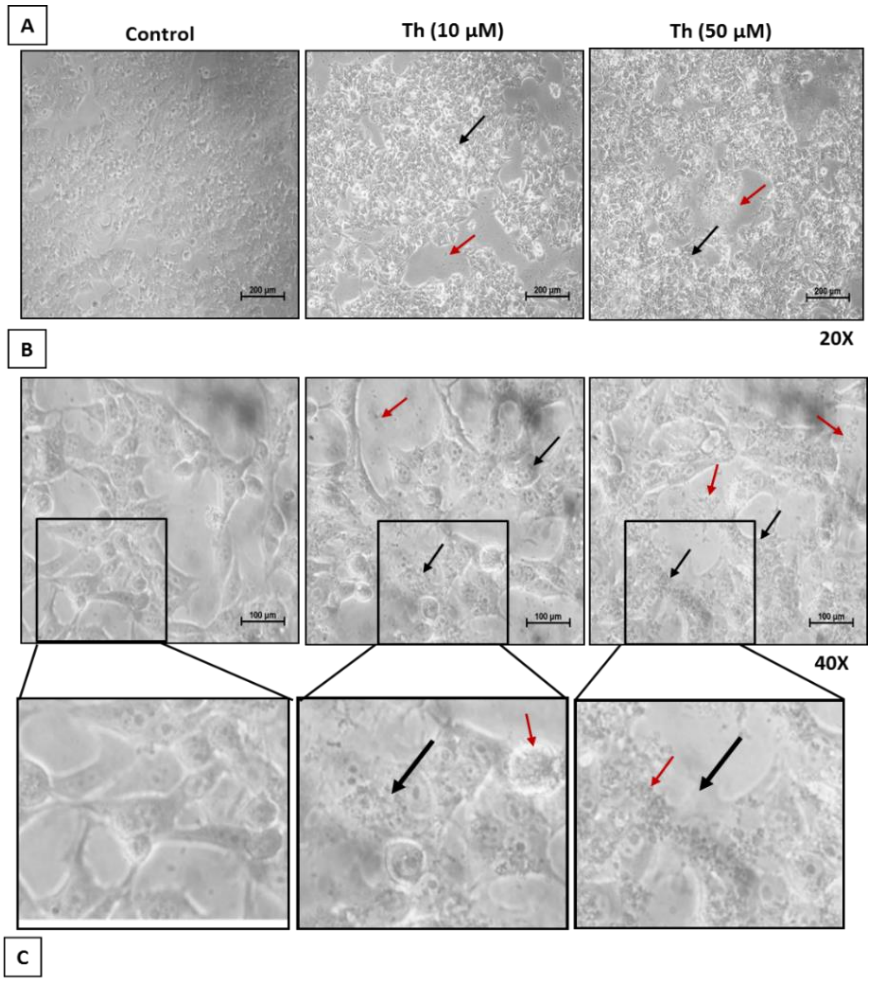

Figure 3.12 (A-C): *Bright field microscopy [**(A)** 20X and **(B)** 40X objective lenses] of WRL68 cells after incubating cells with thorium (10 and 50 µM) for 6 h. Black arrows indicate morphological alterations in cellular architecture and red arrows indicate extracellular granules released by cells after thorium treatment. **(C)** represents 400% digitally magnified images of the selected area from images in **(B)**.*

Cells incubated with thorium showed altered cellular morphology, shrinkage in cellular structure and loss of cell-to-cell contact leading to changes in the cellular architecture as is shown by black arrows in the Figure. Thorium treatment also caused cells to release granule-

like structures into the extracellular matrix. These granules showed increase in their number as the concentration of incubated thorium is increased from 10 to 50 µM (shown by red arrow). These structural alterations, indicating thorium uptake and intracellularization by cells, were better visible at higher magnifications (40X and its 400% digitally magnified view).

3.2.1.2. Optimization of parameters for thorium uptake studies

Thorium uptake studies were performed under *in vitro* conditions using WRL 68 cells to determine the amount of thorium internalized/bound to cells. For this, number of cells, thorium concentration and treatment time were optimized. Experiments were performed using three different cell numbers (i.e., 0.5, 1 and 2 million) and incubating them with two thorium concentrations (10 and 50 µM) for 1, 6, 24 and 48 h. The toxic effects of thorium on the cells causing them to lose their viability (if any) were determined using trypan blue assay. To perform the assay, 0.5, 1 and 2 million WRL 68 cells were incubated with 10 and 50 µM thorium in SFM for varying time points i.e., 1, 6, 24 and 48 h. After incubation, cells were harvested, stained with 0.2% trypan blue solution using suitable cellular dilution and incubated for 2-3 minutes at room temperature. Both live and dead cells were counted using bright field microscope. Live cells did not take up the dye and appeared transparent under the microscope whereas dead cells internalized the dye and appeared as blue coloured cells. Percentage viability was calculated as mentioned in Section 2.2.8 of Materials and Methods chapter in all treatment and control groups and plotted against different time points as shown in Figure 3.13.

After 1 h of thorium incubation, the cellular viability was found to be in the range of 93-97% in control, 10 and 50 µM thorium-treated groups for all the cellular concentrations. At 6 h, ~95% cells were found to be viable in case of control and 10 µM thorium which decreased to ~90% when 50 µM of thorium was used in all cellular concentrations. The viability decreased further when thorium was incubated for 24 h. It was found to be 92% in case of control and 10 µM thorium and < 90% when 50 µM thorium was used for the incubation. The viability further decreased after 48 h of incubation to 85-90% in case of control and 10 µM and < 85% in case of 50 µM across all three cell concentrations.

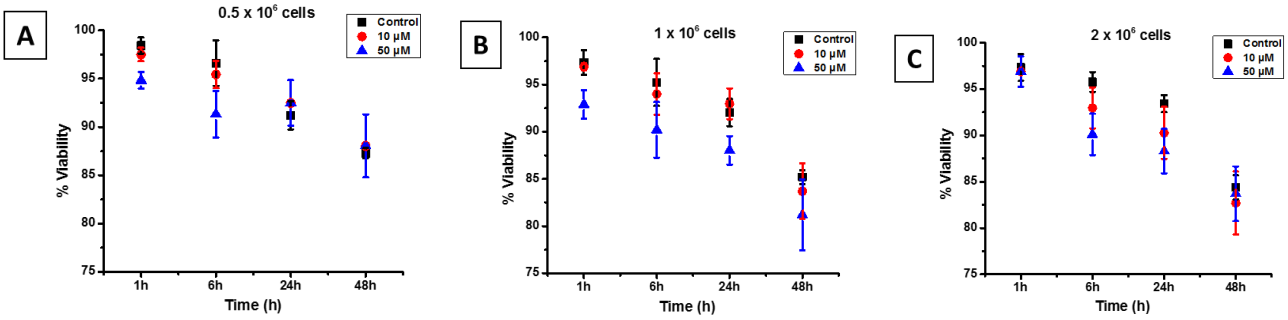

Figure 3.13 (A-C): *Percent viability of WRL 68 cells upon incubation with 10 and 50 µM of thorium as compared with control at 1, 6, 24 and 48 h using trypan blue assay. Different cell numbers i.e.* ***(A)*** *0.5 million* ***(B)*** *1 million and* ***(C)*** *2 million were used. Live, viable cells were counted using bright field microscope with 40X of objective lens.*

These results suggested that upon incubating the cells with 10 µM thorium, the cellular viability was similar to that of control cells whereas 50 µM thorium was found to be comparatively toxic across all cell concentrations. The viability was similar at 1 and 6 h of incubation and starts decreasing gradually after 24 h of incubation. Therefore, for the optimization of thorium uptake, 6 and 24 h incubation time points were used across all the parameters.

Uptake of thorium by cells were studied at all three cell concentrations (0.5, 1 and 2 million) using both 10 and 50 µM concentrations of thorium. The cells were incubated with thorium for 6 and 24 h time points based on the results of trypan blue assay. Since components present in FCS interact with thorium (72) and thus, could interfere in its uptake/internalization by cells, all these experiments were performed in serum-free media (SFM). After incubation, cells were obtained from each treatment group in the form of cell pellet which was acid digested and amount of thorium was determined using arsenazo-III method as described (93). Each experiment was performed in triplicates and repeated three times independently. The values were expressed as the mean of triplicates with standard deviations in Figure 3.14 (A-B).

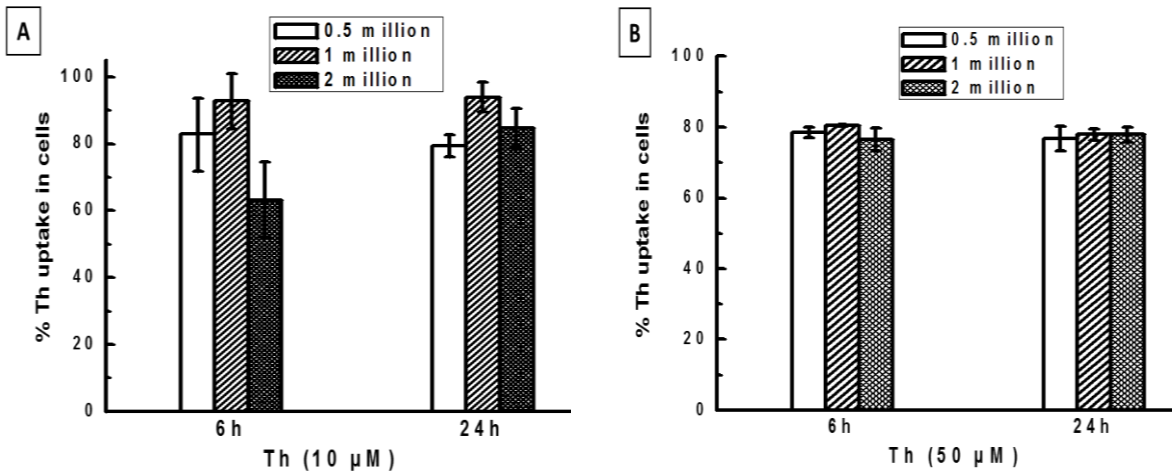

Figure 3.14 (A-B): *Percent thorium uptake by incubating different thorium concentrations* ***(A)****10 µM and* ***(B)****50 µM with different number of WRL 68 cells (0.5, 1 and 2 million) in SFM for 6 and 24 h.*

When 0.5 million WRL 68 cells were incubated with 10 µM thorium, more than 80% of total incubated thorium was taken up in 6 h, whereas 1 million cells internalized around 90%. However, in case of 2 million cells, the amount of thorium internalized gets reduced to

~60%. This decrease in thorium internalization is not significant as compared to thorium uptake at 0.5 and 1 million cells and therefore, could be attributed as an experimental artefact. At 24 h, all three cell concentrations internalized more than 80% of total incubated thorium. When cells were treated with 50 µM thorium, all three cell concentrations (0.5, 1 and 2 million) internalized around 80% of total thorium. This observation remains the same even after 24 h of incubation. No significant difference was found in the amount of thorium internalized by different cell number at both thorium concentrations at 6 and 24 h time points.

Based on the above results of viability (Figure 3.13) and uptake (Figure 3.14) studies, it was found that 1 million cells incubated with 10 µM thorium was optimum for *in-vitro* studies. Although thorium uptake was found to be more than 80% in case of both 6 and 24 h of incubation time, cellular viability was lower at 24 h as compared to 6 h. Similarly, thorium uptake was higher at 6 h incubation time as compared to 1 h. Therefore, 1 million WRL 68 cells incubated with 10 µM thorium for 6 h time point was found to be optimum for *in-vitro* studies.

3.2.1.3. Thorium uptake studies using different chelators (EDTA and DTPA)

Thorium is a positively charged heavy metal ion which, when incubated with cells under culture conditions, will interact with different components of cell culture. The thorium internalized/bound to cell membrane will get collected in the cell pellet fraction upon separation of culture components whereas thorium interacting with medium components and/or excess of thorium will remain suspended in growth medium. Also, a fraction of thorium will interact with proteins found in extracellular membrane matrix. The interaction between these extracellular membrane matrix proteins and thorium would mostly be electrostatic in nature owing to their (thorium and proteins) opposite charges (60). However, other strong

modes of interaction would also be present, binding thorium tightly to extracellular proteins. Most of this thorium would get chelated by chelator EDTA present in trypsin-EDTA solution used for trypsinization and thus, present in trypsin-EDTA fraction of cell culture. However, EDTA is a weak chelator and could not chelate all the removable thorium bound extracellularly. These thorium ions would thus, get pelleted as the cell pellet and present themselves as thorium internalized by the cells. Therefore, to reduce the possibility of this extracellular thorium getting accounted as internalized thorium, EDTA was replaced with a strong chelator which could remove the extracellular protein-bound thorium more effectively. DTPA (diethylenetriaminepentaacetic acid) is a strong chelator which is known to efficiently chelate thorium bound to proteins extracellularly (33,120). DTPA is also known to act extracellularly without entering into the cells (121), making it the ideal chelator to chelate the removable thorium from membrane bound proteins extracellularly. Based on the above facts, DTPA was used in place of EDTA to chelate thorium bound to protein matrix extracellularly. A schematic representation of the differences in action of EDTA and DTPA is shown in Figure 3.15.

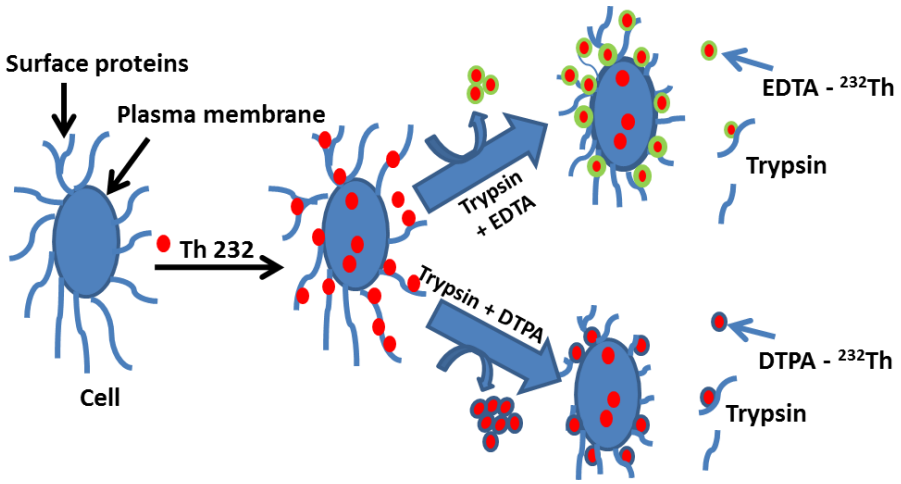

Figure 3.15: *Schematic representation of the differences in the mechanism of action of EDTA and DTPA as thorium chelator. DTPA, when used in combination with trypsin during*

trypsinization, could chelate most of the thorium bound to membrane proteins extracellularly as against EDTA.

For this, increasing concentrations of DTPA ranging from 0.2 to 100 mM was used in combination with 0.25% trypsin during trypsinization. One million cells were seeded as described previously and treated with SFM containing 10 µM thorium and incubated under culture conditions for 6 h. Thorium in various cell culture components (medium, trypsin-EDTA/trypsin-DTPA and cells) was determined using arsenazo assay. It was observed that as the concentration of DTPA increased the percentage of thorium found in cell fraction decreased gradually. This decrease was accompanied with a simultaneous increase in thorium in medium and trypsin-DTPA fraction (shown as extracellular, EC fraction). Percent of thorium continued to decrease in cellular fraction and correspondingly increased in medium and trypsin-DTPA fractions till 25 mM DTPA (Figure 3.16).

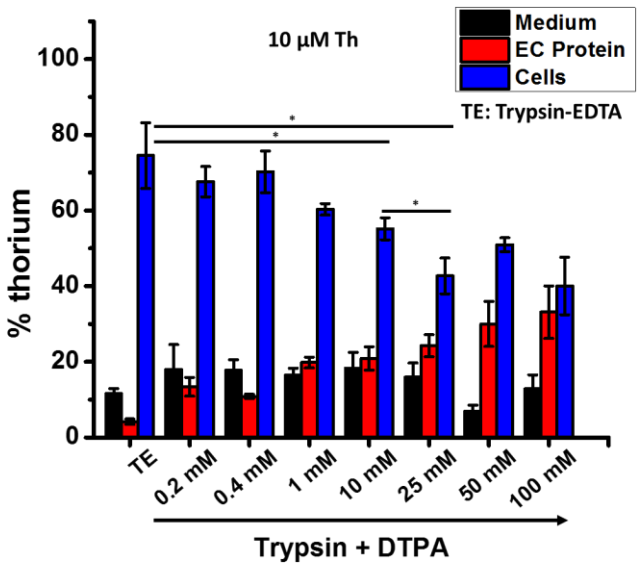

Figure 3.16: *Thorium distribution among different components of cell culture using 0.5 mM EDTA and/or increasing concentrations of DTPA (as chelators) in combination with 0.25% trypsin. DTPA concentrations ranging from 0.2 to 100 mM was used. EC protein: extracellular protein.*

When 25 mM DTPA concentration was used in combination with 0.25% trypsin during trypsinization, only 45-50% of thorium was found in cellular fractions. At higher concentrations of DTPA (50 and 100 mM), 50% of total incubated thorium was found in cells at 50 mM which then decreased to 40% at 100 mM DTPA concentration. There is a significant decrease in the amount of thorium present in cells when 10 and 25 mM DTPA was used for trypsinization as compared to the amount of thorium present in cells when trypsin-EDTA was used. The thorium present in cells when 25 mM DTPA showed a significant reduction as compared to the amount of thorium present in cells when 10 mM DTPA was used. The amount of thorium present in medium showed a marked increase which corresponded with the decrease in thorium in cells at these concentrations of DTPA. These results showed that only ~50% of total incubated thorium (i.e., ~5 µM) enters the cell when cells were treated with 10 µM thorium and the rest is either bound to extracellular protein matrix and/or media components.

3.2.1.4. Mechanism of thorium uptake by cells

A: In presence and absence of transferrin (Tf)

Thorium, being a heavy metal ion, cannot enter cells easily. The mechanism by which thorium gains access to the intracellular environment is still not known. Biologically, thorium has been found to bind iron-transport protein, transferrin (Tf), in blood at physiological pH (72,122). Transferrin protein is synthesized mainly in liver (123). Thorium bound to transferrin is transported in blood and delivered to liver where thorium accumulates (19). One possible explanation for this thorium-transferrin binding could be due to the charge/size ratio of Th (IV) very similar to Fe (III). The ionic radius of Th (IV) is 108 pm and of Fe (III) is 78.5 pm (124). The charge by size ratio of Th (IV) is 4/108 = 0.037 and that of Fe (III) is 3/78.5 = 0.038. Because of this almost same charge/size ratio, Th (IV) interaction may be very similar to Fe (III).

The role of transferrin proteins in thorium uptake by WRL 68 cells was investigated (Figure 3.17). For this, one million cells were seeded onto sterile 60 mm dishes as described previously and incubated with 10 µM thorium in the presence and absence of transferrin in the incubation medium. Thorium uptake in both conditions was estimated using arsenazo method. Since human serum transferrin level ranges between 1 to 2.5 mg/ml (125), a concentration of 2 mg/ml was used for the experiment.

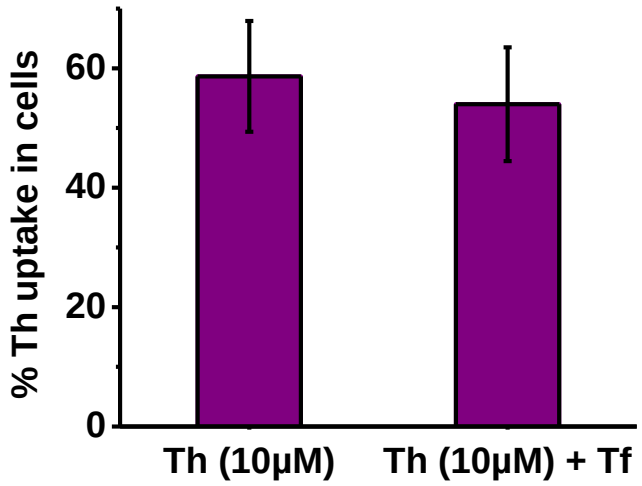

Figure 3.17: *Thorium uptake by WRL 68 cells in presence and absence of transferrin (2 mg/ml) in the incubation medium.*

The results indicate that even in absence of transferrin, ~60% of thorium gets internalized by cells. When transferrin was added, no significant difference in the amount of thorium taken up by cells was found indicating a mechanism of thorium uptake which is independent of transferrin-receptor mediated endocytosis.

B: Active and/or passive uptake of thorium

Thorium uptake at two different temperatures (low temperature, 4˚C and physiological temperature, 37˚C) was studied to elucidate the role of receptor and non-receptor mediated mode of thorium uptake. For this, cells were seeded as describes previously and treated with SFM containing 10 µM thorium. The cells were incubated at two different temperatures i.e., at 4˚C and 37˚C for 6 h. Following incubation, cells were harvested, digested with conc. HNO_3, and heated at ~90˚C for 4-5 h to degrade all organic matter until a clear solution was obtained. Thorium was estimated in each cell sample using arsenazo method. The experiment was performed twice in three independent triplicates and values were presented as their average with standard deviations (Figure 3.18).

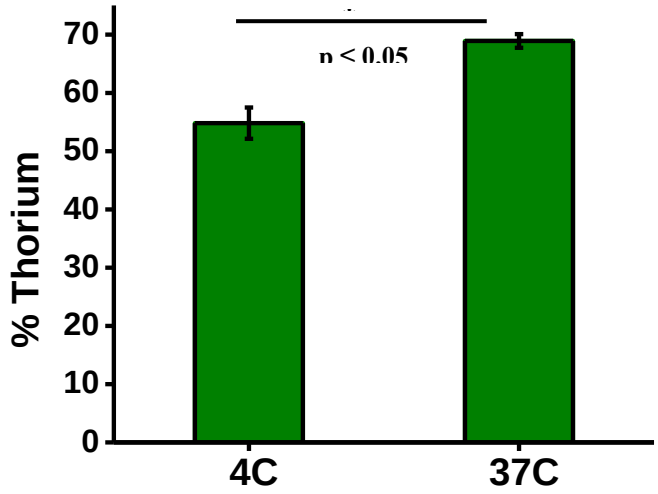

Figure 3.18: *Thorium uptake by WRL 68 cells at different temperatures i.e., 4˚C and 37˚C.*

It was observed that there was a significant difference in the percentage of thorium taken up by cells at both temperatures. At 4˚C, almost 55% of total incubated thorium has been internalized in the cells where are 37˚C, it increases to 70%. Receptor mediated or active transport requires expenditure of energy and occurs at physiological temperature as proteins involved in this mode of transport are mostly enzymatic in nature which gets inactivated at low

temperature and the membrane lipids undergo transition from liquid state at physiological temperature to gel form at low temperature (126,127). Significant thorium uptake (55%) even at low temperature i.e., 4˚C suggested that majority of the thorium is internalized by a mechanism which is independent of receptor mediated transport and might involve some non-receptor mediated pathway. Only a small percentage of thorium i.e., 15% is internalized by receptor-mediated transport.

C: Role of ion channels in thorium uptake

Ion channels are one of the major pathways involved in non-receptor mediated uptake of various ions across cell membrane. As thorium uptake showed a non-receptor mediated i.e., passive mode of uptake mechanism, role of various ion channels present on plasma membrane and endoplasmic reticulum membrane were studied. Various ion channels such as calcium (both voltage-dependent and voltage-independent), potassium, water ion channel (on plasma membrane) and calcium ion channel (on endoplasmic reticulum membrane) were studied for their possible role in thorium uptake by using their respective inhibitors (Figure 3.19).

One million WRL 68 cells were seeded, and experiment was conducted as described in Section 2.2.9. Different inhibitors such as nifedipine (N) and verapamil (V) for calcium ion channel, tetraethyl ammonium (TEA) for potassium ion channel, mercuric chloride ($HgCl_2$) for aquaporins and thapsigargin (TG) for endoplasmic reticulum were screened for their possible role in thorium uptake. Thorium was estimated in each cellular fraction using arsenazo method. The experiment was done in triplicates and repeated two independent times. The result was obtained by averaging all the values of both experiment and expressed as percent thorium uptake with their standard deviations.

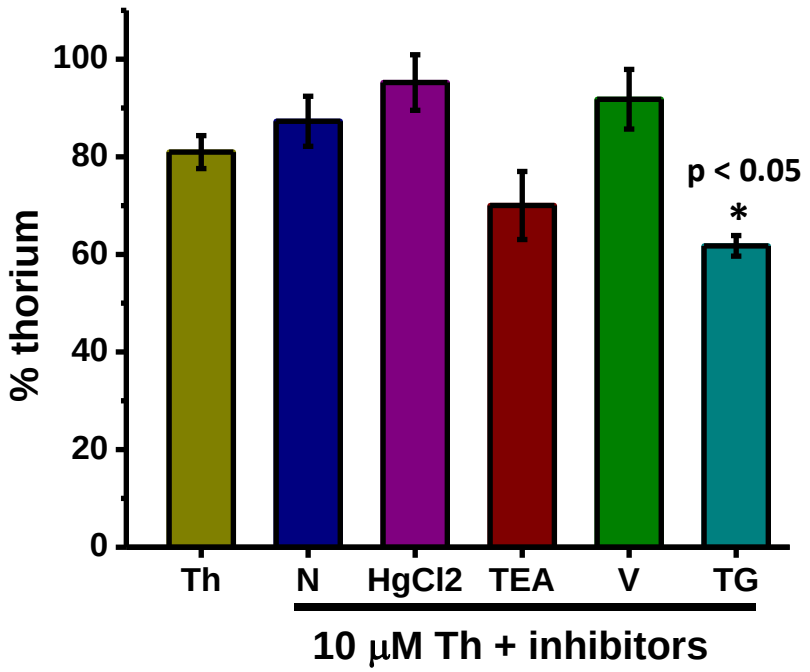

Figure 3.19: *Effects of different ion channel inhibitors for their possible role in thorium uptake in WRL68 cells. The concentration of each inhibitor used was 10 μM. Abbreviations used are Th – thorium, N – nifedipine, $HgCl_2$ - mercuric chloride, TEA – tetraethyl ammonium, V – verapamil, TG – thapsigargin.*

Of all the inhibitors used, only endoplasmic reticulum calcium ion channel inhibitor/mobilizer, thapsigargin, was able to reduce thorium uptake significantly. Other ion channel inhibitors such as nifedipine, mercuric chloride, and verapamil increased thorium uptake to a certain extent, however, the increase was not significantly high. Tetraethyl ammonium, however, reduced the uptake of thorium in cells but the reduction was not significant enough to conclusively suggest the role of potassium ion channel in the uptake of thorium.

D: Role of calcium ion channels in thorium uptake

Since thapsigargin, a calcium ion channel inhibitor, significantly reduces thorium uptake, it was decided to study, the role of different calcium ion channels present on plasma membrane for their possible involvement in thorium uptake. There are different types of calcium ion channels present on plasma membrane which responds to different kinds of stimuli for their activation/inactivation e.g. voltage-dependent, voltage-independent, sodium-calcium ion exchanger, ligand-gated etc. (128–130). Different inhibitors were used to study the role of different calcium ion channels to elucidate the possible mechanism involved in thorium uptake. A diagrammatic representation of different types of calcium ion channels present on eukaryotic cells is shown in Figure 3. 20.

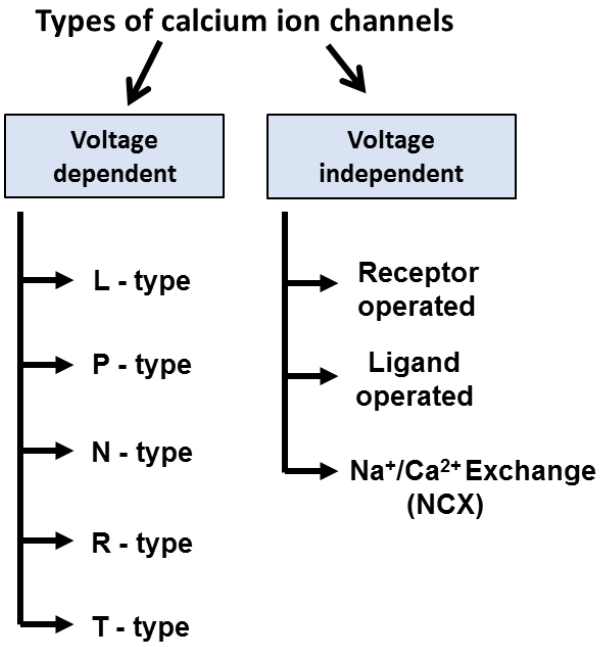

Figure 3.20: *Different types of calcium ion channels present on eukaryotic cells.*

Of the different types of voltage-dependent calcium ion channels, L-type is the most common among non-excitable cells (131) and hence was studied for their role in thorium

uptake in liver cells by using their specific inhibitors such as nifedipine and bepridil. Other ion channels such as P-, N-, R- and T- type were mostly found in excitable cells such as cardiac cells, neurons, other cells of central and peripheral nervous systems. Since, they are not commonly found in liver cells, their role in thorium uptake was not investigated.

In case of voltage-independent or ligand-gated class of calcium ion channels, role of receptor mediated thorium uptake is already studied by studying thorium uptake at different temperatures (i.e., 4˚C and 37˚C). Role of other ligand-gated calcium ion channels such as store-operated calcium ion channel and sodium-calcium ion exchanger (NCX) were studied using their specific inhibitors i.e., CRAC inhibitor BTP2 for store-operated and SN-6 for NCX.

Based on extensive literature review (26,132,141,133–140), a concentration of 10 µM for all inhibitors (thapsigargin, nifedipine, bepridil, SN-6 and BTP2) was used for the study. The experimental protocol followed was the same that was used for the screening of different ion channel inhibitors and is described in Section 2.2.10.3. Thorium was estimated using ICP-MS (Figure 3.21).

It was found that thapsigargin reduced the uptake of thorium by ~20% which was found to be significant as compared to control (without any inhibitor). However, in presence of other inhibitors such as nifedipine (voltage-dependent), SN-6 (sodium-calcium ion exchanger), CRAC BTP2 (store-operated calcium ion channel inhibitor), thorium uptake was found to be significantly higher as compared to only thorium-treated cells. Bepridil hydrochloride also enhanced thorium uptake though the increase was not significantly high.

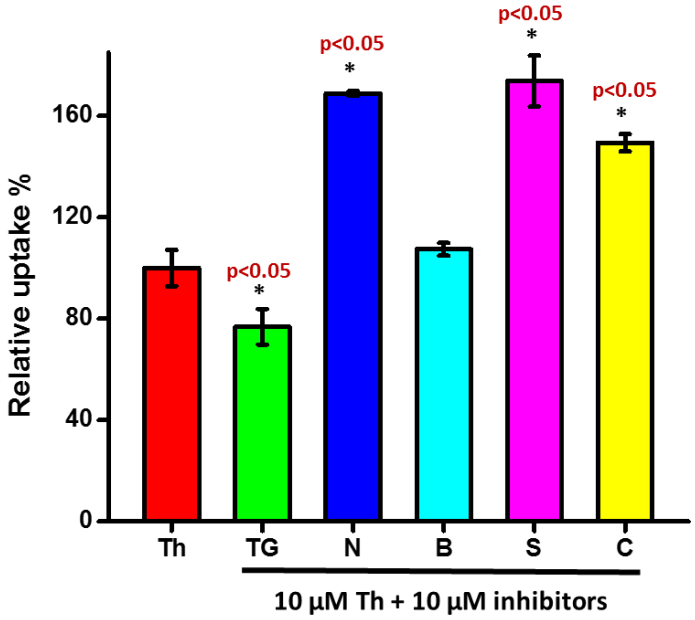

Figure 3.21: *Thorium uptake by WRL68 cells using different ion channel inhibitors (10 µM) in presence of 10 µM thorium. The uptake is shown as relative percent uptake by considering thorium uptake in control to be 100%. The different abbreviations used are Th – thorium, TG – thapsigargin, N – nifedipine, B – bepridil HCl, S – SN-6 and C – CRAC inhibitor, BTP2.*

Thapsigargin is a well-documented endoplasmic reticulum calcium ion channel (SERCA) inhibitor/mobilizer – it depletes endoplasmic reticulum (ER) calcium stores by releasing Ca^{2+} ions stored in endoplasmic reticulum into the cytoplasm. This depletion of calcium ions from ER in turn activates uptake of calcium ion through plasma membrane (142,143). This decrease mainly activates store-operated calcium entry (SOCE) channels such as Orai and STIM1 present in plasma membrane to pump more calcium into the cells (144–147). The resulting increase in intracellular Ca^{2+} could possibly be the reason for reduced uptake of thorium into cells. Based on the above results, a hypothesis has been proposed for the mechanism of thorium uptake by cells in which calcium ion channels and the cytoplasmic concentration of calcium ion has been proposed to play a key role in thorium uptake. However, further studies are required for better understanding of this hypothesis. The mechanism, which

could possibly be playing a key role in the processes has been depicted pictorially below in the Figure 3.22.

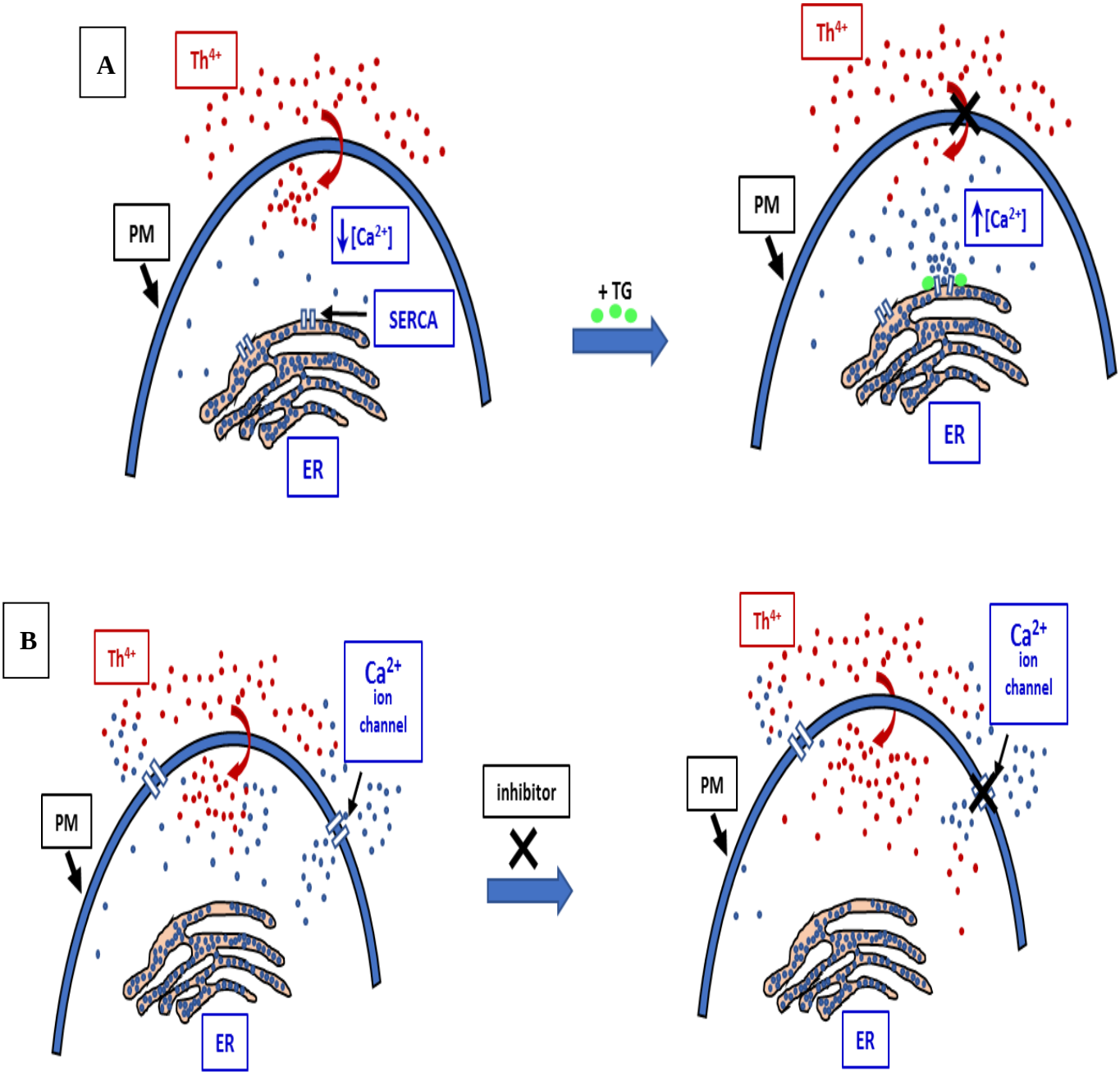

Figure 3.22: *Pictorial depiction of the mechanism proposed to play a key role in thorium uptake by WRL 68 cells.* ***(A)*** *depicts the role of thapsigargin (TG) in the reduction of thorium*

*uptake by cells and **(B)** depicts the role of other calcium ion channel inhibitor in the increase in thorium uptake by cells. PM: Plasma Membrane, ER: Endoplasmic Reticulum, TG: Thapsigargin, SERCA: sarcoendoplasmic reticulum (SR) calcium transport ATPase.*

As thapsigargin causes Ca^{2+} ions to be released from ER, increasing its cytoplasmic concentration, thorium uptake is reduced. On the other hand, when calcium ion channel inhibitors were used, its uptake into the cells was inhibited leading to its low cytoplasmic concentration. A corresponding increase in thorium uptake was also observed.

In the present study, it was established that ~80% of thorium is internalized and/or bound to WRL 68 cells when incubated for 6 h under standard culture conditions. The amount of thorium internalized remains the same even after 24 h of incubation suggesting saturation of uptake by WRL 68 cells. Thorium causes several morphological alterations in WRL 68 cells after its internalization such as shrinkage of cellular structure, loss of cell-to-cell contact, release of certain granules in the extracellular matrix etc. Upon using a strong chelator such as DTPA, for removing excess thorium in thorium uptake studies, it was established that only around 50% of total incubated thorium is internalized by cells and rest are bound to extracellular proteins, which can be removed by DTPA, and/or media components. Thorium uptake appears to be unaffected by the presence of transferrin molecules in the incubation medium. However, in this experiment, the formation of Th-Tf complex and its binding to Tf receptor on liver cells remain to be examined in detail. Moreover, it needs to be determined whether Tf protein has maintained its confirmation essential to bind with Tf receptor after binding with thorium.

A significant proportion of thorium was internalized by receptor-mediated endocytosis pathway indicating the role of certain membrane-bound receptors. This pathway needs to be

examined in detail to ascertain the identity of the receptor(s) involved in active thorium uptake. Experiments performed with ion channel inhibitors to identify the role of ion channels in thorium uptake showed that TG treatment decreases uptake of Th. Since TG mobilizes calcium from ER to cytoplasm leading to change in plasma membrane potential. This will in turn affect the uptake of Th suggesting the role of surface membrane potential in the uptake of thorium by liver cells. Further work is required to determine voltage sensitive ion transport protein for Th intra-cellularization. It is also possible that Orai1 and STIM1 may directly transport Th ions into cytoplasm, which needs to be investigated in detail using molecular models.

3.2.2. Sub-cellular distribution and intra-cellular targets of thorium

3.2.2.1. Thorium localization at sub-cellular protein fractions of WRL 68 cells

Sub-cellular protein fractionation of WRL 68 cells incubated with 10 µM thorium was also performed using sub-cellular protein fractionation kit and thorium bound to these protein fractions was determined using ICP-MS. Proteins from fractions such as cytoplasm, membrane, soluble nuclear protein, chromatin-bound proteins, and cytoskeletal proteins were obtained using protocol provided in the kit. A detailed diagrammatic representation of the protocol followed for sub-cellular protein fractionation is described in scheme 2 under Section 2.2.11. Percentage of thorium found in various protein fractions was calculated and is shown in Figure 3.23.

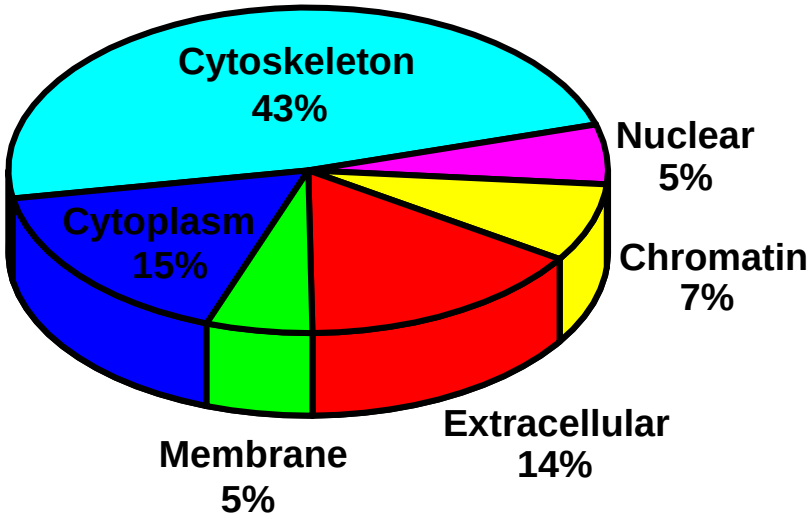

Figure 3.23: *Percentage of thorium bound to different sub-cellular protein fractions.*

In addition to protein fractionation, WRL 68 cells were also incubated with 10 µM thorium for 24 h to estimate total thorium bound to cells. The cells were harvested after trypsinization, total thorium taken up by cells was estimated using arsenazo method.

It was found that 86% of total incubated thorium i.e., 8.6 µM was associated with cells. Rest 14% of thorium which is not taken up by cells was accounted for in medium and trypsin-EDTA fraction of the cell culture. This fraction has been marked as extracellular thorium in the pie chart shown above in Figure 3.23.

To have a better understanding of the distribution of thorium among different sub-cellular protein fractions, the amount of thorium bound to proteins was normalized to thorium in nM bound to per µg of total protein present in each fraction. For this, total protein present in each sub-cellular protein fraction in µg was calculated and the amount of thorium is normalized as nM per µg of protein and is represented in Figure 3.24.

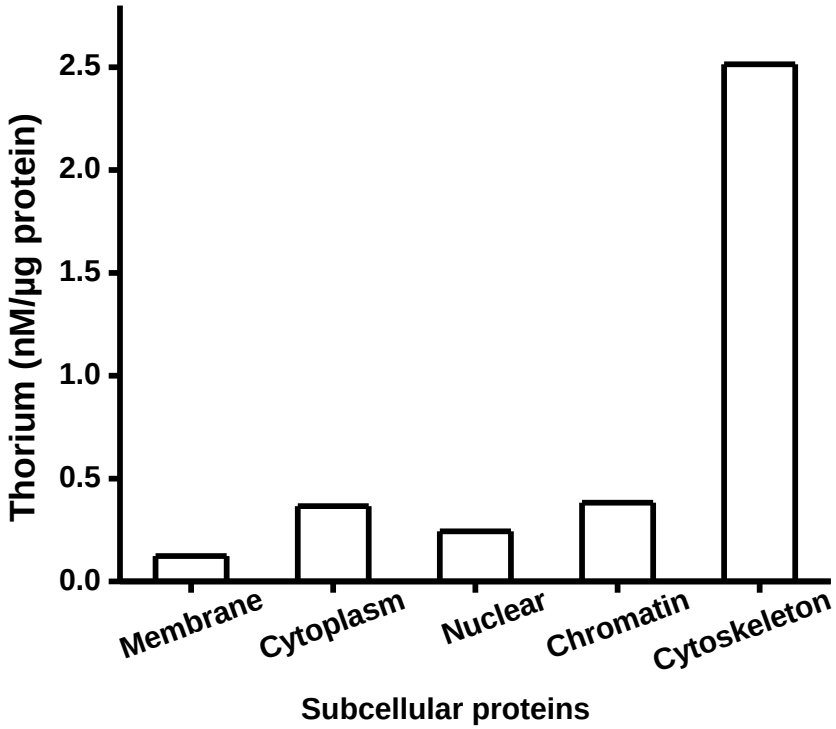

Figure 3.24: *Amount of thorium in nM bound per µg of proteins in different sub-cellular protein fractions.*

It was found that thorium was bound maximally to cytoskeletal proteins followed by cytoplasmic proteins. Chromatin-bound protein also binds substantial amount of thorium per µg of protein followed by soluble nuclear proteins. Membrane proteins bind the least amount of thorium among the sub-cellular protein fraction obtained.

3.2.2.2. TEM studies of thorium treated cells

Transmission electron microscopic (TEM) images of WRL 68 cells incubated with 10 µM thorium for 24 h were obtained to get detailed understanding of thorium distribution inside cells (Figure 3.25).

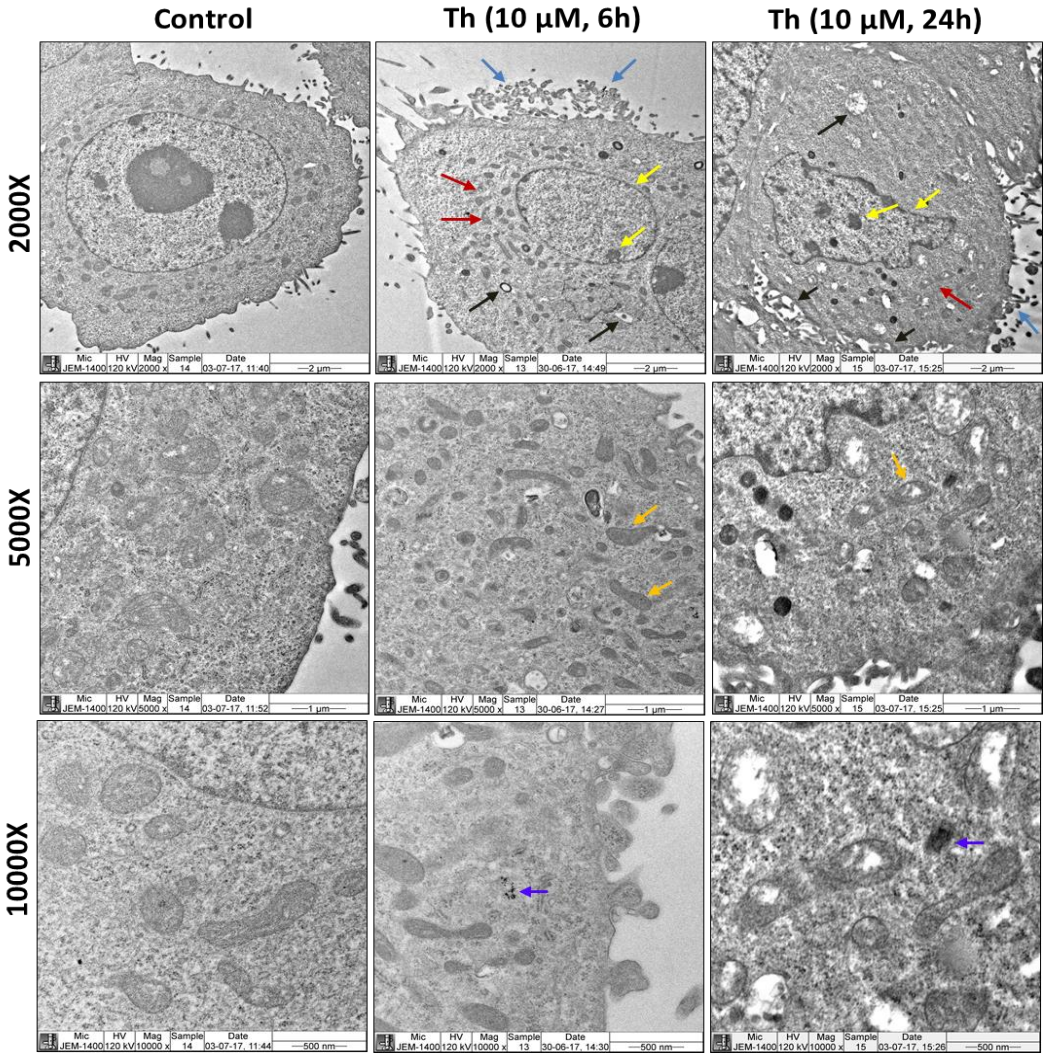

Figure 3.25: *Transmission electron microscopic (TEM) images showing effects of thorium on WRL68 cells. Cells were treated with 10 µM thorium at 6 and 24 h time points and TEM images were obtained at different magnifications i.e., 2000, 5000 and 10000X.*

Images were magnified 2000, 5000 and 10000 times and morphological alterations were studied. It was observed that thorium causes formation and aggregation of several extracellular vesicles attached closely to cellular membrane as membranous extensions indicated by blue colored arrows. These extracellular vesicles are bound very tightly to the cell membrane and could not be removed even after treating cells with trypsin-DTPA (25 mM) and washing them twice in PBS suggesting that they were produced by cells and released into

extracellular space to remove thorium from cells. Inside cytoplasm, thorium treatment led to rearrangement of mitochondria and other cellular organelles from perinuclear in control to towards one end of nucleus in thorium treated samples as shown by red arrows. It also caused nucleus to shrink in its size at 6 h treatment and lose its shape at 24 h with nucleolus disintegration marked by yellow arrows. The number and size of vacuolar structures also increased with thorium treatment in a time-dependent manner as shown by black arrows. At higher magnification, it was observed that thorium treatment led to distortion of mitochondrial structures from oval or circular to flat disc-shaped after 6 h of thorium treatment as shown by orange arrows. On further incubation till 24 h, the flat disc-shaped structures became more transparent towards both its ends indicating decrease in organelle matrix. This could be because thorium incubation upon longer time interval (24 h) may cause cellular stress and its death via mitochondrial leakage and nuclear disintegration. At highest magnification i.e., at 10000X, thorium deposits in the form of black granular aggregates can be seen in the cytoplasm as shown by brown arrows.

Several alterations are caused by incubating cells with thorium which increases with its intensity as incubation time increases. Under *in-vitro* conditions, 10 µM thorium was toxic to cells at 24 h incubation. The cellular stress leading to its death is most possibly caused by mitochondrial leakage and nuclear disintegration. Also, there is also an increased vacuolization of cellular organelles and changes in cytoskeletal structure which increases in time dependent manner. The nucleus first undergoes shrinkage followed by nucleoplasm disintegration. Uniformity in cytoplasm also underwent changes upon thorium treatment with the cytoplasmic content being more heterogeneous in conformation in thorium treated samples at longer durations (24 h) as compared to control samples suggesting possible changes in cytoskeletal structures. At higher magnifications i.e., 10000 X, thorium deposits can be seen in the

cytoplasm in the form of dark granular aggregates as marked by blue arrows in the Figure. Also, smaller dot-like dark spots can be seen in large amounts in the cytoplasm of thorium treated cells at 24 h suggesting presence of free or un-complexed thorium in the cytoplasmic matrix which may account for higher concentration of thorium in cytoskeletal fractions as is observed in sub-cellular protein fractionation experiment.

Upon its internalization, thorium was found to interact mostly with cytoskeletal proteins followed by cytoplasmic and nuclear proteins. Thorium binds to both soluble-nuclear as well as chromatin-bound proteins. A small amount of thorium was also bound to membrane proteins which could also be visualized as small, granules-like aggregates in transmission electron microscopic images. These granules are tightly attached to cell membrane and appear to be small thorium-containing particles excluded by cells into the extracellular matrix. It could also be seen that thorium binding leads to several structural alterations in cellular architecture like shrinkage of nucleus followed by its disintegration, reduction in shape and number of mitochondria and arrangement of various cellular organelles from peri-nuclear to towards one pole of nucleus. Further studies need to be performed to study the binding and interaction of thorium to various soluble-nuclear and chromatin-bound proteins, especially DNA. It would be interesting to study the binding and interaction of thorium with DNA and the effects it would cause to the structure and function of both the DNA and the genes, with thorium being a positively charged alpha emitter. Detailed studies are also required to elucidate the changes caused by the DNA damage introduced by thorium.

3.2.3. Effect of thorium in combination of external alpha radiation in carcinogenic changes in WRL 68 cells

Thorium causes both chemical as well as radiological toxicity (20,27), Since the half-life of thorium is extremely long i.e. ~ 14 billion years, most of the toxic effects exerted by thorium is mainly due to its chemical toxicity. Therefore, to investigate the effect of thorium in humans during long term exposure after its internalization, toxicity caused by radiological effects needs to be simulated to study its effect in combination with chemical toxicity. A schematic diagram describing the toxic effects of thorium under real life conditions and its representation under in-vitro conditions, where WRL 68 cells were treated continually with thorium and are irradiated by alpha particles externally to simulate similar toxic conditions, is shown below in Scheme 5. To accomplish this, an experimental plan was designed where cells were treated with external three doses of alpha particles in continuous presence of thorium. Since objective of the study was to investigate carcinogenic changes after treatment of thorium in combination of external alpha particles, cells were cultured for long-term (up to passage number 15) and alpha irradiation was done at passage 5, 10 and 15^{th}.

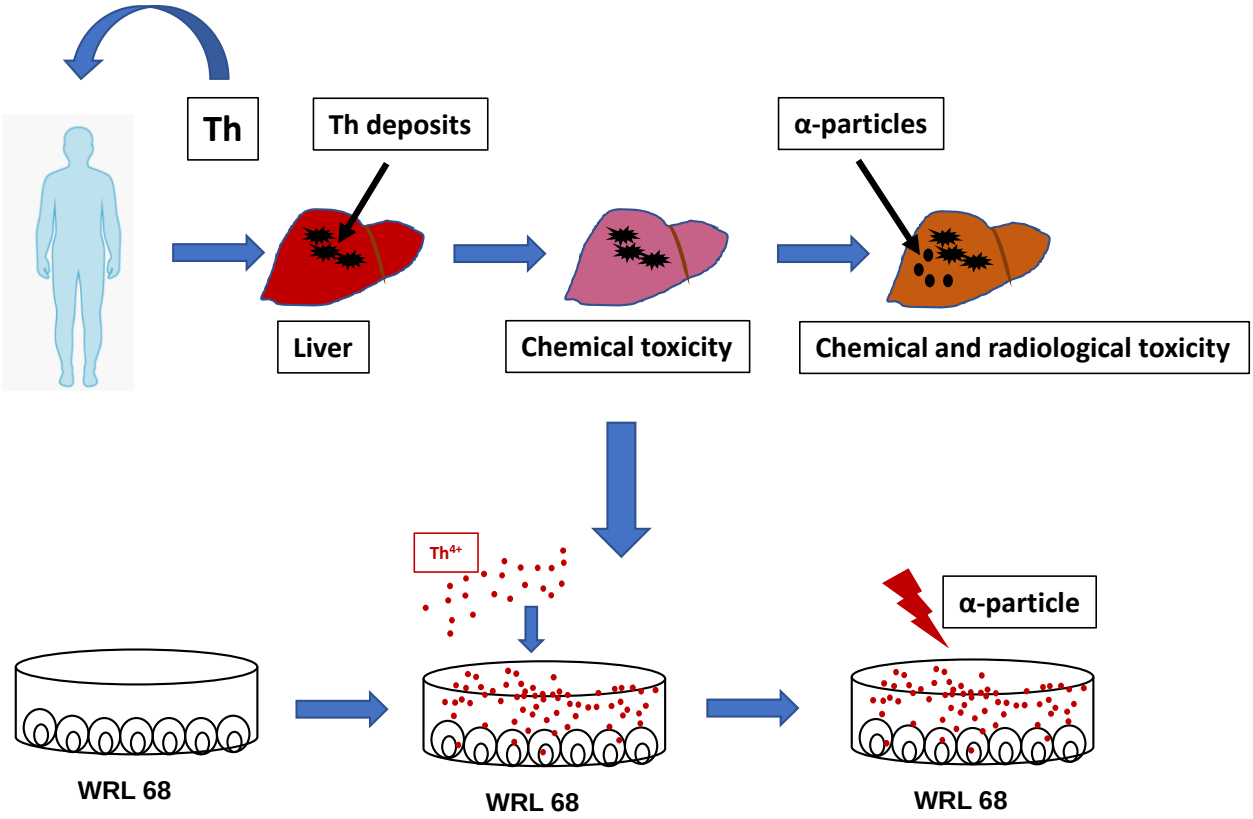

Scheme 5: *Schematic representation of thorium exposure under real life conditions and its representation under in-vitro conditions using WRL 68 cells.*

Before conducting the thorium and/or alpha irradiation experiment, optimization experiments for cell survival/proliferation and thorium uptake at different serum concentrations were done. Moreover, dose for alpha particle radiation was determined based on a clonogenic survival assay.

3.2.3.1. Optimization of serum concentration required for long term culture of WRL 68 cells

All experiments conducted for thorium uptake, its internalization and intra-cellular localization studies under *in-vitro* conditions were performed in the absence of FCS (Fetal Calf Serum) in growth medium. The present experimental plan, requires a long-term culture of cells

to study carcinogenic changes (148–150), which is not possible in the absence of FCS. Moreover, it was shown that in the absence of FCS, 10 µM of thorium causes cellular toxicity within 24 h of incubation. On the other hand, thorium may interact with protein components of FCS, which may affect the net cellular interaction/uptake of thorium. To study the long-term effects of thorium on liver cells, firstly serum concentration was optimized to grow cells and has minimum effect on thorium uptake. For this, WRL 68 cells were incubated with different concentrations of serum and their viability was determined using both MTT assay and cell counting after 72 h of incubation (Figure 3.26 A and B). Longer incubation time was chosen for this study as the main purpose is to continue incubating the cells for multiple passages to study the long-term effect of thorium on liver cells. In both cases, it was found cell viability increases with increasing serum concentration and becomes maximum at 6% serum. Serum concentration more than 6% does not cause any significant change in cell viability as is seen by both MTT assay and cell count.

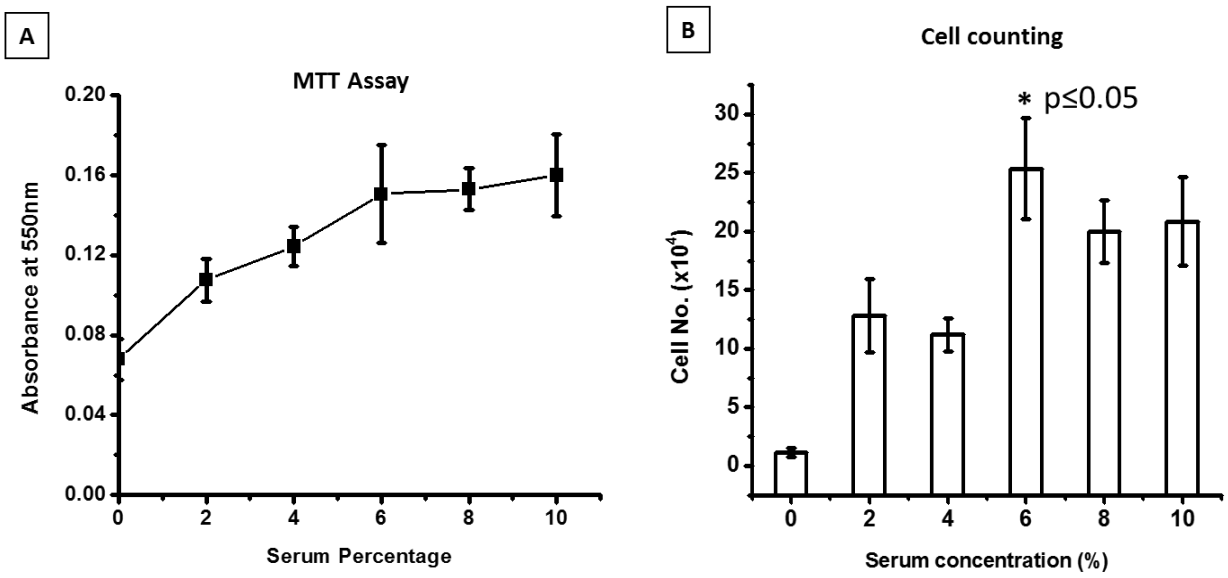

Figure 3.26 (A-B): *Optimization of serum concentration for maximal cell growth by* ***(A)*** *MTT Assay and* ***(B)*** *Cell counting.*

3.2.3.2. Thorium uptake by WRL 68 cells in serum containing media (SCM)

Thorium uptake in the presence and absence of FCS in growth medium was also studied to determine the amount of thorium taken up by cells in SCM. WRL 68 cells were seeded and incubated as described earlier. The cells were incubated with serum-free medium and serum-containing medium (6 and 10%) having thorium maintained at the final concentration of 10 µM for 48 and 72 h. Following trypsinization, different components of cell culture fractions i.e., medium, trypsin-EDTA and cells were obtained. Thorium was estimated in each fraction using arsenazo method (Figure 3.27 A-B).

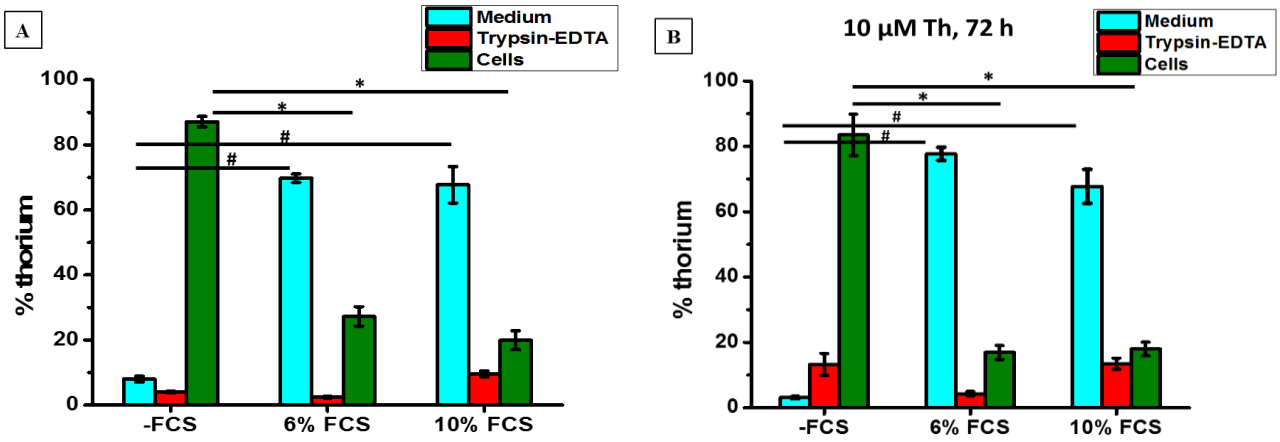

Figure 3.27 (A-B): *Thorium uptake by WRL 68 cells in the presence and absence of FCS at* ***(A)*** *48 h and* ***(B)*** *72 h incubation with 10 µM thorium.*

It was observed that at both time points, in the absence of FCS, more than ~80% of total incubated thorium was found in cells and growth medium contained negligible amount of thorium. However, upon adding 6 and 10% of FCS in growth medium, most of the incubated thorium remained in the growth medium and cells were found to contain only 20-30% of the total incubated thorium at both concentrations of serum. The amount of thorium present in medium showed significant increase upon addition of 6 and 10% FCS as compared to SFM

with a corresponding decrease in the amount of thorium found in cells and is found to be significant even at p value < 0.01. Since 10 % of FCS did not show a significant decrease in thorium uptake compared to 6 % FCS, 10 % FCS was chosen for further experiments, which would have added advantage of better survival during multiple passage experiments.

3.2.3.3. Effect of long-term in vitro thorium treatment in combination of external alpha radiation

Based on the above results, a long-term experiment of thorium exposure to liver cells was designed. For this, the cells were divided into four different groups. First group was treated as control, second group was incubated with 10 µM thorium continuously for all passages, third group was irradiated with alpha particles at 5^{th}, 10^{th}, and 15^{th} passages and the fourth group was treated with 10 µM thorium continuously in addition to external irradiation with alpha particles at 5^{th}, 10^{th}, and 15^{th} passages.

A brief overview of the experimental groups planned for this experiment is shown below.

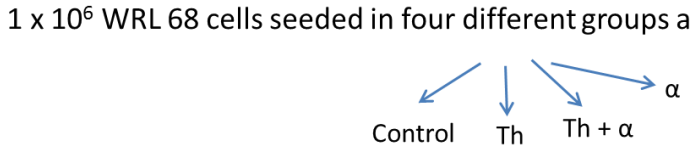

1. **Control** : No treatment. WRL 68 cells grown under standard incubation conditions
2. **Th** : incubation with 10 µM-Th
3. **Alpha (α)** : α-particle irradiation at passage 5, 10 and 15 (each dose 0.1 Gy)
4. **Th + Alpha (α)** : incubation with 10 µM-Th + α-particle irradiation at passage 5, 10 and 15 passage (each dose 0.1 Gy).

Before performing the experiment, the dose of alpha particles was first optimized by irradiating the cells with different doses of alpha particles and calculating the surviving fraction as described in Section 2.2.15. Bright field microscopic images of cells were also obtained using 20X and 40X of objective lens at passage 5, 10 and 15 to study morphological alterations caused by thorium, only alpha and thorium + alpha particle irradiation to WRL 68 cells.

Also, cells were harvested at 5^{th} and 15^{th} passage to study the gene expression alterations caused by the chemical and radiological toxicity of thorium. mRNA was isolated from all these groups and converted into cDNA. Using primers known to play a role in hepatocarcinogenesis, PCR array analysis was done to understand the genetic alterations caused due to thorium exposure and the possible pathways that might be involved in causing thorium induced cytotoxicity and carcinogenesis.

A. Dose optimization of alpha particle irradiation using surviving fraction

The dose of alpha particles used for irradiating the cells was optimized by irradiating the cells with different doses of alpha particles and measuring the surviving fraction (SF) using clonogenic assay as described in Section 2.2.15. Dose optimization of alpha particles is needed as for carcinogenic changes a sub-lethal dose is required, where sufficient fractions of cells should also survive for multiple passage experiments. Survival fraction was calculated, and a semi-logarithmic graph was plotted with survival fraction in log scale on Y-axis and alpha irradiation dose (Gy) in linear scale on X-axis as shown in Figure 3.28.

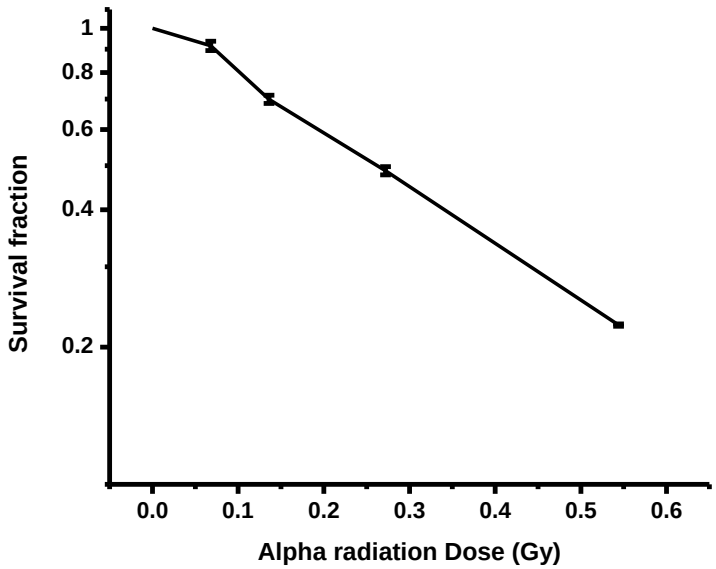

Figure 3.28: *A semi-logarithmic graph showing survival fraction on log scale against alpha irradiation dose (Gy) in linear scale.*

Based on these results, it was observed that a dose of 0.06 Gy caused more than 90% cells to survive whereas a dose of 0.13 Gy caused ~70% cells to survive. Hence, it was decided to use 0.1 Gy of alpha particle irradiation for the studies as the dose was found to be ideal in terms of toxicity as well as survival and hence, suitable for long-term toxicity study of thorium.

B. Morphological changes in thorium and alpha particle irradiated cells*:* Bright field microscopy images as shown in Figure 3.29 A-B indicate that with the treatment of thorium, alpha particle, and thorium treatment in combination with alpha particle irradiation causes release of stress particles in the surrounding medium as shown by black arrows in the 40 X magnified images (Figure 3.29 B). These particles appear to increase in size and density in proportion to the amount of stress they are exposed to. Incubation with thorium (both alone and in combination with alpha particle irradiation) causes immediate stress to cells. This could be attributed mainly to chemical toxicity of thorium, and therefore, can be accounted for the presence of more pronounced stress particles both in number and in density as compared to

alpha particle irradiated only group which mainly causes radiological toxicity and hence, the number and density of stress particles are less pronounced.

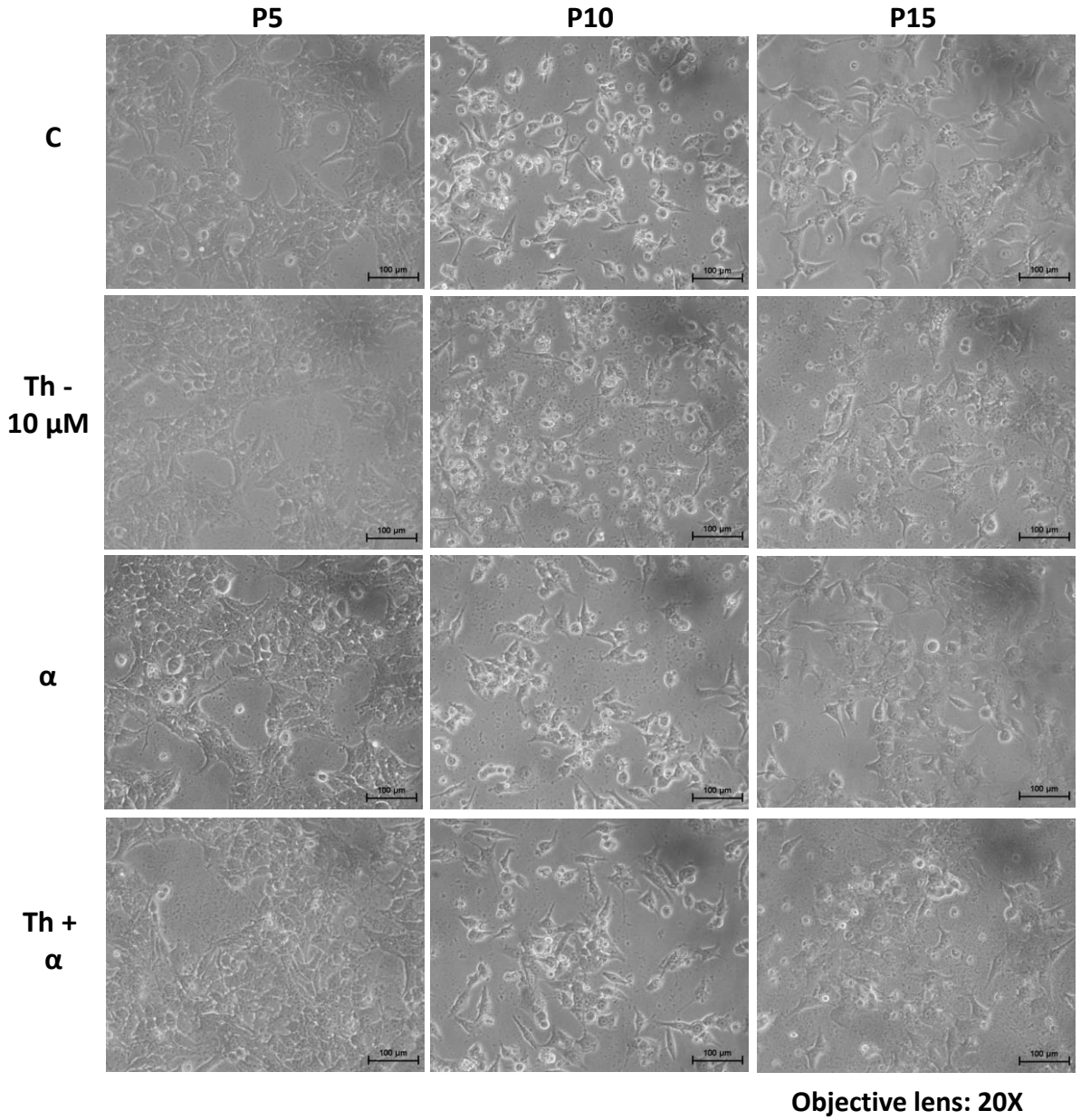

Figure 3.29 A. *Bright field microscopic images of WRL 68 cells of all four groups i.e., control, 10 µM thorium, 0.1 Gy alpha particles each at 5th, 10th and 15th passages, 10 µM thorium + 0.1 Gy alpha particles each at 5th, 10th and 15th passages. Objective: 20X. Scale 100 µM.*

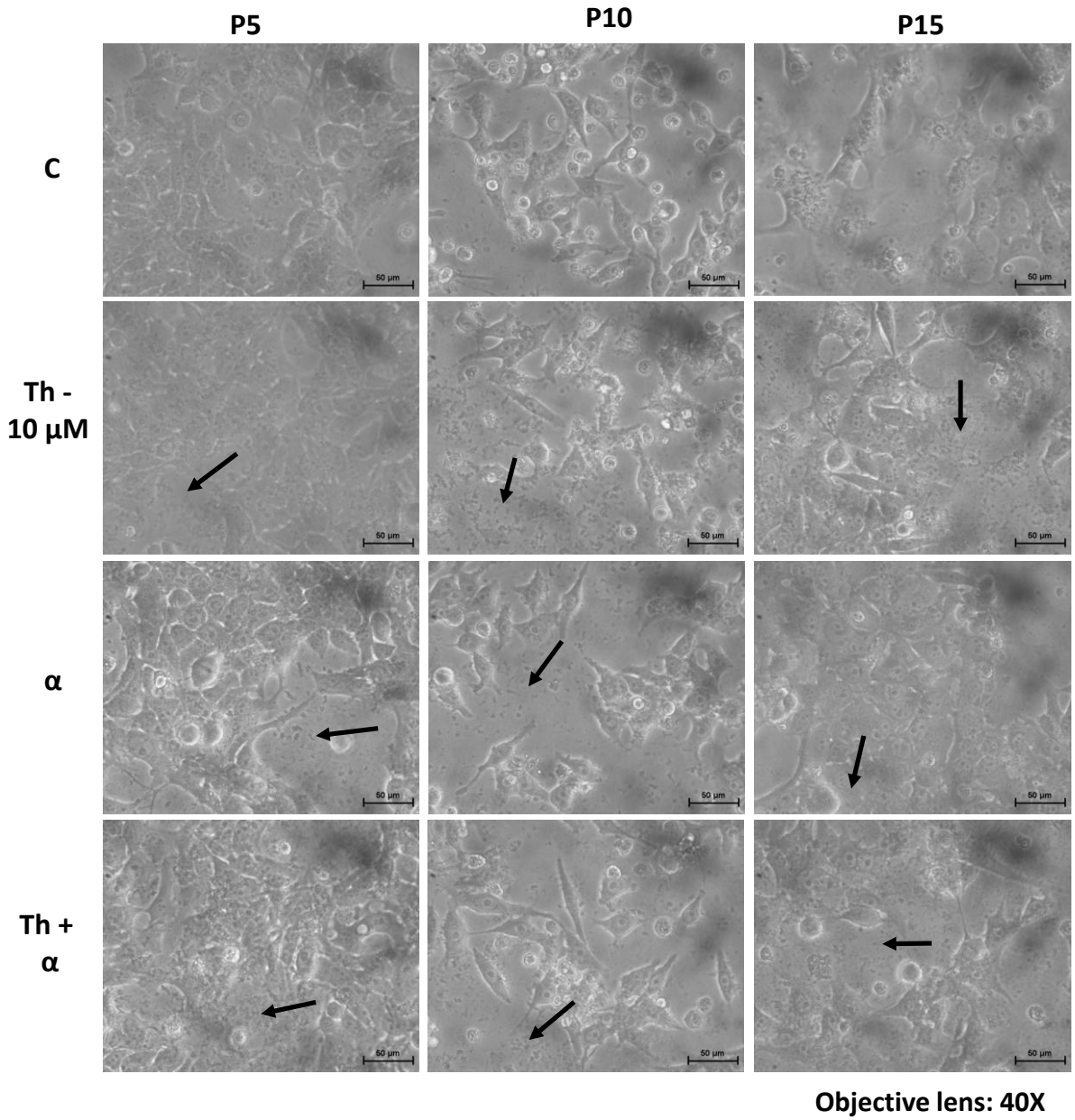

Figure 3.29 B. *Bright field microscopic images of WRL 68 cells of all four groups i.e., control, 10 µM thorium, 0.1 Gy alpha particles each at 5th, 10^{th,} and 15th passages, 10 µM thorium + 0.1 Gy alpha particles each at 5th, 10th and 15th passages. Objective: 40X. Scale 50 µM.*

C. Study of gene expression alterations upon thorium and alpha particle treatment (early passage 5th passage)

To study gene expression alterations in WRL 68 cells exposed to thorium for long-term as mentioned previously, cells from each treatment group were harvested at an early passage (P5) and at late passage (P15) to study gene expression alterations. RNA was isolated from each group using Qiagen's RNeasy® Plus Mini Kit while following the protocol provided in the kit. 2 µg of RNA was then converted into cDNA using Qiagen's RT^2 first strand kit by following the protocol provided in the kit. The cDNA was then added to RT^2 SYBR Green Master mix and added to PCR array well containing pre-fixed primers well defined for causing hepatocarcinogenesis. The PCR was run as per the set program described in detail in Materials and Methods section. A total of 84 primers known to play a role in hepatocarcinogenesis were studied in the PCR array.

Expression profile of different genes of cells treated continuously with 10 µM thorium for 5 passages showed an upregulation of 61 genes and downregulation of 20 genes. Similarly, cells irradiated with alpha-particles only at 5th passage showed an upregulation of 58 genes and downregulation of 22 genes whereas genetic expression profile of cells treated continuously with thorium for 5 passages and irradiated with alpha-particles at 5th passage showed an upregulation of 68 genes and downregulation of 13 genes (Table 3.4)

Thorium		
Symbol	Fold regulation	SD
KDR	-12813.6	0.0
PYCARD	-177.1	0.0
SOCS3	-63.5	0.0

Alpha		
Symbol	Fold regulation	SD
KDR	-265903.4	0.0
PYCARD	-920.0	0.0
SOCS3	-76.2	0.0

Thorium + alpha		
Symbol	Fold regulation	SD
KDR	-38687.8	0.0
PYCARD	-390.4	0.0
PDGFRA	-87.0	0.0

PDGFRA	-13.6	0.0
FLT1	-3.9	0.1
CXCR4	-1.8	0.4
LEF1	-1.8	0.1
RAC1	-1.7	0.6
HHIP	-1.5	0.1
CDH1	-1.3	0.0
CDKN2A	-1.2	0.2
BCL2L1	-1.2	0.1
BIRC5	-1.2	0.2
DAB2IP	-1.2	0.4
CTNNB1	-1.2	0.1
PIN1	-1.1	0.3
MSH3	-1.1	0.3
MYC	-1.0	0.1
SOCS1	-1.0	0.1
YAP1	-1.0	0.3
TP53	1.0	0.2
AKT1	1.0	0.3
ITGB1	1.0	0.1
BCL2	1.0	0.3
TLR4	1.0	0.3
CASP8	1.0	0.3
TCF4	1.0	0.2
CFLAR	1.0	0.1

PDGFRA	-15.5	0.0
TERT	-10.7	0.0
LEF1	-2.6	0.0
HHIP	-1.5	0.3
RUNX3	-1.3	0.4
DAB2IP	-1.3	0.3
MYC	-1.2	0.4
SFRP2	-1.2	0.3
NRAS	-1.1	0.7
MSH2	-1.1	0.1
BIRC5	-1.1	0.7
NFKB1	-1.1	0.4
EGF	-1.1	0.6
CDKN2A	-1.1	0.3
MSH3	-1.0	0.2
YAP1	-1.0	0.7
AKT1	-1.0	0.2
VEGFA	-1.0	0.5
PIN1	-1.0	0.3
ITGB1	1.0	0.0
CASP8	1.0	0.1
RAC1	1.0	0.7
IGFBP3	1.1	0.2
BAX	1.1	0.6
SMAD4	1.1	0.5

SOCS3	-63.0	0.0
TERT	-12.0	0.1
WT1	-5.5	0.0
ITGB1	-2.1	0.1
DLC1	-1.8	0.5
IGFBP3	-1.5	0.1
GADD45B	-1.1	0.2
MCL1	-1.1	0.4
CDH1	-1.1	0.6
MYC	-1.0	0.3
MSH3	1.1	0.0
VEGFA	1.1	0.1
EGFR	1.1	0.1
RB1	1.2	0.1
MTDH	1.2	0.2
EGF	1.2	0.1
CASP8	1.2	0.1
HHIP	1.2	0.4
DAB2IP	1.3	0.0
FZD7	1.3	0.1
CDKN2A	1.3	0.3
YAP1	1.4	0.3
AKT1	1.4	0.1
PIN1	1.5	0.2
FAS	1.5	0.1

GSTP1	1.1	0.2
PTEN	1.1	0.2
NFKB1	1.1	0.6
TGFB1	1.1	0.3
RHOA	1.1	0.2
WT1	1.1	0.6
MSH2	1.1	0.1
VEGFA	1.1	0.3
MTDH	1.1	0.0
EGFR	1.1	0.3
NRAS	1.1	0.4
IRS1	1.1	0.5
TNFRSF10B	1.2	0.2
CDKN1A	1.2	0.0
TNFSF10	1.2	0.3
BAX	1.2	0.5
SMAD4	1.2	0.3
STAT3	1.2	0.4
PTK2	1.2	0.2
XIAP	1.2	0.6
CCND1	1.3	0.3
FZD7	1.3	0.4
MET	1.3	0.4
TGFBR2	1.3	0.5
EGF	1.4	0.8

RB1	1.1	0.4
CFLAR	1.1	0.4
DLC1	1.1	0.8
XIAP	1.1	0.5
RHOA	1.1	0.9
BCL2	1.1	0.2
ANGPT2	1.2	0.3
TNFRSF10B	1.2	0.8
MET	1.2	0.3
STAT3	1.2	0.3
CDKN1A	1.2	0.5
EGFR	1.2	0.0
GADD45B	1.2	0.6
BID	1.2	0.2
TP53	1.2	0.4
TGFB1	1.2	0.5
MTDH	1.3	0.0
PTEN	1.3	0.6
IGFBP1	1.3	0.2
TGFBR2	1.3	0.2
CCND2	1.3	0.6
FZD7	1.3	0.3
CTNNB1	1.4	0.3
RASSF1	1.4	0.5
TGFA	1.4	0.3

TCF4	1.5	0.2
RAC1	1.5	0.2
TNFRSF10B	1.5	0.1
PTGS2	1.5	0.0
TP53	1.5	0.1
TGFB1	1.5	0.2
CDKN1A	1.5	0.3
SOCS1	1.6	0.0
BCL2	1.6	0.2
BCL2L1	1.6	0.2
CFLAR	1.6	0.1
TGFA	1.6	0.3
BIRC5	1.6	0.3
RHOA	1.7	0.5
BAX	1.7	0.2
XIAP	1.7	0.1
STAT3	1.7	0.3
SMAD4	1.7	0.1
PTEN	1.7	0.5
TGFBR2	1.7	0.0
PTK2	1.8	0.2
TLR4	1.8	0.5
ADAM17	1.8	0.3
CTNNB1	1.9	0.3
CXCR4	1.9	0.1

FAS	1.4	0.1
BID	1.5	0.3
CDKN1B	1.5	0.8
GADD45B	1.5	0.4
IGFBP3	1.5	0.5
TGFA	1.5	0.4
IGFBP1	1.5	0.1
E2F1	1.5	0.7
HRAS	1.6	0.8
MCL1	1.6	0.2
SMAD7	1.6	0.6
FADD	1.7	0.3
ANGPT2	1.7	1.1
PTGS2	1.8	0.4
ADAM17	1.8	0.4
EP300	1.8	0.8
RELN	2.2	1.9
RUNX3	2.4	0.3
BIRC2	2.6	0.5
IGF2	2.6	3.0
CCL5	2.9	0.9
CCND2	3.1	0.2
OPCML	4.1	0.7
RB1	4.8	5.5
FHIT	7.0	2.3

TCF4	1.4	0.3
MCL1	1.4	0.2
PTK2	1.4	0.8
CCND1	1.4	0.7
GSTP1	1.4	1.0
FAS	1.4	0.3
SOCS1	1.4	0.5
SMAD7	1.5	1.0
CDH1	1.5	0.5
CDKN1B	1.5	0.5
FLT1	1.5	0.1
HRAS	1.5	0.8
TNFSF10	1.5	0.0
E2F1	1.6	1.0
ADAM17	1.6	0.4
IRS1	1.6	0.5
CXCR4	1.7	0.0
TLR4	1.7	1.3
FADD	1.7	1.2
PTGS2	1.8	0.4
BCL2L1	1.8	1.6
EP300	1.8	0.7
CCL5	1.9	0.3
BIRC2	2.8	1.0
IGF2	3.1	0.5

CCND1	2.0	0.2
BID	2.1	0.7
GSTP1	2.2	0.4
NRAS	2.2	0.9
E2F1	2.2	0.3
SMAD7	2.2	0.3
CDKN1B	2.3	0.3
ANGPT2	2.3	0.8
TNFSF10	2.3	0.5
RUNX3	2.5	2.5
RASSF1	2.5	0.1
HRAS	2.6	0.1
IGFBP1	2.8	2.6
EP300	2.8	0.2
FADD	3.0	0.4
RELN	3.2	1.1
BIRC2	3.3	0.3
FLT1	3.4	0.7
CCND2	3.4	0.3
FHIT	4.0	1.7
CCL5	4.3	1.0
NFKB1	8.2	9.4
IRS1	17.8	22.5
LEF1	137.3	193.9
IGF2	329.2	460.6

TERT	7.5	9.8	RELN	3.7	2.0	CDH13	549.1	69.8
RASSF1	38.1	52.6	FHIT	4.0	1.0	MET	1274.6	1800.5

Table 3.4: *List of genes upregulated and downregulated in WRL 68 cells upon various treatment regimes. The genes which are upregulated are marked in red color and the genes downregulated are marked in blue color.*

The data was further analyzed, and genes with fold change (2 or more folds) differential gene expression (DEGs) were also studied. In case of cells treated continuously with 10 µM thorium for 5 passages, genes such as *FADD, PTGS2, ADAM17, EP300, RUNX3, BIRC2, CCL5, CCND2, OPCML, FHIT* (total 10 genes) were found to be upregulated and genes such as *KDR PYCARD, SOCS3, PDGFRA, FLT1, CXCR4, LEF1, RAC1* (total 08 genes) were found to be downregulated by 2 or more folds (Figure 3.30 A). Similarly, when cells were irradiated with 0.1 Gy alpha particles at 5th passage, genes such as *CXCR4, PTGS2, EP300, CCL5, BIRC2, IGF2, FHIT* (total 07 genes) were found to be upregulated and genes such as *KDR, PYCARD, SOCS3, PDGFRA, TERT, LEF1* (total 06 genes) were found to be downregulated by 2 or more folds (Figure 3.30B). When cells were treated continuously with 10 µM thorium for 5 passages followed by 0.1 Gy alpha-particle irradiation at 5th passage, a total of 28 genes i.e. *SMAD4, PTEN, TGFBR2, PTK2, TLR4, ADAM17, CTNNB1, CXCR4, CCND1, BID, GSTP1, NRAS, E2F1, SMAD7, CDKN1B, ANGPT2, TNFSF10, RASSF1, HRAS, EP300, FADD, RELN, BIRC2, FLT1, CCND2, FHIT, CCL5, CDH13* were found to be upregulated and around 08 genes namely, *KDR, PYCARD, PDGFRA, SOCS3, TERT, WT1, ITGB1, DLC1* were found to be downregulated (Figure 3.30C). The extent of increase and decrease of fold regulation of these DEGs were plotted and is shown in Figure 3.30 (A-C).

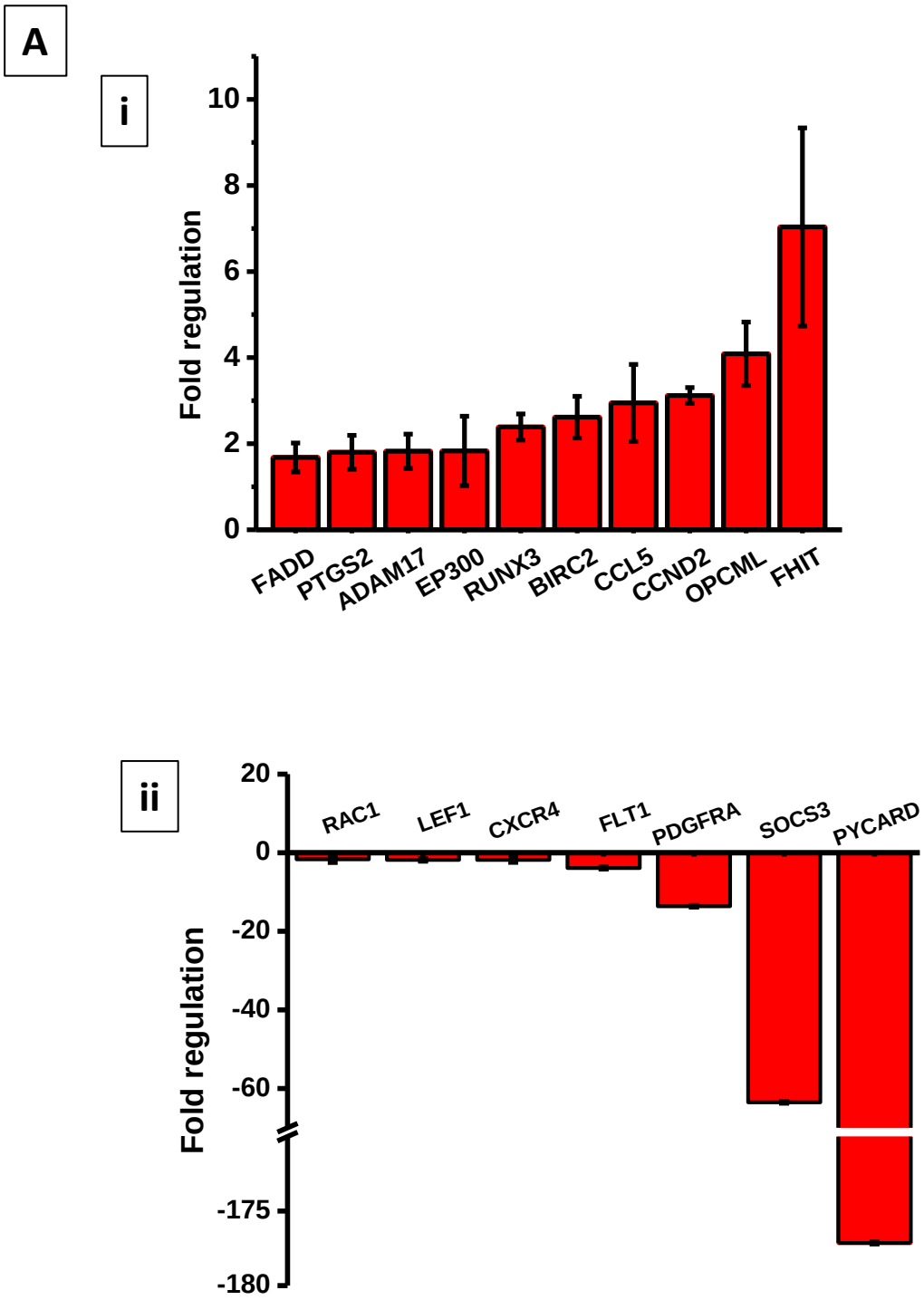
A
i
Fold regulation
10
8
6
4
2
0
FADD
PTGS2
ADAM17
EP300
RUNX3
BIRC2
CCL5
CCND2
OPCML
FHIT
ii
Fold regulation
20
0
-20
-40
-60
-175
-180
RAC1
LEF1
CXCR4
FLT1
PDGFRA
SOCS3
PYCARD

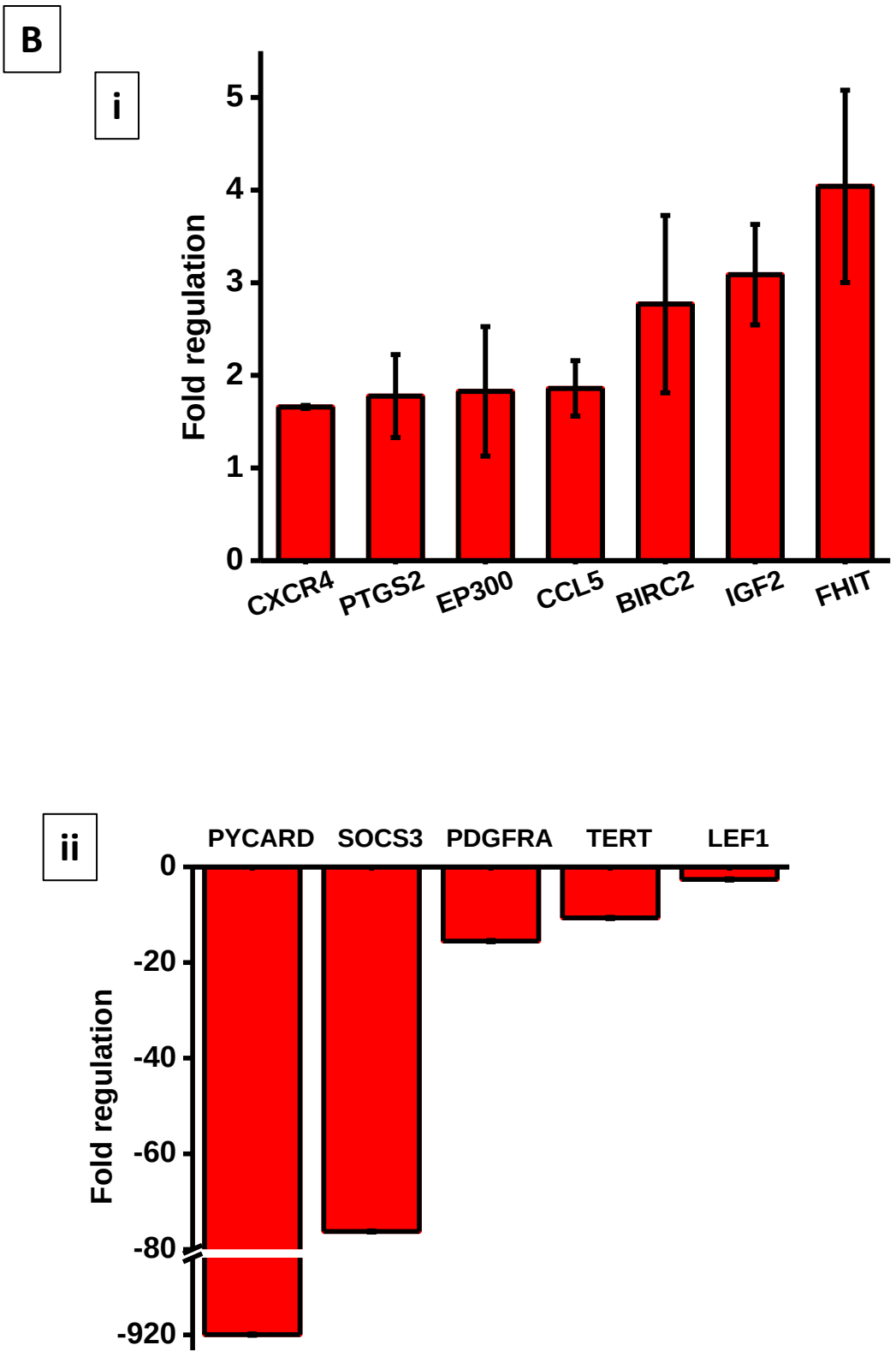
B
i
Fold regulation
0
1
2
3
4
5
CXCR4
PTGS2
EP300
CCL5
BIRC2
IGF2
FHIT
ii
PYCARD
SOCS3
PDGFRA
TERT
LEF1
Fold regulation
0
-20
-40
-60
-80
-920

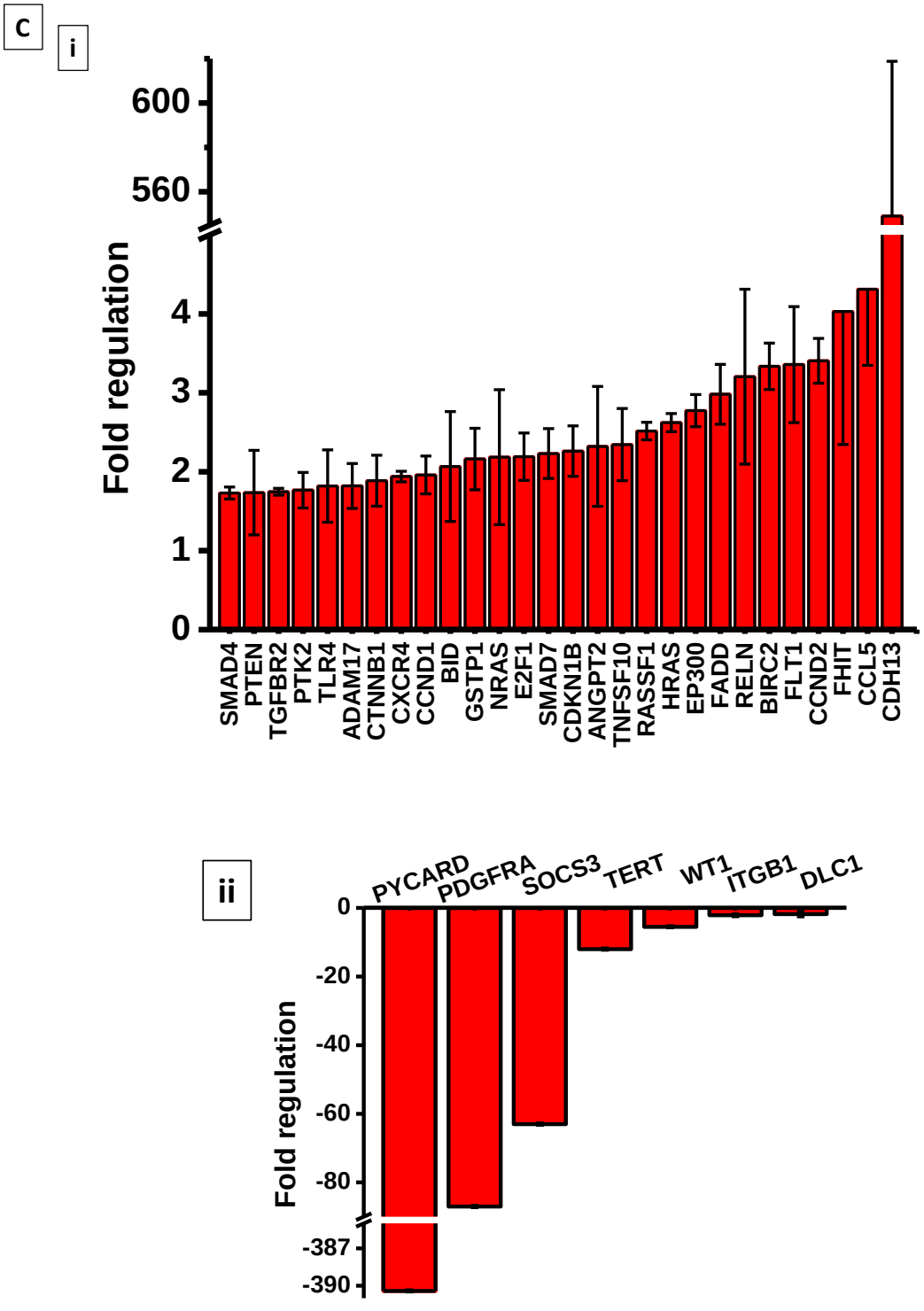

Figure 3.30: *Expression profile of differentially expressed genes (DEGs) with two or more folds differential expression in human liver cells (WRL 68) after* ***(A)*** *continuous treatment with*

10 µM thorium for 5 passages ***(i)*** *upregulated (10 genes) and* ***(ii)*** *downregulated (07 genes),* ***(B)*** *treatment with 0.1 Gy alpha-particle irradiation after 5th passage* ***(i)*** *upregulated (07 genes) and* ***(ii)*** *downregulated (05 genes) and* ***(C)*** *continuous treatment with 10 µM thorium for 5 passages followed by alpha-particle irradiation at 5th passage* ***(i)*** *upregulated (28 genes) and* ***(ii)*** *downregulated (07 genes).*

Further studies were carried out using these DEGs with two or more folds differential expression. String Network Functional Enrichment Analysis was performed with these DEGs across all groups and various protein interactions were mapped (Figure 3.31 A-C).

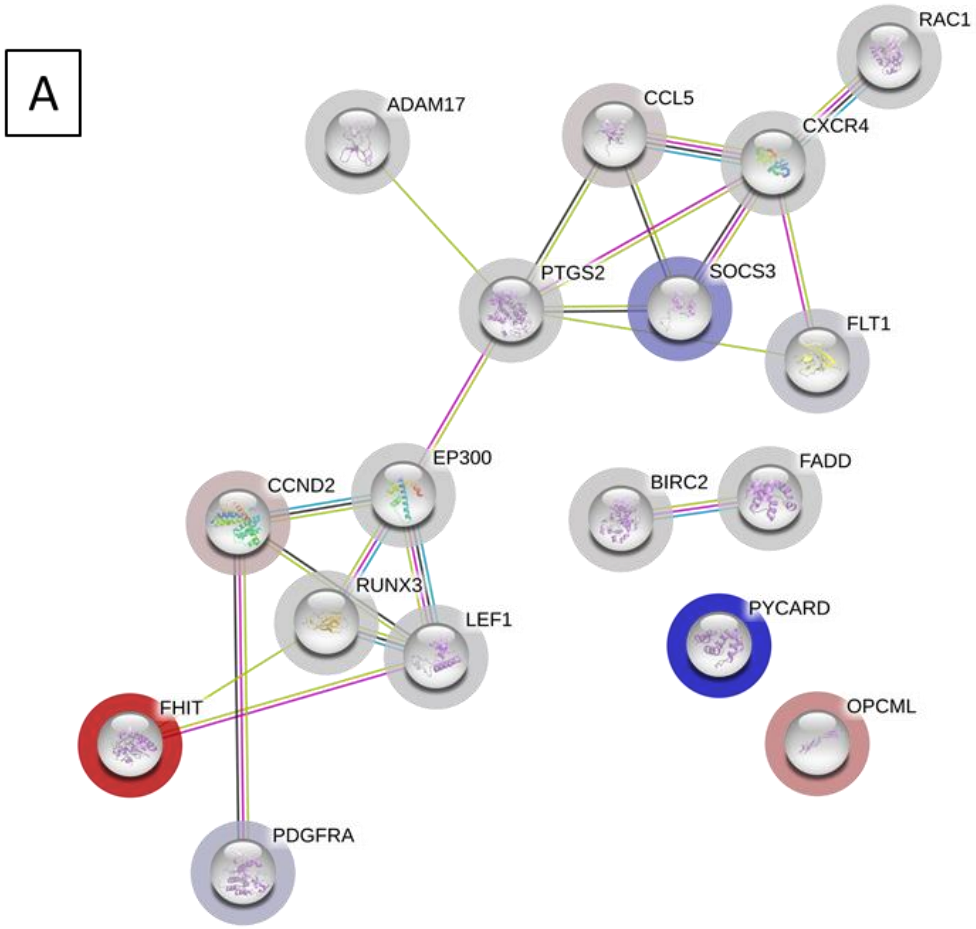

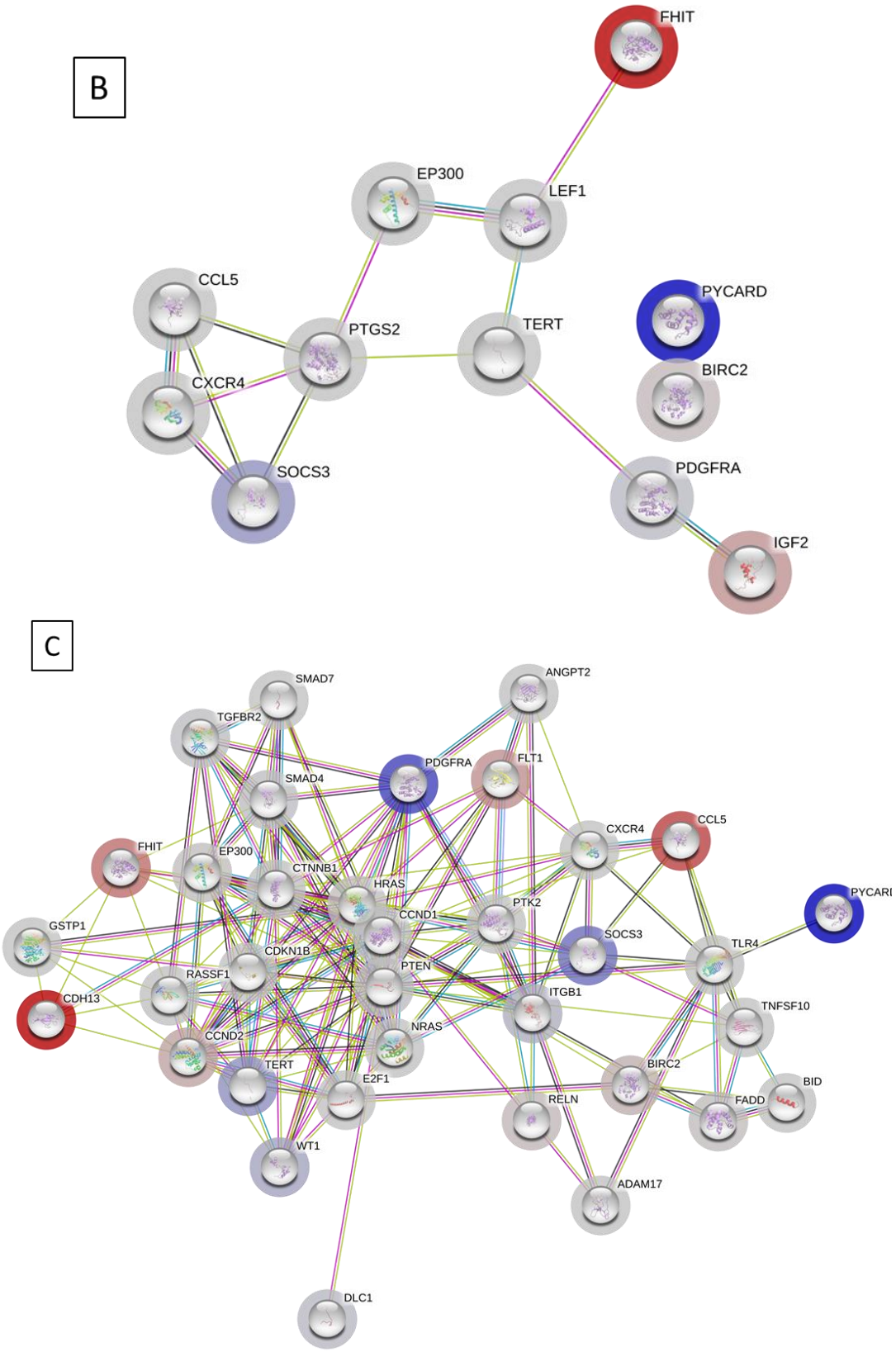

Figure 3.31: *Interaction among two or more folds differentially expressed genes (DEGs) in*

WRL 68 cells as shown by String Network Functional Enrichment Analysis, version 11.0, after ***(A)*** *continuous treatment with 10 µM thorium* ***(B)*** *irradiation with 0.1 Gy alpha-particle* ***(C)*** *continuous treatment with 10 µM thorium followed by bombarding the cells with α-particles at 5th passage. The proteins shown with red coloration showed maximum upregulation and in blue coloration showed maximum downregulation.*

Venn diagram was made to study the common genes which were upregulated and downregulated across all treatment groups after 5 passages of growth and is shown in Figure 3.32. Figure 3.32 A shows all the common genes across all three treatment groups which were upregulated, and Figure 3.32 B shows all common genes downregulated after treatment across all three groups after 5 passages. The total number of genes upregulated and downregulated in each group is expressed in brackets. All common genes upregulated and downregulated are listed out among each group while the number of unique genes among all groups are expressed in numbers.

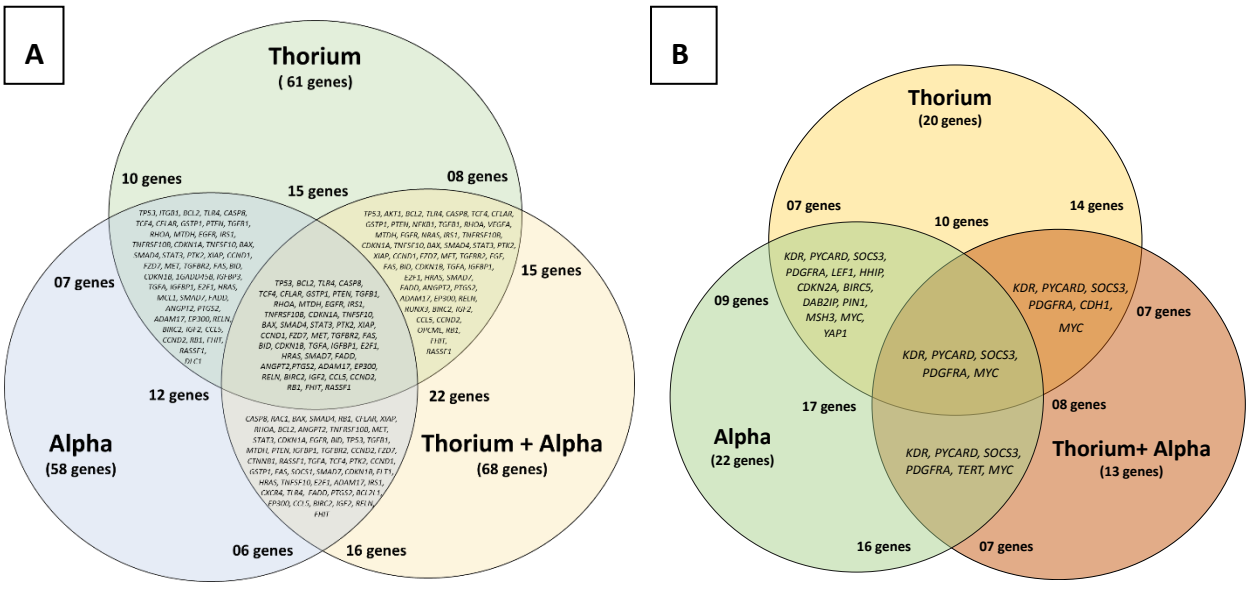

Figure 3.32: *Venn diagram showing all common genes which were* ***(A)*** *upregulated and* ***(B)*** *downregulated across all three treatment groups after 5 passages. The total number of genes*

upregulated and downregulated are shown in brackets. Common genes are listed out and number of unique genes are written in numbers.

Table 3.5 below lists the five most highly upregulated and downregulated genes across all three groups at P5.

Group	Upregulated genes	Downregulated genes
Thorium	*FHIT (7.0±2.3), OPCML (4.1±0.7), CCND2 (3.1±0.2), CCL5 (2.9±0.9), BIRC2 (2.6±0.5)*	*KDR (-12813.6±0.00), PYCARD (-177.1±0.01), SOCS3 (-63.5±0.00), PDGFRA (-13.6±0.01), FLT1 (-3.9±0.07)*
Alpha	*FHIT (4.0±1.0), IGF2 (3.1±0.5), BIRC2 (2.8±0.9), CCL5 (1.9±0.3), EP300 (1.8±0.7)*	*KDR (-265903.3±0.00), PYCARD (-920±0.001), SOCS3 (-76.2±0.01), PDGFRA (-15.5±0.05), TERT (-10.7±0.02)*
Th +Alpha	*CDH13 (549.1±69.8), CCL5 (4.3±1), FHIT (4±1.7), CCND2 (3.4±0.3), FLT1 (3.4±0.7)*	*KDR (-12813.6±0.00), PYCARD (-390.4±0.00), PDGFRA (-87±0.01), SOCS3 (-63±0.00), TERT (-12±0.06)*

Table 3.5: *List of 05 most highly upregulated and downregulated genes across all three groups at P5. The genes upregulated are marked in red color and downregulated genes are marked in blue color and the number in bracket shows the fold regulation with standard deviation of each gene as compared to control.*

All these DEGs with two or more-fold regulation were also studied for their role in different pathways using KEGG pathway software analysis. The top 15 pathways are presented below in a tabular form (Table 3.6 A-C):

No.	Altered pathways	Number of genes altered in each pathway ()
1	**Pathways in cancer**	*BID, BIRC2, CCND2, CDKN1B, EP300, FADD, GADD45B, HRAS, IGF2, PTGS2, RAC1, RASSF1, RB1, TERT, TGFA, CXCR4, HHIP, LEF1, PDGFRA* **(20)**
2	**PI3K-Akt signaling**	*ANGPT2, CCND2, CDKN1B, HRAS, IGF2, MCL1, RELN, TGFA, FLT1, PDGFRA, KDR, RAC1* **(12)**
3	**Human papillomavirus infection**	*CCND2, CDKN1B, E2F1, EP300, FADD, HRAS, PTGS2, RB1, RELN, TERT* ***(10)***
4	**Human cytomegalovirus infection**	*BID, CCL5, E2F1, FADD, HRAS, PTGS2, RB1, CXCR4, RAC1, PDGFRA* ***(10)***
5	**Kaposi sarcoma-associated herpesvirus infection**	*ANGPT2, BID, E2F1, EP300, FADD, HRAS, PTGS2, RB1, LEF1, RAC1* ***(10)***
6	**Epstein-Barr virus infection**	*BID, CCND2, CDKN1B, E2F1, FADD, GADD45B, RB1, RUNX3, RAC1* ***(9)***
7	**MAPK signaling**	*ANGPT2, GADD45B, HRAS, IGF2, TGFA, FLT1, KDR, PDGFRA, RAC1* ***(9)***
8	**Ras signaling**	*ANGPT2, HRAS, IGF2, RASSF1, TGFA, FLT1, KDR, PDGFRA, RAC1* ***(9)***
9	**MicroRNAs in cancer**	*CCND2, CDKN1B, E2F1, EP300, HRAS, MCL1, PTGS2, RASSF1, PDGFRA* ***(9)***

10	**Hepatocellular carcinoma**	*E2F1, GADD45B, HRAS, IGF2, RB1, TERT, TGFA, LEF1* ***(8)***
11	**Prostate cancer**	*CDKN1B, E2F1, EP300, HRAS, RB1, TGFA, LEF1, PDGFRA* ***(8)***
12	**Focal adhesion**	*BIRC2, CCND2, HRAS, RAC1, RELN, FLT1, KDR, PDGFRA* ***(8)***
13	**Gastric cancer**	*CDKN1B, E2F1, GADD45B, HRAS, RB1, TERT, LEF1* ***(7)***
14	**Non-small cell lung cancer**	*E2F1, FHIT, GADD45B, HRAS, RASSF1, RB1, TGFA* ***(7)***
15	**Small cell lung cancer**	*BIRC2, CDKN1B, E2F1, FHIT, GADD45B, PTGS2, RB1* ***(7)***

A: Thorium treatment continuously for 5 passages

No.	Altered pathways	Number of genes altered in each pathway ()
1	**Pathways in cancer**	*BCL2L1, BIRC2, CDH1, CDKN1B, CXCR4, E2F1, EP300, FADD, HRAS, IGF2, PTGS2, HHIP, LEF1, PDGFRA, TERT* **(15)**
2	**PI3K-Akt signaling**	*BCL2L1, CDKN1B, FLT1, HRAS, IGF2, IRS1, RELN, TLR4, KDR, PDGFRA* ***(10)***
3	**Human papillomavirus infection**	*CDKN1B, E2F1, EP300, FADD, HRAS, PTGS2, RELN, TERT* ***(8)***
4	**Influenza A**	*CCL5, EP300, FADD, TLR4, TNFSF10, PYCARD, SOCS3* ***(7)***

5	**Salmonella infection**	*BIRC2, FADD, HRAS, TLR4, TNFSF10, LEF1, PYCARD* ***(7)***
6	**Human cytomegalovirus infection**	*CCL5, CXCR4, E2F1, FADD, HRAS, PTGS2, PDGFRA* ***(7)***
7	**MicroRNAs in cancer**	*CDKN1B, E2F1, EP300, HRAS, IRS1, PTGS2, PDGFRA* ***(7)***
8	**Hepatocellular carcinoma**	*BCL2L1, E2F1, HRAS, IGF2, LEF1, TERT* ***(6)***
9	**NOD-like receptor signaling**	*BCL2L1, BIRC2, CCL5, FADD, TLR4, PYCARD* ***(6)***
10	**Small cell lung cancer**	*BCL2L1, BIRC2, CDKN1B, E2F1, FHIT, PTGS2* ***(6)***
11	**Gastric cancer**	*CDH1, CDKN1B, E2F1, HRAS, LEF1, TERT* ***(6)***
12	**Prostate cancer**	*CDKN1B, E2F1, EP300, HRAS, LEF1, PDGFRA* ***(6)***
13	**Focal adhesion**	*BIRC2, FLT1, HRAS, RELN, KDR, PDGFRA* ***(6)***
14	**Kaposi sarcoma-associated herpesvirus infection**	*E2F1, EP300, FADD, HRAS, PTGS2, LEF1* ***(6)***
15	**Ras signaling**	*BCL2L1, FLT1, HRAS, IGF2, KDR, PDGFRA* ***(6)***

B: Irradiated with 0.1 Gy alpha particles at 5thpassage

No.	Altered pathways	Number of genes altered in each pathway ()
1	**Pathways in cancer**	*BAX, BCL2, BCL2L1, BID, BIRC2, BIRC5, CCND1, CCND2, CDKN1A, CDKN1B, CTNNB1, CXCR4, E2F1, EP300, FADD, FAS, GSTP1, HRAS, IGF2, LEF1, MET, NFKB1, NRAS, PTEN, PTGS2, PTK2, RAC1, RASSF1, RHOA, SMAD4, STAT3, TGFA, TGFB1, TGFBR2, TP53, XIAP, ITGB1, PDGFRA, TERT* **(39)**
2	**PI3K-Akt signaling**	*ANGPT2, BCL2, BCL2L1, CCND1, CCND2, CDKN1A, CDKN1B, FLT1, HRAS, IGF2, IRS1, ITGB1, MET, NFKB1, NRAS, PTEN, PTK2, RAC1, RELN, TGFA, TLR4, TP53, KDR, PDGFRA* ***(24)***
3	**Human papillomavirus infection**	*BAX, CCND1, CCND2, CDKN1A, CDKN1B, CTNNB1, E2F1, EP300, FADD, FAS, HRAS, ITGB1, NFKB1, NRAS, PTEN, PTGS2, PTK2, RELN, TP53, TERT* ***(20)***
4	**Human cytomegalovirus infection**	*BAX, BID, CCL5, CCND1, CDKN1A, CTNNB1, CXCR4, E2F1, FADD, FAS, HRAS, NFKB1, NRAS, PTGS2, PTK2, RAC1, RHOA, STAT3, TP53, PDGFRA* ***(20)***
5	**MicroRNAs in cancer**	*BCL2, CCND1, CCND2, CDKN1A, CDKN1B, E2F1, EP300, HRAS, IRS1, MET, NFKB1, NRAS, PTEN, PTGS2, RASSF1, RHOA, SOCS1, STAT3, TP53, PDGFRA* ***(20)***
6	**Hepatocellular carcinoma**	*BAX, BCL2L1, CCND1, CDKN1A, CTNNB1, E2F1, GSTP1, HRAS, IGF2, LEF1, MET, NRAS, PTEN, SMAD4, TGFA, TGFB1, TGFBR2, TP53, TERT* ***(19)***

7	**Hepatitis B**	*BAX, BCL2, BID, BIRC5, CDKN1A, E2F1, EP300, FADD, FAS, HRAS, NFKB1, NRAS, SMAD4, STAT3, TGFB1, TGFBR2, TLR4, TP53* ***(18)***
8	**Kaposi sarcoma-associated herpesvirus infection**	*ANGPT2, BAX, BID, CCND1, CDKN1A, CTNNB1, E2F1, EP300, FADD, FAS, HRAS, LEF1, NFKB1, NRAS, PTGS2, RAC1, STAT3, TP53* ***(18)***
9	**Proteoglycans in cancer**	*CCND1, CDKN1A, CTNNB1, FAS, HRAS, IGF2, ITGB1, MET, NRAS, PTK2, RAC1, RHOA, STAT3, TGFB1, TLR4, TP53, KDR* ***(17)***
10	**Human T-cell leukemia virus 1 infection**	*BAX, BCL2L1, CCND1, CCND2, CDKN1A, E2F1, EP300, HRAS, NFKB1, NRAS, PTEN, SMAD4, TGFB1, TGFBR2, TP53, XIAP, TERT* ***(17)***
11	**Focal adhesion**	*BCL2, BIRC2, CCND1, CCND2, CTNNB1, FLT1, HRAS, ITGB1, MET, PTEN, PTK2, RAC1, RELN, RHOA, XIAP, KDR, PDGFRA* ***(17)***
12	**Colorectal cancer**	*BAX, BCL2, BIRC5, CCND1, CDKN1A, CTNNB1, HRAS, LEF1, NRAS, RAC1, RHOA, SMAD4, TGFA, TGFB1, TGFBR2, TP53* ***(16)***
13	**Prostate cancer**	*BCL2, CCND1, CDKN1A, CDKN1B, CTNNB1, E2F1, EP300, GSTP1, HRAS, LEF1, NFKB1, NRAS, PTEN, TGFA, TP53, PDGFRA* ***(16)***
14	**Apoptosis**	*BAX, BCL2, BCL2L1, BID, BIRC2, BIRC5, CFLAR, FADD, FAS, HRAS, NFKB1, NRAS, TNFRSF10B, TNFSF10, TP53, XIAP* ***(16)***

15	**Gastric cancer**	*BAX, BCL2, CCND1, CDKN1A, CDKN1B, CTNNB1, E2F1, HRAS, LEF1, MET, NRAS, SMAD4, TGFB1, TGFBR2, TP53, TERT* ***(16)***

C: Thorium treatment continuously for5 passages in combination with 0.1 Gy α-particle irradiation at 5th passage.

Table: 3.6. List *of pathways altered by more than two folds differentially expressed genes (DEGs) after* ***(A)*** *continuous treatment with 10 µM thorium* ***(B)*** *alpha-particle irradiation of dose 0.1 Gy at 5th passage* ***(C)*** *continuous treatment with 10 µM thorium followed by bombarding the cells with α-particles at 5th passages as mapped by KEGG pathway. Genes upregulated are represented in red color and downregulated genes are represented in blue color and the total number of DEGs expressed in brackets.*

Alterations of gene expression when WRL 68 cells were treated with all three treatment groups as described above continuously for 5 passages were obtained by PCR array and it was observed that many oncogenes and genes which promote onset and progression of hepatocellular carcinoma (HCC) were genes upregulated and many tumor suppressor genes which suppress the growth of HCC were downregulated suggesting a strong probability of development of HCC in humans upon thorium exposure. Genes such as *TP53, BCL2, TLR4, CASP8, TCF4, CFLAR, GSTP1, PTEN, TGFB1, RHOA, MTDH, EGFR, IRS1, TNFRSF10B, CDKN1A, TNFSF10, BAX, SMAD4, STAT3, PTK2, XIAP, CCND1, FZD7, MET, TGFBR2, FAS, BID, CDKN1B, TGFA, IGFBP1, E2F1, HRAS, SMAD7, FADD, ANGPT2,PTGS2, ADAM17, EP300, RELN, BIRC2, IGF2, CCL5, CCND2, RB1, FHIT, RASSF1 etc.* which play a key role in HCC were over-expressed in all three treatment groups and tumor suppressor genes such as *KDR, PYCARD, SOCS3, PDGFRA, MYC* were downregulated which augmented the probability of growth and development of HCC upon treatment with all three groups. These

genes altered expression also led to the activation of various carcinogenic pathways. Pathways such as PI3K-Akt signaling, Human papillomavirus infection, Human cytomegalovirus infection, Kaposi sarcoma-associated herpesvirus infection, MicroRNAs in cancer, Hepatocellular carcinoma, Prostate cancer, Focal adhesion, Gastric cancer pathways were the topmost carcinogenic pathways whose genes were found to have altered expression upon treatment across all groups.

D. Study of gene expression alterations upon thorium and alpha particle treatment (late passage 15th passage)

As mentioned earlier, the same treatments were continued, and cells were harvested after 15 passages also. PCR array was performed with cells and same set of analysis across all experimental groups were performed to study the effects of chemical as well as radiological toxicity of thorium on cells upon exposure for longer-duration.

When cells were treated continuously with 10 µM thorium for 15 passages, PCR array data analysis showed an increased regulation of 43 genes and downregulation of 38 genes out of all the 84 genes studied for their role in hepatocarcinogenesis. In another set where cells were irradiated with 0.1 Gy alpha-particles at 5th passage were continued to grow under standard cell culture growth conditions and irradiated again with 0.1 Gy alpha-particles at 10th and 15th passage. The cells were harvested after 15th passage and studied for genetic alterations using PCR array. The data analysis of these cells showed an upregulation of 39 genes and downregulation of 42 genes. Similar experiment performed on third group of cells where cells were treated continuously with 10 µM thorium and irradiated with 0.1 Gy alpha particles at 5th passage were continued to grow under standard culture conditions while being exposed continuously with 10 µM thorium and irradiated again with 0.1 Gy alpha particles at 10th and 15th passage. The cells were harvested after 15th passage and PCR array analysis were

performed on them as mentioned above. It was found that this group of cells showed an upregulation of 55 genes while a total of 27 genes were found to be downregulated as shown in Table 3.7.

Thorium			Alpha			Thorium + Alpha		
Symbol	Fold regulation	SD	Symbol	Fold regulation	SD	Symbol	Fold regulation	SD
CDH13	-1019.8	0.0	CDH1	-70.1	0.0	CDH13	-1453.1	0.0
CDH1	-89.2	0.0	OPCML	-57.7	0.0	OPCML	-12.3	0.1
OPCML	-20.6	0.0	NFKB1	-21.6	0.0	NFKB1	-10.2	0.0
CCND2	-17.4	0.0	CCND2	-18.3	0.0	CDH1	-3.5	0.4
NFKB1	-13.7	0.0	FZD7	-2.5	0.1	GADD45B	-2.6	0.0
RELN	-4.9	0.0	RASSF1	-2.4	0.1	GSTP1	-2.3	0.3
IGFBP3	-4.4	0.1	DAB2IP	-2.4	0.1	RAC1	-1.9	0.2
SOCS3	-4.1	0.2	CDKN1B	-2.3	0.1	RASSF1	-1.8	0.0
CDKN1B	-2.9	0.1	RUNX3	-2.2	0.4	E2F1	-1.7	0.1
STAT3	-2.3	0.6	E2F1	-2.2	0.0	IGFBP1	-1.6	0.8
RAC1	-2.0	0.1	ANGPT2	-2.2	0.0	ITGB1	-1.3	0.5
MSH3	-2.0	0.0	BCL2	-2.2	0.1	CTNNB1	-1.3	0.4
RASSF1	-1.8	0.1	SMAD4	-2.1	0.2	PTGS2	-1.3	0.0
YAP1	-1.8	0.7	RELN	-2.0	0.0	TP53	-1.3	0.3
TP53	-1.8	0.3	STAT3	-2.0	0.3	STAT3	-1.3	0.1
DAB2IP	-1.6	0.2	MSH3	-1.7	0.2	FADD	-1.3	0.1
NRAS	-1.6	0.1	PYCARD	-1.7	0.1	LEF1	-1.2	0.7
SMAD4	-1.6	0.1	CASP8	-1.6	0.2	FAS	-1.2	1.1
FZD7	-1.5	0.2	SOCS3	-1.5	0.2	SMAD4	-1.2	0.3

TGFB1	-1.4	0.2
RB1	-1.4	0.2
E2F1	-1.4	0.1
HRAS	-1.4	0.2
XIAP	-1.3	0.4
CTNNB1	-1.3	0.2
VEGFA	-1.3	0.9
RUNX3	-1.3	0.7
PIN1	-1.3	0.1
GADD45B	-1.3	0.8
CFLAR	-1.3	0.1
RHOA	-1.2	0.0
TCF4	-1.2	0.1
SOCS1	-1.2	0.1
IRS1	-1.1	0.7
EP300	-1.1	0.3
PTGS2	-1.0	0.1
PTK2	-1.0	0.0
CDKN2A	-1.0	0.1
BAX	1.0	0.2
EGFR	1.1	0.1
GSTP1	1.1	0.1
MCL1	1.2	0.2
MYC	1.3	0.0
MTDH	1.3	0.1

CTNNB1	-1.5	0.2
RAC1	-1.5	0.3
TGFB1	-1.4	0.2
PTGS2	-1.4	0.3
MCL1	-1.4	0.1
CFLAR	-1.4	0.2
NRAS	-1.4	0.3
TLR4	-1.4	0.5
GADD45B	-1.3	0.2
BCL2L1	-1.3	0.2
TNFSF10	-1.3	0.4
TP53	-1.3	0.3
WT1	-1.3	1.1
PIN1	-1.3	0.2
EP300	-1.2	0.3
TGFA	-1.2	0.4
FADD	-1.1	0.4
IRS1	-1.1	0.6
SOCS1	-1.1	0.6
EGFR	-1.1	0.1
IGF2	-1.1	0.8
MTDH	-1.0	0.3
FAS	-1.0	0.5
AKT1	1.0	0.3
XIAP	1.1	0.3

CDKN2A	-1.2	0.4
MCL1	-1.2	0.1
CFLAR	-1.1	0.3
EGFR	-1.1	0.2
NRAS	-1.1	0.3
CDKN1B	-1.1	0.7
BID	-1.0	0.4
RHOA	-1.0	0.3
CASP8	1.0	0.0
MYC	1.0	0.2
TGFB1	1.1	0.2
MTDH	1.1	0.2
RB1	1.1	0.2
HRAS	1.1	0.2
BCL2	1.1	0.1
PTEN	1.1	0.1
CXCR4	1.1	0.2
BCL2L1	1.3	0.0
YAP1	1.3	0.3
PDGFRA	1.3	0.1
AKT1	1.3	0.3
DAB2IP	1.3	0.8
PTK2	1.3	0.0
VEGFA	1.3	0.0
ADAM17	1.4	0.4

TNFSF10	1.3	0.3
CDKN1A	1.3	0.0
TNFRSF10B	1.3	0.5
BID	1.3	0.7
PTEN	1.4	0.3
MSH2	1.4	0.0
ITGB1	1.4	0.1
BCL2L1	1.6	1.4
IGFBP1	1.6	0.5
CCND1	1.6	0.9
FAS	1.7	0.1
MET	1.8	0.0
BIRC5	1.8	0.6
TLR4	1.8	0.2
PYCARD	1.9	0.5
BIRC2	2.0	1.3
HHIP	2.3	0.3
CXCR4	2.3	0.4
PDGFRA	2.4	0.8
SMAD7	2.5	0.4
EGF	2.6	0.1
IGF2	2.9	2.0
BCL2	3.6	4.1
FADD	4.9	4.1
SFRP2	5.4	5.6

RHOA	1.1	0.3
YAP1	1.1	0.7
PTK2	1.1	0.3
MYC	1.1	0.3
HRAS	1.1	0.3
RB1	1.1	0.4
ITGB1	1.1	0.2
IGFBP3	1.1	0.2
TNFRSF10B	1.1	0.4
CXCR4	1.1	0.3
LEF1	1.2	0.7
MET	1.2	0.3
BID	1.3	0.3
TCF4	1.3	0.5
BAX	1.3	0.6
MSH2	1.4	0.5
TERT	1.5	0.1
GSTP1	1.5	0.7
HHIP	1.5	0.2
CCND1	1.5	0.7
PTEN	1.5	0.5
KDR	1.7	0.2
VEGFA	1.8	0.5
CDKN2A	1.8	0.2
CDKN1A	1.9	0.9

MSH3	1.5	1.1
TCF4	1.6	0.7
XIAP	1.7	0.3
EP300	1.7	0.6
CDKN1A	1.7	0.0
TLR4	1.7	0.4
BIRC5	1.7	0.7
BAX	1.7	0.2
CCND1	1.8	0.6
TNFRSF10B	1.8	0.2
TGFA	2.0	1.0
PIN1	2.4	1.8
ANGPT2	2.5	1.5
MET	2.8	1.3
WT1	2.9	0.4
PYCARD	2.9	0.4
CCL5	3.5	3.4
BIRC2	3.8	1.3
SMAD7	4.6	1.6
TNFSF10	4.7	5.6
SFRP2	5.8	1.8
IRS1	5.9	6.8
CCND2	6.5	9.1
RELN	8.4	11.2
TGFBR2	13.0	3.1

TGFBR2	6.3	1.4	BIRC5	1.9	0.5	FZD7	13.7	2.3
ADAM17	6.9	7.8	CDH13	2.2	0.2	SOCS3	17.5	24.2
CCL5	7.2	2.4	SMAD7	2.4	1.3	TERT	20.5	25.2
CASP8	7.2	9.3	IGFBP1	2.4	0.4	HHIP	33.0	37.5
TGFA	8.4	10.0	EGF	2.7	0.3	EGF	70.8	74.8
DLC1	8.7	10.9	SFRP2	3.0	0.9	MSH2	339.7	478.3
AKT1	12.8	16.9	BIRC2	3.8	0.3	RUNX3	406.2	573.6
LEF1	51.1	71.2	TGFBR2	4.5	1.9	DLC1	420.8	510.0
ANGPT2	56.4	78.4	CCL5	9.1	4.0	SOCS1	514.4	725.7
KDR	243.1	343.7	ADAM17	14.8	19.0	IGF2	794.0	1118.3
WT1	1291.7	1826.7	FHIT	15.4	3.4	FHIT	1555.5	2190.2
TERT	1370.7	1936.6	DLC1	167.0	235.0	KDR	29611.2	4625.3

Table 3.7: *List of genes upregulated and downregulated in WRL 68 cells upon various treatment regimes. The genes which are upregulated are marked in red color and the genes downregulated are marked in blue color.*

The genetic expression profiles were studied in further detail with genes having differential expression (both upregulated and downregulated) of two or more folds. The expression levels of these DEGs were plotted and compared across all three treatment groups for the possible pathways causing genetic alterations in cells upon long-term thorium exposure in humans. When cells were treated continuously with 10 µM thorium for 15 passages and their genetic expression profile were studied for DEGs with fold regulation 2 or more as compared to control, it was found that genes such as *FAS, MET, BIRC5, TLR4, PYCARD, BIRC2, HHIP, CXCR4, PDGFRA, SMAD7, EGF, IGF2, BCL2, FADD, SFRP2, TGFBR2, ADAM17, CCL5, CASP8, TGFA, DLC1, AKT1, LEF1, ANGPT2, KDR, WT1, TERT*(total 27)

were upregulated two or more folds whereas genes such as *CDH13, CDH1, OPCML, CCND2, NFKB1, RELN, IGFBP3, SOCS3, CDKN1B, STAT3, RAC1, MSH3, RASSF1, YAP1, TP53*(total 15 genes) were downregulated (Figure 3.33 A). In case when cells were grown under standard culture conditions and irradiated with 0.1 Gy alpha particles only at 5^{th}, 10^{th} and 15^{th} passages, a total of 13 genes were found to be significantly upregulated whereas 17 genes were significantly downregulated. Genes such as *KDR, VEGFA, CDKN2A, CDKN1A, BIRC5, CDH13, IGFBP1, EGF, SFRP2, BIRC2, TGFBR2, CCL5, FHIT* were upregulated and *CDH1, OPCML, NFKB1, CCND2, FZD7, RASSF1, DAB2IP, CDKN1B, RUNX3, E2F1, ANGPT2, BCL2, SMAD4, RELN, STAT3, MSH3, PYCARD* were found to be downregulated (Figure 3.33 B). Similarly, in third experimental group where cells were treated continuously with 10 µM thorium and irradiated with 0.1 Gy alpha particles at 5^{th}, 10^{th} and 15^{th} passages showed a total of 18 genes i.e., *XIAP, EP300, CDKN1A, TLR4, BIRC5, BAX, CCND1, TNFRSF10B, TGFA, ANGPT2, MET, WT1, PYCARD, BIRC2, SMAD7, SFRP2, TGFBR2, FZD7*to be upregulated and genes such as *CDH13, OPCML, NFKB1, CDH1, GADD45B, GSTP1, RAC1, RASSF1, E2F1*(total 09 genes) to be downregulated (Figure 3.33 C).

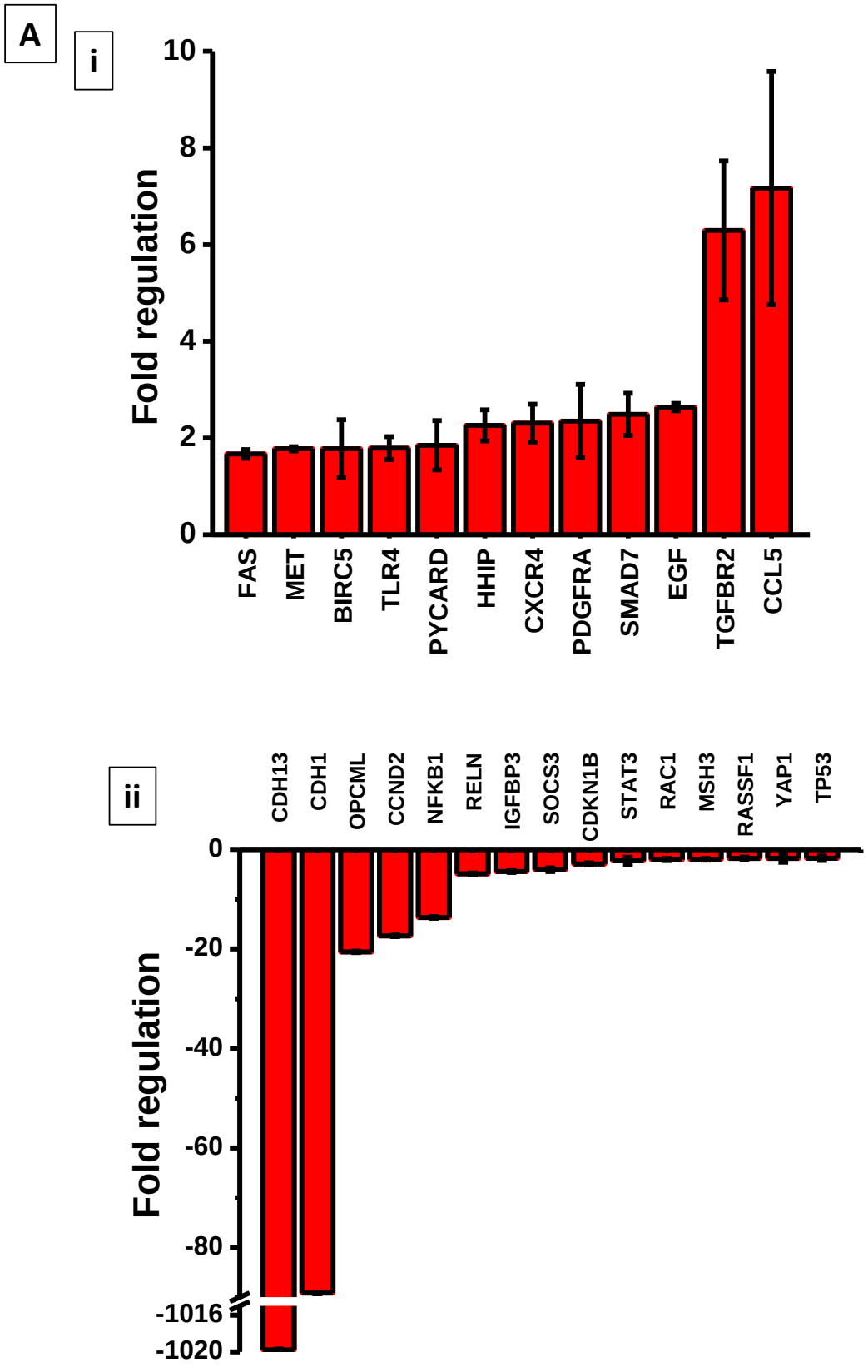
A
i
Fold regulation
10
8
6
4
2
0
FAS
MET
BIRC5
TLR4
PYCARD
HHIP
CXCR4
PDGFRA
SMAD7
EGF
TGFBR2
CCL5
ii
Fold regulation
0
-20
-40
-60
-80
-1016
-1020
CDH13
CDH1
OPCML
CCND2
NFKB1
RELN
IGFBP3
SOCS3
CDKN1B
STAT3
RAC1
MSH3
RASSF1
YAP1
TP53

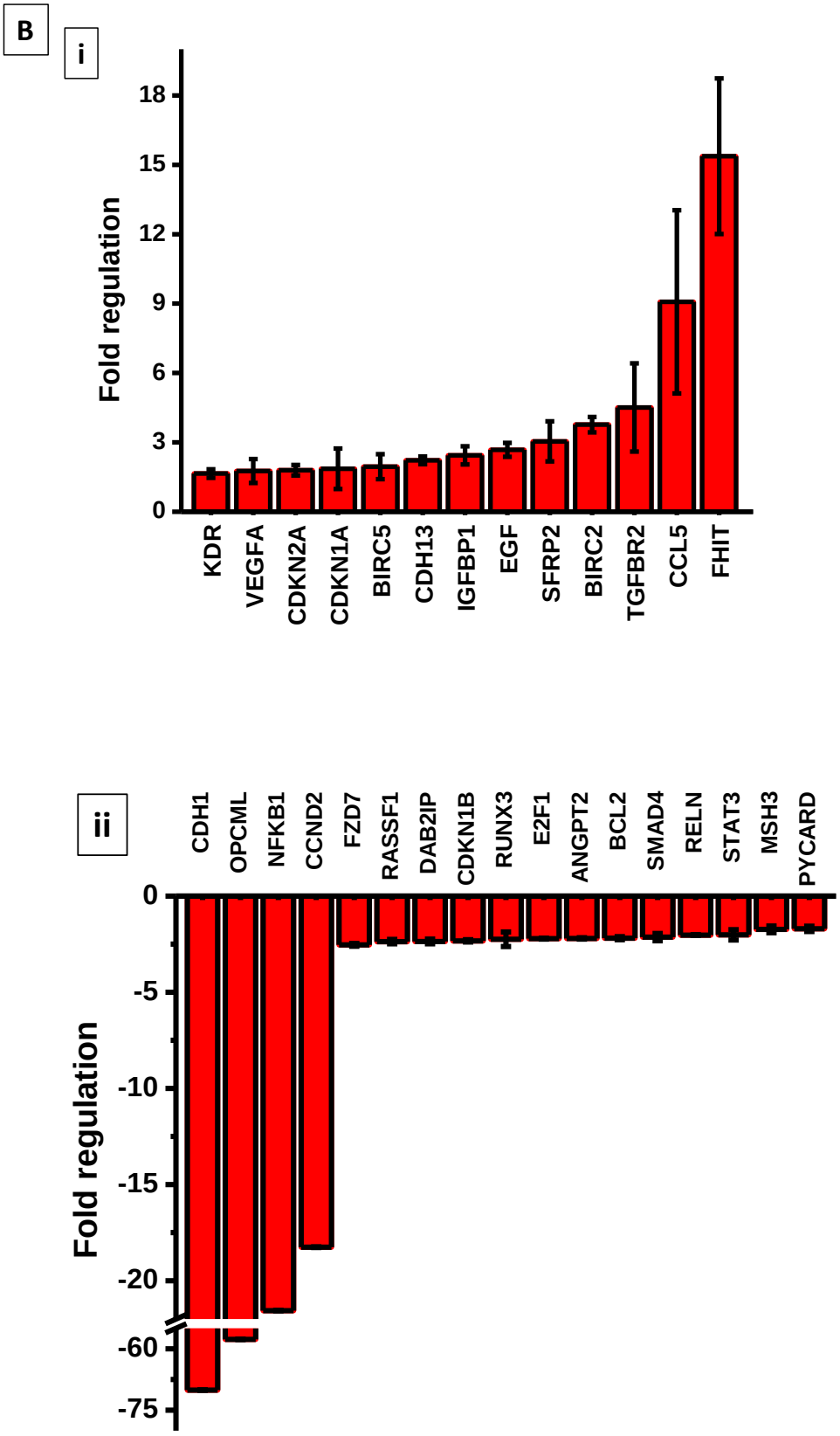
B
i
Fold regulation
18
15
12
9
6
3
0
KDR
VEGFA
CDKN2A
CDKN1A
BIRC5
CDH13
IGFBP1
EGF
SFRP2
BIRC2
TGFBR2
CCL5
FHIT
ii
Fold regulation
0
-5
-10
-15
-20
-60
-75
CDH1
OPCML
NFKB1
CCND2
FZD7
RASSF1
DAB2IP
CDKN1B
RUNX3
E2F1
ANGPT2
BCL2
SMAD4
RELN
STAT3
MSH3
PYCARD

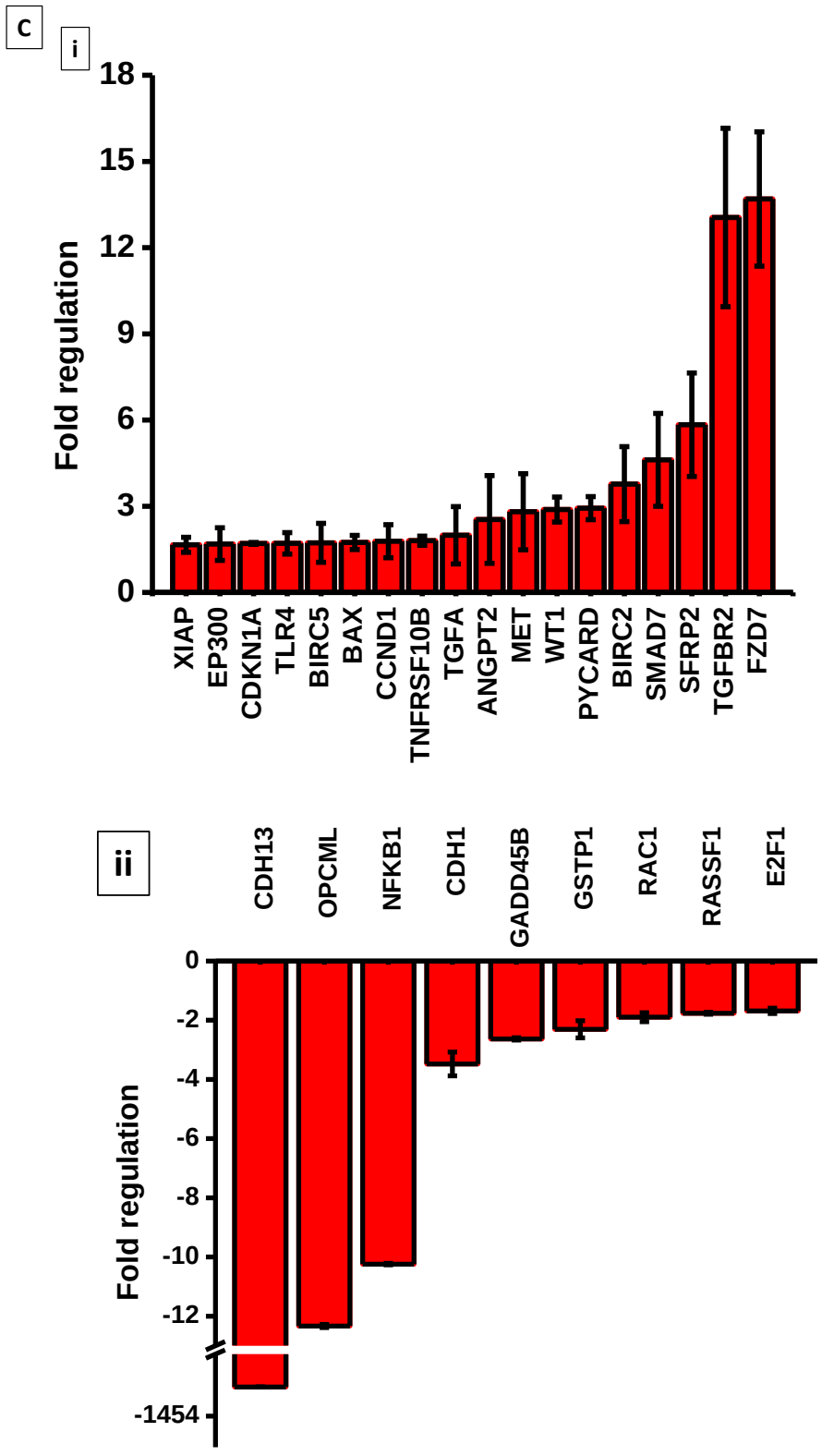

Figure 3.33: *Expression profile of differentially expressed genes (DEGs) with two or more folds of differential expression in human liver cells (WRL 68) after* ***(A)*** *continuous treatment*

with 10 µM thorium for 15 passages ***(i)*** *upregulated (27 genes) and* ***(ii)*** *downregulated (15 genes),* ***(B)*** *treatment with 0.1 Gy alpha-particle irradiation after 5th, 10th and 15th passage* ***(i)*** *upregulated (13 genes) and* ***(ii)*** *downregulated (17 genes) and* ***(C)*** *continuous treatment with .10 µM thorium for 15 passages followed by alpha-particle irradiation at 5th, 10th and 15th passage* ***(i)*** *upregulated (18) genes and* ***(ii)*** *downregulated (09 genes).*

The proteins encoded by these DEGs were studied for their interaction amongst each other using String Network Functional Enrichment Analysis. Proteins playing a key role in the interactions were mapped and are shown in Figure 3.34 A-C.

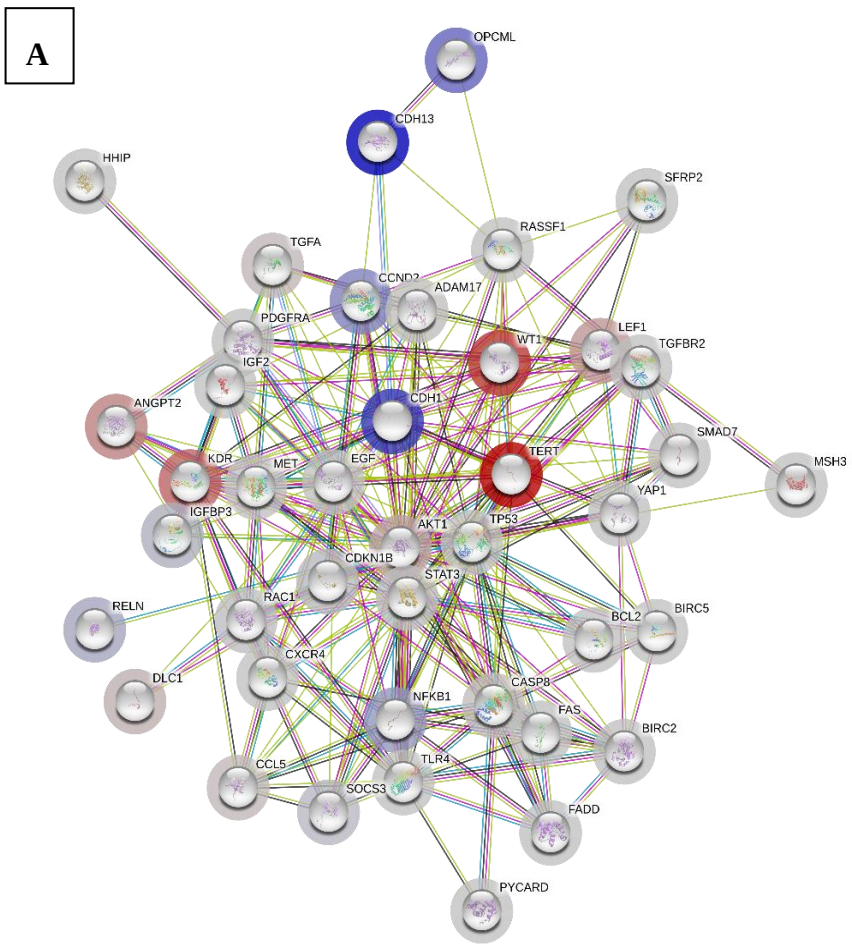

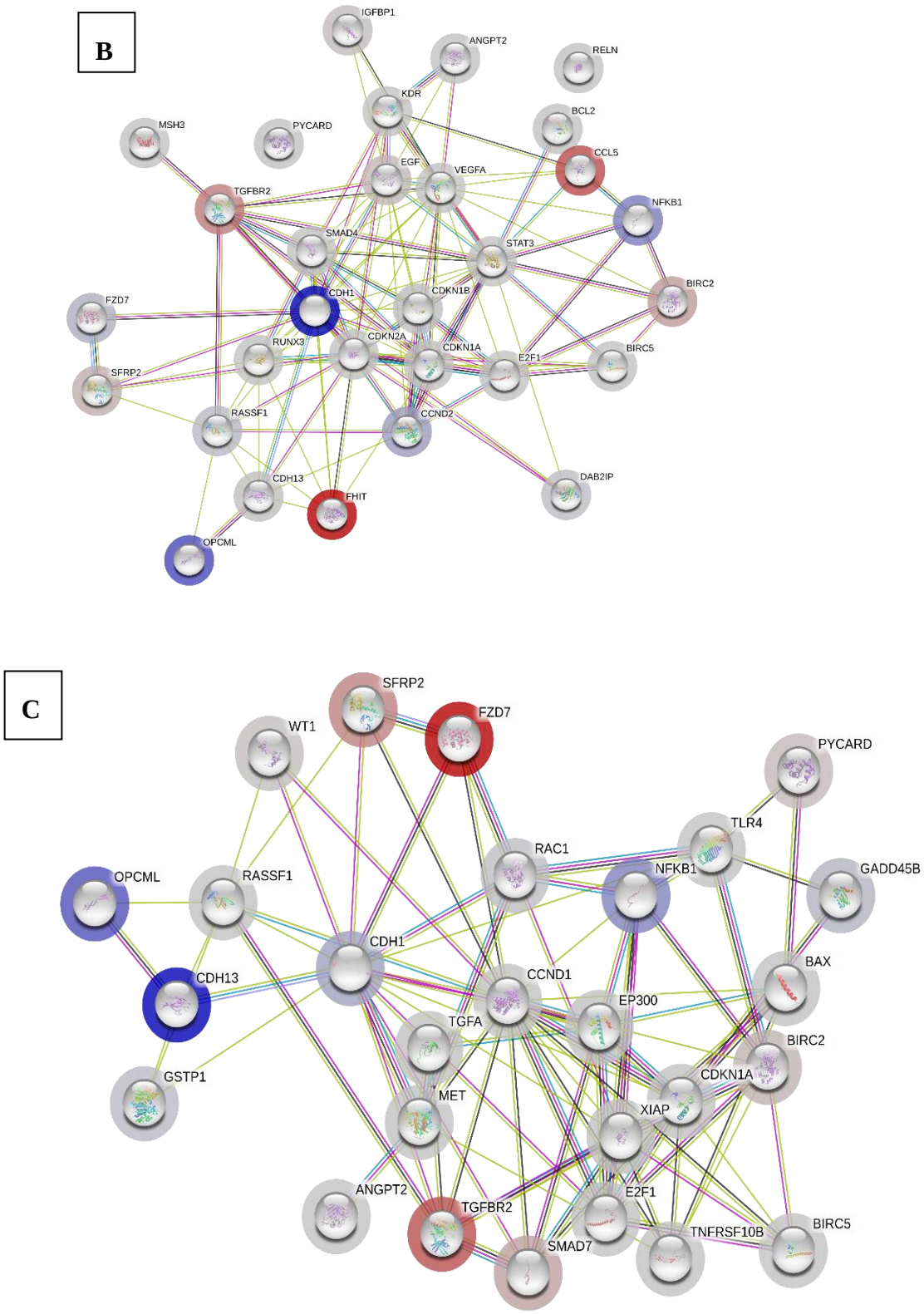

Figure 3.34: *Interaction among two or more folds differentially expressed genes (DEGs) in WRL 68 cells as shown by String Network Functional Enrichment Analysis after* ***(A)***

continuous treatment with 10 µM thorium till 15 passage ***(B)*** *irradiation with 0.1 Gy alpha-particle at 5th, 10^{th,} and 15th passage* ***(C)*** *continuous treatment with 10 µM thorium till 15th passage in combination with bombardment of cells with α-particles at 5th, 10th and 15th passage. The proteins shown with red coloration showed maximum upregulation and in blue coloration showed maximum downregulation.*

Venn diagram was made to study the common genes which were upregulated and downregulated across all treatment groups after 15 passages of growth and is shown in Figure 3.35. Figure 3.35 A shows all the common genes across all three treatment groups which were upregulated, and figure 3.35 B shows all common genes downregulated after treatment across all three groups after 15 passages. The total number of genes upregulated and downregulated in each group is expressed in brackets. All common genes upregulated and downregulated are listed out among each group while the number of unique genes among all groups are expressed in numbers.

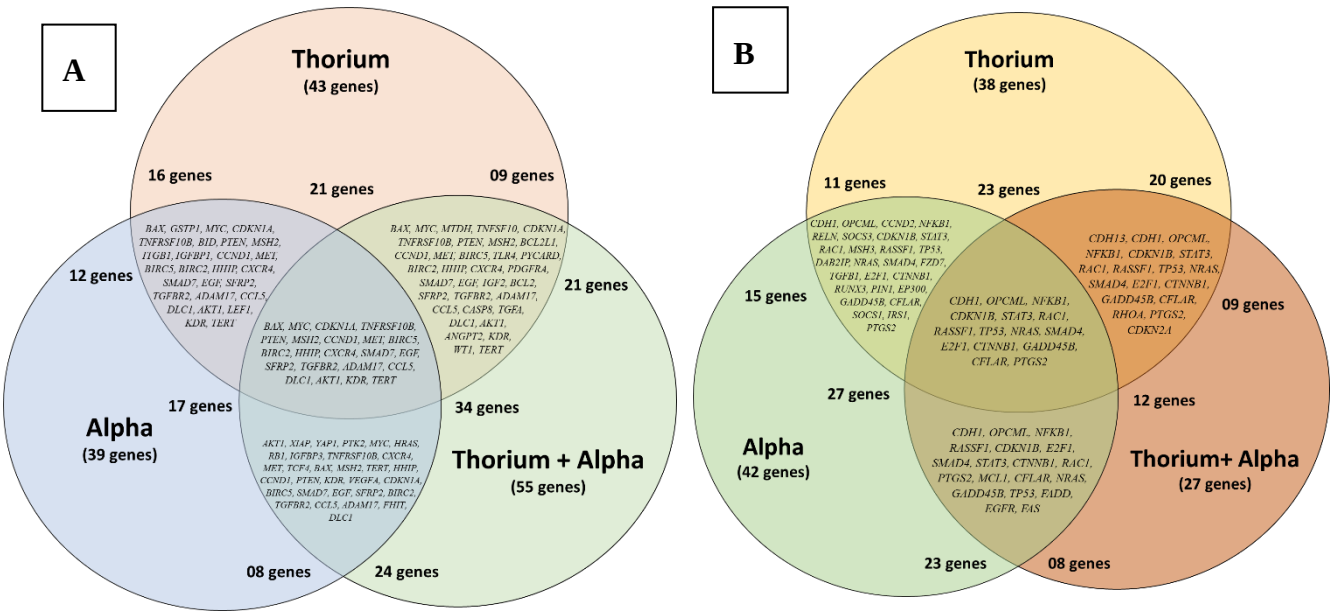

Figure 3.35: *Venn diagram showing all common genes which were* ***(A)*** *upregulated and* ***(B)***

downregulated across all three treatment groups after 15 passages. The total number of genes upregulated and downregulated are shown in brackets. Common genes are listed out and number of unique genes are written in numbers.

Table 3.8 below lists the top 05 most highly upregulated and downregulated genes in each group at P15.

Group	Upregulated genes	Downregulated genes
10 µM thorium	*CCL5 (7.2 ± 2.4), TGFBR2 (6.3 ± 1.4), EGF (2.6 ± 0.1), SMAD7 (2.5 ± 0.4), PDGFRA (2.4 ± 0.8)*	*CDH13(-1019.8 ± 0.00), CDH1 (-89.2 ± 0.00), OPCML (-20.6 ± 0.00), CCND2 (-17.4 ± 0.00), NFKB1 (-13.7 ± 0.00)*
Alpha	*FHIT (15.4 ± 3.4), CCL5 (9.1 ± 4.0), TGFBR2 (4.5 ± 1.9), BIRC2 (3.8 ± 0.3), SFRP2 (3.0 ± 0.9)*	*CDH1 (-70.01 ± 0.01), OPCML (-57.7 ± 0.00), NFKB1 (-21.6 ± 0.00), CCND2 (-18.3 ± 0.00), FZD7 (-2.5 ± 0.1)*
Thorium + Alpha	*FZD7 (13.7 ± 2.3), TGFBR2 (13.0 ± 0.1), SFRP2 (5.8 ± 1.8), SMAD7 (4.6 ± 1.6), BIRC2 (3.8 ± 1.3)*	*CDH13 (-1453.1 ± 0.00), OPCML (-12.3 ± 0.1), NFKB1 (-10.2 ± 0.00), CDH1 (-3.5 ± 0.4), NFKB1 (-10.2 ± 0.00)*

Table 3.8: *List of 05 most highly upregulated and downregulated genes across all three groups at P5. The genes upregulated are marked in red color and downregulated genes are marked in blue color and the number in bracket shows the fold regulation of each gene as compared to control.*

The pathways playing a key role using differentially expressed genes (DEGs) in each

experimental group (both significantly upregulated and downregulated) were analyzed using KEGG pathway analysis and mapped in a tabular form (Table 3.9).

No.	Altered pathways	Number of genes altered in each pathway ()
1	**Pathways in cancer**	*AKT1, BCL2, BCL2L1, BIRC2, BIRC5, CASP8, CCND1, CXCR4, EGF, FADD, FAS, HHIP, IGF2, LEF1, MET, MSH3, PDGFRA, SMAD4, TERT, TGFA, TGFBR2, CCND2, CDH1, CDKN1B, FZD7, NFKB1, NRAS, RAC1, RASSF1, STAT3, TP53* **(31)**
2	**PI3K-Akt signaling**	*AKT1, ANGPT2, BCL2, BCL2L1, CCND1, EGF, IGF2, KDR, MET, PDGFRA, TGFA, TLR4, CCND2, CDKN1B, NFKB1, NRAS, RAC1, RELN, TP53* ***(19)***
3	**Gastric cancer**	*AKT1, BCL2, CCND1, EGF, LEF1, MET, SMAD4, TERT, TGFBR2, CDH1, CDKN1B, FZD7, NRAS, TP53* ***(14)***
4	**Human papillomavirus infection**	*AKT1, CASP8, CCND1, EGF, FADD, FAS, TERT, CCND2, CDKN1B, FZD7, NFKB1, NRAS, RELN, TP53* ***(14)***
5	**MAPK signaling**	*AKT1, ANGPT2, EGF, FAS, IGF2, KDR, MET, PDGFRA, TGFA, TGFBR2, NFKB1, NRAS, RAC1, TP53* ***(14)***
6	**Hepatitis B**	*AKT1, BCL2, BIRC5, CASP8, FADD, FAS, TGFBR2, TLR4, NFKB1, NRAS, SMAD4, STAT3, TP53* ***(13)***
7	**Measles**	*AKT1, BCL2, BCL2L1, CASP8, CCND1, FADD, FAS, TLR4, CCND2, CDKN1B, NFKB1, STAT3, TP53* ***(13)***
8	**Colorectal cancer**	*AKT1, BCL2, BIRC5, CCND1, EGF, LEF1, TGFA, TGFBR2, MSH3, NRAS, RAC1, SMAD4, TP53* ***(13)***

9	**Human cytomegalovirus infection**	*AKT1, CASP8, CCL5, CCND1, CXCR4, FADD, FAS, PDGFRA, NFKB1, NRAS, RAC1, STAT3, TP53* ***(13)***
10	**Ras signaling**	*AKT1, ANGPT2, BCL2L1, EGF, IGF2, KDR, MET, PDGFRA, TGFA, NFKB1, NRAS, RAC1, RASSF1* ***(13)***
11	**Hepatocellular carcinoma**	*AKT1, BCL2L1, CCND1, IGF2, LEF1, MET, TERT, TGFA, TGFBR2, NRAS, SMAD4, FZD7, TP53* ***(13)***
12	**Kaposi sarcoma-associated herpesvirus infection**	*AKT1, ANGPT2, CASP8, CCND1, FADD, FAS, LEF1, NFKB1, NRAS, RAC1, STAT3, TP53* ***(12)***
13	**Epstein-Barr virus infection**	*AKT1, BCL2, CASP8, CCND1, FADD, FAS, CCND2, CDKN1B, NFKB1, RAC1, STAT3, TP53* ***(12)***
14	**Apoptosis**	*AKT1, BCL2, BCL2L1, BIRC2, BIRC5, CASP8, FADD, FAS, DAB2IP, NFKB1, NRAS, TP53* ***(12)***
15	**Hippo signaling**	*BIRC2, BIRC5, CCND1, LEF1, SMAD7, TGFBR2, CCND2, CDH1, FZD7, RASSF1, SMAD4, YAP1* ***(12)***

A: Thorium treatment continuously for 15 passages

No.	Altered pathways	Number of genes altered in each pathway ()
1	**Pathways in cancer**	*BIRC2, BIRC5, CCND1, CDKN1A, CDKN2A, EGF, GSTP1, HHIP, PTEN, TERT, TGFBR2, VEGFA, BCL2, CASP8, CCND2, CDH1, CDKN1B, CTNNB1, E2F1, FZD7, MSH3, NFKB1, RAC1, RASSF1, SMAD4, STAT3* ***(26)***

2	**Human papillomavirus infection**	*CCND1, CDKN1A, EGF, PTEN, TERT, VEGFA, CDKN1B, CTNNB1, E2F1, FZD7, NFKB1, RELN, CASP8, CCND2* ***(14)***
3	**PI3K-Akt signaling**	*CCND1, CDKN1A, EGF, KDR, PTEN, VEGFA, ANGPT2, BCL2, CCND2, CDKN1B, NFKB1, RAC1, RELN* ***(13)***
4	**MicroRNAs in cancer**	*CCND1, CDKN1A, CDKN2A, PTEN, VEGFA, BCL2, CCND2, CDKN1B, E2F1, NFKB1, RASSF1, STAT3* ***(12)***
5	**Gastric cancer**	*CCND1, CDKN1A, EGF, TERT, TGFBR2, BCL2, CDH1, CDKN1B, CTNNB1, E2F1, FZD7, SMAD4* ***(12)***
6	**Pancreatic cancer**	*CCND1, CDKN1A, CDKN2A, EGF, TGFBR2, VEGFA, E2F1, NFKB1, RAC1, SMAD4, STAT3* ***(11)***
7	**Hepatocellular carcinoma**	*CCND1, CDKN1A, CDKN2A, GSTP1, PTEN, TERT, TGFBR2, CTNNB1, E2F1, FZD7, SMAD4* ***(11)***
8	**Epstein-Barr virus infection**	*CCND1, CDKN1A, BCL2, CASP8, CCND2, CDKN1B, E2F1, NFKB1, RAC1, RUNX3, STAT3* ***(11)***
9	**Hippo signaling**	*BIRC2, BIRC5, CCND1, SMAD7, TGFBR2, CCND2, CDH1, CTNNB1, FZD7, RASSF1, SMAD4* ***(11)***
10	**Focal adhesion**	*BIRC2, CCND1, EGF, KDR, PTEN, VEGFA, BCL2, CCND2, CTNNB1, RAC1, RELN* ***(11)***
11	**Human cytomegalovirus infection**	*CCND1, CDKN1A, CDKN2A, VEGFA, CASP8, CCL5, CTNNB1, E2F1, NFKB1, RAC1, STAT3* ***(11)***
12	**Kaposi sarcoma-associated herpesvirus infection**	*CCND1, CDKN1A, VEGFA, ANGPT2, CASP8, CTNNB1, E2F1, NFKB1, RAC1, STAT3* ***(10)***

13	**Human T-cell leukemia virus 1 infection**	*CCND1, CDKN1A, CDKN2A, PTEN, TERT, TGFBR2, CCND2, E2F1, NFKB1, SMAD4* ***(10)***
14	**Prostate cancer**	*CCND1, CDKN1A, EGF, GSTP1, PTEN, BCL2, CDKN1B, CTNNB1, E2F1, NFKB1* ***(10)***
15	**Colorectal cancer**	*BIRC5, CCND1, CDKN1A, EGF, TGFBR2, BCL2, CTNNB1, MSH3, RAC1, SMAD4* ***(10)***

B: Irradiated with 0.1 Gy alpha particles at 5th, 10th and 15thpassage

No.	Altered pathways	Number of genes altered in each pathway ()
1	**Pathways in cancer**	*BAX, BIRC2, BIRC5, CCND1, CCND2, CDKN1A, EGF, EP300, FZD7, HHIP, IGF2, MET, MSH2, MSH3, TERT, TGFA, TGFBR2, XIAP, CDH1, E2F1, GADD45B, GSTP1, NFKB1, RAC1, RASSF1* ***(25)***
2	**PI3K-Akt signaling**	*ANGPT2, CCND1, CCND2, CDKN1A, EGF, IGF2, IRS1, KDR, MET, RELN, TGFA, TLR4, NFKB1, RAC1* ***(14)***
3	**Hepatocellular carcinoma**	*BAX, CCND1, CDKN1A, FZD7, IGF2, MET, TERT, TGFA, TGFBR2, E2F1, GADD45B, GSTP1* ***(12)***
4	**Colorectal cancer**	*BAX, BIRC5, CCND1, CDKN1A, EGF, MSH2, MSH3, TGFA, TGFBR2, GADD45B, RAC1* ***(11)***
5	**Human papillomavirus infection**	*BAX, CCND1, CCND2, CDKN1A, EGF, EP300, FZD7, RELN, TERT, E2F1, NFKB1* ***(11)***

6	**Gastric cancer**	*BAX, CCND1, CDKN1A, EGF, FZD7, MET, TERT, TGFBR2, CDH1, E2F1, GADD45B* ***(11)***
7	**Transcriptional mis regulation in cancer**	*BAX, BIRC2, CCND2, CDKN1A, IGFBP3, MET, TGFBR2, WT1, GADD45B, NFKB1* ***(10)***
8	**MicroRNAs in cancer**	*CCND1, CCND2, CDKN1A, EP300, IRS1, MET, NFKB1, RASSF1, SOCS1, E2F1* ***(10)***
9	**Human T-cell leukemia virus 1 infection**	*BAX, CCND1, CCND2, CDKN1A, EP300, TERT, TGFBR2, XIAP, NFKB1* ***(10)***
10	**MAPK signaling**	*ANGPT2, EGF, IGF2, KDR, MET, TGFA, TGFBR2, GADD45B, NFKB1, RAC1* ***(10)***
11	**Pancreatic cancer**	*BAX, CCND1, CDKN1A, EGF, TGFA, TGFBR2, E2F1, GADD45B, NFKB1, RAC1* ***(10)***
12	**Non-small cell lung cancer**	*BAX, CCND1, CDKN1A, EGF, FHIT, MET, TGFA, E2F1, GADD45B, RASSF1* ***(10)***
13	**Epstein-Barr virus infection**	*BAX, CCND1, CCND2, CDKN1A, RUNX3, E2F1, GADD45B, NFKB1, RAC1* ***(09)***
14	**Focal adhesion**	*BIRC2, CCND1, CCND2, EGF, KDR, MET, RELN, XIAP, RAC1* ***(09)***
15	**Hippo signaling**	*BIRC2, BIRC5, CCND1, CCND2, FZD7, SMAD7, TGFBR2, CDH1, RASSF1* ***(09)***

C: Thorium treatment continuously for 15 passages in combination with 0.1 Gyα-particle

irradiation at 5th, 10th and 15th passage.

Table: 3.9. *List of pathways altered by more than two folds differentially expressed genes (DEGs) after* ***(A)*** *continuous treatment with 10 µM thorium* ***(B)*** *alpha-particle irradiation of dose 0.1 Gy at 5th, 10th, and 15th passage* ***(C)*** *continuous treatment with 10 µM thorium followed by bombarding the cells with α-particles at 5th, 10th and 15th passages as mapped by KEGG pathway. Genes upregulated are represented in red color and downregulated genes are represented in blue color and the total number of DEGs expressed in brackets.*

Long term exposure of human liver cells to thorium causes several alterations both morphologically and genetically. Morphological studies of cells exposed continuously with thorium, doses of alpha particles, and thorium in combination with alpha particles causes changes such as release of granules in the extracellular matrix which increases with the increase in the stress after continued incubation with thorium and/or irradiation with alpha particles.

When the same treatment was continued till 15 passages and genetic alteration data were obtained, it was found that genes such as *BAX, MYC, CDKN1A, TNFRSF10B, PTEN, MSH2, CCND1, MET, BIRC5, BIRC2, HHIP, CXCR4, SMAD7, EGF, SFRP2, TGFBR2, ADAM17, CCL5, DLC1, AKT1, KDR, TERT* were found to be upregulated whereas genes such as *CDH1, OPCML, NFKB1, CDKN1B, STAT3, RAC1, RASSF1, TP53, NRAS, SMAD4, E2F1, CTNNB1, GADD45B, CFLAR, PTGS2* were found to be downregulated across all treatment groups after continuous treatment for 15 passages. Various carcinogenic pathways which involve these altered genes were found to be activated across all three groups. Carcinogenic pathways such as PI3K-Akt signaling, gastric cancer, human papillomavirus infection, colorectal cancer, hepatocellular

carcinoma, Epstein-Barr virus infection, hippo signaling were found to be involved in all three groups. At P5, upregulation of genes such as *AKT, IRS1, STAT 3, HGF* AND *MET* causes increased cell survival, proliferation, and motility through PI3k-Akt pathway. Upregulation of *ADAM17* has also been implicated in the development of hypoxia-induced drug resistant in HCC cells through activation of Egfr/PI3K/Akt pathway (151). Also, upregulation of genes such as *FZD7, PTK2* indicate role of Wnt/β-catenin pathway (152). Another pathway which was found to be upregulated is insulin-like growth factor pathway with genes such as *IRS1, IGFBP1, IGF2* being over-expressed (153). Various genes such as *BCL2, XIAP* control apoptosis and their upregulation on thorium treatment leads to dysregulation of apoptosis and increased cell survival (154). Other proteins which act as various contributing factors in the onset and progression of cancer were also found to be upregulated in cells e.g., *E2F1, CCND1, SMAD4, RHOA, TLR4, TCF4, CFLAR, CDKN1B, PTGS2, ANGPT2, CCL5* etc. Ccl5 is an inflammatory cytokine which is highly over-expressed in cancer cells and promotes cancer progression (155). *Ep300* in combination with CBP acts as histone acetyltransferase (HATs) and its overexpression has been involved in liver metabolism and development of fibrosis (156). Over-expression of Angpt2 is known to play a role in angiogenesis and is closely related to development and prognosis of HCC (157).Similarly, at P15, pathways such as PI3K-Akt, Wnt/β-catenin, Tgfb and insulin-like growth factor pathway have been found to be involved in carcinogenesis via the altered expression of genes such as *AKT1, BAX, MYC, CDKN1A,*

TNFRSF10B, MSH2, CCND1, MET, BIRC5, BIRC2, HHIP, CXCR4, SMAD7, EGF, SFRP2, TGFBR2, ADAM17, CCL5, TERT.

Section 3.3: Thorium-induced anatomical, histopathological and carcinogenic changes in mice

Thorium studies under *in-vitro* conditions provided insights about the uptake mechanism, intracellular targets of thorium and gene expression alterations in cells upon long term exposure with thorium without or with alpha particle irradiation. This long-term treatment accounted for its effect on human liver cells due to both its chemical toxicity as well as radiological toxicity. In order to study the effect of thorium under *in vivo* conditions, experiments were performed using Swiss mice after short (1 and 30 days) and long-term (6 and 12 months) of treatment. Initially short-term treatment experiment was performed, where low (4 mg/Kg) and high (40 mg/Kg) doses of thorium were administered intravenously (*i.v.*). Rationale of choosing the doses has been mentioned in the subsequent Section (3.3.1.2: thorium bio-distribution). In addition, the short-term exposure (1 day and 30 days) study provided an idea about the doses which could be used for long-term (6 and 12 months) treatment required to study carcinogenic changes. As short-term exposure studies were intended more towards acute toxicity, the long-term treatment was aimed towards carcinogenic changes.

The bio-distribution of thorium was studied after short and long-term treatment by ICP-MS. The anatomical/cytological changes caused due to thorium treatment were studied using techniques such as synchrotron imaging, transmission electron microscopy. Further studies were also conducted to determine the effects of thorium on different tissues using histopathological techniques (hematoxylin and eosin staining), immunohistochemistry and periodic acid Schiff staining. Effects of thorium on mice were also studied using different serum biochemical parameters like glucose, total protein, total bilirubin, creatinine, urea,

cholesterol. Cytokine and chemokine profiling of serum samples were also performed in serum samples obtained from mice after long-term thorium treatment. Alterations in gene expression of liver tissues samples were also analyzed to correlate their possible role in carcinogenic effects of thorium. Overall, different approaches were adopted to determine the effect of thorium under *in-vivo* conditions especially in the context of carcinogenesis.

3.3.1: Effects of Thorium in Mice at Short Period (At Day 1 And 30)

3.3.1.1: Gross health effects

Mice treated with thorium were carefully observed for any gross visible changes in their health parameters and/or phenotypic changes after thorium treatment in the course of one month. The weight of mice was monitored over the period of one month and compared to control, it did not show any significant difference after thorium treatment as is shown in Figure 3.36. It was observed that at higher concentration of thorium (40 mg/Kg), blackening of the tail (from the point of injection onwards till tail's end) was observed. Such blackening of tail may be due to necrosis caused by thorium induced damage to blood vessels. However, no such alteration was observed in case of 4 mg/Kg dose. During day-to-day observations, thorium treated mice remained visibly similar to control in other general health aspects (like movement, feed/water intake), which however was not recorded.

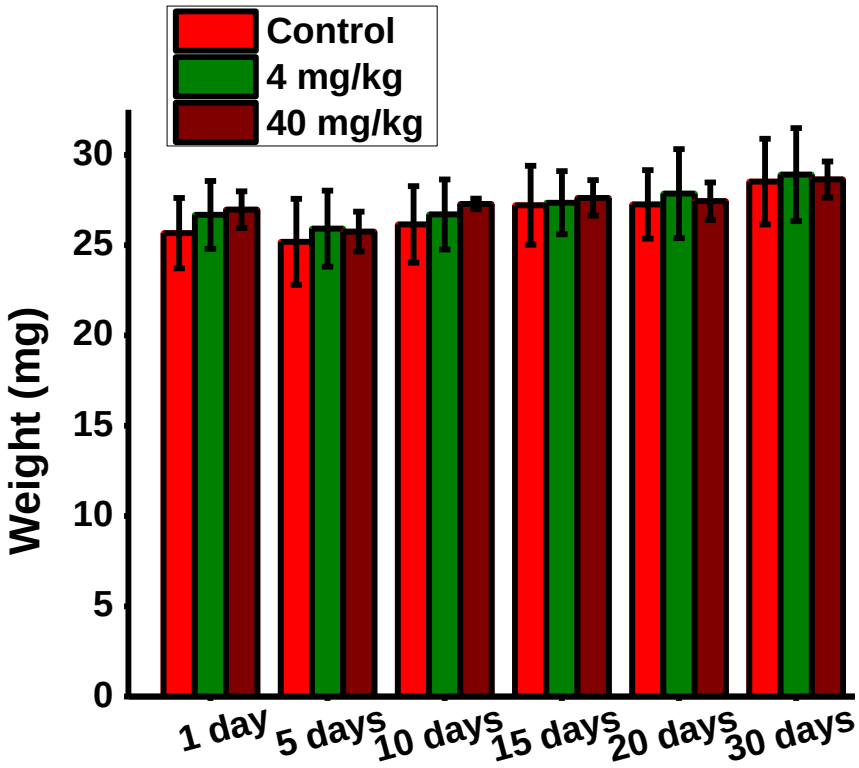

Figure 3.36: *Weight of mice in control and thorium treated groups (4 and 40 mg/Kg) as observed over a period of one month. 8 mice per group were used for the study and the values were obtained by averaging the weight of all mice in each group. No significant difference in the weight of mice was observed in thorium treated groups compared to their respective control.*

3.3.1.2: Thorium bio-distribution

Localization of thorium in its different target organs would govern its short and long terms health effects. Hence, to study the major target organs for deposition/accumulation, bio-distribution study was performed in 8-10-weeks old Swiss albino male mice after short and long-term treatment of thorium. For this, the doses were first optimized by injecting thorium into mice for shorter duration i.e., 1 and 30 days. This was done to study the bio-distribution as well as to select the doses appropriate for long-term studies. The mice were injected

intravenously with two different concentrations of thorium, low concentration (4 mg/Kg) and high concentration (40 mg/Kg). Since LD_{50} of thorium nitrate in small rodents is reported to be 48 mg/Kg following intravenous injection (158), the dose of 40 mg/Kg was chosen for higher dose and a dose ten times lower than this dose, i.e. 4 mg/Kg was chosen as low dose of thorium. The mice were sacrificed after one and thirty days of thorium injection. Different target organs such as liver, spleen and bone [as known from a previous study from our laboratory after intramuscular injection of thorium at acute and chronic doses, (33)] were obtained for thorium accumulation studies. The organs were washed with saline, acid-digested and thorium was estimated in each organ as described in Materials and Methods (Section 2.2.4.2). Results were expressed as both absolute thorium (in µg) and specific thorium (in µg/g of tissue weight) as shown in Figure 3.37 (A-F). In addition to absolute concentration of thorium in each organ, specific thorium (µg per g of organ/tissue) was also calculated to know about the density of thorium accumulation, which would indicate the binding affinity/preference of thorium for each organ.

At both time points, i.e., 1 and 30 days, maximum amount of total thorium (µg) was found to be deposited in liver followed by spleen and skeleton for both concentrations of thorium (4 and 40 mg/Kg). In liver, at low dose, i.e., 4 mg/Kg, there was a marginal decrease in the amount of total thorium deposited from day 1 to day 30, but the decrease was insignificant. However, the decrease was significant in case of specific thorium (µg per g of organ weight) from day 1 to day 30. At high dose of thorium, i.e., 40 mg/Kg, the amount of thorium (total thorium and specific thorium) was increased (compared to 4 mg/Kg) but was similar at both time points. Although, specific thorium decreases in liver from day 1 to day 30, the decrease was insignificant at 40 mg/Kg. In case of liver, at 4 mg/Kg dose, 17% of the total thorium which was deposited on day 1 was cleared from the organ by day 30 while in case of

40 mg/Kg, there was an accumulation of ~3% of total thorium after exposure for 30 days. However, when specific thorium is considered, there was a clear pattern of clearance of thorium from liver at both doses. Specific thorium gets cleared/removed from liver at day 30 and the percent of clearance is higher at 4 mg/Kg as compared to 40 mg/Kg. At 4 mg/Kg, a total of 37% of thorium is cleared from liver as compared to its initial deposition at day 1. At 40 mg/Kg, 9% of thorium is cleared from liver at day 30 as compared to its initial deposition.

In spleen, at low dose, i.e., 4 mg/Kg, the amount of thorium deposited on day 1 and day 30 remains similar in case of both total thorium and specific thorium. However, at higher dose, i.e., 40 mg/Kg, the amount of thorium (total thorium as well as specific thorium) deposited on day 30 is significantly higher as compared to day 1. It is clear from the Figure 3.37, there is an accumulation of thorium at both the doses in terms of total thorium and specific thorium. In case of total thorium, there is 30-35% accumulation of thorium in the spleen over a period of 30 days. However, when specific thorium is considered, the percentage of thorium accumulation in spleen increases drastically to more than 200 percent (230% in case of 4 mg/Kg and 285% in case of 40 mg/Kg).

Skeleton shows clearance of thorium in terms of total thorium and specific thorium at low dose i.e., at 4 mg/Kg. However, at 40 mg/Kg, there is slight removal of thorium in case of total thorium but when specific thorium is considered, there is an accumulation of 42% of thorium in bones after 30 days. Total thorium deposited in skeleton does not show any major difference at 4 and 40 mg/Kg at both time points i.e., day 1 and day 30. However, specific thorium deposited is significantly higher at day 30 as compared to day 1 at 40 mg/Kg.

The higher specific activity of thorium in spleen at 30 days suggest, it as an organ of deposition of thorium at higher density than liver and bone. Moreover, from day 1 to 30, an

accumulation of thorium was observed in bone and spleen which was different than liver, where a clearance was observed at day 30. These results may be attributed to facilitated clearance of thorium from liver due to its relatively higher blood flow and dividing cells, which however, needs further investigation. Compared to day 1, an accumulation of thorium (at 40 mg/Kg) in spleen and bone at day 30, suggest either slower clearance from these organs or still available cellular/molecular sites for thorium deposition.

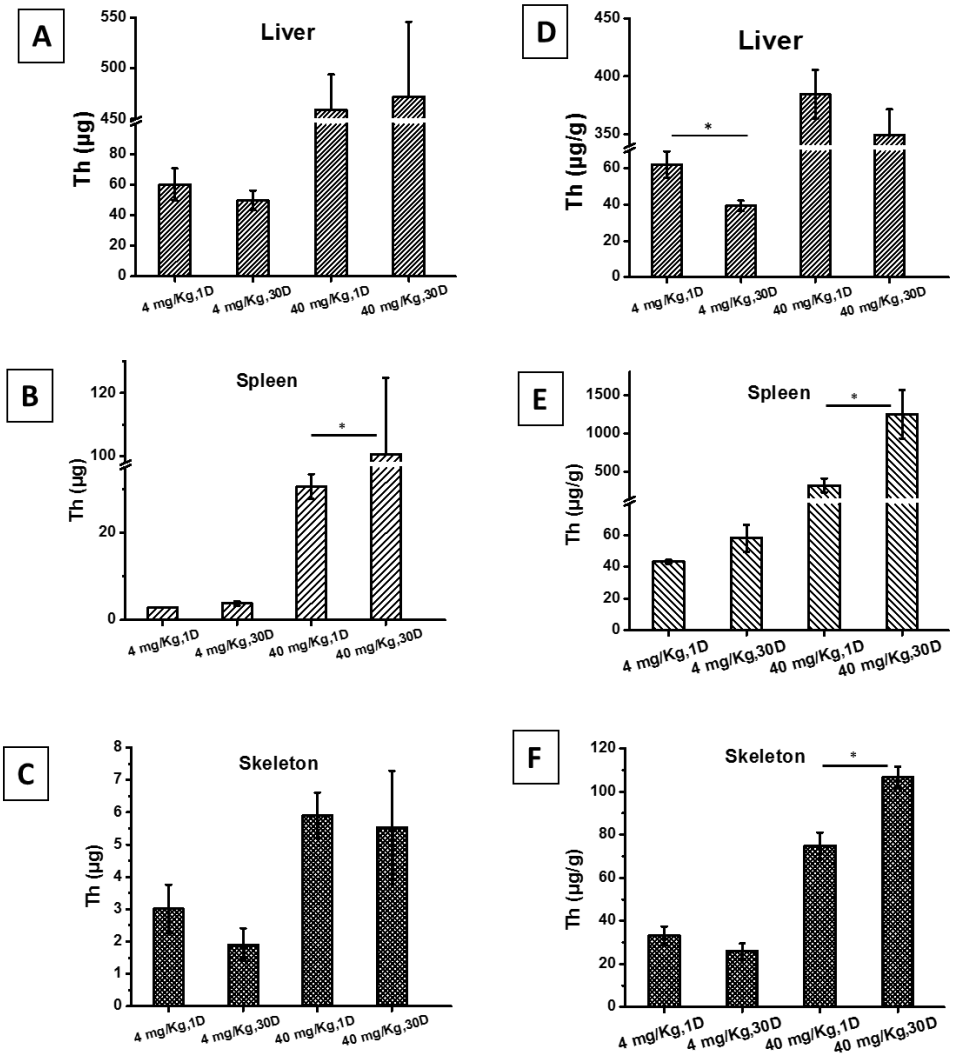

Fig. 3.37 A-F: *Thorium bio-distribution at low (4 mg/Kg) and high (40 mg/Kg) doses of thorium injected intra-venously in Swiss albino male mice after day 1and 30. Thorium was estimated in liver, spleen, and skeleton by ICP-MS.* ***(A-C)*** *total thorium (µg) and* ***(D-F)*** *specific*

*thorium (thorium in µg per gram of organ weight) (µg/g) in liver, spleen and skeleton (N = 3). *significantly different at p value <0.05*

3.3.1.3: ANATOMICAL CHANGES IN MAJOR TARGET ORGANS

In the previous section, localization of thorium in different organs was observed, which would result in anatomical and histopathological changes in these organs, thereby, contributing to health effects of thorium. These anatomical and histopathological changes were studied using synchrotron imaging and H&E staining described in subsequent sections.

3.3.1.4: SYNCHROTRON IMAGING

In order to study anatomical changes caused by thorium in mice, 4 and 40 mg/Kg of thorium was injected in Swiss mice intra-venously for one month. The mice were sacrificed after 30 days and major organs of thorium deposition i.e., liver, spleen and bone were obtained followed by fixation in paraformaldehyde. To study the three dimensional structural changes in these organs caused by thorium treatment, synchrotron-based micro computed tomography (SR-µCT) was employed (103) at Indus-2 Synchrotron, RRCAT, Indore, India as mentioned in materials and Methods. Slice images obtained in X-ray µCT provide a local map of attenuation co-efficient in the sample to visualize the local microstructures. Synchrotron source produces X-ray beam of very high intensity with high collimation (159,160) which can be monochromatized to produce images without any beam hardening artefacts and hence, this technique is more suitable to study quantitative structure and density variation measurements as compared to conventional µCT (103). The imaging facility based on synchrotron produces X-ray phase contrast images which, due to their high coherence, enables to distinguish anatomical features with very fine differences in densities (161). Structural details of liver,

spleen and bone were obtained through these X-ray phase contrast images based on synchrotron.

3.3.1.4.1: LIVER

Liver tissue samples treated with 4 and 40 mg/Kg thorium for 30 days were used to study the effect of thorium accumulation on its anatomy using SR-μCT. Similar area from same lobe of liver from each group were used to obtain projection images (Figure 3.38). Some of the prominent changes in thorium treated samples as compared to control were studied. In control samples, the blood vessels and their various entanglements were clearly visible throughout the liver sample. However, in thorium treated liver samples, the number of these blood vessels per unit volume decreased in a dose-dependent manner. The vessels in case of 4 mg/Kg thorium treated liver were reduced in number as compared to control. This reduction in the number of blood vessels was even more pronounced in 40 mg/Kg thorium treated liver samples. It was also observed that in addition to the reduction in the number of blood vessels per unit volume, the length and diameter of these blood vessels also decreased in thorium treated groups.

The blood vessels were thicker in diameter and spread-out till the peripheral edges of the liver spanning the entire organ in case of control tissue. In case of 4 mg/Kg, the diameter of blood vessels and their length got reduced. The blood vessels were comparatively thinner and only a few spread-out till the periphery suppling blood to the edges of the organ. The effect was more pronounced in case of 40 mg/Kg where blood vessels further decreased in number and hardly any blood vessel reached out to the periphery of the organ.

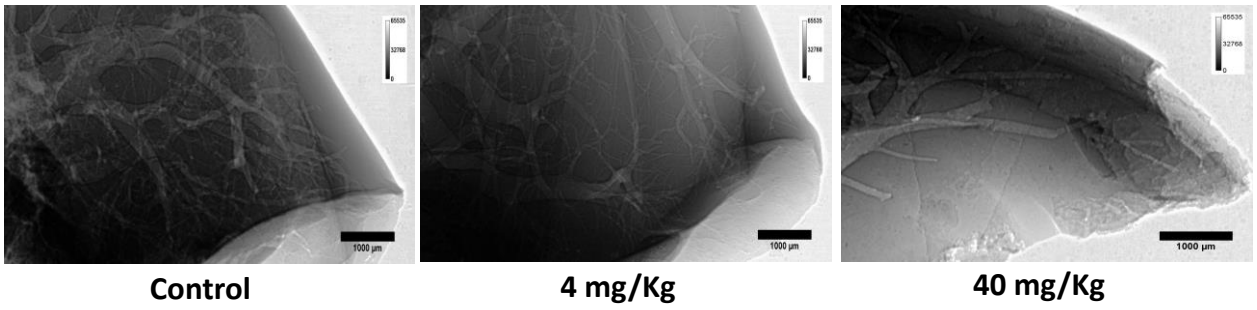

Figure 3.38: *Projection images showing alterations in the number and structure of blood vessels and capillaries in mice liver injected with 4 and 40 mg/Kg thorium intravenously for 30 days as compared with control liver. Scale represents 1000 µM.*

These initial observations were further confirmed by tomographic slice images obtained at approximately similar elevations of liver from all the groups (Figure 3.39).

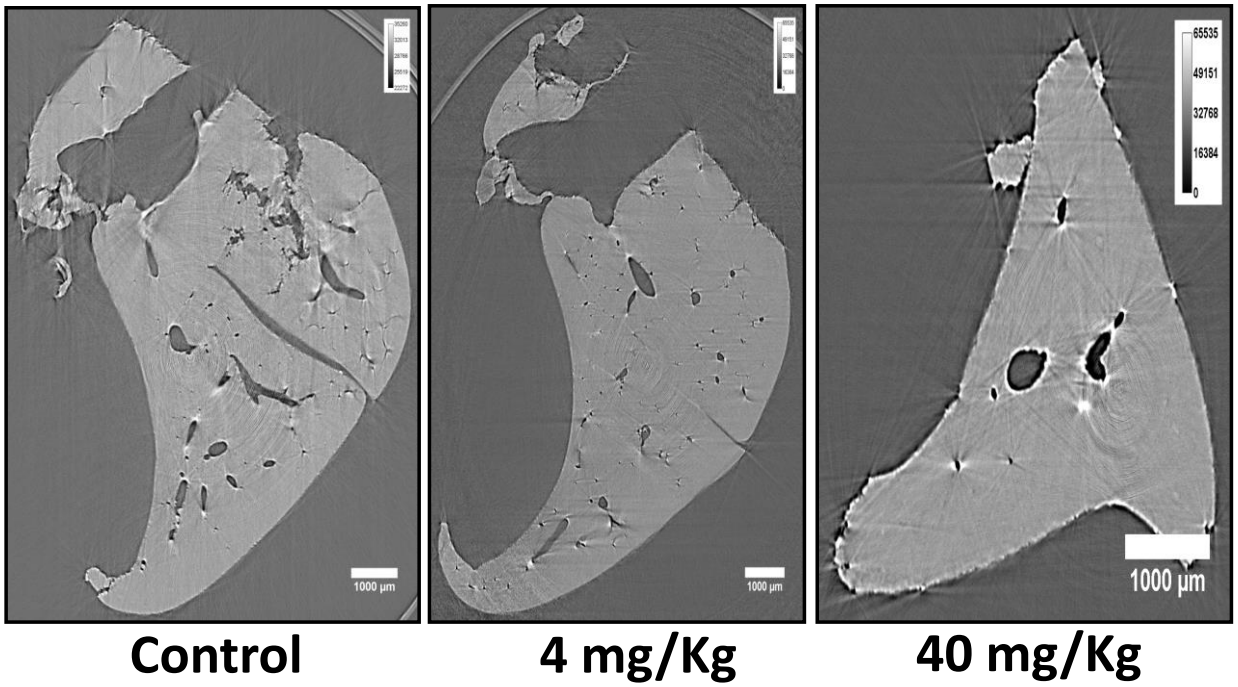

Figure 3.39: *Tomographic slice image of liver showing decrease in number as well as diameter of blood vessels and capillary in liver upon thorium treatment. Scale represents 1000 µM.*

These cross-sectional tomographic images showed a finite number of intersections at a given elevation which decreased in a dose-dependent manner. The number of these blood vessels was also more in case of control liver and covered the entire liver tissue till its periphery, which is in agreement of projection image results (Fig. 3.39). In 4 mg/Kg thorium treated liver tissue, the number of these intersecting blood vessels decreased in number as well as in diameter. The number of blood vessels towards the periphery were also lesser as compared to control. Similar but more pronounced effect was observed in 40 mg/Kg thorium treated. It was observed that when mice were treated with 40 mg/Kg of thorium for one month, the number of intersecting blood vessels reduced significantly as compared to control and low dose of thorium. Additionally, the number of intersecting blood vessels towards the peripheral edges and their local entanglements were also absent in 40 mg/Kg treated group.

These structural alterations were further analyzed in greater detail using three dimensional (3-D) images (Figure 3.40). In these 3-D images, major features of liver and its background were removed using volume rendering and blood vessels were highlighted. It could be clearly observed that in case of control, all the blood vessels and their branches such as arterioles and venules were clearly visible across all sections. They were much denser and spanned the entire tissue. In case of 4 mg/Kg, there was a reduction in the number of blood vessels and its branches such as arterioles and venules. In addition to decrease in the density of blood vessels, there was also marked thinning of blood vessels towards the end. The same effect was even more prominently visible in case of 40 mg/Kg where the number of blood vessels and their density was significantly reduced ($p \leq 0.05$). Hardly any blood vessel could be seen in the peripheral edges covering the organ.

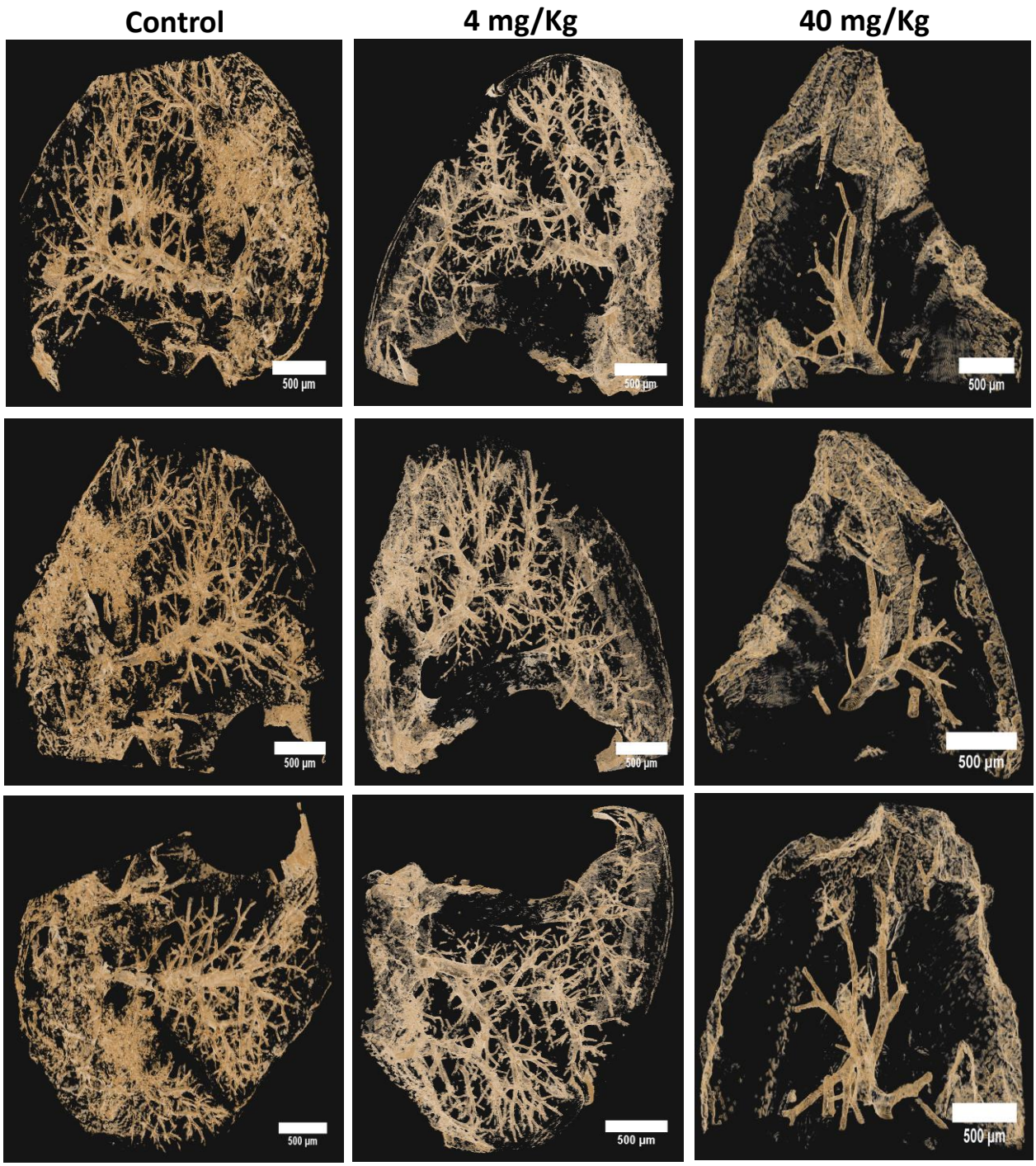

Figure 3.40: *Three-dimensional view of alterations in liver blood vessels caused by 4 and 40 mg/Kg thorium treatment as compared with control. Scale represents 500 µm. Three images are at three tomographic rotations*

The qualitative changes observed in these images were confirmed by studying these alterations quantitatively in terms of vessel density, their surface area and total volume using quantitative image analysis on micro-tomography volume data (Table 3.10).

Parameters	**Control**	**4 mg/Kg**	**40 mg/Kg**
Integrated Volume (μm^3) ($x10^8$)	2.38	1.24	0.76
Integrated Surface Area (μm^2) ($x10^7$)	2.04	1.46	0.21

Table 3.10: *Alterations in capillary parameters of liver of mice treated with thorium. Values presented are mean of two liver samples from two animals*

Alteration in blood vasculature of liver tissue as observed under synchrotron imaging were further correlated with performing immunohistochemical staining for the marker of blood vessels/angiogenesis (CD31) in the liver tissue samples (103). Increase in its expression is an indicator of increased angiogenesis and vice-versa. Loss of vasculature would result in decrease in CD31 expression (103,162). Liver tissues from the control animals showed prominent expression of CD31, which was substantially decreased in thorium treated liver tissue sections (Figure 3.41)

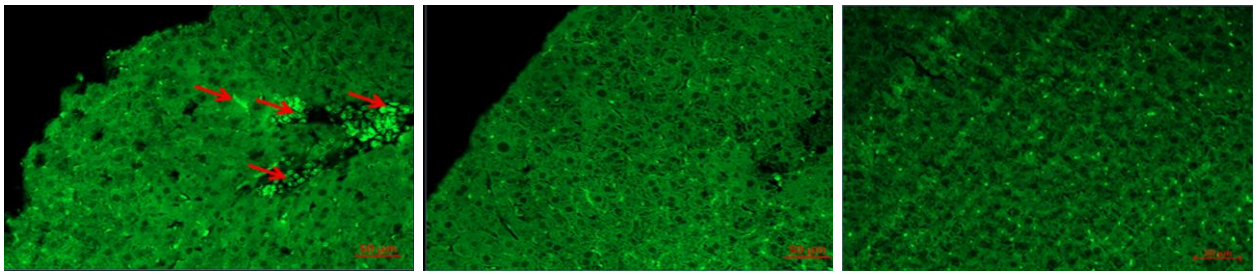

Figure 3.41: *Immuno-histochemistry of liver tissue for CD 31 expression. Arrows indicate CD 31 positive regions. Scale bar: 50 µM.*

To further correlate the anatomical changes, hematoxylin and Eosin (H & E) staining of control and thorium treated liver tissues was performed to study the histopathological changes after thorium treatment at different time points. Figure 3.42 shows H & E-stained images of liver treated with 4 and 40 mg/Kg thorium for one month. Control tissues showed typical histological organization of normal mouse liver (163) having well-organized cellular architecture with central/portal venules, sinusoidal capillaries and hepatocytes. At low magnification (10X), each view field showed one or two portal venules and a few central venules (relatively smaller diameter). Analysis of slides at higher magnification (20X) showed sinusoidal capillaries radiating from these venules whose boundaries were arranged with hepatocytes. The features observed at lower magnifications (10X and 20X) could be better visualized at magnification of 40X. Compared to control, the number of central and portal venules visualized per field showed a significant decrease in a dose-dependent manner. The number of venules per field was highest in control which decreased a little in case of 4 mg/Kg thorium. At 40 mg/Kg, the number of venules per field was the lowest providing further evidence of shrinkage in blood vessels upon thorium treatment. At 40X, several double nucleated hepatocytes were also observed in control liver samples which decreased in thorium treated samples. However, the decrease in double nucleated hepatocytes was found to be uniform in thorium treated samples and was not dose dependent.

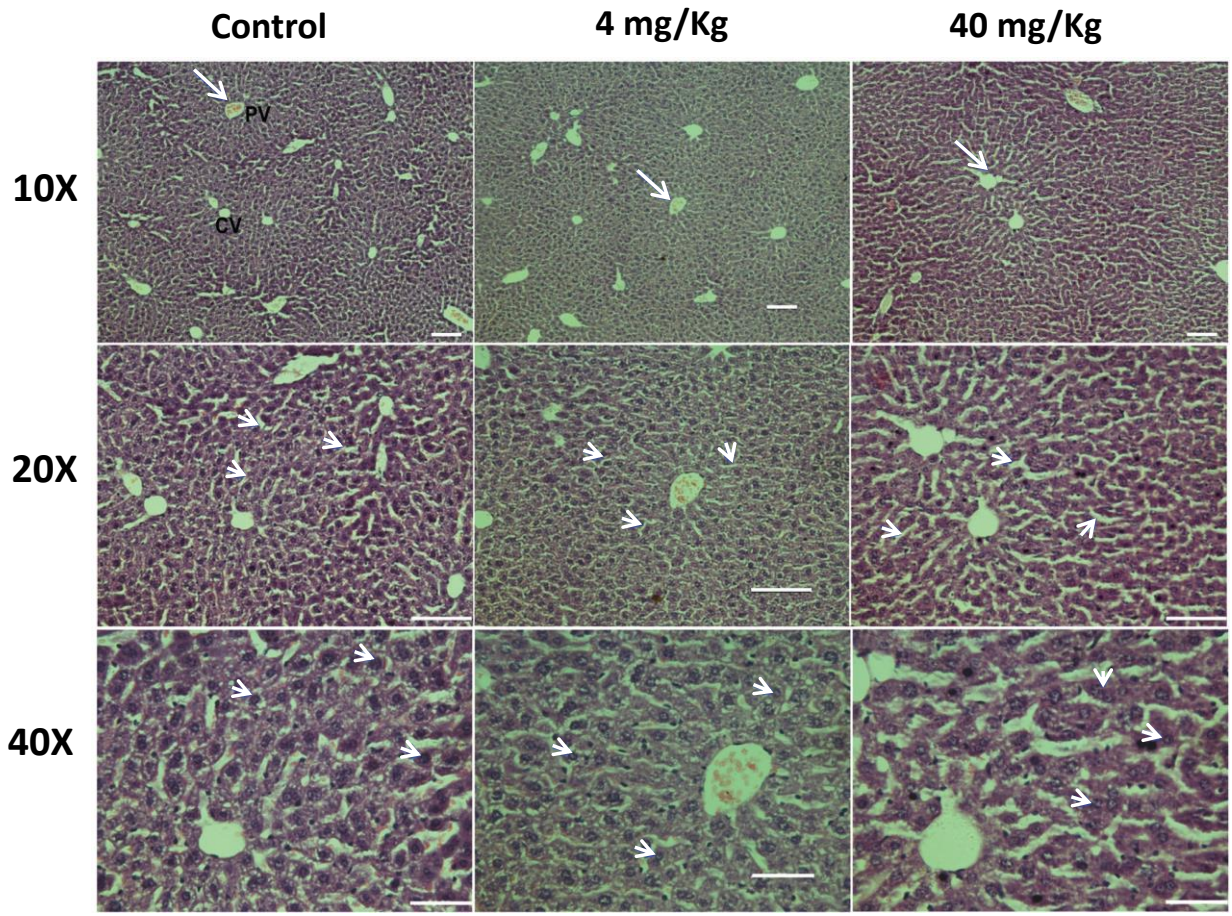

Figure 3.42: *Hematoxylin and eosin-stained bright field microscopic images of liver treated with thorium for one month. Images were obtained at 10X, 20X and 40X. Scale bar represents 100 µm (10X, 20X); 50 µm (40X). Arrows show change in number of venules (at 10X), change in width of sinusoidal capillaries (at 20X) and double nucleated hepatocytes (at 40X). CV: central venules, PV: portal venules.*

3.3.1.4.2: Spleen

SR-µCT studies were also performed in spleen tissues obtained from control and thorium treated mice. Tomographic projection images showed that control spleen was uniformly translucent throughout indicating absolute absence of any heavy X-ray opaque object in the spleen (Figure 3.43). Tomographic projection images of spleen samples from

mice treated with 4 mg/Kg thorium showed dark lines along with the length of blood vessels and its various arterioles. Venules were observed which were projecting perpendicular to the plane in both directions (shown as arrows). In 40 mg/Kg, the same effect was observed but was more pronounced. Thorium is a contrasting agent which has been used as an X-ray contrast in the form of thorotrast to develop better X-ray images in 1930s before its toxic effects were discovered (79). The dark lines observed in this experiment, seemed to be generated out of thorium deposition along the length of blood vessels, which however needs to be confirmed by other suitable technique.

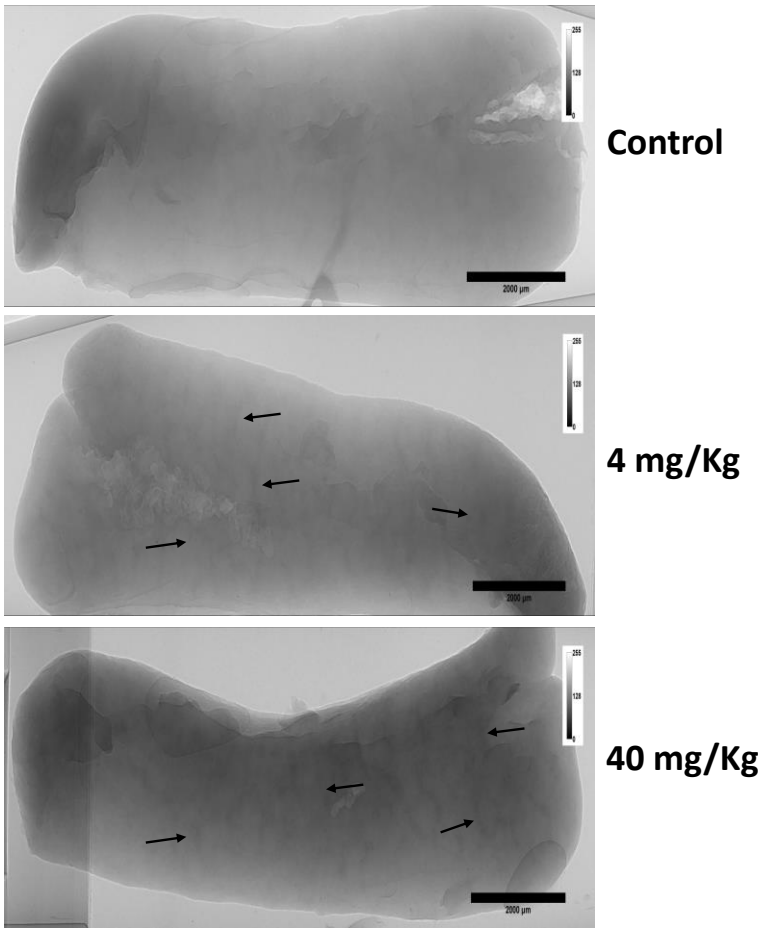

Figure 3.43: *Projection image of thorium deposition along blood vessels and capillaries in mice spleen injected with 4 and 40 mg/Kg of thorium intravenously for 30 days as compared*

with control spleen. The scale bar represents 200 µM. Arrows show x-ray opaque areas in the images

The deposition of thorium along the length of blood vessels and capillaries appeared to be uniform throughout the tissue. Rest of the tissue morphology appeared to be similar in control as well as both treatment groups. When tomographic slice images of spleen were studied, it was observed that in thorium treated group, there was a formation of white patches which appeared along the walls of blood vessels and were therefore, seen in closed patches. These white patches were absent in control and could be clearly seen in 4 and 40 mg/Kg treated spleen. The effect was more prominent in case of 40 mg/Kg as compared to 4 mg/Kg treated spleen. In 40 mg/Kg, these white patches were much darker in nature and were more prominently visible along the blood vessel wall in one region of spleen suggesting significant thorium deposition in that region (Figure 3.44).

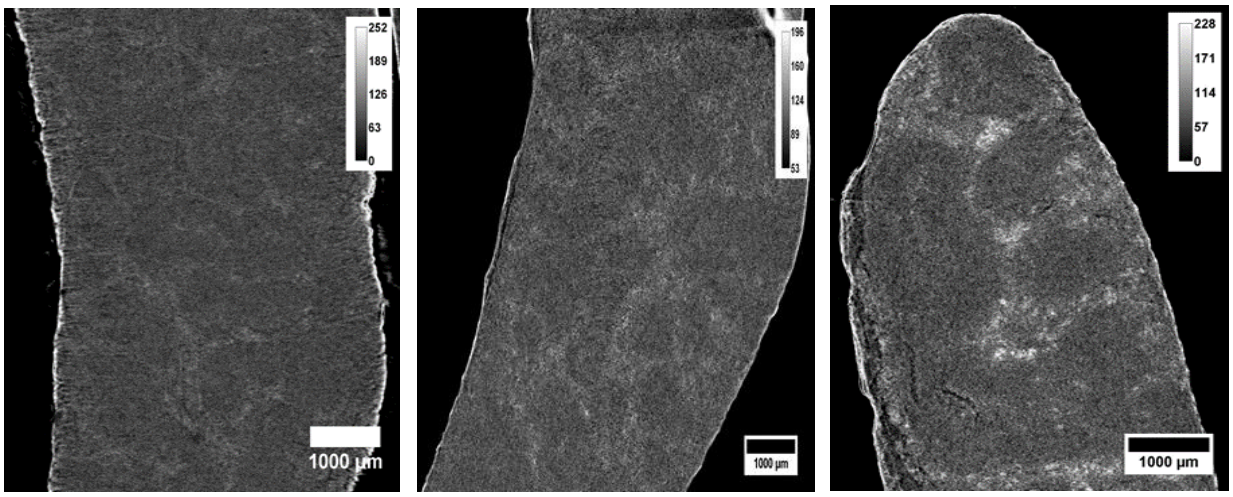

Control 4 mg/Kg 40 mg/Kg

Figure 3.44: *Tomographic slice images of spleen showing deposition of thorium along blood vessels in spleen upon thorium treatment*.

Same results were obtained when images were observed under their three-dimensional structure. In the three-dimensional images also, thorium deposition could be seen along the walls of blood vessels in spleen (Figure 3.45). All three different synchrotron images (projection, slice and three-dimensional) providing the result suggesting thorium deposition along the wall of blood vessels and capillaries of the spleen.

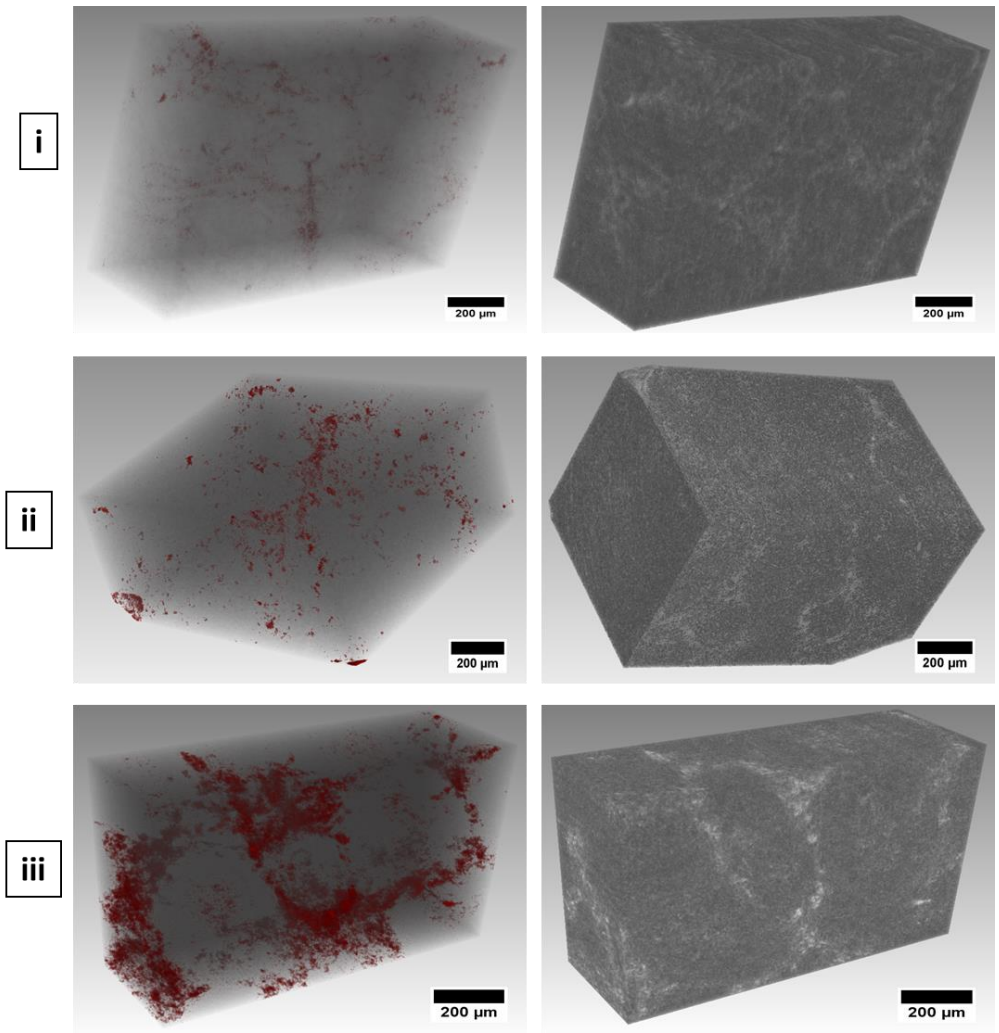

Figure 3.45: *Three-dimensional view of thorium deposition along blood vessels in spleen after thorium treatment, 4 mg/Kg(ii) and 40 mg/Kg(iii) as compared to control (i).*

Like in liver, these qualitative structural alterations observed in spleen were also studied quantitatively. The changes were studied in terms of mean intensity of white patches,

the number of closed patchy structures formed by white colored thorium deposits namely, voxels, the number of voxels per unit area, their percentage per unit area and the total volume occupied by these voxels (Table 3.11). The same technique of quantitative analysis with three major steps i.e., thresholding and feature segmentation, labelling or tagging and geometrical measurement which were used for liver analysis were applied.

Parameters	**Control**	**4 mg/Kg**	**40 mg/Kg**
Mean	45,261	49,236	56,326
No. of voxels	8,943	36,823	2,35,241
% of voxels	0.06	0.25	1.57
Volume occupied by voxels (μm^3)	8,14,930	33,55,495	2,14,36,336

Table 3.11: *Quantitative analysis of thorium treatment in spleen. Threshold value= 46000 in 16-bit images for all images.* ***Values presented are mean of two spleen samples from two animals.***

It was observed that the mean of white patches is highest in 40 mg/Kg as compared to 4 mg/Kg and is the least in control spleen. The number of voxels, their percentage and the volume occupied by them is significantly high in case of 40 mg/Kg as compared to 4 mg/Kg which in turn is significantly higher as compared to control spleen.

3.3.1.4.3: Bone

SR-µCT images of mice femoral bone were also obtained for control and thorium (40 mg/Kg) tissue samples. Approximately 900 raw projection images of each sample were obtained. Flat field correction was performed to remove the excess background and non-uniformity in images arising due to effects of incident-beam. Figure 3.46 shows the projection image of control and thorium treated mice femoral bone which has been flat-field corrected.

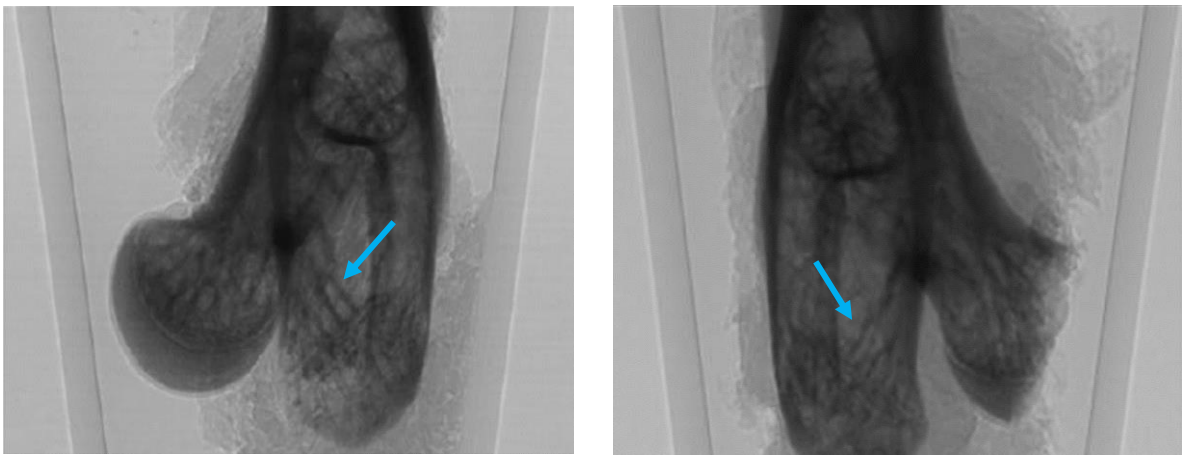

Control Thorium treated

Figure 3.46: Projection image of control and thorium treated mice femoral bone. Arrow indicates loss of inter-connections of trabecular bone in thorium treated samples as compared to control.

Tomographic slice images were reconstructed from these projection images by using Filtered-back projection algorithm (164). Figure 3.47 shows the cross-sectional tomographic slice images of these projections obtained in horizontal plane. These slice images were used to study the image intensity over a selected pixel. Image intensity, also referred to as gray value, is directly proportional to local image density averaged over the volume of pixel. In addition to studying the image intensity, tomographic slice images were also used to study local micro-

architecture of bone including the shape, size and various inter-connections of trabecular bone. The fine details of outer bone wall (cortical bone) were also clearly visible in both the groups.

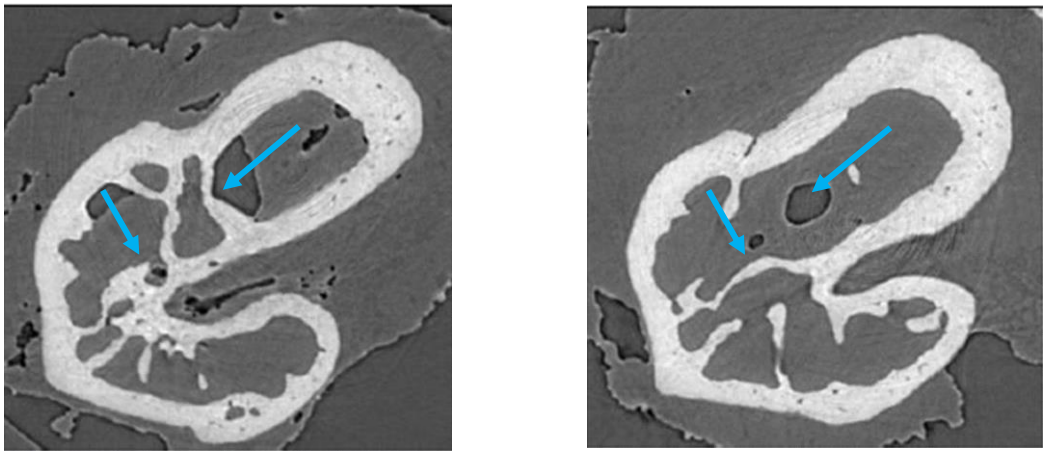

Control Thorium treated

Figure 3.47. Tomographic slice images of control and thorium treated samples where arrow indicates loss of inter-connections of trabecular bone in thorium treated bone as compared to control.

These micro-structures of bone were studied in greater detail in three-dimensional images which were obtained by stacking and volume rendering these tomographic slice images (165). Figure 3.48 (A) shows the three-dimensional volume rendered images of the bottom region of mice femoral bone of both control and thorium treated samples. Figure 3.48 (B) shows their internal cropped images. Both two- and three-dimensional images shows the alterations in structural architecture, various openings, and connections of trabecular bone of mice in both control and thorium treated samples.

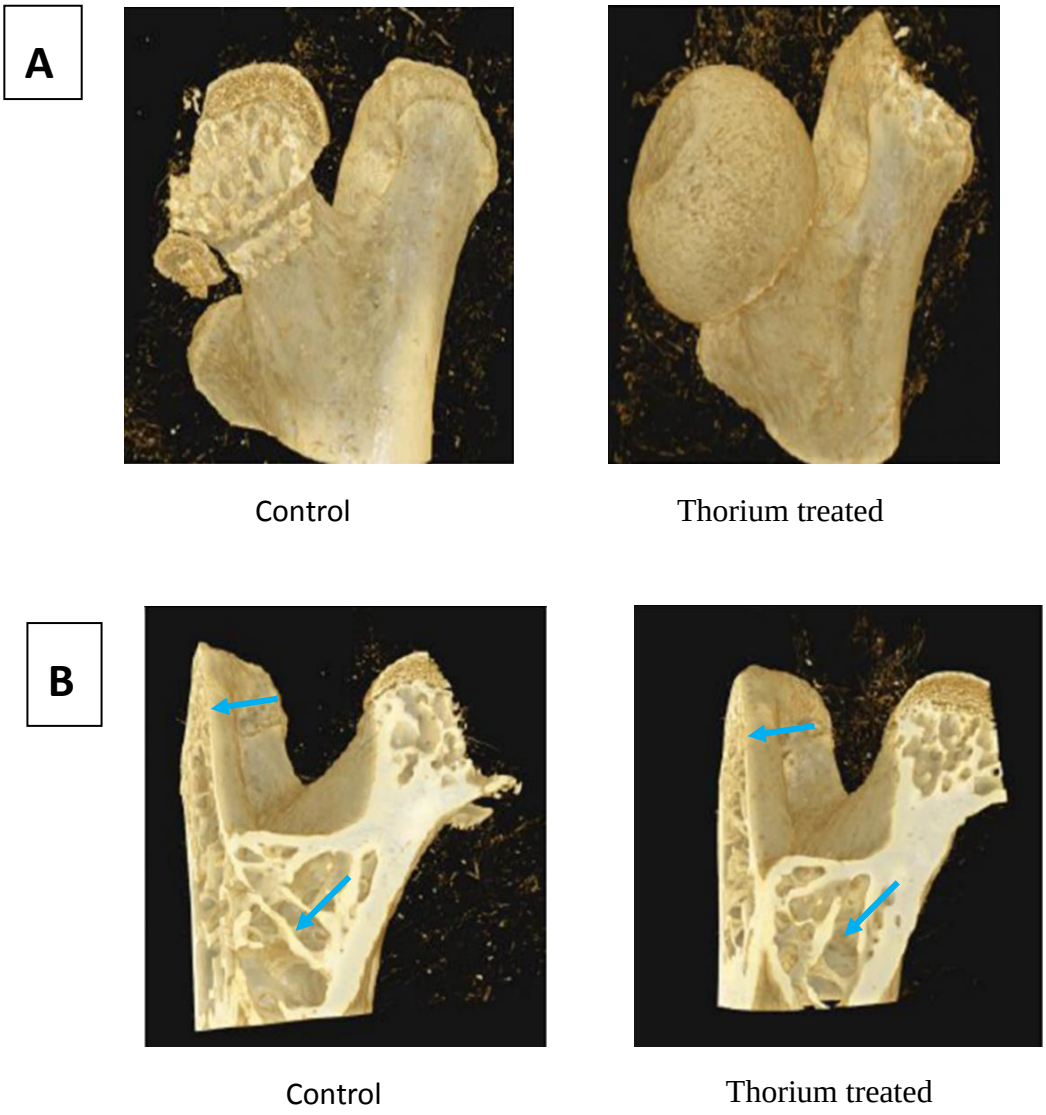

*Figure 3.48. Three-dimensional image **(A)** and their internal cropped image **(B)** of bottom section of mice bone in both control and thorium treated samples. Arrows indicate loss of porosity and inter-connections in trabecular bone in thorium treated bone as compared to control.*

Thorium treatment causes major structural alterations in mice femoral bone. Both trabecular as well as cortical bone undergoes bone degeneration as well as loss of physical density and connectivity in case of thorium treated samples as compared to control. These results were corroborated by all three forms of images i.e., projection, tomographic slices, and

3D images. There was a consistent thinning of trabecular as well as cortical bone which led to increased spacing between various structures in trabecular bone. At places, the thinning of trabeculae was so intense that it was completely lost or degenerated.

Small angle X-ray scattering (SAXS) study of control and thorium treated samples were performed to study the micro-structural details. These micro-structural details of bone were associated with the degree of order in collagen fibers and roughness of bone surface at sub-micrometer scale (166). In order to study these micro-structural details, small angle X-ray scattering experiment was performed on control and thorium treated bone samples using SWAX beamline (BL-18) at Indus-2 synchrotron. The detail of the experimental procedure is as described in Materials and Methods chapter, Section 2.2.18. When mineral particles are aligned perfectly parallel, the SAXS profiles generally show a narrow streak perpendicular to the orientation of the long axis of mineral nanoparticles. The scattering profiles were anisotropic in nature indicating preferred orientation of the nano-meter sized mineral crystallites in bone (Figure 3.49).

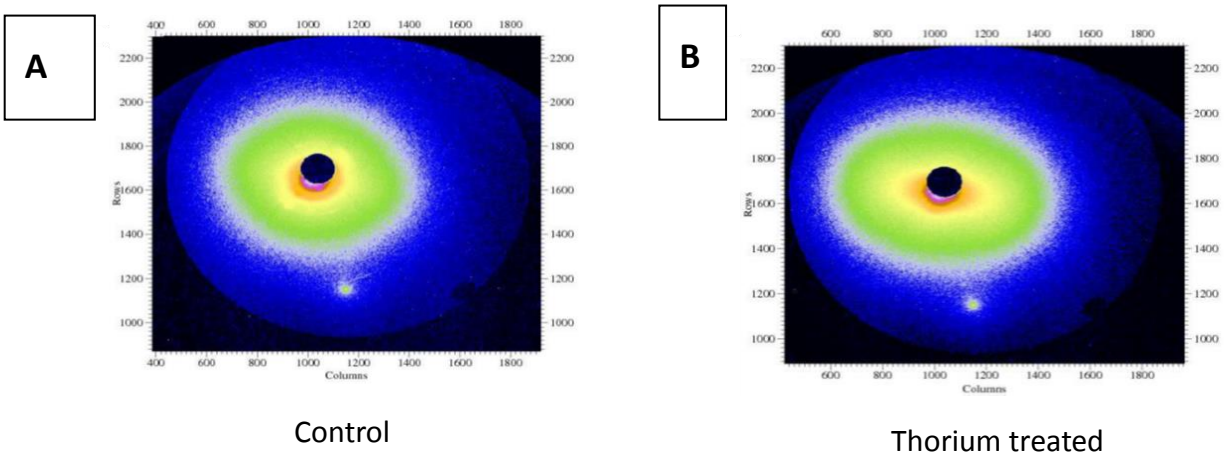

Figure 3.49: *2D SAXS profile of* ***(A)*** *control and* ***(B)*** *thorium treated samples. Arrows indicate change in shape from circular in control to elliptical in thorium-treated bones.*

3.3.1.6: Serum biochemical parameters

To study the effect of thorium on metabolism and homeostasis, different metabolic parameters and their levels in mice serum were studied by various biochemical studies. Serum samples obtained after 1 month were analyzed using automated serum biochemical analyzer and various parameters such as creatinine, total protein, total bilirubin, urea, cholesterol, and glucose etc. were measured (Figure 3.50)

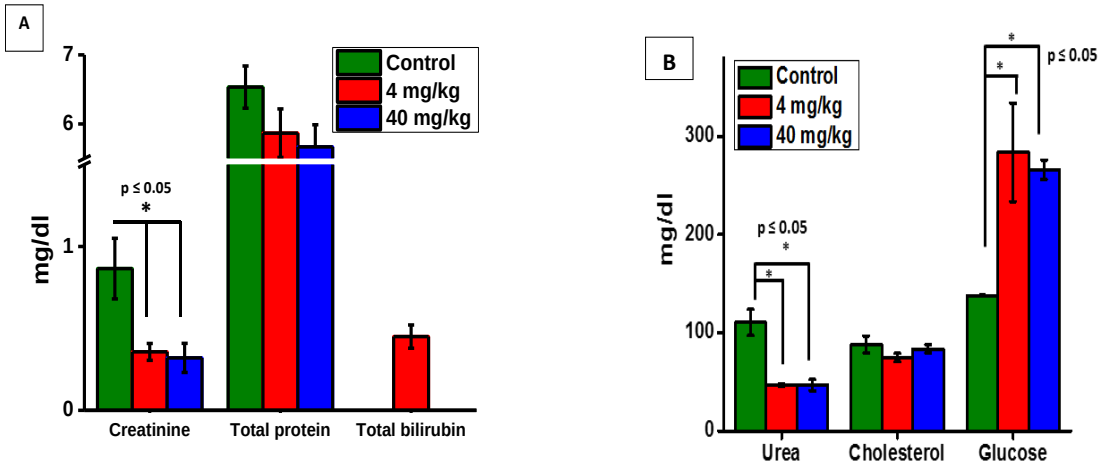

Figure 3.50: *Serum biochemical tests for* ***(A)*** *creatinine, total protein, and total bilirubin and* ***(B)*** *urea, cholesterol, and glucose levels after intra-venous injection of thorium for one month at 4 mg/Kg and 40 mg/Kg dose of thorium. * means $p \leq 0.05$.*

For kidney function, amount of creatinine, total protein, and urea were studied in mice. Amount of glucose and cholesterol in blood were also studied to obtain a simplistic overview of carbohydrate and fat metabolism upon thorium treatment. The amount of creatinine in serum was found to decrease in a dose-dependent manner when treated with thorium as shown in Figure 3.50 A. The decrease in the amount was found to be significant in case of thorium treated groups as compared to control. Normal range of creatinine varies from 0.3 to 1 mg/dl

in mice (167). Thus, the amount of creatinine, even after significantly reducing in treatment group, was found to fall within the normal range. Levels of total protein did not show any significant changes in their amounts in control and thorium treated mice serum. Total bilirubin could be measured only in 4 mg/Kg group, which could be due to experimental artefact.

The level of urea in serum is another marker of kidney function. After one month of thorium treatment, it was observed that the level of urea decreased significantly ($p \leq 0.05$) in both the thorium treated groups (4 and 40 mg/Kg) as shown in Figure 3.50 B. The level of cholesterol and glucose were also studied in mice treated with thorium in order to understand the effect of thorium on carbohydrate and fat metabolism. It was observed that the amount of cholesterol in mice treated with 4 and 40 mg/Kg of thorium for one month did not show any change their expression level (Figure 3.50 B). When glucose levels in serum sample were studied, it was observed that there was a profound increase ($p \leq 0.05$) in the amount of glucose in mice treated with thorium as compared to control after one month. This finding of higher blood glucose is also correlated by higher amount of glycogen in thorium treated liver tissue as compared to control, the results of which is shown below in Figure 3.51 (103).

Liver is the prime site for glucose and glycogen metabolism which is transported mainly by blood. Since, both liver and blood vessels are affected by thorium accumulation, it is impertinent that this would cause an imbalance on glucose and glycogen metabolism. The effect of thorium on glycogen metabolism was studied in liver using glycogen staining technique i.e., Periodic acid-Schiff (PAS) staining. Thin liver tissue sections obtained on glass slides were subjected to PAS staining of glycogen. The result indicated higher glycogen staining of hepatocytes (with stained cytoplasm) in thorium treated mice liver sections than control suggesting higher glycogen content in thorium treated mice liver tissues (Figure 3.51). It was also interesting to observe that the glycogen areas are peri-nuclear to hepatocytes in

controls, which extends up to whole cytoplasm in case of thorium treated mice liver tissue samples (103).

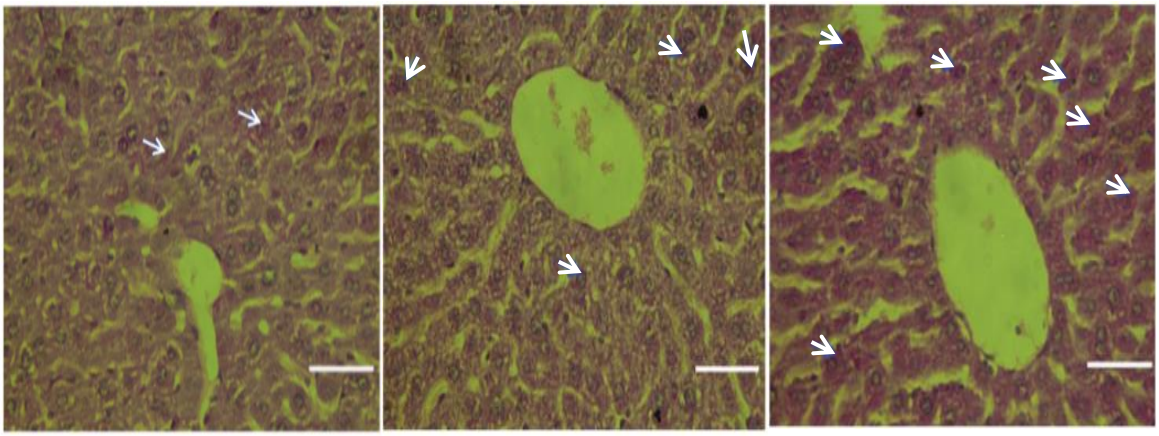

Control 4 mg/Kg 40 mg/Kg

Figure 3.51: *Glycogen staining of liver tissue sections obtained from control and thorium treated mice. Images were acquired using bright field microscopy at 40X (eye piece 10X). Arrows indicate stained cytoplasm (glycogen) either located peri-nuclear (control) or cytoplasmic (4 and 40 mg/Kg thorium) to hepatocytes. Scale bars 50 µm.*

3.3.2: Effects of thorium in mice at long period (6 and 12 months)

Thorium bio-distribution and gross health parameters study at short time periods (day 1 and 30) in previous Section (3.3.1.1 and 3.3.1.2) showed substantial localization of thorium to different target organs but unnoticeable toxicity in mice at single and acute low dose of thorium i.e., 4 mg/Kg. However, at 40 mg/Kg causes toxicity in mice as is observed by tissue necrosis at site of injection. Moreover, high dose of thorium showed death of a few mice within a few hours after intravenous injection. Even though, quantification and exact reasons of the morbidity could not be established but it seemed to be associated with acute toxicity of thorium. Based on these observations, it was decided to use lower doses of thorium (10 mg/Kg and 20

mg/Kg in addition to 4 mg/Kg) than 40 mg/Kg followed by measurement of different endpoints at long-term (6 and 12 months) time periods. Different animal groups were planned for long-term thorium treatment as shown in detail in Scheme 4 in Section 2.2.17 in Chapter 2. For this, thorium was injected intravenously to 8-10-week-old Swiss albino male mice followed by measurement of different endpoints as mentioned below in subsequent Sections.

3.3.2.1.: Gross Health Parameters

During course of this treatment period (6 and 12 months) mice were intermittently observed for gross health parameters/changes due to thorium treatment and wherever required observations were recorded. It was observed that like 30-day period, at 6-month time also, in thorium treated group of mice tail underwent blackening which started from the point of injection and continued till tail end. This was followed by tissue necrosis after which the tails were slowly shed off. This change was more prominently observed in case of 20 mg/Kg of thorium dose as compared to 10 and 4 mg/Kg of thorium. Since, the dose of 20 mg/Kg is half of 40 mg/Kg, the phenotypic changes observed took longer than 30-days to appear (approx. 3-4 months). This blackening of tail was observed in ~50% of total mice injected with 20 mg/Kg thorium. In case of 10 mg/Kg thorium-treated mice, two mouse showed complete blackening and subsequent shedding of tail while three other showed partial blackening of tail. The rest of mice and mice in group treated with 4 mg/Kg of thorium did not show such changes in their tail. Images of the mice were obtained using Kodak digital photographic camera after 4 months of injection (Figure 3.52 A-D). It could be clearly observed that mice tail appeared to be normal in case of control and 4 mg/Kg thorium (Figure 3.52 A and B). At 10 mg/Kg, there was a dark spot, as is shown by blue arrow, which could be observed at the site of injection. The tail vein in the lower part was darker and hence, more clearly observable (marked by red arrow, Figure 3.52 C).

However, at 20 mg/kg dose of thorium, mice tail became completely dark starting from the point of thorium injection and continued till tail end as is shown by blue arrow (Figure 3.52 D). This led to tissue necrosis and subsequent shedding off mice tail which was observed in later months of incubation period.

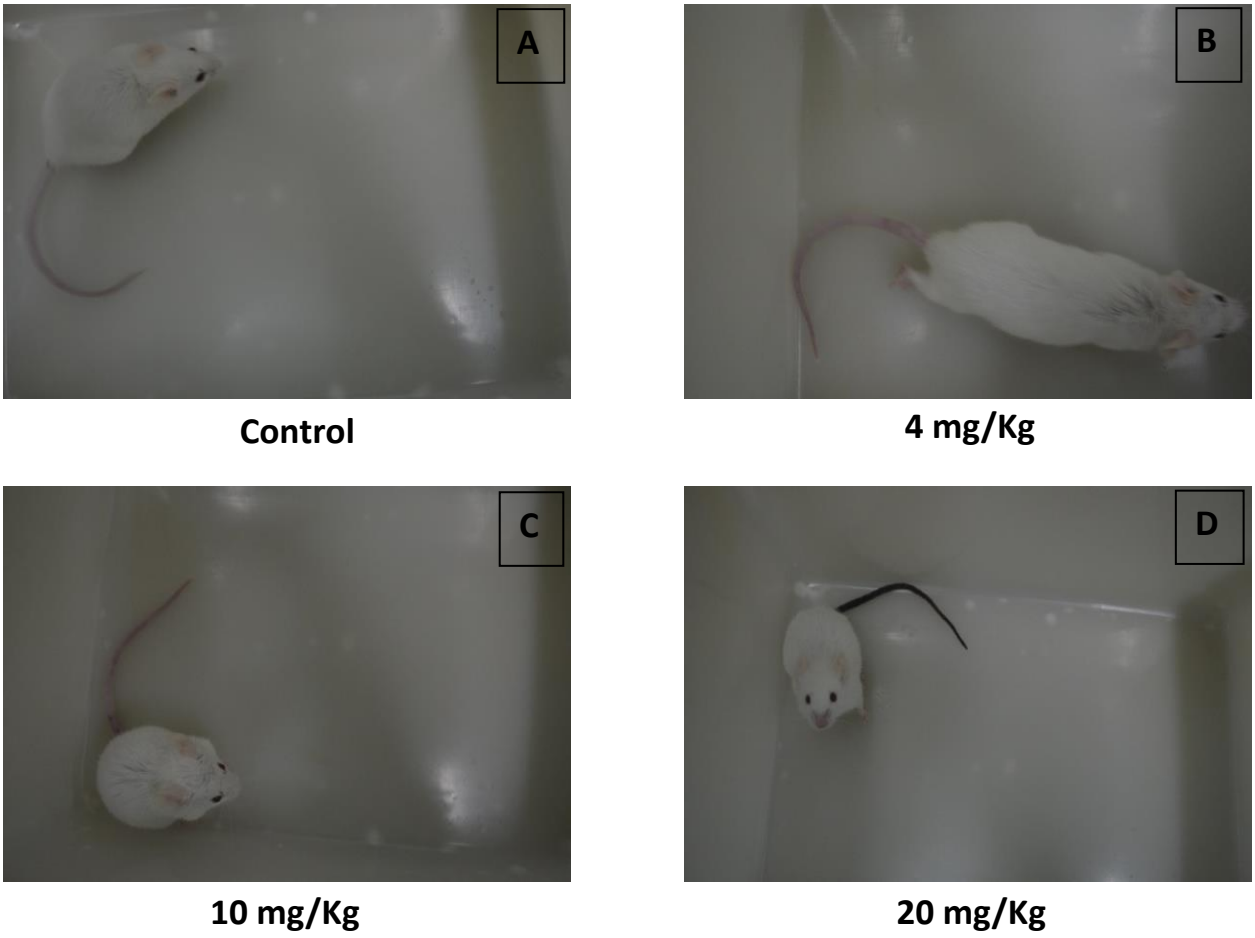

Figure 3.52 A-D. *Photographic images of mice showing changes caused by different doses of thorium after ~6 months. No observable changes were observed in* ***(A)*** *control and* ***(B)*** *4 mg/Kg mice. At* ***(C)*** *10 mg/Kg thorium dose, site of thorium injection was found to have a dark spot as marked by blue arrow and the lower half of mice tail vein was darker compared to upper half tail vein as is shown by red arrow.* ***(D)*** *20 mg/Kg dose of thorium showed complete darkening of tail from point of injection till the end, marked by blue arrow.*

Monitoring of features of mice continued till twelve months and mice were photographed before their sacrifice at twelve months. After one year of treatment with different doses of thorium, various phenotypic changes were observed in mice (Figure 3.53). In control mice, hair fall, and balding pattern was seen between the eyes which continued till nose as is marked by blue colored arrow (Figure 3.53 A). This hair fall could be attributed to one of the many effects of aging in mice. This hair fall, and balding was seen in all thorium treated mice as well (shown by blue arrow in each pic). At 4 and 10 mg/Kg thorium dose, in addition to hair fall, discoloration of eyes was also observed as is shown by red arrow (Figure 3.53 B and C). At 20 mg/Kg, all these effects were present in addition to shortening of tail (marked by black arrow) (Figure 3.53 D).

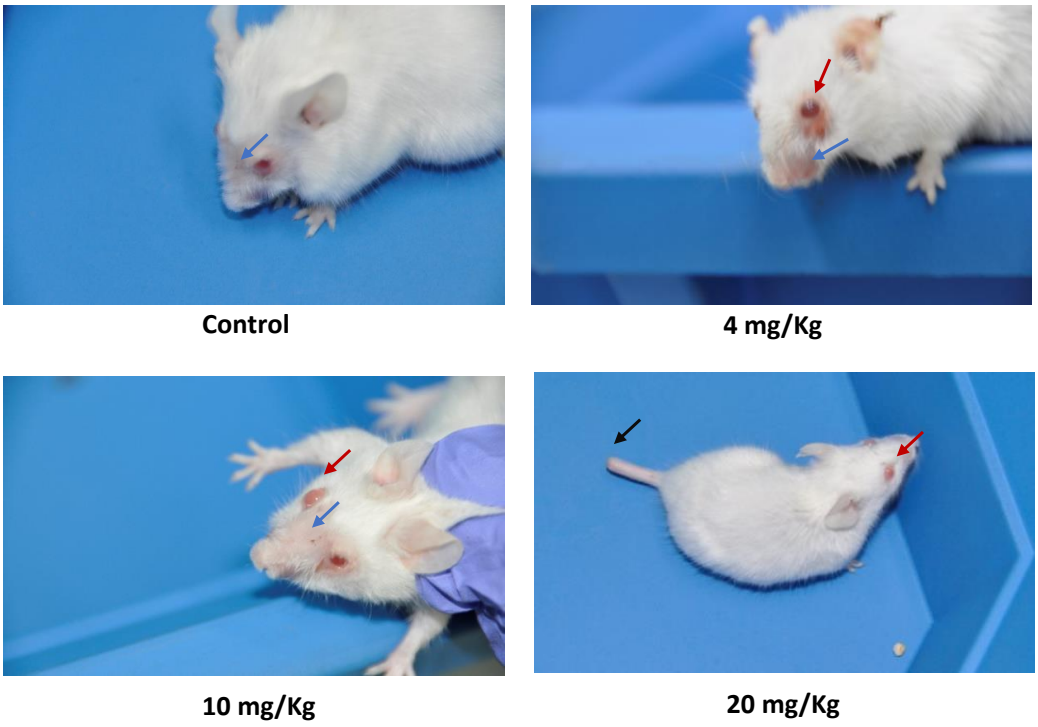

Figure 3.53 A-D. *Photographic images of mice showing various changes caused by different doses of thorium after ~12 months. Hair fall and balding was observed in control* ***(A)*** *hair fall and balding along with discoloration of eyes at 4 mg/Kg* ***(B)*** *and 10 mg/Kg* ***(C)*** *20 mg/Kg dose of thorium showed tail shortening in addition to hair fall and discoloration of eye* ***(D)*** *Blue*

color arrow indicates hair fall, red color arrow indicates discoloration of eyes and black arrow indicates shortening of tail.

The hair fall and balding pattern was seen in 80-85% of mice after twelve months. Discoloration of eye color was observed in ~90% of mice in thorium treated groups whereas blackening and subsequent tail shortening was observed only in 10 and 20 mg/Kg thorium treated groups. 70-75% mice in 10 mg/Kg group showed tail blackening and shortening while in 20 mg/Kg, the same effect was 100%.

Apart from these visible changes, weight of mice was also monitored at regular intervals for 6-and 12-month time-period groups. Mice weight is expressed as its average with standard deviation (Figure 3.54 A-B).

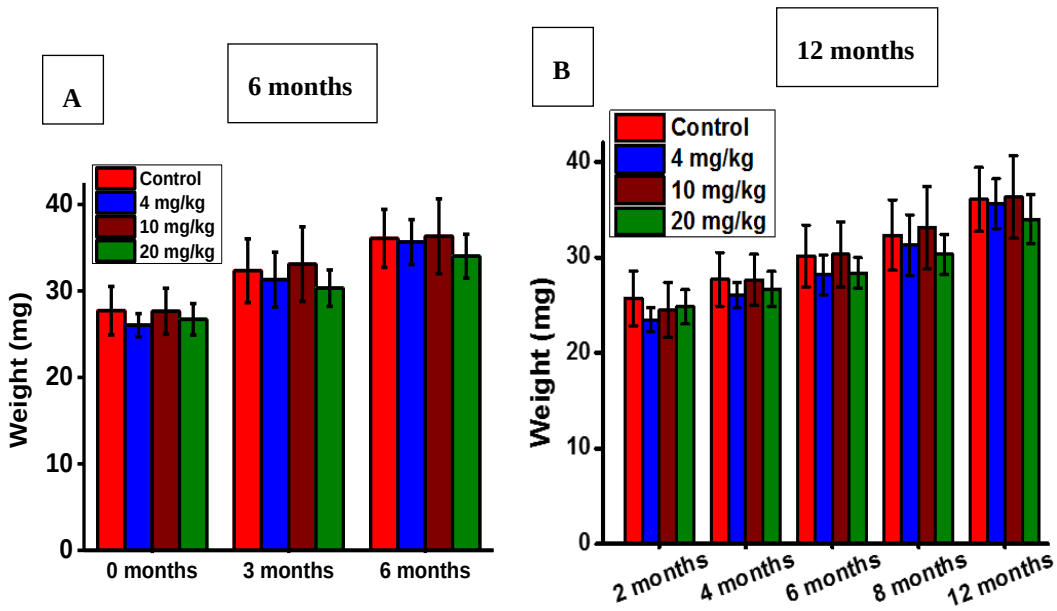

Figure 3.54 A-B. *Weight of mice after thorium injection in case of* ***(A)*** *6 months and* ***(B)*** *12 months treatment groups. (n=5)*

The weight of control animals increased with respect to time. However, compared to respective controls, the weight the mice in thorium treated groups (4 mg/Kg and 10 mg/Kg; 6

and 12 months) did not vary significantly. At longer periods (more than 3 months), animals in 20 mg/Kg, showed decrease in weight but it was insignificant. Hence, in terms of gross health parameters, following thorium treatment mice showed hair fall, discoloration of eyes, tail blackening (followed by tissue necrosis and tail shedding) while insignificant effect on weight.

3.3.2.2: Bio-distribution of Thorium after 6 and 12 months of Treatment

Thorium bio-distribution after long-term treatment (6 and 12 months) under *in-vivo* conditions were performed for 4, 10 and 20 mg/Kg of thorium doses. For this, animals were administered with thorium intravenously as described in Scheme 4 in Section 2.2.17 of Chapter 2. Animals were housed in standard conditions with intermittent gross observations for any morbidity or health issues. The mice were sacrificed after 6 and 12 months. Different organs/tissues (such as blood, brain, lungs, kidneys, liver, spleen, and bone) were collected, and one set of tissue were used for biodistribution studies. Except blood samples all organs were washed in saline and digested in cHNO_3 for thorium estimation by ICP-MS (as mentioned in Materials and Methods Section 2.2.17). Results were obtained by averaging the values from 3-5 mice. Total thorium in µg in each organ and specific thorium (thorium in µg per gram of organ weight) in µg/g was calculated/plotted for each organ (Figure 3.55 A-D). At these optimized doses of thorium and longer time periods (6 and 12 months), bio-distribution was performed in additional organs/tissues (kidney, brain, blood, and lung) including known major targets organs (liver, spleen, and skeleton) studied in previous experiment.

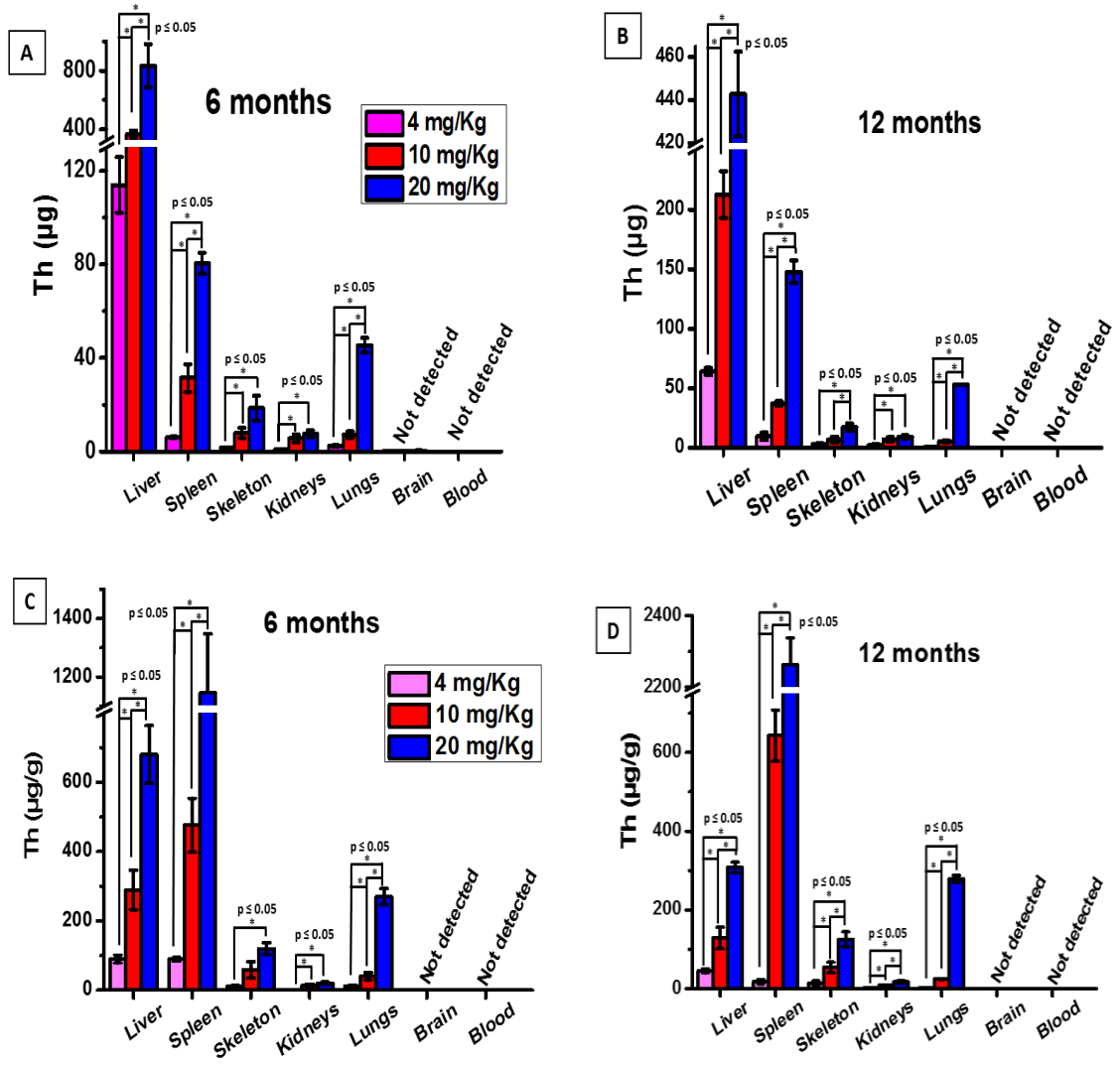

Fig. 3.55 (A-D): *Thorium bio-distribution at 4, 10 and 20 mg/Kg dose of thorium injected intra-venously in Swiss albino male mice after 6 and 12 months. Thorium was estimated in liver, spleen, skeleton, kidneys, lungs, brain, and blood by ICP-MS.* ***(A-B)*** *total thorium (µg) at 6 and 12 months and* ***(C-D)*** *specific thorium (thorium in µg per gram of organ weight) (µg/g) at 6 and 12 months in liver, spleen, skeleton, kidneys, lungs, brain, and blood (N = 3-5).*

At both time points, i.e., 6 and 12 months, maximum amount of thorium was found to be deposited in liver across all doses followed by spleen, skeleton, and kidneys. Among skeleton, kidney and lungs, the amount of thorium detected in each of these organs were similar at 4 and 10 mg/Kg. However, at higher thorium concentration, i.e., 20 mg/Kg, maximum amount of thorium was detected in lungs followed by skeleton and kidneys at both time points (Figure 3.55 A-D). The pattern of thorium localization in different organs were similar to day 1 and 30 biodistribution studies (Figure 3.37) except observing localization of significant level in lungs especially at high dose of thorium (20 mg/Kg). Since in previous experiment, level of thorium was not determined in lungs, the results could not be compared. No thorium was detected in brain and blood after 6 and 12 months of treatment. When liver, spleen and lungs were compared, it was found that at 20 mg/Kg, the amount of thorium deposited was significantly higher as compared to 4 and 10 mg/Kg and the amount of thorium deposited at 10 mg/Kg is significantly higher than 4 mg/Kg. This pattern of thorium deposition for all three doses remains same at both time interval i.e., 6 and 12 months. In case of skeleton, thorium deposition at thorium dose of 10 and 20 mg/Kg was significantly higher as compared to 4 mg/Kg. However, between 10 and 20 mg/Kg, the increase in thorium deposition is not significant at 6 months. At 12 months, the thorium deposition at dose 20 mg/Kg was significantly higher as compared to 4 and 10 mg/Kg. Between 4 and 10 mg/Kg, thorium deposition increased with the increase in dose, but the difference was insignificant. In kidneys, the amount of thorium deposited at 10 and 20 mg/Kg was significantly higher than 4 mg/Kg. However, between 10 and 20 mg/Kg, the difference in thorium uptake was not significantly higher at both 6-and 12 months-time point.

It was observed that specific thorium i.e., thorium in µg deposited per gram of organ weight is same in case of liver and spleen at 4 mg/Kg. However, at 10 and 20 mg/Kg, specific

thorium deposited in spleen is significantly higher as compared to the thorium deposited in liver at corresponding doses. Although total thorium deposited in liver is much higher as compared to spleen, low specific thorium in liver indicates that spleen stores much higher amount of thorium per gram of its weight and hence, has higher density of thorium deposits. In contrast, although liver has much higher organ weight and surface area as compared to spleen, it contains less amount of thorium per gram of its weight and hence, is less dense in terms of thorium deposits in comparison to spleen. The specific thorium in spleen remains higher at both time points i.e., 6 and 12 months at 10 and 20 mg/Kg thorium concentrations. Skeleton, kidney, and lungs showed deposition in terms of specific thorium and followed the same pattern at both 6 and 12 months. Total thorium and specific thorium showed similar deposition in skeleton, kidney, and lungs according to the doses. The absolute values of total thorium and specific thorium found in each organ after 6 and 12 months of thorium treatment is shown in detail in Table 3.12 (A-B).

Thorium Dose	**4 mg/Kg**		**10 mg/Kg**		**20 mg/Kg**	
Time (⟹) / **Organs (⇩)**	**6 Months**	**12 Months**	**6 Months**	**12 Months**	**6 Months**	**12 Months**
Liver (n=3-5)	114 ± 12	64 ± 3	368 ± 26	213 ± 20	835 ± 147	443 ± 20
Spleen (n=3-5)	6 ± 0.2	10 ± 3	31 ± 6	37 ± 2	80 ± 5	148 ± 9
Skeleton (n=3-5)	2 ± 0.1	3 ± 0.3	8 ± 2	7 ± 3	19 ± 5	17 ± 3
Kidneys (n=3-5)	1 ± 0.1	2 ± 0.9	6 ± 2	7 ± 2	8 ± 2	9 ± 1

Lungs (n=3-5)	2 ± 0.3	0.6 ± 0.2	7 ± 1	5 ± 0.8	45 ± 3	53 ± 0.2

Table 3.12 (A): *Total thorium in µg deposited in different organs such as liver, spleen, skeleton, kidney, and lungs in Swiss albino male mice with three different concentrations of thorium i.e., 4, 10 and 20 mg/Kg after 6 and 12 months. Organs were digested and thorium was estimated using ICP-MS. Final values were normalized by subtracting the control values. No thorium was detected in blood and brain after 6 and 12 months. (N = 3-5)*

Thorium Dose	**4 mg/Kg**		**10 mg/Kg**		**20 mg/Kg**	
Time (⟹) / **Organs (⇓)**	**6 Months**	**12 Months**	**6 Months**	**12 Months**	**6 Months**	**12 Months**
Liver (n=3-5)	90 ± 12	45 ± 5	289 ± 57	129 ± 27	680 ± 84	308 ± 13
Spleen (n=3-5)	89 ± 5	18 ± 6	476 ± 78	643 ± 65	1145 ± 203	2263 ± 75
Skeleton (n=3-5)	12 ± 1	14 ± 5	59 ± 23	54 ± 13	119 ± 17	126 ± 18
Kidneys (n=3-5)	2 ± 0.2	3 ± 0.0	14 ± 3	9 ± 2	20 ± 3	17 ± 4
Lungs (n=3-5)	12 ± 1.4	3 ± 0.0	39 ± 11	24 ± 0.7	270 ± 23	279 ± 8.6

Table 3.12 (B): *Specific thorium in µg/g deposited in different organs such as liver, spleen, skeleton, kidney, and lungs after injecting Swiss mice with three different concentrations of thorium i.e., 4, 10 and 20 mg/Kg after 6 and 12 months. Organs were digested and thorium was estimated using ICP-MS. Final values were normalized by subtracting the control values. No thorium was detected in blood and brain after 6 and 12 months. (N = 3-5)*

As described earlier, maximum amount of total thorium was found in liver after 6 and 12 months of thorium treatment followed by spleen. However, when specific thorium deposited in each organ was studied, it was found that except 4 mg/Kg, spleen contained much higher concentration of thorium at both 6 and 12 months indicating a much denser distribution of thorium in spleen as compared to liver. At low dose i.e., 4 mg/Kg, specific thorium in liver and spleen are similar at 6-month time point and decreases in spleen at 12 months. On the other hand, specific thorium in spleen at 10 and 20 mg/Kg is almost 1.7 times higher at 6-month time interval which further increases to ~5 times at 10 mg/Kg and ~7 times at 20 mg/Kg at 12-month time intervals. This increase in the amount of specific thorium was dose dependent at higher time point, which suggested higher thorium binding efficiency and capacity of spleen as compared to liver. Skeleton, kidney, and lungs also showed an increase in their specific thorium but since their accumulation is low, the amount of thorium bound per g of organ weight is comparatively not very high.

Thorium once accumulated inside body is transported across various target organs until stability is achieved. Percentage of thorium cleared and/or accumulated from/on different target organs over a period of 12 months was therefore calculated and is expressed in terms of both total thorium and specific thorium in Table 3.13 (A-B).

A

Total thorium (μg) percentage clearance/accumulation after 12 months

Thorium Dose (⇒) / Organs (⇓)	4 mg/Kg	10 mg/Kg	20 mg/Kg
Liver	-43.8	-42.2	-47.0
Spleen	57.7	18.4	83.9
Skeleton	92.1	-14.8	-7.4
Kidneys	172.7	27.6	21.0
Lungs	-76.6	-24.6	16.2

B			
Specific thorium (µg/g) percentage clearance/accumulation after 12 months			
Thorium Dose (⇒) / **Organs (⇓)**	**4 mg/Kg**	**10 mg/Kg**	**20 mg/Kg**
Liver	-49.7	-55.3	-54.7
Spleen	-79.7	35.1	97.6
Skeleton	13.1	-8.7	5.0
Kidneys	72.9	-36.6	-13.6
Lungs	-79.3	-38.6	3.5

Table 3.13: *Percentage of clearance/accumulation among various target organs on exposure with thorium over a period of 12 months (compared with 6 month) and expressed in terms of* ***(A)*** *total thorium (µg) and* ***(B)*** *specific thorium (µg/g). Positive values represent accumulation and negative values represent clearance.*

It could be clearly seen that over a period of 12 months, approximately 50% of thorium initially deposited in liver is cleared/removed from it. Similarly, spleen showed an accumulation of thorium over a period of 12 months. At 20 mg/Kg, there is an ~80-90% increase in the amount of thorium deposited in spleen both in terms of total thorium and specific thorium. Bone, also, showed an increase in accumulation of thorium. The increase is more prominent in terms of specific thorium at 20 mg/Kg dose of thorium.

3.3.2.3.: Transmission electron microscopy (TEM)

Since liver was major target organ of thorium, its effects on mice liver tissue obtained from highest dose of thorium i.e., 20 mg/Kg for 1 year were studied using transmission electron microscopy. Liver tissue obtained from sacrificed mice was preserved in 10% formaldehyde solution and subjected to further processing (as mentioned in Materials and Methods Section 2.2.12) for TEM imaging (Figure 3.56 A-B). The images were studied at two different scale magnifications (0.5 and 1 µm). Figure 3.56 A details images with scale magnification of 1 µm. There was an increase in intracellular spacing in thorium treated liver sample (shown by red arrows in the Figure) as compared to control. Similarly, as is observed in synchrotron imaging of liver, there was a distortion of membrane surrounding the blood vessel and shrinkage of blood vessels in thorium treated liver as compared to control (shown by yellow arrows). It is clearly observed that the walls surrounding the blood vessel was smooth and well-demarcated in case of control samples. However, after thorium treatment, this smooth and well demarcated lining of blood vessel was lost and there was an invasion of extracellular matrix in the blood vessel indicating extensive damage to blood vessel. The effects of thorium treatment in liver were studied in further detail by doubling the magnification scale so that the scale represents the magnification of 0.5 µm (Figure 3.56 B). At this magnification, it was observed that there was a disintegration of endoplasmic reticulum network inside cells as is marked by orange arrows. There was a marked decrease in the number of endoplasmic reticulum folds in liver samples exposed to thorium for one year as compared to control liver. Also, as was observed in Figure 3.56 A, there is a loss of integration and demarcation of cell wall boundary leading to the invasion of extracellular matrix components inside the blood vessels. This loss of demarcation and invasion of components inside the vessels is marked by white arrow in the image. It is thus, clear that thorium treatment leads to damage of blood vessels in liver as is

seen by both synchrotron imaging as well as transmission electron microscopic images. Also, the loss of endoplasmic reticulum network indicates possible impairment of protein structure and function as well as of inter-cellular network connections.

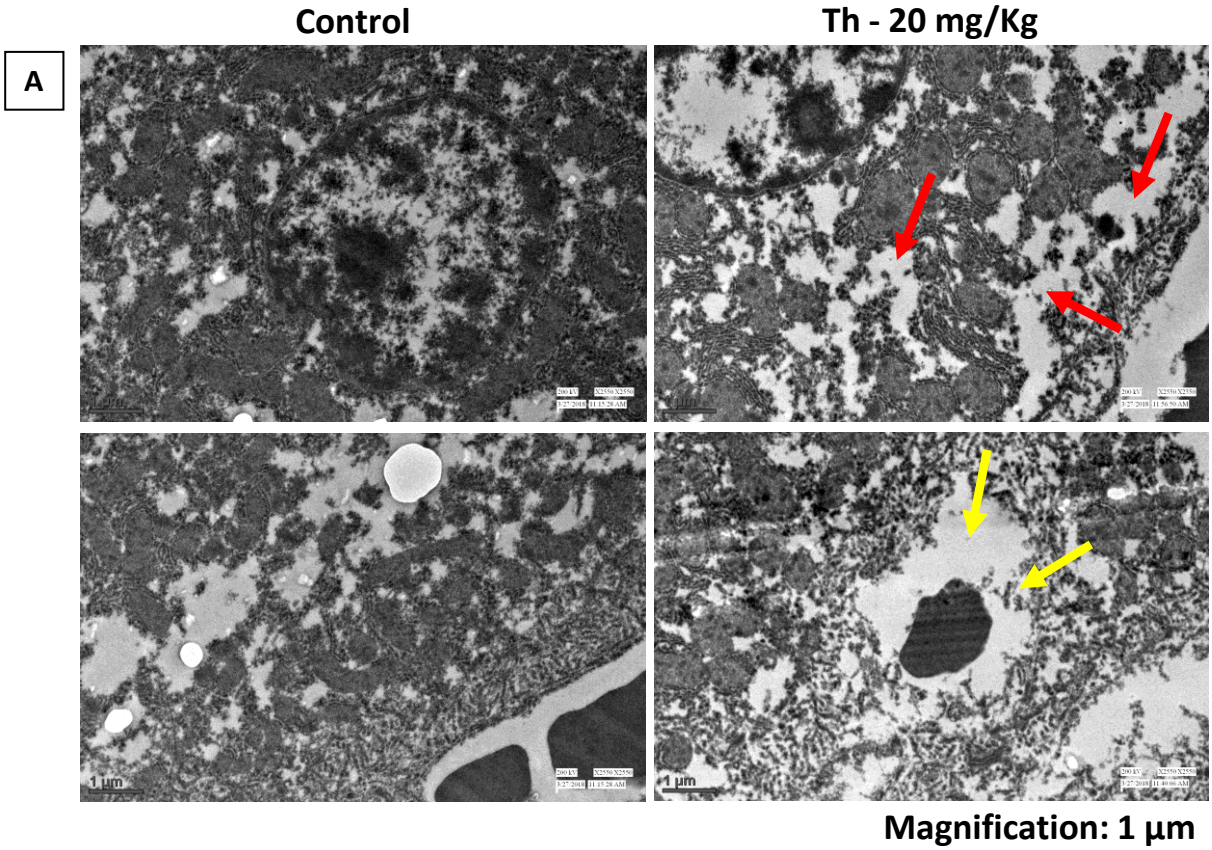

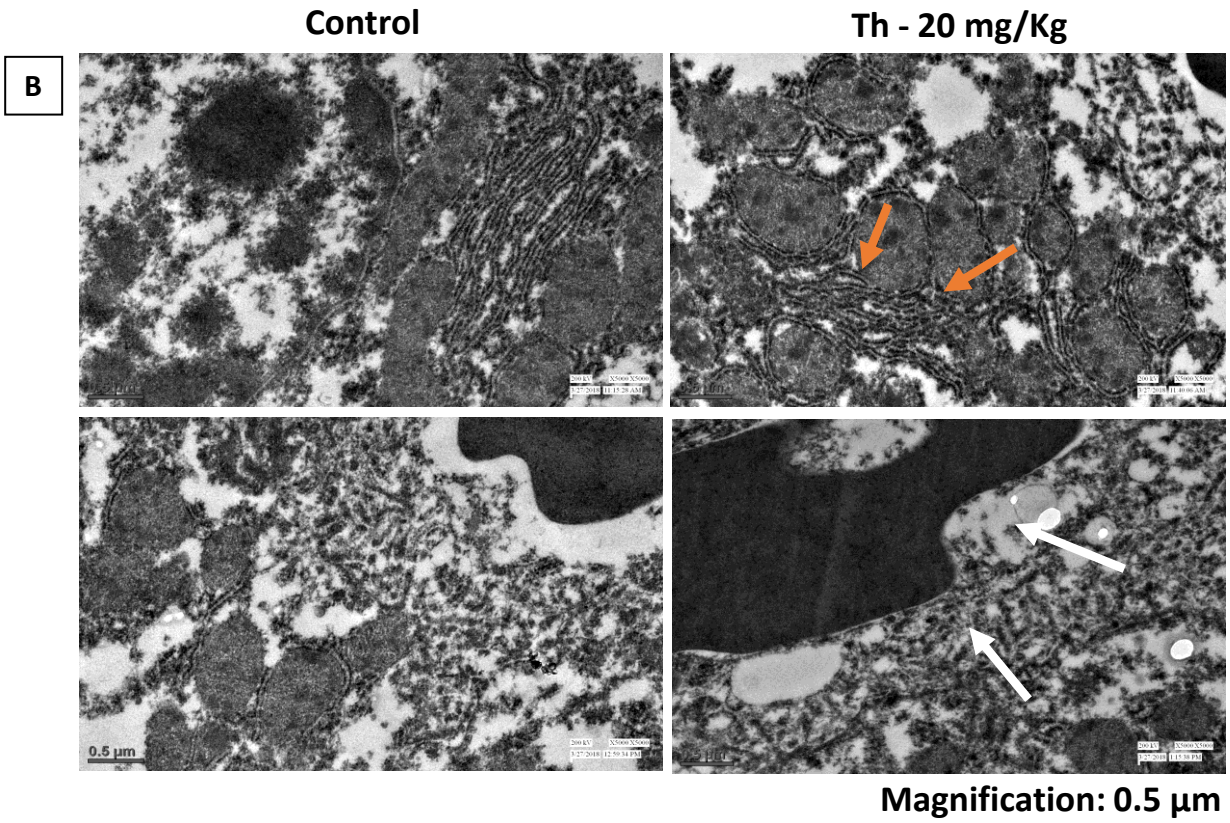

Figure 3.56 (A-B): *Anatomical changes in liver treated with 20 mg/Kg of thorium for 12 months as compared with control. (**A**) has magnification of 1 µm and (**B**) of 0.5 µm. Red arrows indicate increased intracellular spaces probably due to organelle damage; Yellow arrows indicate shrinkage of blood vessels; orange arrow indicates disintegration of endoplasmic reticulum and white arrows shows enlarged view of reduced blood capillaries.*

3.3.2.4. Histopathological changes in major organs

Histopathological changes were studied in major organs of mice after for long duration study of thorium treatment injected with 4, 10 and 20 mg/Kg of thorium for 6 and 12 months. Bright field microscopic images of H & E-stained slides were obtained for liver, spleen, bone, brain, and lungs.

Liver, 6 months

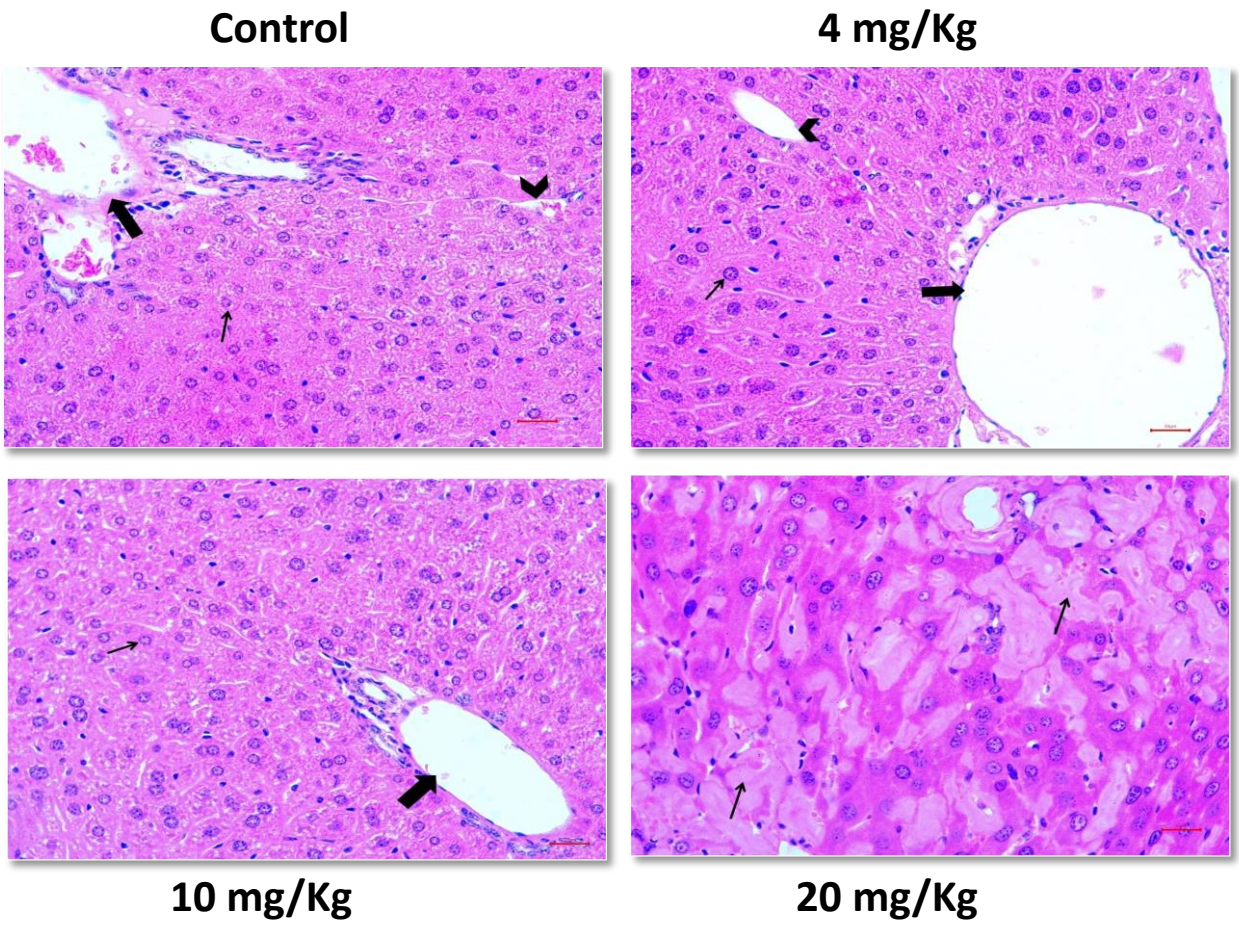

Figure 3.57: *Hematoxylin and eosin staining of liver treated with 4, 10 and 20 mg/Kg of thorium as compared to control at 40X after 6 months of treatment. Control, 4 and 10 mg/Kg liver showed normal histopathology where large arrow indicates portal triad, arrowhead indicates central vein and small arrow indicates hepatocytes. 20 mg/Kg treated liver showed deposition of amorphous proteinaceous material (amyloid) at hepatocytes as is indicated by small arrow. Objective lens: 40X.*

Liver, 12 months

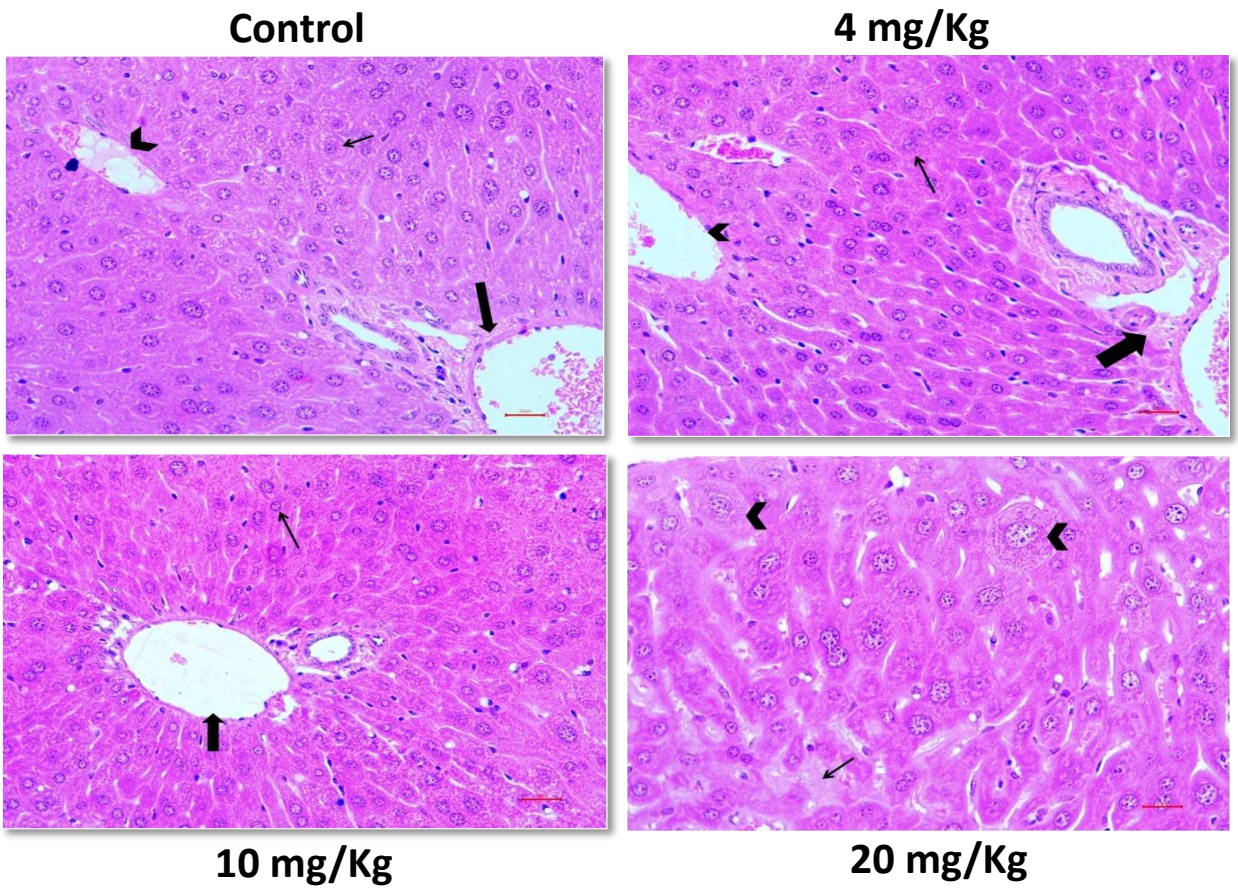

Figure 3.58: *Hematoxylin and eosin staining of liver treated with 4, 10 and 20 mg/Kg of thorium as compared to control at 40X after 12 months of treatment. In case of control, 4 and 10 mg/Kg, the liver tissue showed normal histology where large arrow indicated portal triad, arrowhead indicated central vein, and small arrow indicated hepatocytes. At 20 mg/Kg thorium treatment after 12 months, deposition of amorphous proteinaceous material (possibly amyloid) in hepatocytes as is indicated by small arrows and hypertrophy of hepatocytes as indicated by arrowhead is observed. Objective lens: 40X.*

Spleen, 6 months

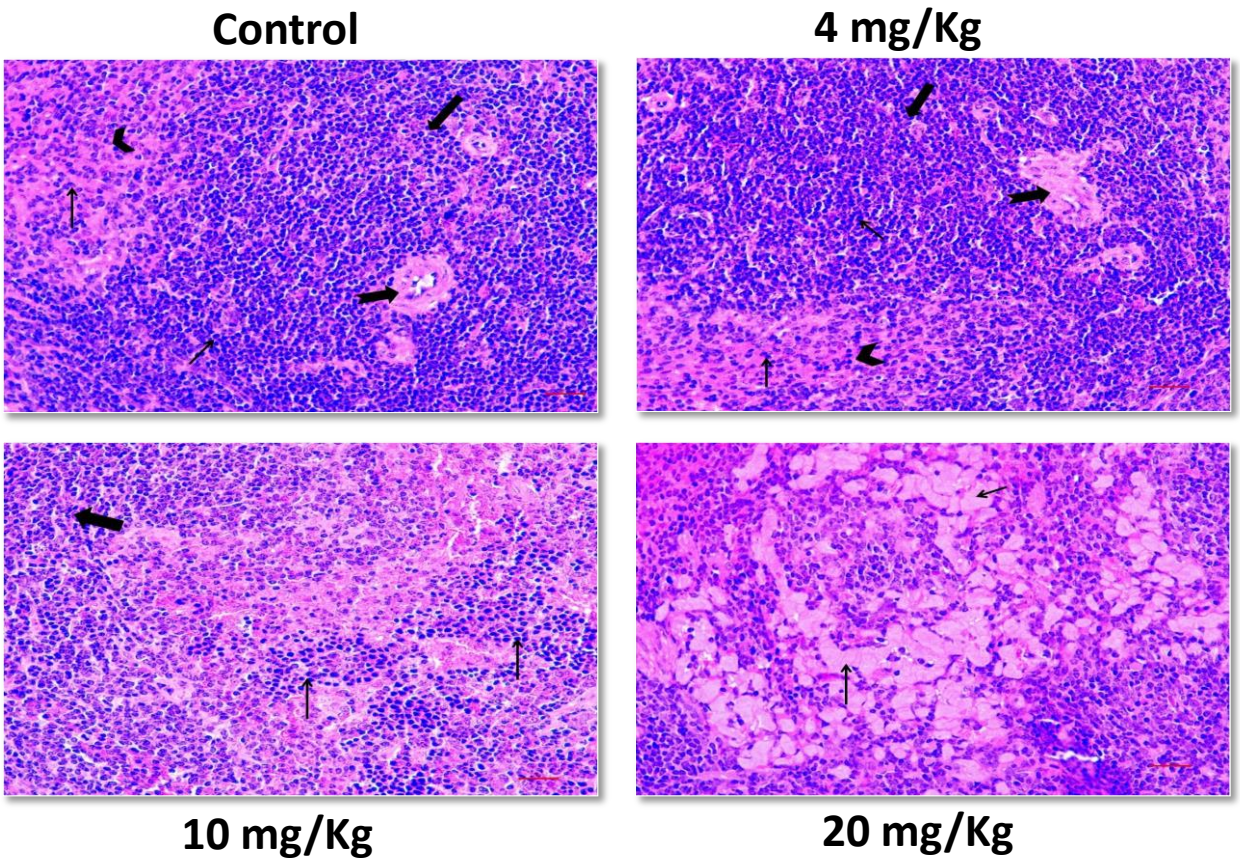

Figure 3.59: *Hematoxylin and eosin staining of spleen treated with 4, 10 and 20 mg/Kg of thorium as compared to control at 40X after 6 months of treatment. Control as well as 4 mg/Kg spleen shows normal histology with large arrow indicating white pulp, arrowhead indicating red pulp, lymphocytes in red and white pulp is indicated using small arrow while notched arrow indicates splenic artery. In case of 10 mg/Kg, large arrow indicates normal white pulp and increased extramedullary hematopoiesis (EMH) was observed at red pulp which is shown by small arrows. At 20 mg/Kg, deposition of amorphous proteinaceous material – possibly amyloid was observed which was indicated by small arrows. Objective lens: 40X*

Spleen, 12 months

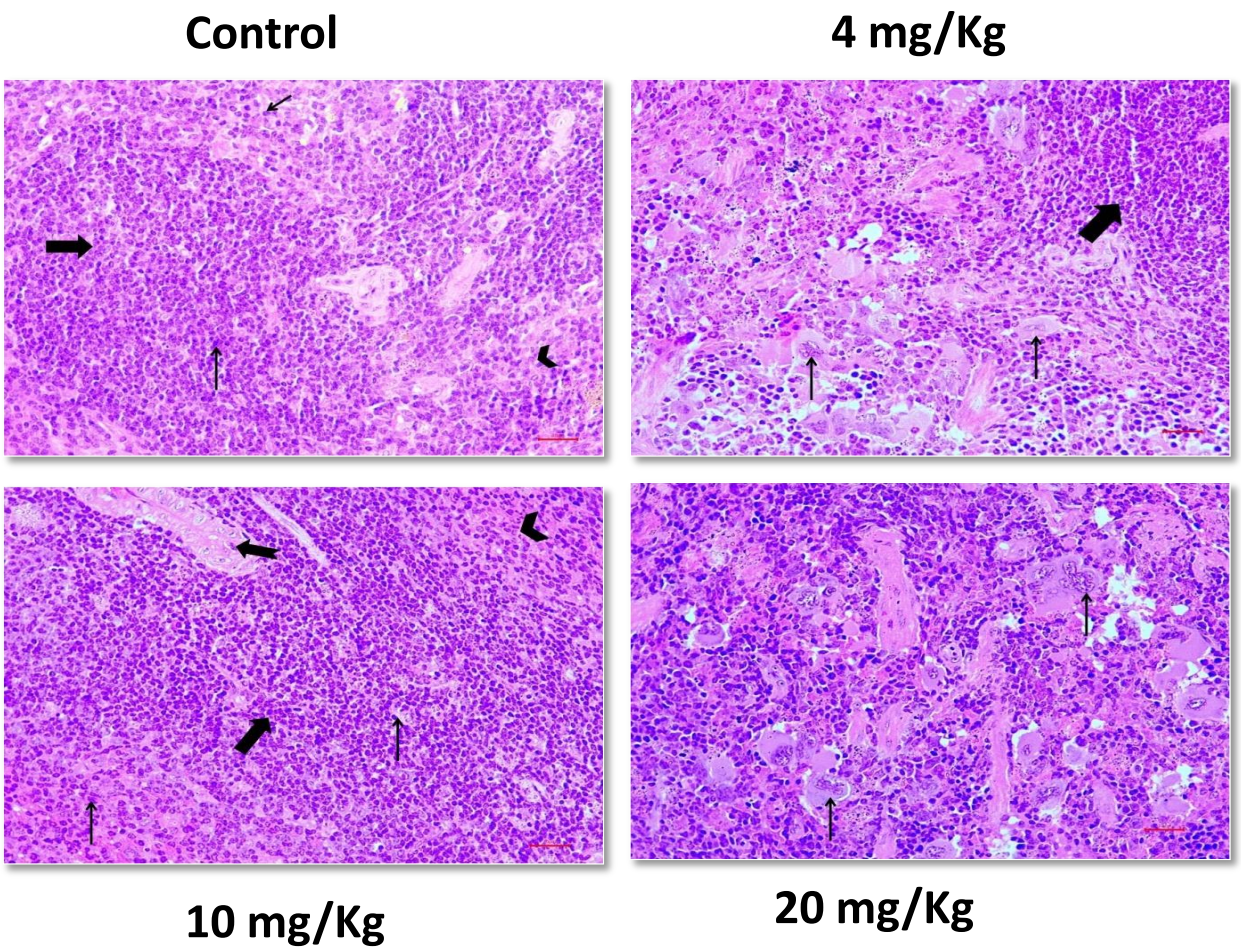

Figure 3.60: *Hematoxylin and eosin staining of spleen treated with 4, 10 and 20 mg/Kg of thorium as compared to control at 40X after 12 months of treatment. Control showed normal histology where large arrow shows white pulp, arrowhead shows red pulp, lymphocytes is indicated by small arrows while notched arrow shows splenic artery. 4 mg/Kg thorium treated spleen showed megakaryocytes in red pulp as indicated by small arrow and large arrow indicated normal white pulp. At 10 mg/Kg, however, normal histology of spleen similar to control was observed. At 20 mg/Kg, extensive megakaryocytosis was observed as indicated by small arrows. Objective lens: 40X.*

Bone, 6 months

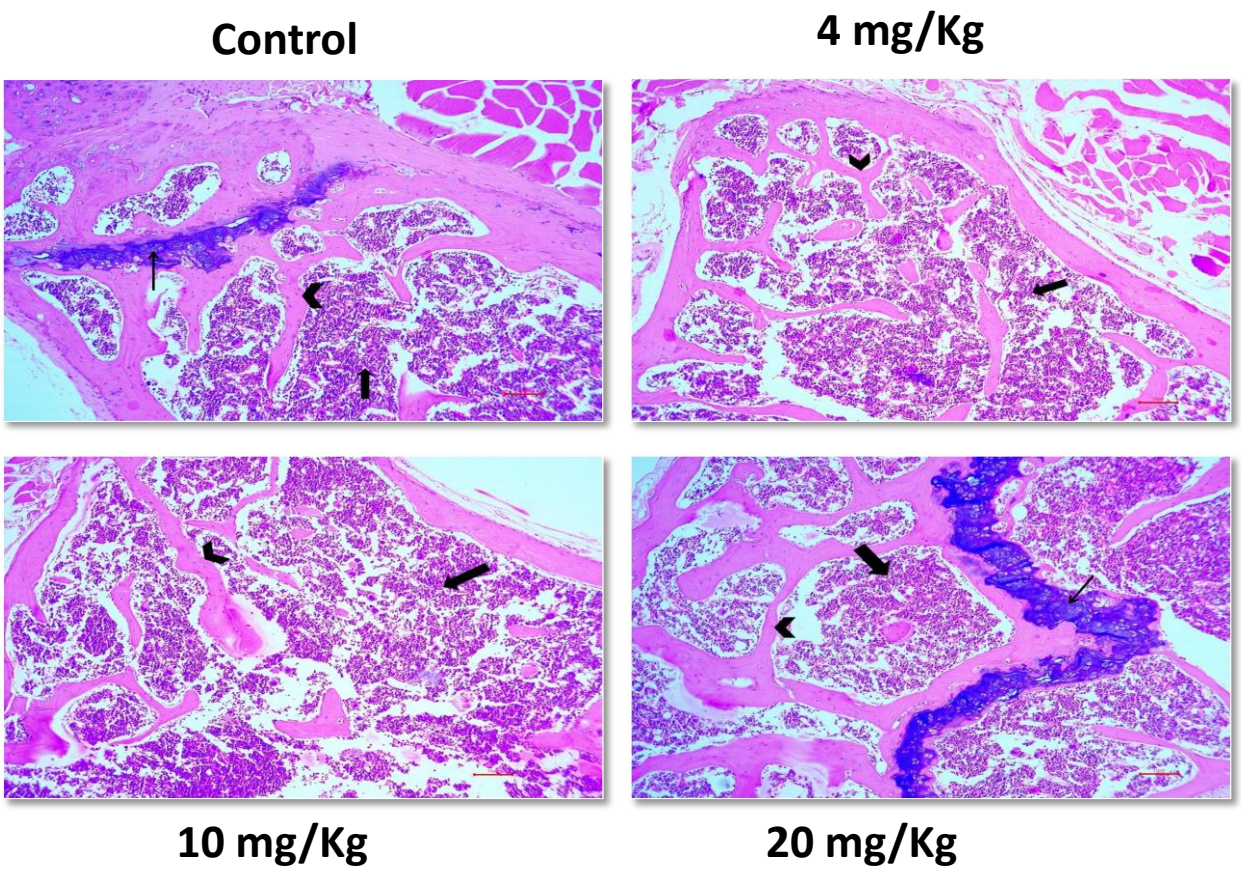

Figure 3.61: *Hematoxylin and eosin staining of bone treated with 4, 10 and 20 mg/Kg of thorium as compared to control at 10X after 6 months of treatment. Control and all other thorium treated bone samples showed normal histology where large arrow indicated bone marrow, small arrow indicates cartilage and arrowhead indicated trabecular bone. Objective lens: 10X.*

Bone, 12 months

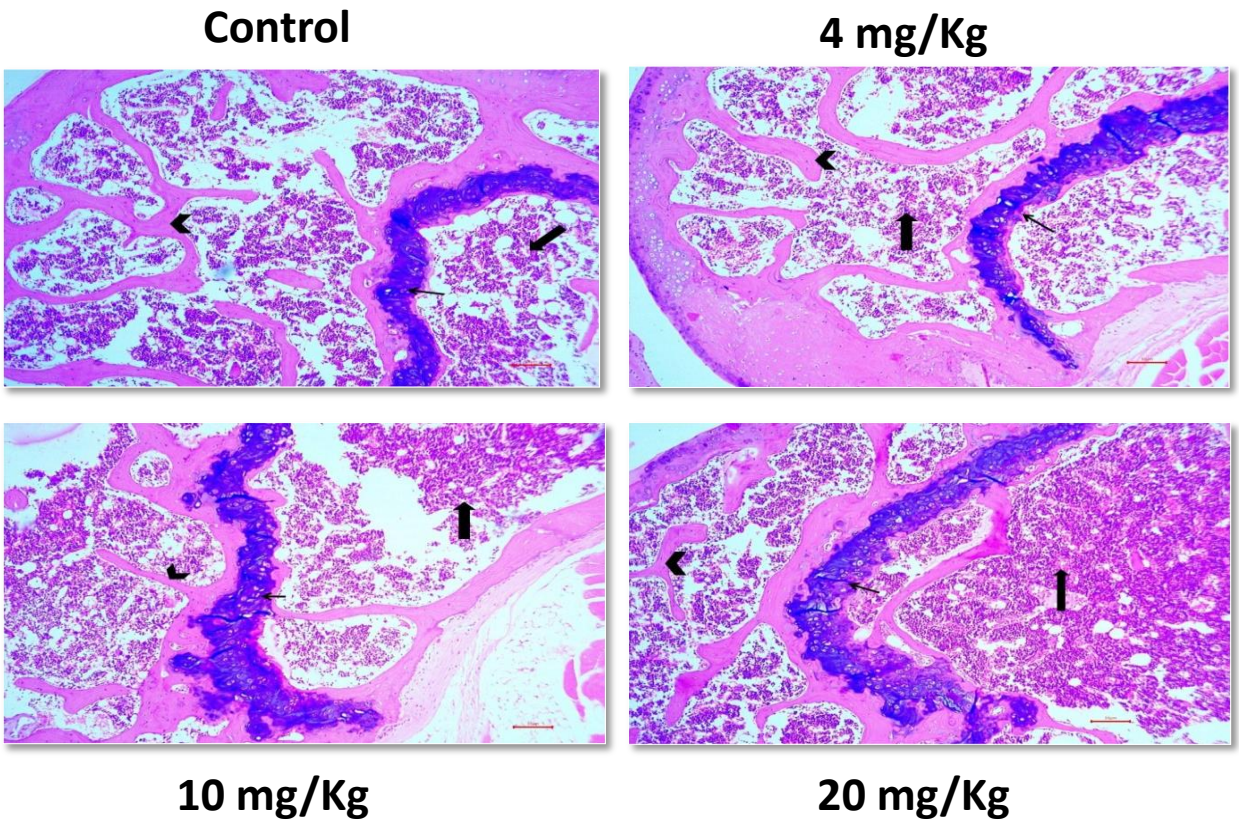

Figure 3.62: *Hematoxylin and eosin staining of bone treated with 4, 10 and 20 mg/Kg of thorium as compared to control at 10X after 12 months of treatment. Control and all other thorium treated bone samples showed normal histology where large arrow indicated bone marrow, small arrow indicates cartilage and arrowhead indicated trabecular bone. Objective lens: 10X.*

Lungs, 6 months

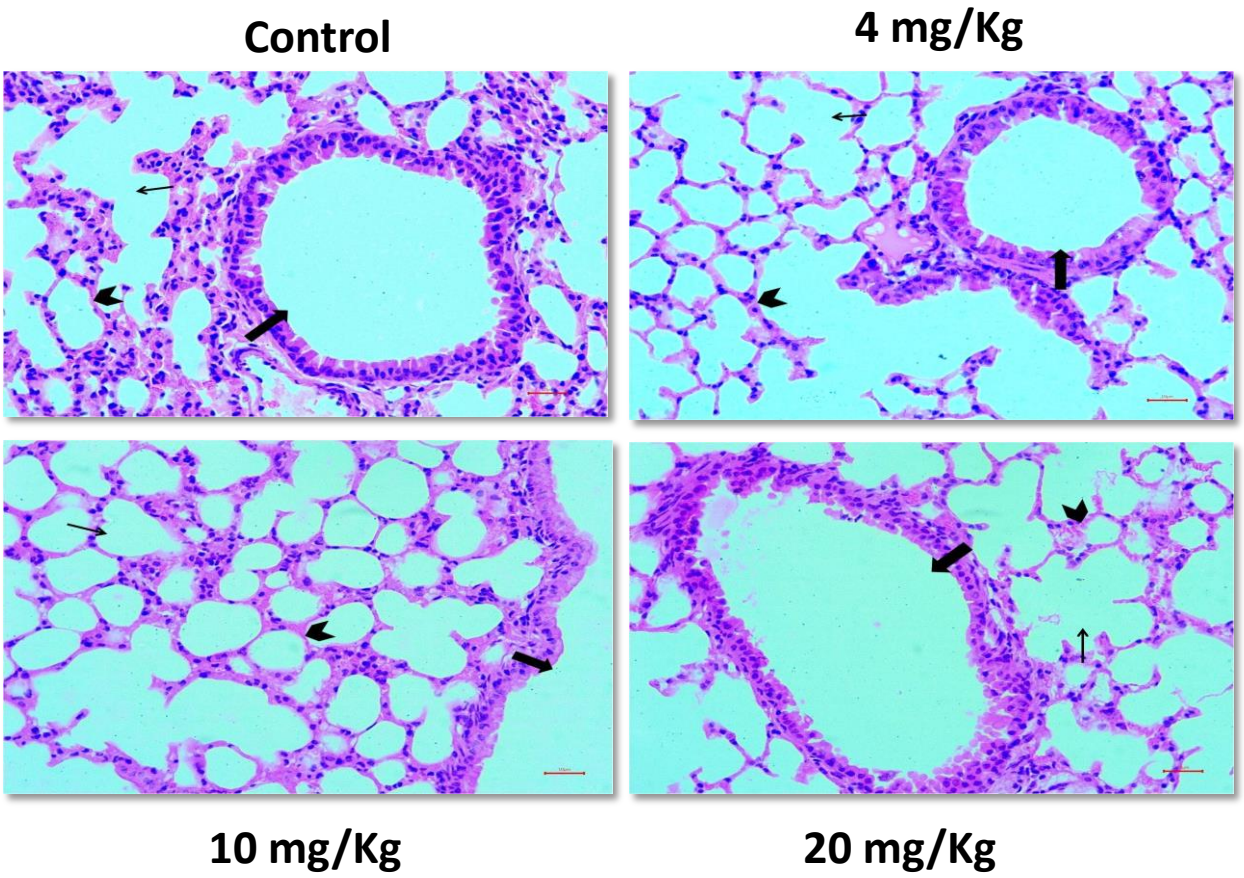

Figure 3.63: *Hematoxylin and eosin staining of lungs treated with 4, 10 and 20 mg/Kg of thorium as compared to control at 40X after 6 months of treatment. Control and all other thorium treated lungs samples showed normal histology where large arrow indicated bronchiole, small arrow indicates alveoli and arrowhead indicated normal alveolar wall. Objective lens: 40X.*

Lungs, 12 months

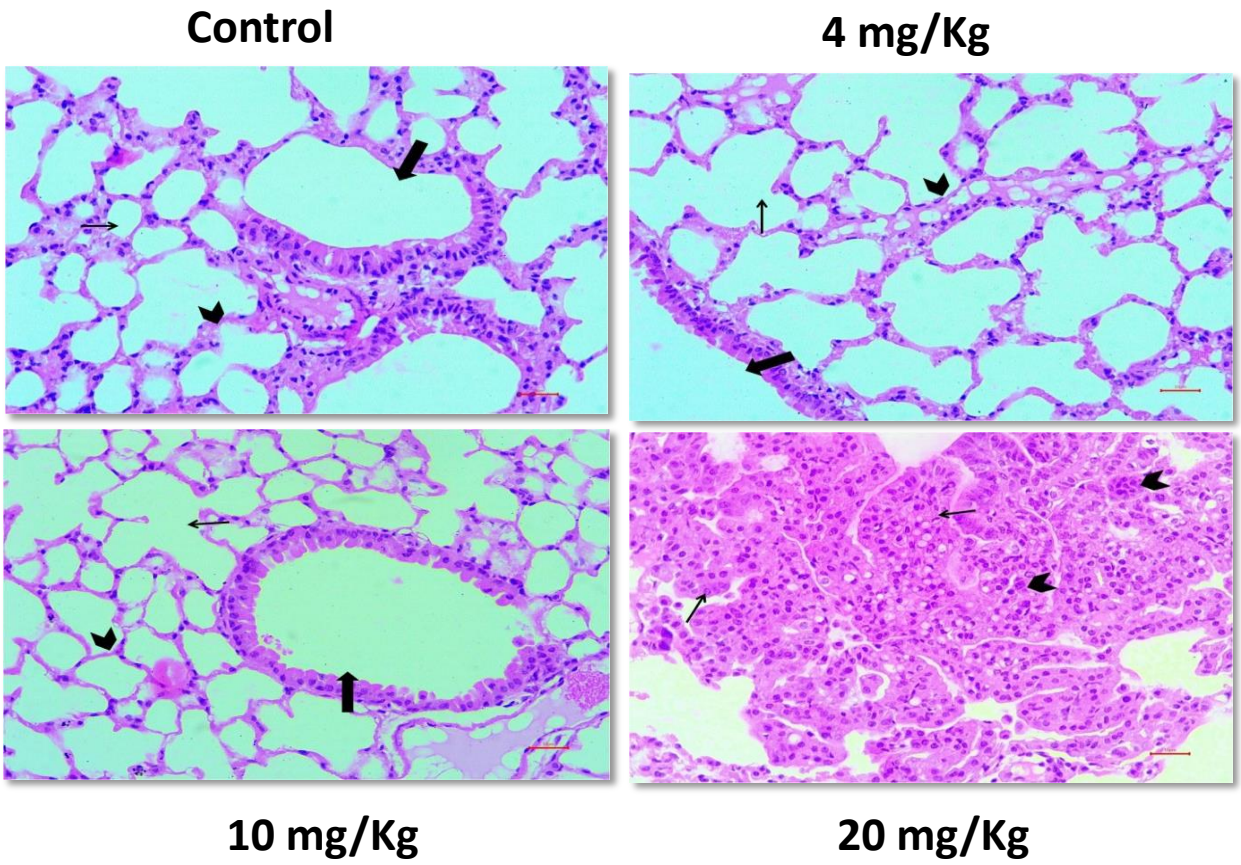

Figure 3.64: *Hematoxylin and eosin staining of lungs treated with 4, 10 and 20 mg/Kg of thorium as compared to control at 40X after 12 months of treatment. Control, 4 and 10 mg/Kg thorium treated lungs samples showed normal histology where large arrow indicated bronchiole, small arrow indicates alveoli and arrowhead indicated normal alveolar wall. At 20 mg/Kg, papillary adenoma neoplastic cuboidal cells were seen with papillary growth having round to oval nucleus which is indicated by small arrow. Increased basophilia with eosinophilic cytoplasm was also observed which is indicated by arrowhead. Objective lens: 40X.*

Brain, 6 months

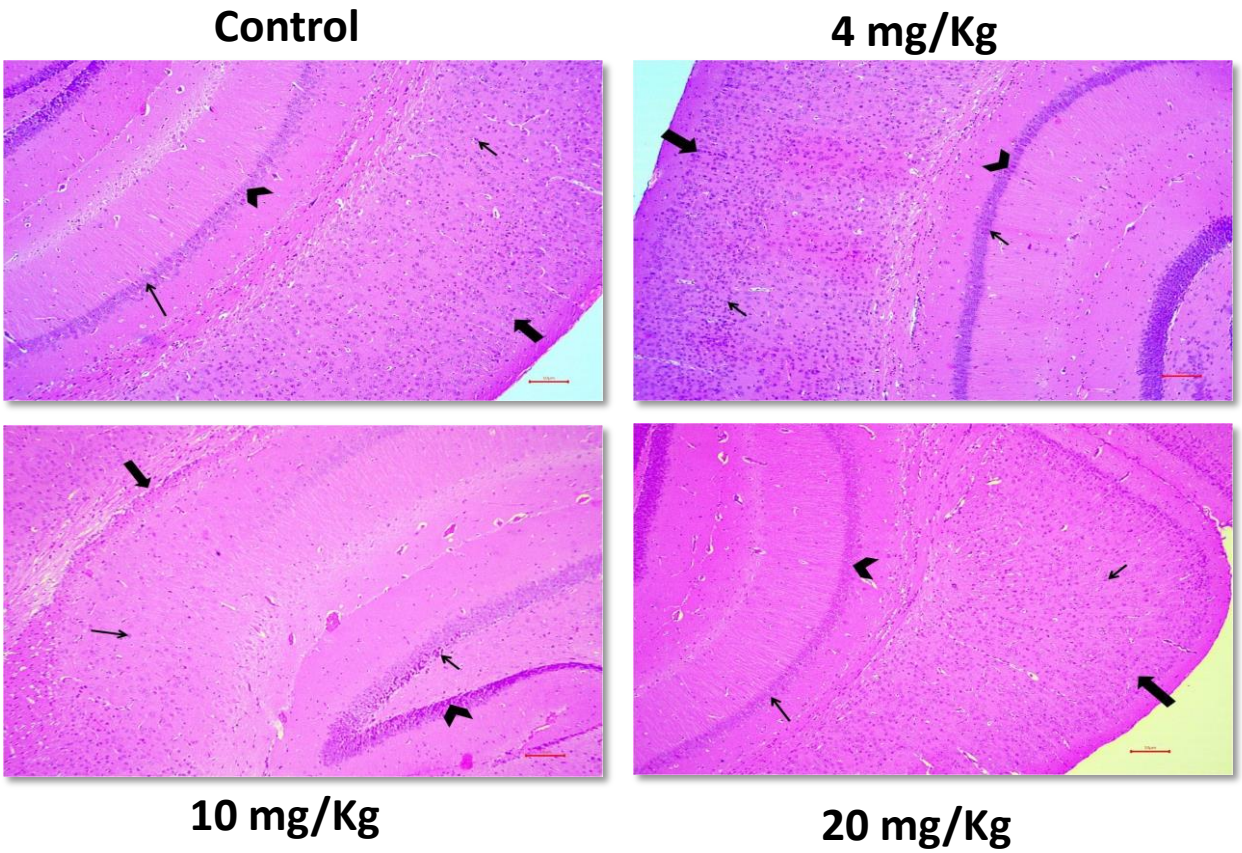

Figure 3.65: *Hematoxylin and eosin staining of brain treated with 4, 10 and 20 mg/Kg of thorium as compared to control at 10X after 6 months of treatment. Control and all other thorium treated brain samples showed normal histology where large arrow indicates cerebral cortex, small arrow indicates neurons and arrowhead indicates hippocampus. Objective lens:10X.*

Brain, 12 months

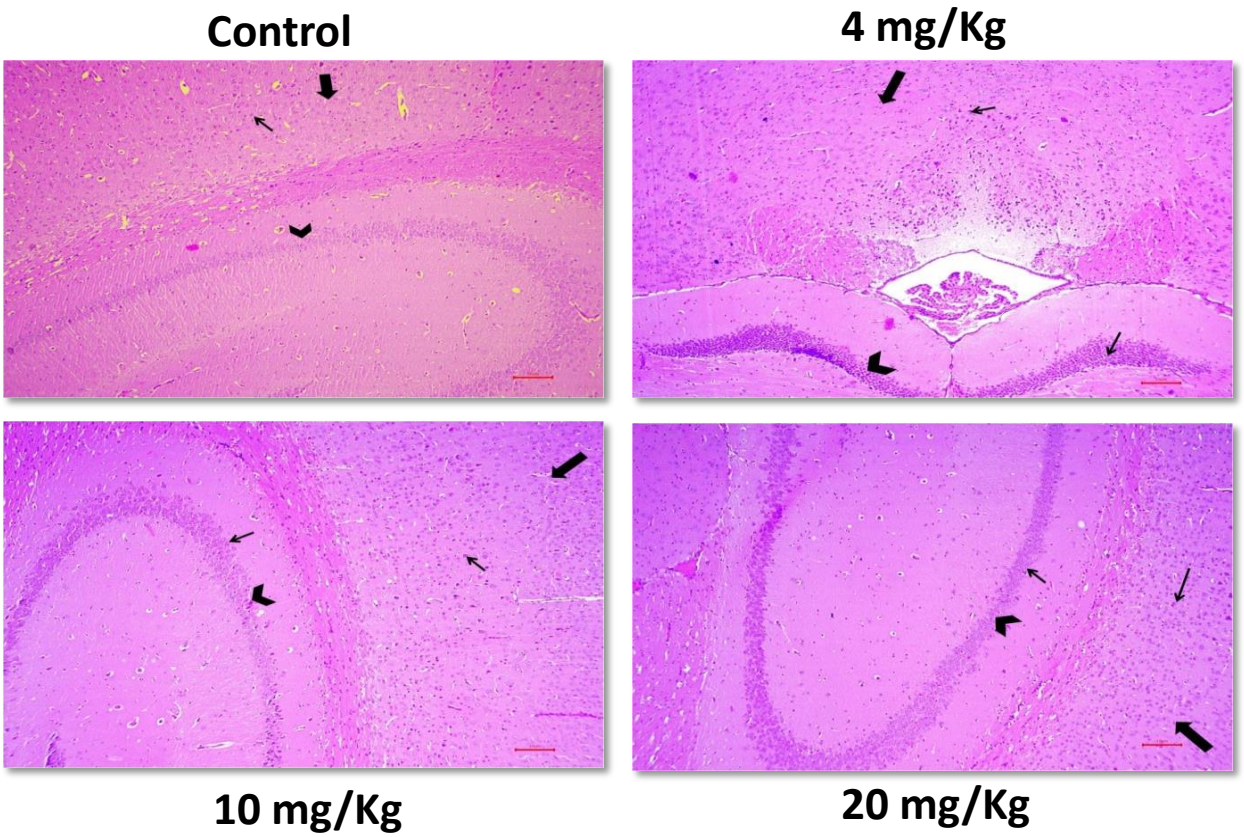

Figure 3.66: *Hematoxylin and eosin staining of brain treated with 4, 10 and 20 mg/Kg of thorium as compared to control at 10X after 12 months of treatment. Control and all other thorium treated brain samples showed normal histology where large arrow indicates cerebral cortex, small arrow indicates neurons and arrowhead indicates hippocampus. Objective lens: 10X.*

Overall, at six-month time point, the hematoxylin and eosin staining showed that the control group mice across all treatments did not show any lesion of pathological significance. Mice treated with 4 mg/Kg of thorium for six months also did not show any abnormality in their histology. However, the spleen of mice treated with 10 mg/Kg dose of thorium revealed multifocal marked amorphous proteinaceous-like material deposition at splenic red pulp and

diffused mild increase in extramedullary hematopoiesis. The proteinaceous material which is most commonly found deposited around the cells is amyloid deposition. The deposits seen is this case might also be amyloid deposition, however, further specialized staining is required to confirm its deposition. When mice were treated with 20 mg/Kg of thorium for six months, the histopathology of their liver and spleen showed multifocal marked amorphous proteinaceous material (possibly amyloid) deposition at hepatocyte and splenic red pulp, respectively. Multifocal mild lymphoid hyperplasia was also observed in white pulp of spleen at this dose in six months. Similarly, when mice were subjected to different doses of thorium for one year followed by their H&E studies, mild focal megakaryocytosis was observed in the red pulp of spleen from mice treated with 4 mg/Kg of thorium. However, surprisingly, treatment with 10 mg/Kg of thorium did not reveal any abnormality and/or lesion of pathological significance in liver and/or spleen after one year. At 20 mg/Kg. the splenic red pulp revealed focal minimal to mild megakaryocytosis. Similarly, at lower doses, lungs showed normal histology whereas at 20 mg/Kg, papillary adenoma was observed with cuboidal cells. Papillary growth showed cells with round to oval nucleus and an increased basophilia with eosinophilic cytoplasm was observed. Brain and bone showed normal histopathology after thorium treatment at all doses even after 12 months. To summarize, thorium treatment in mice at different doses for longer time duration (6 and 12 months) caused maximum histological changes in liver and spleen. Spleen showed presence of hyperplastic lesions while spleen and liver both indicated presence of multifocal amorphous proteinaceous material (possibly amyloid) deposition. Lungs showed presence of papillary adenoma with cuboidal cells. Bone and brain, however, did not show any effect on its histology upon thorium treatment at both time intervals.

3.3.2.5: Biochemical parameters of mice serum

To study the effect of long-term exposure of thorium on health and metabolism, different metabolic parameters and their levels in mice serum were studied by various biochemical studies. Serum samples were analyzed for various parameters as described above in Section 3.3.1.6 and values were averaged from at least three to five mice to obtain result.

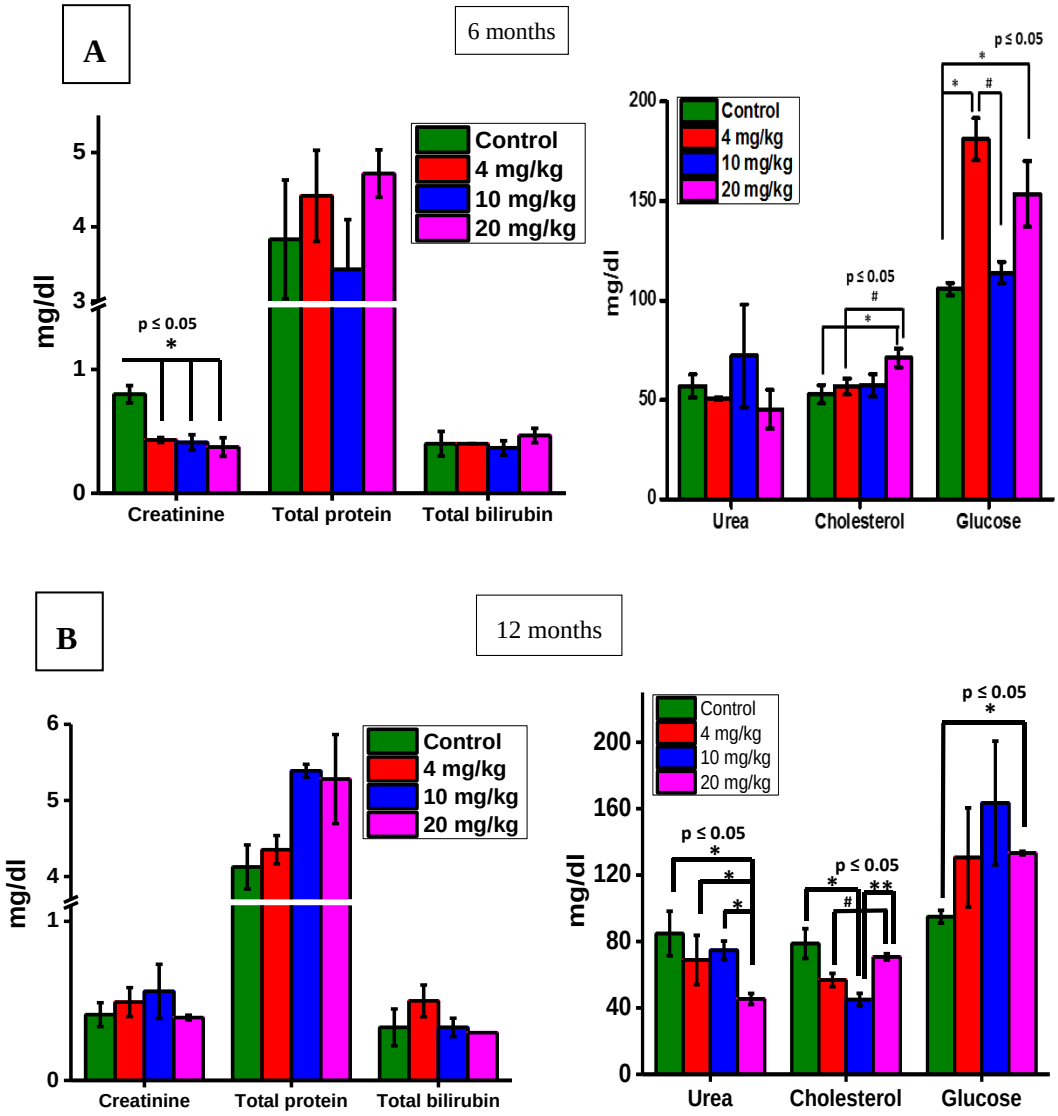

Figure 3.67: *Serum biochemical tests for creatinine, total protein, total bilirubin, urea, cholesterol, and glucose levels after intra-venous injection with thorium for* ***(A)*** *six months and* ***(B)*** *twelve months at 4, 10 and 20 mg/Kg dose of thorium. *Significantly different at $p \leq 0.05$.*

Amount of creatinine, total protein, total bilirubin, and urea in serum were studied as kidney function markers. At six months, the amount of creatinine was found to decrease significantly in thorium treated group as compared to control. Creatinine level in thorium treatment group were found to be at similar level. At one year, thorium treated group showed a minimal increase in the amount of creatinine in serum, but the increase was not significant (Figure 3.67). Nevertheless, the levels of creatinine observed in mice serum in both control and treated group were within the normal range (167). The amount of total protein and total bilirubin did not show any significant difference among control and thorium treated group at all time points (1, 6 and 12 months). When amount of urea in the serum of mice treated with 4, 10 and 20 mg/Kg of thorium was compared at six months, its level did not show significant difference as compared to control across all three doses of thorium (Figure 3.67). At 10 mg/Kg, the amount of urea showed an increase, which was insignificant when compared to other groups. In case of twelve months, level of urea in serum of mice treated with 20 mg/Kg of thorium showed significant decrease when compared with control as well as 4 and 10 mg/Kg thorium treated mice. At other doses, i.e., at 4 and 10 mg/Kg thorium, there was a decrease in the level of urea as compared to control, but the decrease was not significant. The levels of cholesterol and glucose were also studied in mice treated with thorium in order to understand the effect of thorium on carbohydrate and fat metabolism. At six months, 4, 10 and 20 mg/Kg thorium treated mice serum samples showed a gradual increase in the level of cholesterol which was found to be dose-dependent (Figure 3.67). This increase was not significant in case of 4 and 10 mg/Kg thorium as compared to control. However, at 20 mg/Kg thorium dose, the increase was significant as compared to control and 4 mg/Kg thorium treated mice. However, after twelve months of thorium treatment, there was a decrease in the level of cholesterol in thorium treated serum samples as compared to control. The thorium treated samples showed a

gradual decrease in the amount of cholesterol as compared to control however, only 10 mg/Kg thorium treated sample showed a significant ($p \leq 0.05$) decrease as compared to control. Surprisingly, among the thorium treated groups, there is a significant increase in the amount of cholesterol at 20 mg/Kg group as compared to 4 and 10 mg/Kg thorium treatment groups. Although there is an increase in the amount of cholesterol in 20 mg/Kg group compared to 4 and 10 mg/Kg, the level in this group is still lower compared to control. When glucose level in serum samples was studied, it was observed that there was a profound increase ($p \leq 0.05$) in the amount of glucose in blood serum levels at six and twelve months. At six months, 4 and 20 mg/Kg thorium treated group showed a significant increase in glucose level in the serum as compared to control. The increase at 10 mg/Kg was not in a dose-dependent manner. After twelve months of thorium treatment as well, serum glucose level followed the same pattern of increment. At 4, 10 and 20 mg/Kg of thorium, a marked increase in serum glucose level was observed as compared to control. However, only in case of 20 mg/Kg, the increase was found to be significant as compared to control.

In some parameters such as urea at 6 months, creatinine at 12 months, levels of total protein etc. the insignificant changes in thorium treated animals may be due to lower sample size (n=3-5), which may be verified using more samples from a greater number of mice. The amount of total bilirubin studied in serum samples showed no difference in their measured levels in control and thorium treated samples. Bilirubin attached by the liver to glucuronic acid is called direct or conjugated bilirubin and bilirubin not attached to glucuronic acid is called indirect or unconjugated, bilirubin. All the bilirubin in blood together is called total bilirubin. Since in here only total bilirubin was measured, measurement of direct bilirubin also could have better information about effect of thorium on bilirubin.

Creatinine, a marker of kidney function showed a significant decrease in its measured level in thorium treated group as compared to control group at six months. At twelve months, the levels measured were approximately equal in all groups. At six months, even though there is a significant drop in the level of creatinine in mice serum in thorium treated group as compared to control, the levels are within normal reference range. As mentioned above in Section 3.3.1.6, the normal range of creatinine is from 0.3 to 1 mg/dl. Similarly, at twelve months, although all groups showed similar level of creatinine in their serum, the amount of creatinine is well within the normal reference range (167) indicating no significant damage to kidney functions after thorium treatment. At six months, the level of blood urea was maintained at approximately equal levels with no significant difference in their measured amount. The same pattern was observed at twelve months. However, the amount of urea at 20 mg/Kg thorium treated serum sample was found to be significantly less as compared to control and other treatment groups at twelve months. Low amount of urea in blood serum is not a cause of concern until the amount is severely less. In the present experimental group, both control and treated ones, the amount of urea, even after reducing as compared to other groups is well within the normal reference range. The normal reference range of blood urea in small rodents is 64-120 mg/dl (168). Study of fat metabolism in the form of levels of cholesterol in blood serum showed that at six months, the amount of cholesterol in serum was significant higher at 20 mg/Kg thorium concentration as compared to control and 4 mg/Kg thorium treated group. When serum concentrations of cholesterol were studied after one year of thorium treatment, it was found that the amount of cholesterol decreased in treated groups till 10 mg/Kg. The decrease at 10 mg/Kg was significant as compared to control and 4 mg/Kg. Surprisingly, 20 mg/Kg showed an increase in the amount of serum cholesterol which was found to be significant as compared to other thorium treated groups. Like other serum parameters, this

variation in the amount of serum cholesterol level is also within the normal reference range (167). Levels of blood glucose after thorium treatment showed a marked increase in their levels in thorium treatment group which remains significantly higher as compared to control. At 6 months, it is 1.5 to 2 times higher as compared to control (depending on thorium dose) and at 12 months, it is increased by 1.3 times. Even though, the amount of blood glucose is higher in thorium treated groups but are within normal reference range of 62–175 mg/dl (167). But an increasing pattern in blood glucose in thorium treated animals was consistent for 6 and 12 months as well as serum samples analyzed at 30 days. These results suggested diabetic condition of thorium treated animals, which however requires validation using other serum biomarkers like HbA1c. The diabetic condition is associated with symptoms like poly urea, which may result in dehydration. Such changes may be associated with decrease in level of serum urea and creatinine observed in thorium treated animals observed at 6 months and 1 year of thorium treatment, respectively.

Biochemical parameters are an important tool to study normal body metabolism and homeostasis. Their levels when measured in body fluids such as blood serum gives an important indication about the onset and/or progress of various clinical disorder in body (169). Treatment to thorium causes its accumulation in various body organs leading to disorders owing to chemical as well as radiological toxicity of thorium (170). When Swiss mice were treated with different doses of thorium for different time intervals, thorium gets accumulated in organs over time. Biochemical tests in blood serum were performed to observe any abnormality which might have developed due to thorium treatment and accumulation. However, kidney function test showed insignificant toxicity studied using the levels of creatinine and urea in the blood serum. Cholesterol also showed insignificant difference over a period of one year. However, when glucose metabolism was studied, it was found that in

thorium treated groups, the amount of glucose was significantly higher as compared to control. Though with time, the amount of glucose in blood serum reduces but still the levels were significantly higher implying impairment of glucose metabolism in liver indicating a diabetic condition of mice.

3.3.2.6: Cytokine and chemokine profile of mice serum

Treatment to thorium and its accumulation in various body organs causes its toxic effects, which can also be determined by studying the types of cytokines/chemokines circulating in the body. Cytokines are small proteins, peptides and glycoproteins released by cells. They have specific effects on the interactions and communications between cells. It is a general name with broad classification. There are various types of cytokines such as lymphokine (cytokines made by lymphocytes), monokine (Cytokines made by monocytes), chemokine (cytokine with chemotactic activities), and interleukins (cytokines which are made by one leukocyte and acts on another leukocyte). They can be either autocrine, paracrine or endocrine in nature and can be broadly classified as pro-inflammatory and anti-inflammatory based on their action (171). Thorium treatment and accumulation may also cause release of different cytokines and chemokines into the blood. A cytokine array of 32 cytokines and 13 chemokines were studied in serum samples obtained from control and thorium treated mice. It was observed that out of 32 cytokines, only 10 cytokines and 9 chemokines showed an altered profile upon thorium treatment. Rest all cytokines and chemokines either did not show any alteration and/or their levels were below the detection limit of the kit used.

Levels of cytokines such as G-CSF, Eotaxin, IL-1α, IL-13, LIX, IP-10, KC, MIG, RANTES, TNF-α showed alteration in their levels in blood stream upon thorium treatment (Figure 3.71) whereas cytokines such as GM-CSF, IFN-γ, IL-1α, IL-1β, IL-2, IL-4, IL-3, IL-5, IL-6, IL-7, IL-9, IL-10, IL-12p40, IL-12p70, LIF, IL-15, IL-17, MCP-1, MIP-1α, MIP-1β,

MCSF, MIP-2, VEGF showed no alteration. Similarly, out of the 13 chemokines studied, sIL-1R1, sIL-1RII, sIL-2Rα, sIL-4R, sIL-6R, sTNFR1, sTNFRII, sVEGFR1, sVEGFR2 showed altered level (Figure 3.72) whereas Scd30, SGP130, sRAGE, sVEGFR3 did not showed any change in their level.

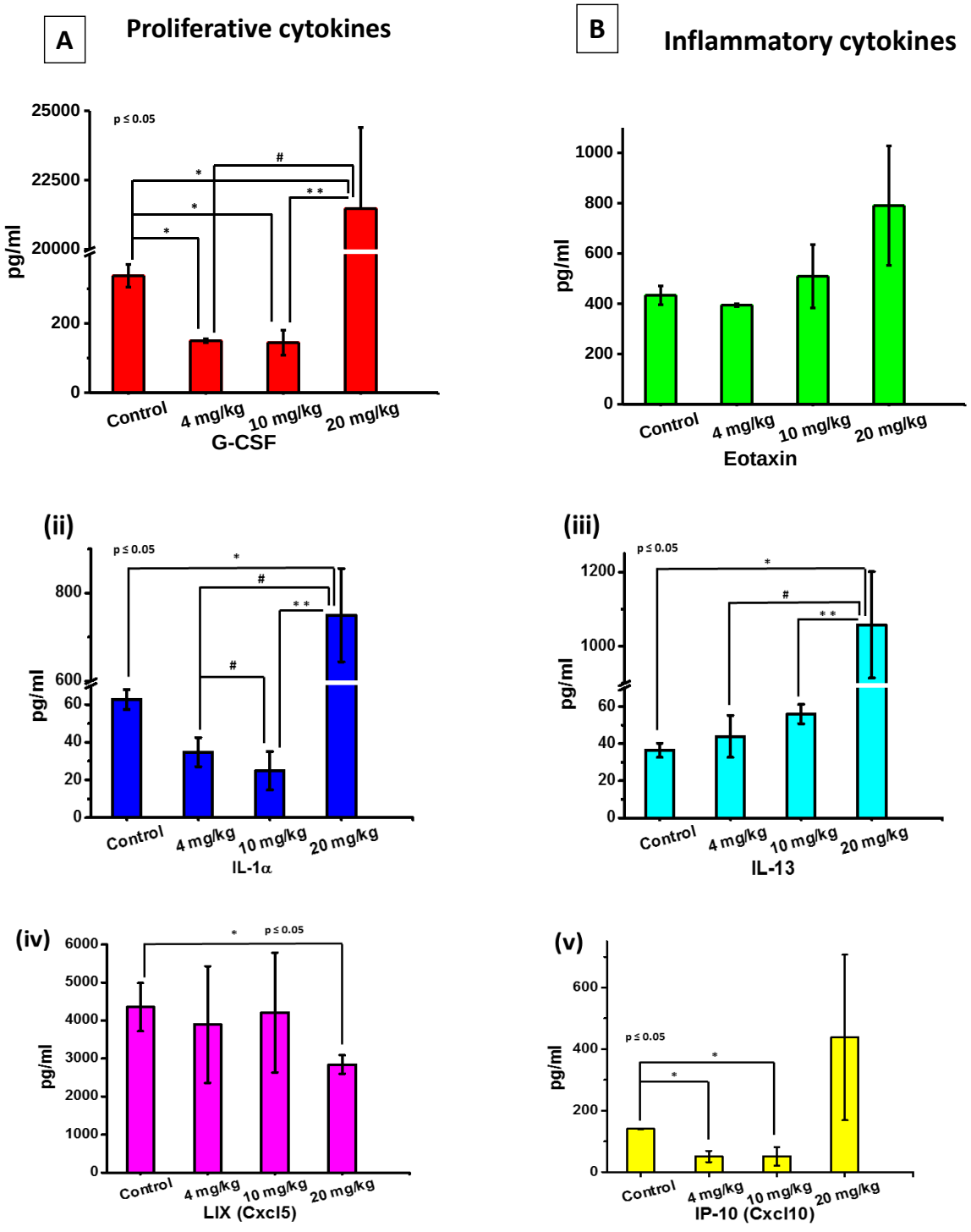

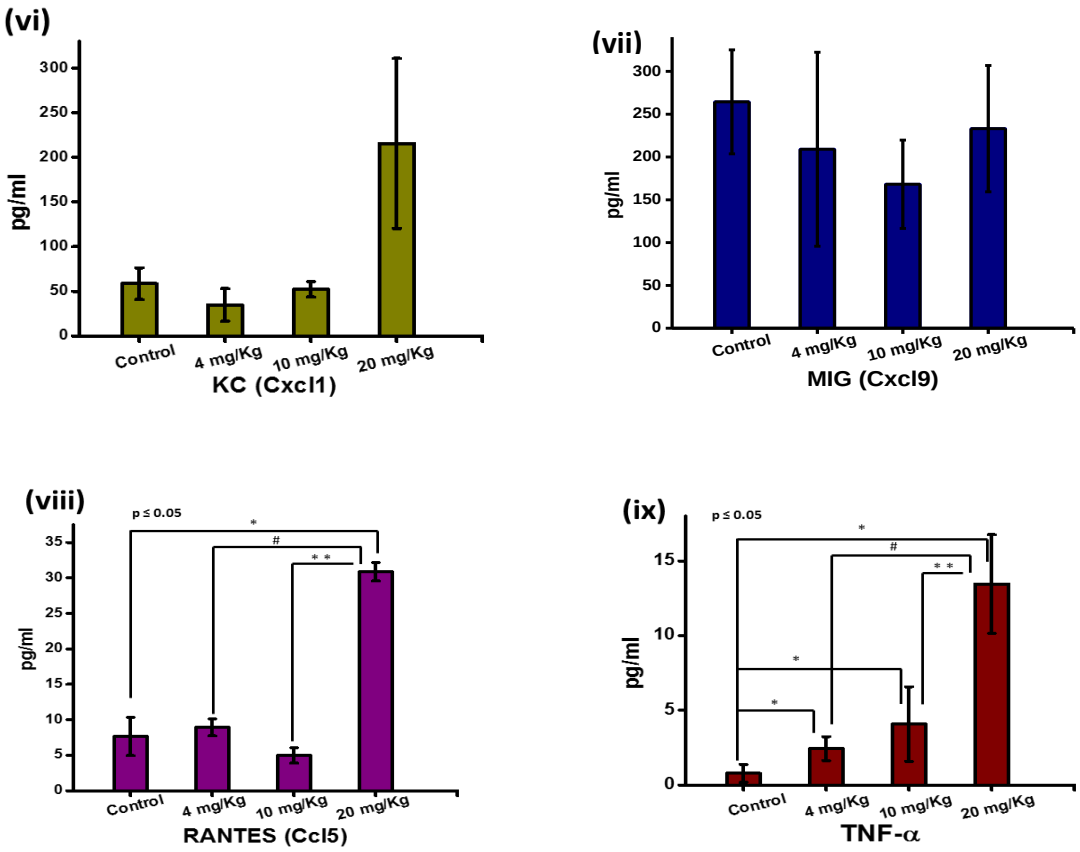

Figure 3.68: *Expression levels of various serum cytokines in mice after treatment with 4, 10 and 20 mg/Kg of thorium for 12 months. The values are a mean of three to five independent mice serum (n=3-5). Changes in level of* ***(A)*** *proliferative cytokine such as G-CSF and* ***(B)*** *inflammatory cytokine such as Eotaxin (v) Inducible protein (IP)-10, (vi) keratinocyte chemoattractant (KC), (vii) MIG, (viii) RANTES, (ix) TNF-α.*

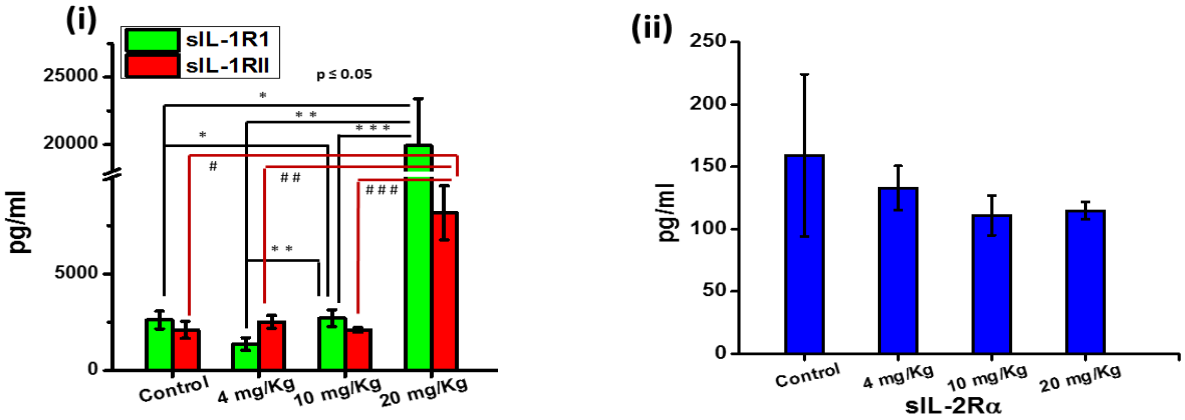

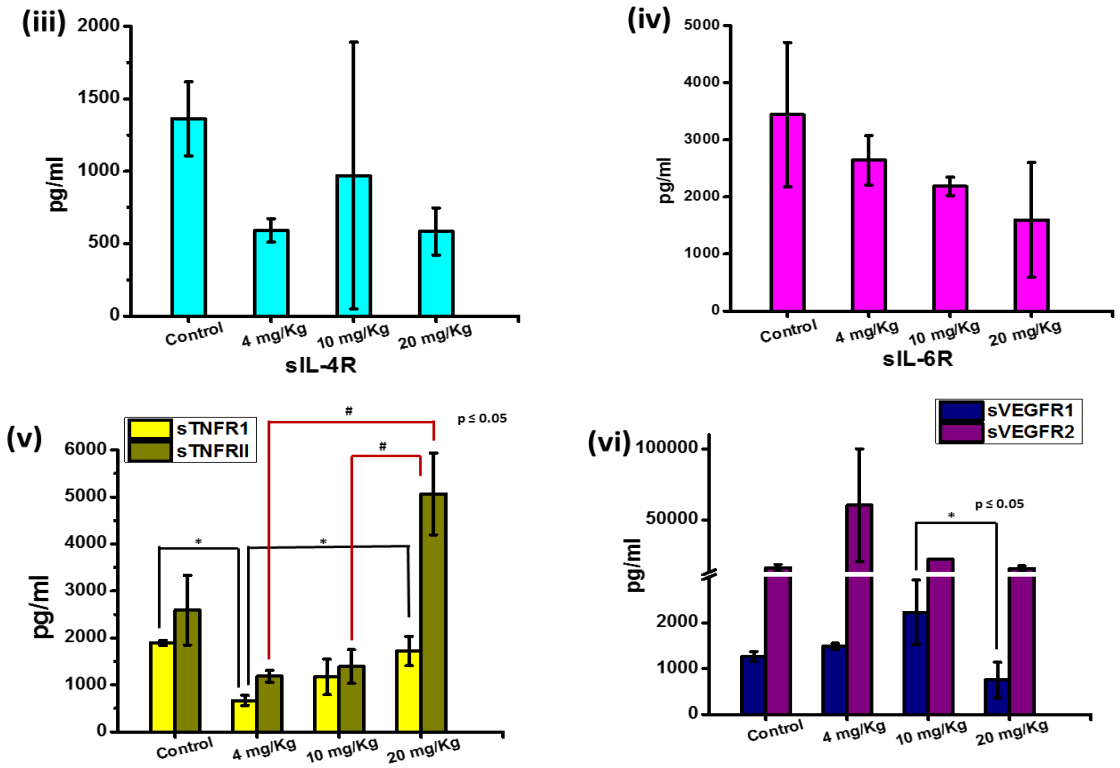

Figure 3.69: *Chemokine profile of mice serum samples treated with 4,10 and 20 mg/Kg of thorium intravenously for 12 months. Expressions of chemokines such as sIL-1R1, sIL-1RII, sIL-2Rα, sIL-4R, sIL-6R, sTNFR1, sTNFR2, sVEGFR1, sVEGFR2 showed changes in their expression level upon thorium treatment after 12 months as compared to control.*

It was observed that following thorium treatment for one year, granulocyte-colony stimulating factor (G-CSF), a proliferative cytokine showed a significant decrease in its expression at 4 and 10 mg/Kg thorium but at 20 mg/Kg, there was an increase in the level of G-CSF which was significantly high as compared to control and other thorium treated groups. The same pattern of n was observed for other inflammatory cytokines such as IL-1α, IP-10 and KC. Other inflammatory cytokines such as Eotaxin, IL-13, and TNF-α showed a gradual increase in their levels in thorium treated groups as compared to control. The increase at 4 and 10 mg/Kg of thorium is slow and gradual however, at 20 mg/Kg, they show a marked increase

in their level which is significantly higher as compared to control. LIX also known as Cxcl5 and MIG (Cxcl9) did not show any difference in their profile in thorium treated samples as compared to control. RANTES also known as Ccl5 showed no significant difference in the expression profile of 4 and 10 mg/Kg thorium treated samples when compared to control. However, at 20 mg/Kg, there was a marked increase in the level of RANTES which is significantly higher compared to control and thorium treated samples (4 and 10 mg/Kg). Further studies on chemokines showed that sIL-1R1 and sIL-1R2 did not have any effect on its level at 4 and 10 mg/Kg as compared to control. However, at 20 mg/Kg, the marked increase in their level indicates that thorium treatment causes body to produce these chemokines in large quantities. Similar pattern was observed for sTNFR1 and sTNFR2 whereas sIL-2Rα and sIl-6R showed a gradual decline in their level in thorium treated samples. sIL-4α and sVEGFR1 and sVEGFR2 showed no significant change in their level. The marked increase in various inflammatory cytokine and chemokine at 20 mg/Kg indicates that this dose is toxic to mice even after one year of treatment and might be playing an active role in carcinogenesis. Some of the cytokines like Il-1 alpha and G-CSF showed decrease in its level at lower doses of thorium (4 and 10 mg/Kg), which showed increase at higher doses (20 mg/Kg) suggesting biphasic dose response of thorium at low and high doses. Soluble tumor necrosis factor receptors (sTNFR) are the cleaved-off extracellular domains of transmembrane TNF receptors, which enter the bloodstream either via shedding or through exocytosis of the full-length receptor in exosome-like vesicles. These soluble receptors are known to play role in malignancy and infection. A similar pattern was observed for sTNFR1 and sTNFR2. Based on inflammatory cytokine/chemokine profile of IL-1 alpha and G-CSF in thorium treated animals, it seems thorium at lower doses induce anti-inflammatory but at high dose result in pro-inflammatory conditions, which may result in carcinogenesis. At lower doses of thorium, body

would try to adapt the effect and hence may induce some cyto-protective mechanisms. However, at higher doses, balance may tilt towards toxic effects. These results are in agreement of induction of lung carcinogenesis at higher dose of thorium (20 mg/Kg) not at lower doses (4 and 10 mg/Kg).

3.3.3: Expression of genes involved in hepatocarcinogenesis in liver tissues obtained from thorium treated mice

To study the carcinogenic effects of thorium treatment, expression of genes involved in carcinogenesis of liver was studied in liver samples obtained after 6 months and 12 months after thorium treatment. Liver was used for this study, as it is the major known target organ for exerting health effects of thorium and major site of accumulation of thorium after *i.v.* administration (Figure 3.40 and 3.58). For this study, Swiss mice were treated with 4, 10 and 20 mg/Kg of thorium and gene expression alterations were studied using mouse hepatocarcinogenesis RT^2 PCR array (Qiagen, Germany make and catalogue no. 330231 with GeneGlobe ID: PAMM–133Z) in liver tissue of these mice. The 84 genes in the array are listed in Section 2.2.25.

At six months, the studies were carried out using low and high concentration of thorium i.e., 4 and 20 mg/Kg dose. 4 mg/Kg being the low concentration of thorium will be responsible for slow toxic effects of thorium both chemically as well as radiologically on liver and might be the optimum dose involved in carcinogenicity and hence, it would be appropriate to study the gene expression alterations caused by them at intermediate interval of treatment i.e., six months. Highest dose used in the study i.e., 20 mg/Kg would be the dose causing the most toxic effects on mice and therefore, this dose was also chosen to study its toxic effects on liver

at the time interval of 6 months. At one-year, gene expression alterations caused by all three concentrations of thorium used *viz.*, 4, 10 and 20 mg/Kg were studied.

3.3.3.1: Gene expression changes in liver tissue six months after thorium treatment

Gene expression profile of liver tissue obtained after six months of mice injected with 4 mg/Kg thorium intravenously showed an upregulation of 17 genes and downregulation of 47 genes. Similarly, when mice were injected with 20 mg/Kg of thorium, an upregulation of 60 genes and downregulation of 06 genes was observed. A list of all these genes with their respective fold regulations are listed below in Table 3.11 A-B.

A

4 mg/Kg		
Symbol	**Fold regulation**	**SD**
Igfbp3	-205.3	0.0
Igfbp1	-165.6	0.0
Opcml	-31.2	0.0
Pten	-20.4	0.0
Fhit	-18.6	0.0
Dab2ip	-12.2	0.1
Fzd7	-9.9	0.1
Rhoa	-7.8	0.1
Egfr	-7.7	0.0
Vegfa	-7.1	0.0

B

20 mg/Kg		
Symbol	**Fold regulation**	**SD**
Runx3	-18.9	0.1
Opcml	-5.5	0.0
Sfrp2	-4.6	0.1
Lef1	-3.4	0.1
Wt1	-3.0	0.2
Igf2	-2.7	0.1
Egfr	1.5	0.4
Xiap	1.5	0.0
Vegfa	1.5	0.2
Cdkn1a	1.6	0.6

E2f1	-6.7	0.0
Hgf	-6.6	0.0
Kdr	-6.6	0.2
Ccnd1	-6.6	0.0
Cxcr4	-6.3	0.1
Tnfsf10	-5.5	0.0
Pycard	-5.5	0.1
Xiap	-5.3	0.0
Yap1	-5.3	0.1
Nfkb1	-5.1	0.1
Birc5	-4.3	0.0
Dlc1	-4.2	0.1
Tlr4	-4.0	0.0
Fas	-4.0	0.1
Irs1	-3.9	0.3
Cflar	-3.9	0.2
Tnfrsf10b	-3.7	0.0
Tgfa	-3.5	0.1
Birc2	-3.3	0.1
Ctnnb1	-3.0	0.0
Ptk2	-2.9	0.0
Gstp1	-2.9	0.1

Akt1	1.6	0.3
Ptk2	1.6	0.3
Angpt2	1.6	0.2
Trp53	1.6	0.1
Rac1	1.6	0.4
Tnfsf10	1.6	0.7
Fzd7	1.7	0.2
Mcl1	1.7	0.4
Birc2	1.7	0.2
Tlr4	1.7	0.3
Fas	1.7	0.3
Hhip	1.7	0.4
Igfbp3	1.7	0.5
Ptgs2	1.8	0.2
Egf	1.8	0.8
Birc5	1.9	0.2
Hras	2.0	0.4
Bax	2.0	0.3
Pdgfra	2.0	0.3
Nras	2.0	0.4
Met	2.1	0.5
Cdh13	2.1	0.4

Tcf4	-2.8	0.2
Rac1	-2.7	0.1
Smad7	-2.7	0.3
Igf2	-2.6	0.0
Adam17	-2.5	0.1
Lef1	-2.5	0.5
Ccnd2	-2.5	0.1
Tgfb1	-2.2	0.1
Fadd	-2.1	0.1
Stat3	-2.1	0.2
Mtdh	-2.0	0.1
Gadd45b	-2.0	0.4
Cdkn1a	-2.0	0.2
Flt1	-1.9	0.2
Egf	-1.9	0.1
Smad4	1.2	1.3
Ep300	1.3	0.4
Msh3	2.1	2.5
Hhip	2.2	0.9
Socs3	2.6	0.5
Tgfbr2	2.7	0.9
Rassf1	2.8	0.9

Ccnd2	2.2	0.5
Pten	2.2	0.2
Bcl2l1	2.2	0.2
Rhoa	2.3	0.7
Bid	2.4	0.1
Smad7	2.4	0.5
Cflar	2.6	0.2
Flt1	2.7	0.1
Msh3	2.7	0.3
Tcf4	2.8	0.1
Fadd	2.8	1.1
Pin1	2.9	0.2
Casp8	2.9	1.1
E2f1	3.0	0.2
Socs3	3.6	0.0
Itgb1	3.6	0.8
Dlc1	3.7	1.2
Tgfbr2	3.9	0.5
Igfbp1	4.0	0.9
Cdkn1b	4.1	0.1
Msh2	4.1	0.6
Stat3	4.4	0.2

Msh2	2.8	0.6
Pdgfra	3.0	3.8
Cdh13	3.5	3.2
Rb1	4.9	2.4
Bcl2	5.7	1.9
Reln	5.8	1.0
Tert	6.1	3.0
Cdkn2a	13.8	5.0
Ptgs2	18.3	2.6
Myc	47.6	26.3

Ep300	4.6	0.6
Ctnnb1	4.8	1.4
Hgf	5.8	0.4
Gadd45b	7.0	0.9
Rassf1	9.0	1.0
Rb1	11.2	0.8
Bcl2	11.3	2.5
Smad4	17.3	4.8
Reln	35.3	4.5
Myc	148.7	9.5

Table 3.14: *Fold regulation of total genes in mice liver tissue after treatment with* ***(A)*** *4 mg/Kg, upregulated (17 genes) and downregulated (47 genes), and* ***(B)*** *20 mg/Kg, upregulated (58 genes) and downregulated (06 genes), thorium injected intravenously after six months of treatment. Genes in red were upregulated and genes in blue were downregulated upon thorium treatment.*

These expression profiles were further analyzed, and it was found that when 4 mg/Kg of thorium was injected intravenously in mice, 12 genes (*Hhip, Socs3, Tgfbr2, Rassf1, Msh2, Rb1, Bcl2, Reln, Tert, Cdkn2a, Ptgs2, Myc)* were found to be upregulated more than 2 folds and while 47 genes (*Igfbp3, Igfbp1, Opcml, Pten, Fhit, Dab2ip, Fzd7, Rhoa, Egfr, Vegfa, E2f1, Hgf, Kdr, Ccnd1, Cxcr4, Tnfsf10, Pycard, Xiap, Yap1, Nfkb1, Birc5, Dlc1, Tlr4, Fas, Irs1, Cflar, Tnfrsf10b, Tgfa, Birc2, Ctnnb1, Ptk2, Gstp1, Tcf4, Rac1, Smad7, Igf2, Adam17, Lef1, Ccnd2, Tgfb1, Fadd, Stat3, Mtdh, Gadd45b, Cdkn1a, Flt1, Egf)* were found to be

downregulated by more than 2 folds (Figure 3.74 A). Also, when the gene alteration data for 20 mg/Kg of thorium dose for six months was similarly analyzed, it was found that a total of 41 genes *viz., Birc5, Hras, Bax, Pdgfra, Nras, Met, Cdh13, Ccnd2, Pten, Bcl2l1, Rhoa, Bid, Smad7, Cflar, Flt1, Msh3, Tert, Tcf4, Fadd, Pin1, Casp8, E2f1, Socs3, Itgb1, Dlc1, Tgfbr2, Igfbp1, Cdkn1b, Msh2, Stat3, Ep300, Ctnnb1, Hgf, Cdkn2a, Gadd45b, Rassf1, Rb1, Bcl2, Smad4, Reln, Myc* were found to be upregulated more than 2 folds and a total of 06 genes *viz., Runx3, Opcml, Sfrp2, Lef1, Wt1, Igf2* were found to be downregulated more than 2 folds (Figure 3.74 B).

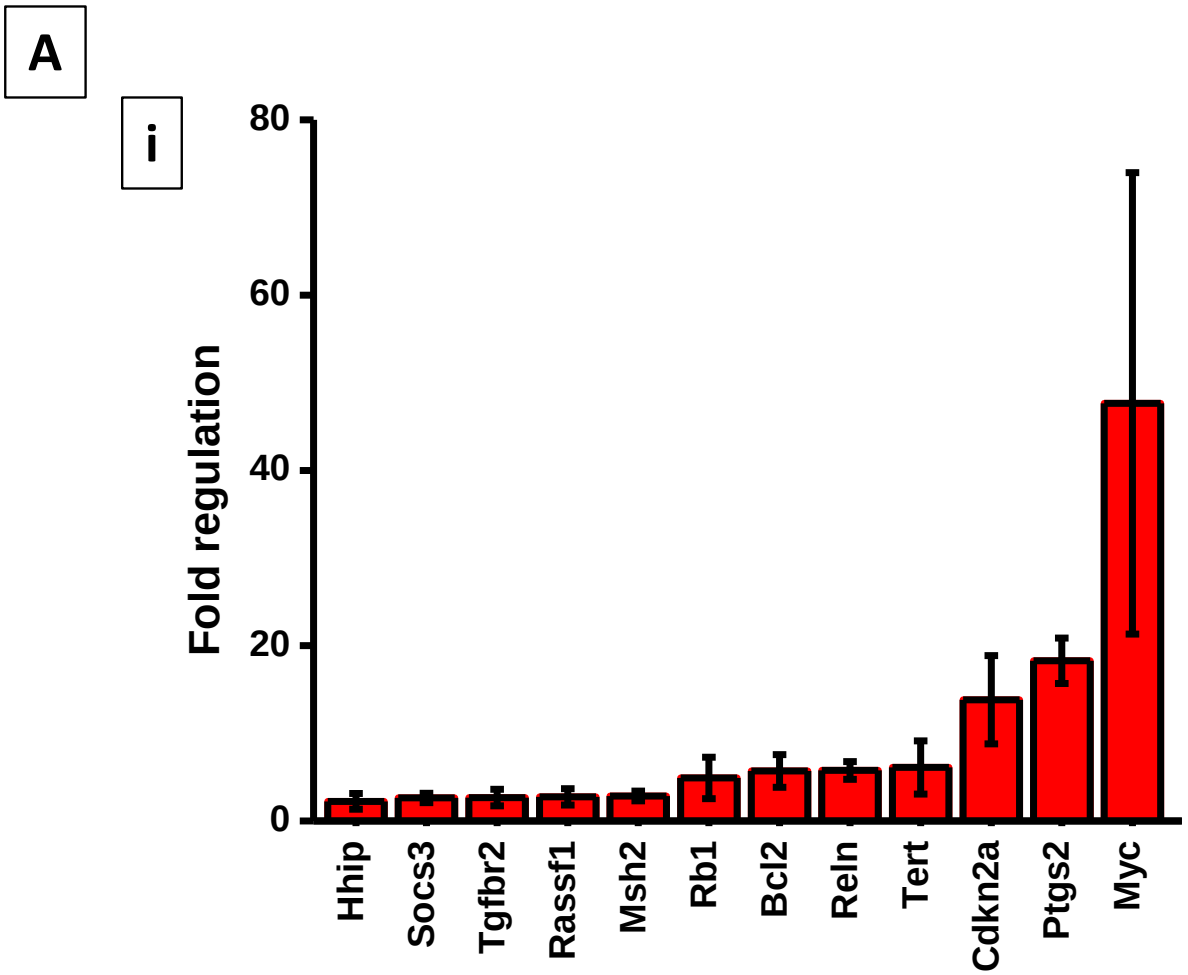

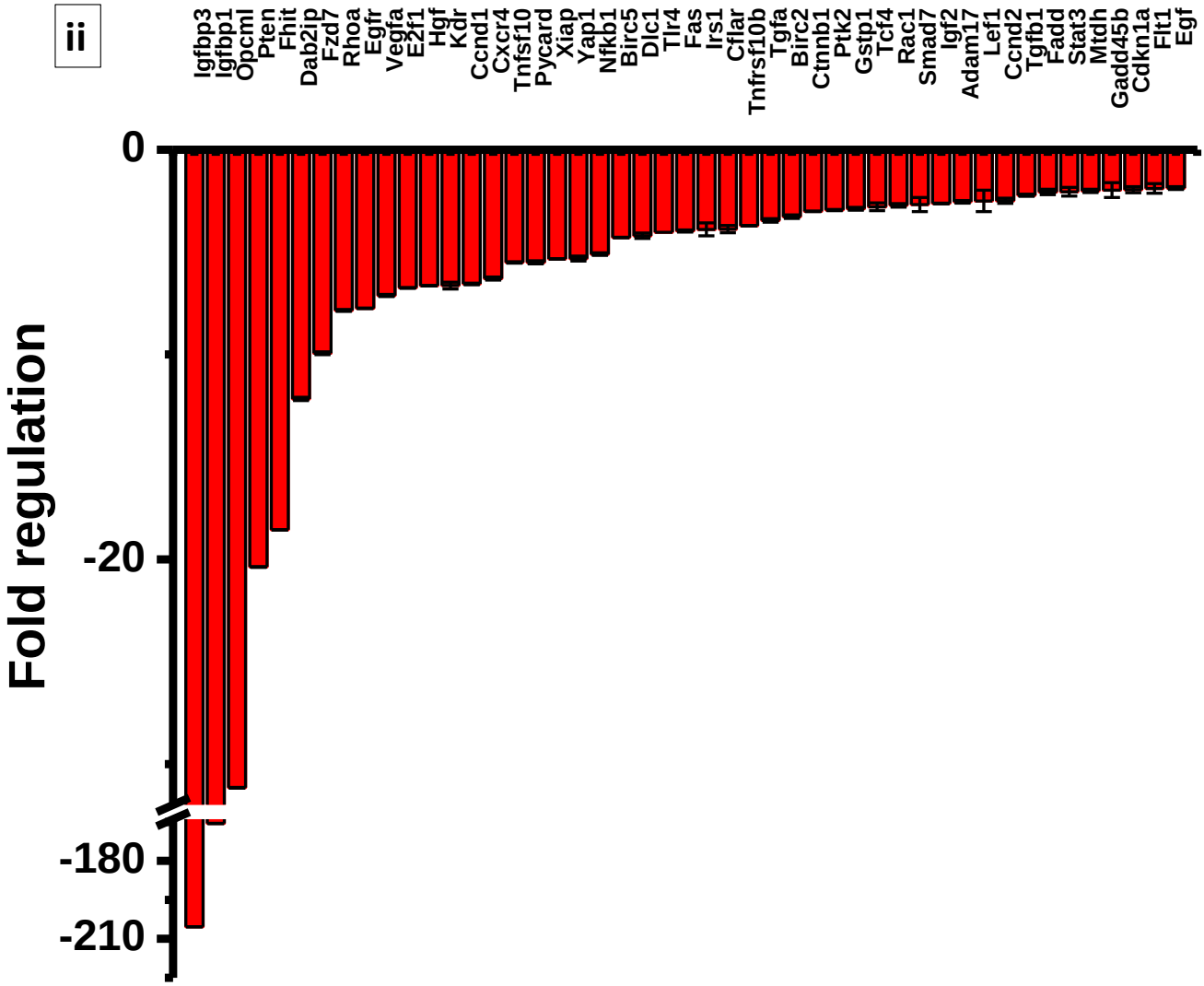
ii
Igfbp3
Igfbp1
Opcml
Pten
Fhit
Dab2ip
Fzd7
Rhoa
Egfr
Vegfa
E2f1
Hgf
Kdr
Ccnd1
Cxcr4
Tnfsf10
Pycard
Xiap
Yap1
Nfkb1
Birc5
Dlc1
Tlr4
Fas
Irs1
Cflar
Tnfrsf10b
Tgfa
Birc2
Ctnnb1
Ptk2
Gstp1
Tcf4
Rac1
Smad7
Igf2
Adam17
Lef1
Ccnd2
Tgfb1
Fadd
Stat3
Mtdh
Gadd45b
Cdkn1a
Flt1
Egf
Fold regulation
0
-20
-180
-210

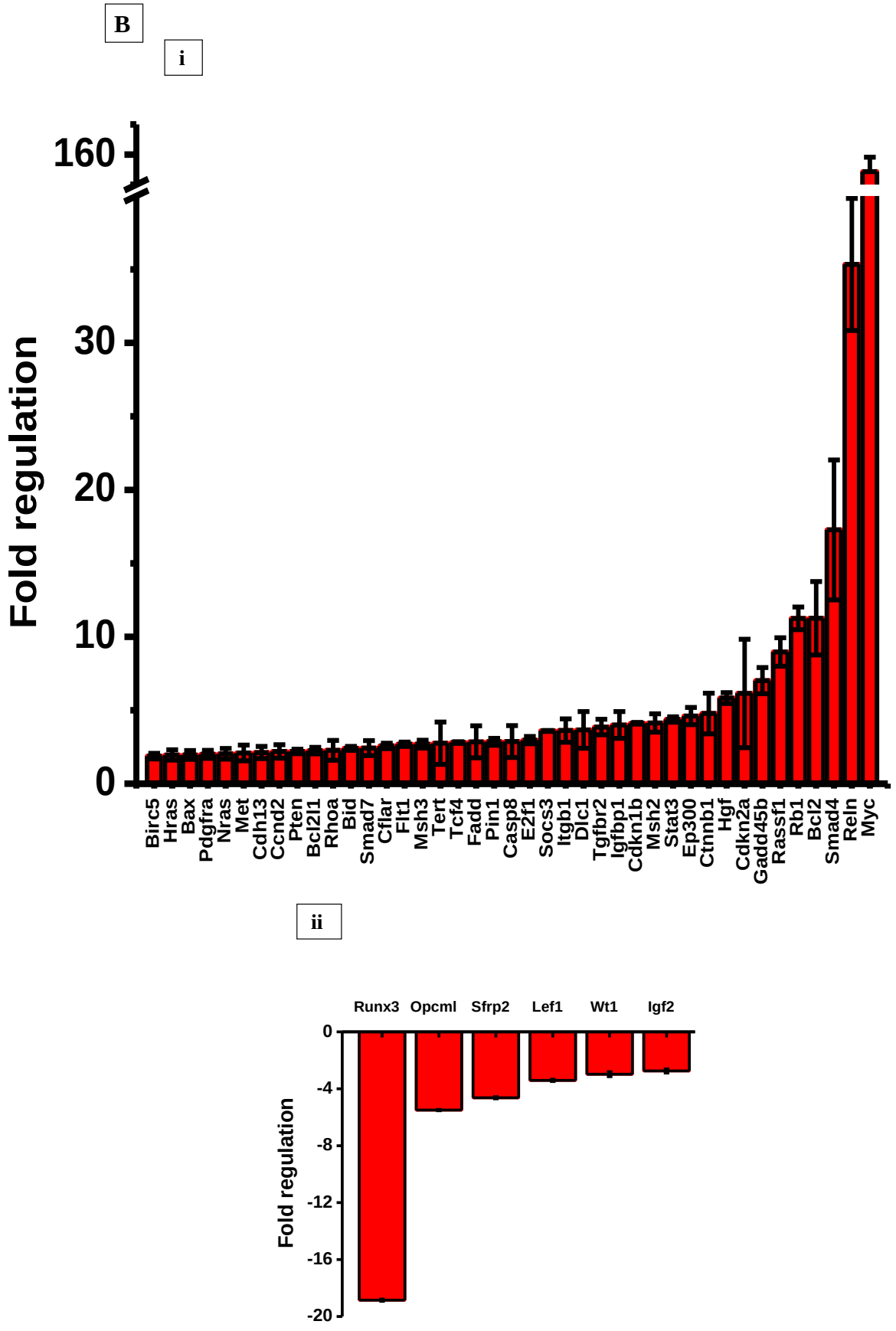
B
i
Fold regulation
160
30
20
10
0
Birc5
Hras
Bax
Pdgfra
Nras
Met
Cdh13
Ccnd2
Pten
Bcl2l1
Rhoa
Bid
Smad7
Cflar
Flt1
Msh3
Tert
Tcf4
Fadd
Pin1
Casp8
E2f1
Socs3
Itgb1
Dlc1
Tgfbr2
Igfbp1
Cdkn1b
Msh2
Stat3
Ep300
Ctnnb1
Hgf
Cdkn2a
Gadd45b
Rassf1
Rb1
Bcl2
Smad4
Reln
Myc
ii
Runx3
Opcml
Sfrp2
Lef1
Wt1
Igf2
Fold regulation
0
-4
-8
-12
-16
-20

Figure 3.70: *Expression profile of differentially expressed genes (DEGs) with more than two folds differential expression in mice liver tissue after treatment with* ***(A)*** *4 mg/Kg* ***(i)*** *upregulated (12 genes) and* ***(ii)*** *downregulated (47 genes),* ***(B)*** *20 mg/Kg* ***(i)*** *upregulated (41 genes) and* ***(ii)*** *downregulated (06 genes), thorium for six months.*

In order to understand the role of genes in thorium toxicity and carcinogenic pathways, a list of 05 most upregulated and downregulated genes have been prepared for both thorium doses and is shown below in Table 3.12. It can be observed that in case of 4 mg/Kg, oncogenes such as *Myc* and *Tert* have been found to be highly upregulated whereas tumor suppressor genes such as *Pten* have been found to downregulated. Similarly, in case of 20 mg/Kg, oncogenes such as *Myc*, *Rb1* and *Tert* have been found to be highly upregulated.

Group	Upregulated genes	Downregulated genes
4 mg/Kg	*Myc (47.6 ± 26.3), Ptgs2 (18.3 ± 2.6), Cdkn2a (13.8 ± 5), Tert (6.1 ± 3.0), Reln (5.8 ± 1.0)*	*Igfbp3 (-205.3 ± 0.00), Igfbp1 (-165.6 ± 0.00), Opcml (-31.2 ± 0.00), Pten (-20.4 ± 0.00), Fhit (-18.6 ± 0.00)*
20 mg/Kg	*Myc (148.7 ± 9.5), Reln (35.3 ± 4.5), Smad4 (17.3 ± 4.8), Bcl2 (11.3 ± 2.5), Rb1 (11.2 ± 0.8)*	*Runx3 (-18.9 ± 0.1), Opcml (-5.5 ± 0.00), Sfrp2 (-4.6 ± 0.1), Lef1 (-3.4 ± 0.1), Wt1 (-3.0 ± 0.2)*

Table 3.15: *Top five upregulated and downregulated genes when mice were treated with 4 and 20 mg/Kg of thorium for six months. The genes in red were upregulated while genes in blue were downregulated while the numbers in brackets indicate the fold regulation of each gene*

The proteins coded by these DEGs with more than two folds differential expression were studied for their mutual interaction using String Network Functional Enrichment

Analysis. The interaction of these proteins was mapped and is shown in Figure 3.75 A-B for 4 mg/Kg and 20 mg/Kg thorium treated liver samples, respectively. The proteins most upregulated are marked by red color halo and the most downregulated proteins are marked by blue color halo. Based on these mapping, it was found that Myc, Ptgs2, Stat3, Pten, Egfr, Egf, Vegfa, Tgfb1, Ctnnb1, Hgf, Igf2, Igfbp1, Cdkn2a, Tert, Rhoa, Kdr, Nfkb1, Birc2, Xiap, Cflar etc. were found to be key proteins involved in thorium toxicity caused by 4 mg/Kg thorium treatment in mice liver after six months. Similarly, for 20 mg/Kg thorium treatment in mice liver, it was found that Myc, Pten, Hras, Nras, Wt1, Smad4, Rassf1, Tert, Ctnnb1, Met, Hgf, Smad7, Igf2 etc. were some of the key proteins involved in thorium induced gene expression alterations after six months.

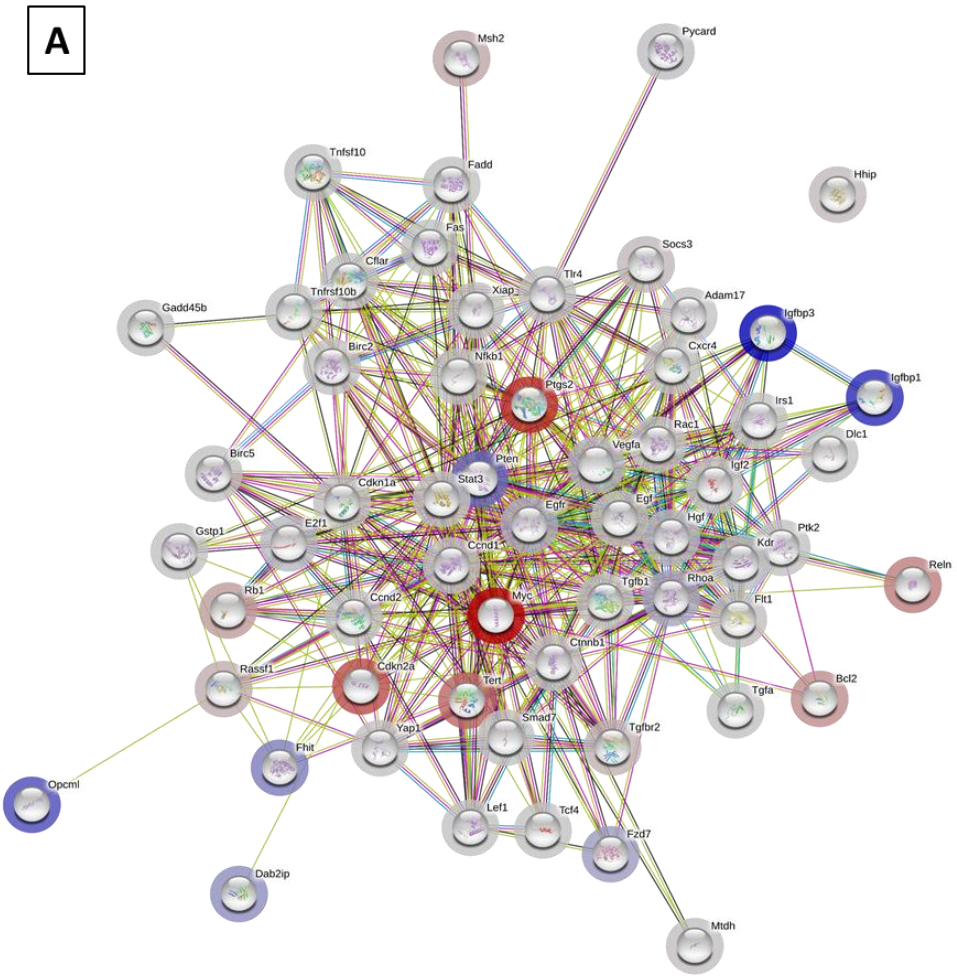

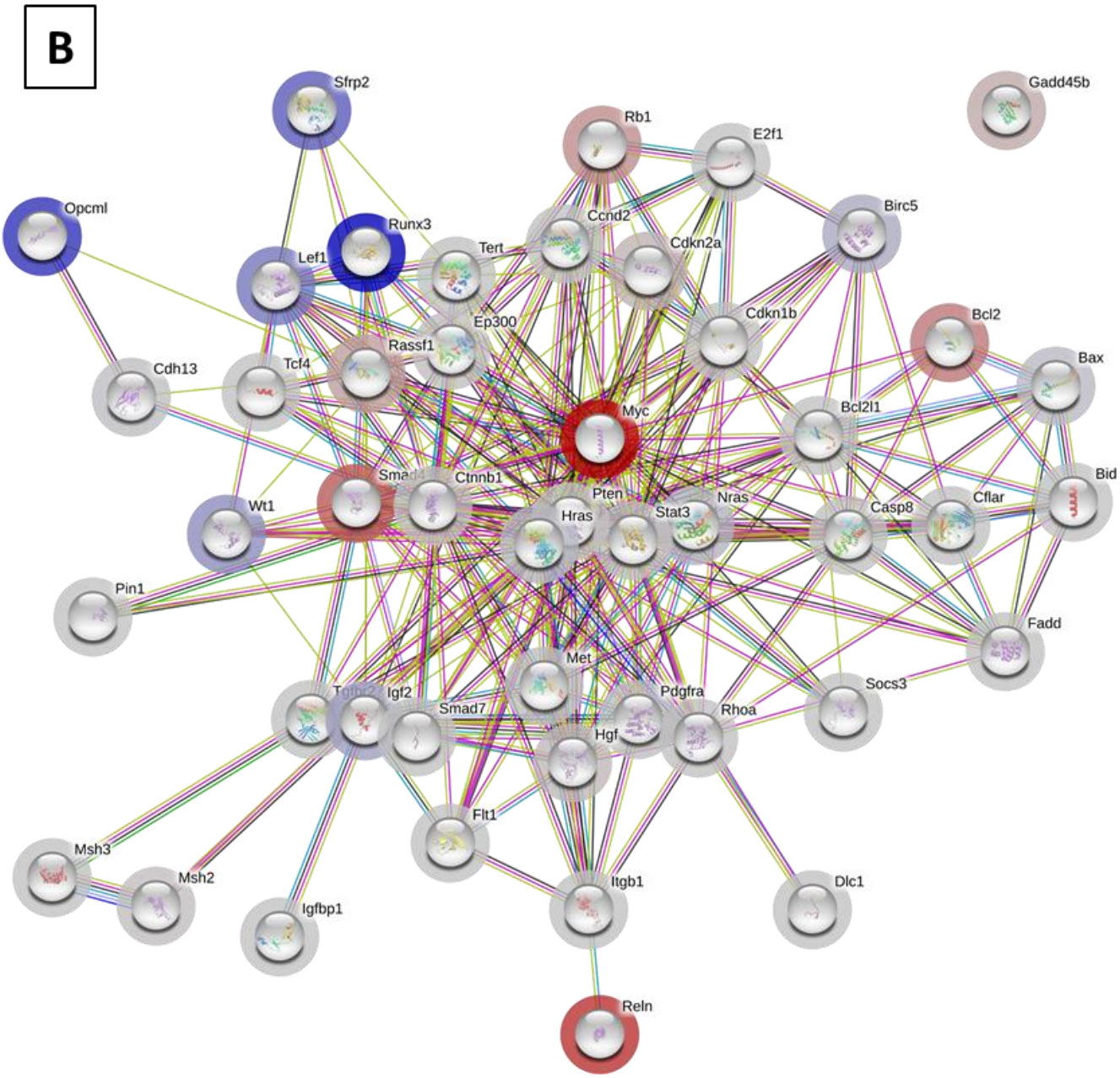

Figure 3.71: *Interaction among different proteins coded by DEGs with fold regulation more than two in mice liver tissue as was mapped by String Network Functional Enrichment Analysis after treatment with* ***(A)*** *4 mg/Kg* ***(B)*** *20 mg/Kg thorium after six months. The proteins shown with red coloration showed maximum upregulation and in blue coloration showed maximum downregulation.*

Venn diagram was prepared to study the genes commonly upregulated and downregulated after treating mice with 4 and 20 mg/Kg of thorium for 6 months (Figure 3.76). It was found that a total of 16 upregulated (Figure 3.76 A) and 41 downregulated (Figure 3.76 B) genes were commonly expressed at 6 months-time between these two doses. Only 4 genes at 4 mg/Kg and 7 genes at 20 mg/Kg were uniquely upregulated whereas 23 genes at 4 mg/Kg and 4 genes at 20 mg/Kg were uniquely downregulated.

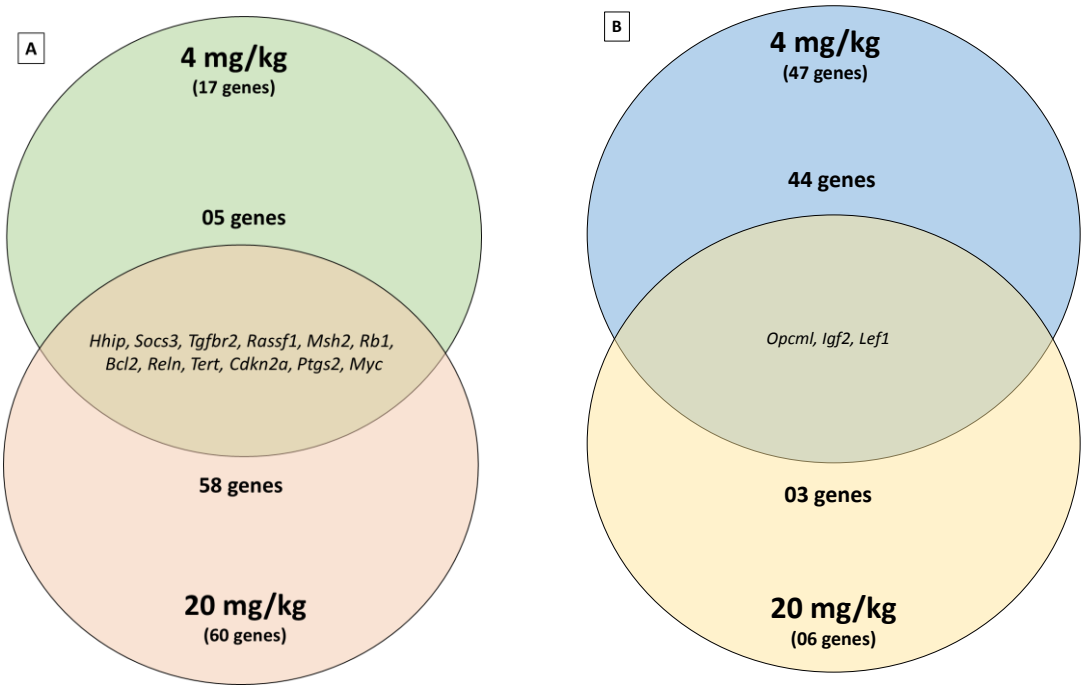

Figure 3.72: *Venn diagram showing genes commonly* ***(A)*** *upregulated and* ***(B)*** *downregulated after treating mice with 4 and 20 mg/Kg of thorium for six months. The total number of genes upregulated and downregulated are shown in brackets. Common genes are listed out and number of unique genes are written in numbers.*

In addition to protein-protein interactions and mapping of genes commonly upregulated and downregulated, the role of all these DEGs with fold regulation more than two were also studied in different pathways using KEGG pathway software analysis. The top 15 pathways in which these proteins play a key role were chosen and presented below in a tabular form (Table

3.13 A-B):

No.	Altered pathways	Genes altered in each pathway (number of genes)
1	**Pathways in cancer**	*Bcl2, Cdkn2a, Hhip, Msh2, Ptgs2, Rassf1, Rb1, Tert, Tgfbr2, Birc2, Birc5, Ccnd1, Ccnd2, Cdkn1a, Ctnnb1, Cxcr4, E2f1, Egf, Egfr, Fadd, Fas, Fzd7, Gadd45b, Gstp1, Hgf, Igf2, Lef1, Myc, Nfkb1, Pten, Ptk2, Rac1, Rhoa, Stat3, Tgfa, Tgfb1, Vegfa, Xiap* ***(38)***
2	**PI3K-Akt signaling**	*Bcl2, Myc, Reln, Ccnd1, Ccnd2, Cdkn1a, Egf, Egfr, Flt1, Hgf, Igf2, Irs1, Kdr, Nfkb1, Pten, Ptk2, Rac1, Tgfa, Tlr4, Vegfa* ***(20)***
3	**Hepatocellular carcinoma**	*Cdkn2a, Myc, Rb1, Tert, Tgfbr2, Ccnd1, Cdkn1a, Ctnnb1, E2f1, Egfr, Fzd7, Gadd45b, Gstp1, Hgf, Igf2, Lef1, Pten, Tgfa, Tgfb1* ***(19)***
4	**Human cytomegalovirus infection**	*Cdkn2a, Myc, Ptgs2, Rb1, Ccnd1, Cdkn1a, Ctnnb1, Cxcr4, E2f1, Egfr, Fadd, Fas, Nfkb1, Ptk2, Rac1, Rhoa, Stat3, Vegfa* ***(18)***
5	**Human papillomavirus infection**	*Ptgs2, Rb1, Reln, Tert, Ccnd1, Ccnd2, Cdkn1a, Ctnnb1, E2f1, Egf, Egfr, Fadd, Fas, Fzd7, Nfkb1, Pten, Ptk2, Vegfa* ***(18)***
6	**Focal adhesion**	*Bcl2, Reln, Birc2, Ccnd1, Ccnd2, Ctnnb1, Egf, Egfr, Flt1, Hgf, Kdr, Pten, Ptk2, Rac1, Rhoa, Vegfa, Xiap* ***(17)***

7	**Proteoglycans in cancer**	*Myc, Ccnd1, Cdkn1a, Ctnnb1, Egfr, Fas, Fzd7, Hgf, Igf2, Kdr, Ptk2, Rac1, Rhoa, Stat3, Tgfb1, Tlr4, Vegfa* ***(17)***
8	**Gastric cancer**	*Bcl2, Myc, Rb1, Tert, Tgfbr2, Ccnd1, Cdkn1a, Ctnnb1, E2f1, Egf, Egfr, Fzd7, Gadd45b, Hgf, Lef1, Tgfb1* ***(16)***
9	**MicroRNAs in cancer**	*Bcl2, Cdkn2a, Irs1, Myc, Ptgs2, Rassf1, Ccnd1, Ccnd2, Cdkn1a, E2f1, Egfr, Nfkb1, Pten, Rhoa, Stat3, Vegfa* ***(16)***
10	**Colorectal cancer**	*Bcl2, Msh2, Myc, Tgfbr2, Birc5, Ccnd1, Cdkn1a, Ctnnb1, Egf, Egfr, Gadd45b, Lef1, Rac1, Rhoa, Tgfa, Tgfb1* ***(16)***
11	**MAPK signaling**	*Myc, Tgfbr2, Egf, Egfr, Fas, Flt1, Gadd45b, Hgf, Igf2, Kdr, Nfkb1, Rac1, Tgfa, Tgfb1, Vegfa* ***(15)***
12	**Pancreatic cancer**	*Cdkn2a, Rb1, Tgfbr2, Ccnd1, Cdkn1a, E2f1, Egf, Egfr, Gadd45b, Nfkb1, Rac1, Stat3, Tgfa, Tgfb1, Vegfa* ***(15)***
13	**Hepatitis C**	*Myc, Rb1, Socs3, Ccnd1, Cdkn1a, Cflar, Ctnnb1, E2f1, Egf, Egfr, Fadd, Fas, Nfkb1, Stat3* ***(14)***
14	**Kaposi sarcoma-associated herpesvirus infection**	*Myc, Ptgs2, Rb1, Ccnd1, Cdkn1a, Ctnnb1, E2f1, Fadd, Fas, Lef1, Nfkb1, Rac1, Stat3, Vegfa* ***(14)***
15	**Small cell lung cancer**	*Bcl2, Myc, Ptgs2, Rb1, Birc2, Ccnd1, Cdkn1a, E2f1, Fhit, Gadd45b, Nfkb1, Pten, Ptk2, Xiap* ***(14)***

A: 4 mg/Kg of thorium treatment for six months

No.	Altered pathways	Genes altered in each pathway (number of genes)
1	**Pathways in cancer**	*Bax, Bcl2, Bcl2l1, Bid, Casp8, Ccnd2, Cdkn1b, Cdkn2a, Ctnnb1, E2f1, Ep300, Fadd, Gadd45b, Hgf, Hras, Itgb1, Met, Msh2, Msh3, Myc, Nras, Pdgfra, Pten, Rassf1, Rb1, Rhoa, Smad4, Stat3, Tert, Tgfbr2, Igf2, Lef1* ***(32)***
2	**Hepatocellular carcinoma**	*Bax, Bcl2l1, Cdkn2a, Ctnnb1, E2f1, Gadd45b, Hgf, Hras, Met, Myc, Nras, Pten, Rb1, Smad4, Tert, Tgfbr2, Igf2, Lef1* ***(18)***
3	**Gastric cancer**	*Bax, Bcl2, Cdkn1b, Ctnnb1, E2f1, Gadd45b, Hgf, Hras, Met, Myc, Nras, Rb1, Smad4, Tert, Tgfbr2, Lef1* ***(16)***
4	**PI3K-Akt signaling**	*Bcl2, Bcl2l1, Ccnd2, Cdkn1b, Flt1, Hgf, Hras, Itgb1, Met, Myc, Nras, Pdgfra, Pten, Reln, Igf2* ***(15)***
5	**Human papillomavirus infection**	*Bax, Casp8, Ccnd2, Cdkn1b, Ctnnb1, E2f1, Ep300, Fadd, Hras, Itgb1, Nras, Pten, Rb1, Reln, Tert* ***(15)***
6	**MicroRNAs in cancer**	*Bcl2, Ccnd2, Cdkn1b, Cdkn2a, E2f1, Ep300, Hras, Met, Myc, Nras, Pdgfra, Pten, Rassf1, Rhoa, Stat3* ***(15)***
7	**Human cytomegalovirus infection**	*Bax, Bid, Casp8, Cdkn2a, Ctnnb1, E2f1, Fadd, Hras, Myc, Nras, Pdgfra, Rb1, Rhoa, Stat3* ***(14)***
8	**Human T-cell leukemia virus 1 infection**	*Bax, Bcl2l1, Ccnd2, Cdkn2a, E2f1, Ep300, Hras, Myc, Nras, Pten, Rb1, Smad4, Tert, Tgfbr2* ***(14)***

9	**Hepatitis B**	*Bax, Bcl2, Bid, Casp8, E2f1, Ep300, Fadd, Hras, Myc, Nras, Rb1, Smad4, Stat3, Tgfbr2* ***(14)***
10	**Kaposi sarcoma-associated herpesvirus infection**	*Bax, Bid, Casp8, Ctnnb1, E2f1, Ep300, Fadd, Hras, Myc, Nras, Rb1, Stat3, Lef1* ***(13)***
11	**Colorectal cancer**	*Bax, Bcl2, Ctnnb1, Gadd45b, Hras, Msh2, Msh3, Myc, Nras, Rhoa, Smad4, Tgfbr2, Lef1* ***(13)***
12	**Hepatitis C**	*Bax, Bid, Casp8, Cflar, Ctnnb1, E2f1, Fadd, Hras, Myc, Nras, Rb1, Socs3, Stat3* ***(13)***
13	**Epstein-Barr virus infection**	*Bax, Bcl2, Bid, Casp8, Ccnd2, Cdkn1b, E2f1, Fadd, Gadd45b, Myc, Rb1, Stat3, Runx3* ***(13)***
14	**Chronic myeloid leukemia**	*Bax, Bcl2l1, Cdkn1b, Cdkn2a, E2f1, Gadd45b, Hras, Myc, Nras, Rb1, Smad4, Tgfbr2* ***(12)***
15	**Focal adhesion**	*Bcl2, Ccnd2, Ctnnb1, Flt1, Hgf, Hras, Itgb1, Met, Pdgfra, Pten, Reln, Rhoa* ***(12)***

B: 20 mg/Kg of thorium treatment for six months

Table: 3.16. *List of pathways altered by more than two folds differentially expressed genes (DEGs) after treatment with* ***(A)*** *4 mg/Kg* ***(B)*** *20 mg/Kg thorium after six months as mapped by KEGG pathway. Genes upregulated are represented in red color and downregulated genes are represented in blue color and the total number of DEGs expressed in brackets.*

It is clear from the pathways studies that when 4 mg/Kg of thorium was injected in

mice intravenously for six months interval, apart from genes involved in cancer pathogenesis, genes involved mainly in the development of PI3K-Akt signaling pathway, hepatocellular carcinoma pathway, human cytomegalovirus infection pathway, human papillomavirus infection pathway, pathway for proteoglycans in cancer, focal adhesion pathway and gastric cancer pathway are the main pathways activated/induced by thorium treatment of 4 mg/Kg after six months. Similarly, thorium treatment of 20 mg/Kg for six months activated/induced various genes involved in cancer pathway. Apart from this, genes responsible for hepatocellular carcinoma, gastric cancer pathway, PI3K-Akt signaling pathway, human papillomavirus infection pathway, pathway involved in microRNAs in cancer, human cytomegalovirus infection were also found to be playing a key role.

3.3.3.2: Gene expression changes in liver tissue Twelve months after thorium treatment

Gene alterations caused by thorium toxicity after twelve months treatment to 4, 10 and 20 mg/Kg of thorium were also studied by RT^2 PCR array analysis as was done for six months treatment. At dose 4 mg/Kg, it was found that out of 84 genes known to play a role in hepatocarcinogenesis which were studied, a total of 26 genes were upregulated and 32 genes were downregulated (Table 3.14 A). Similar study for 10 mg/Kg of thorium showed an upregulation of 53 genes and downregulation of 05 genes (Table 3.14 B) whereas 20 mg/Kg thorium treatment for one year caused 47 genes to be upregulated and 11 genes to be downregulated (Table 3.14 C).

A

4 mg		
Genes	Fold regulation	SD
Adam17	-60.06	0.01
Akt1	-241.54	0.001
Trp53	-6.71	0.1
Angpt2	-6.31	0.0
Runx3	-5.34	0.1
Myc	-5.18	0.1
Egfr	-4.92	0.0
Msh3	-3.63	0.3
Dab2ip	-3.11	0.0
Rhoa	-3.00	0.2
Bax	-2.89	0.3
Fadd	-2.86	0.1
Cdkn1b	-2.66	0.1
Gstp1	-2.60	0.2
Irs1	-2.44	0.1
Pten	-2.42	0.1
Bid	-2.40	0.3
Smad4	-2.35	0.2
Cdkn1a	-2.22	0.3
Egf	-2.01	0.0

B

10 mg		
Genes	Fold regulation	SD
Akt1	-15.98	0.0
Adam17	-11.19	0.0
Angpt2	-5.79	0.0
Egf	-3.15	0.1
Trp53	-2.62	0.1
Egfr	1.59	0.3
Hras	1.65	0.2
Ccl5	1.67	0.0
Fadd	1.81	0.2
Birc5	1.88	0.1
Dlc1	1.92	0.3
Ep300	1.93	0.2
Rhoa	2.10	0.1
Pten	2.14	0.3
Cdh1	2.17	0.4
Rac1	2.30	0.4
Ccnd1	2.47	0.5
Wt1	2.55	0.3
Fhit	2.58	0.6
Tnfsf10	2.63	0.1

C

20 mg		
Genes	Fold regulation	SD
Egfr	-352.03	0.0
Mcl1	-33.61	0.0
Kdr	-20.86	0.1
Fadd	-17.81	0.0
Akt1	-13.91	0.0
Ep300	-12.80	0.1
Adam17	-10.61	0.0
Trp53	-3.06	0.1
Hras	-2.33	0.0
Egf	-1.93	0.1
Fas	-1.73	0.5
Ccl5	1.01	0.3
Irs1	1.04	0.1
Pten	1.39	0.3
Rhoa	1.44	0.2
Cdkn1b	1.80	0.5
Cdh1	1.87	0.2
Rac1	2.41	0.2
Socs3	2.45	0.4
Smad4	2.60	0.2

Ccl5	-1.95	0.3
Cflar	-1.88	0.3
Tert	-1.76	0.5
Tgfa	-1.61	0.8
Kdr	-1.61	0.6
Hras	-1.54	0.2
Vegfa	-1.54	0.2
Tcf4	-1.30	0.0
Fhit	-1.28	0.2
Cdh1	-1.19	0.7
Ep300	-1.09	0.1
Cdkn2a	-1.04	0.2
Yap1	1.14	0.1
Reln	1.19	0.5
Rb1	1.31	0.1
Pdgfra	1.34	0.3
Stat3	1.37	0.4
Tgfb1	1.42	0.2
Tnfsf10	1.59	0.3
Ptk2	1.68	0.8
Hgf	1.83	0.4
Dlc1	1.84	0.1
Rac1	1.87	0.5
Nras	2.21	0.5

Mcl1	2.88	0.6
Dab2ip	3.16	0.2
Smad4	3.17	0.2
Vegfa	3.30	0.5
Tcf4	3.63	0.3
Cflar	4.06	1.0
Msh2	4.17	1.0
Yap1	4.53	0.4
Flt1	4.59	1.4
Smad7	4.98	0.9
Hgf	5.32	1.0
Tert	5.66	1.0
Bax	5.91	0.9
Reln	6.01	1.7
Hhip	6.23	1.6
Ptk2	6.57	0.4
Pin1	7.01	1.8
Fas	7.11	2.5
Pycard	7.30	0.0
Pdgfra	7.42	0.3
Tgfb1	7.98	1.7
Cdkn1a	8.19	1.6
Bid	8.29	1.1
Nfkb1	8.44	1.9

Birc5	2.75	0.7
Fhit	2.81	1.0
Gstp1	2.87	0.7
Dlc1	3.01	1.3
Cdkn2a	3.04	1.2
Vegfa	3.30	0.5
Ccnd1	3.31	0.3
Msh2	3.36	1.5
Cflar	3.48	0.8
Smad7	3.67	0.7
Flt1	4.18	0.0
Bax	4.20	1.8
Tcf4	4.35	0.5
Wt1	4.74	0.1
Yap1	5.40	0.4
Pdgfra	5.41	0.6
Pycard	5.79	0.3
Tnfsf10	6.28	0.3
Tgfa	7.24	0.3
Bid	7.27	2.4
Rb1	7.29	0.7
Met	7.63	0.9
Tgfb1	8.43	1.0
Tert	8.59	1.1

Pin1	2.71	0.0	Tgfa	8.54	0.9	Reln	9.40	1.5
Pycard	2.82	0.6	Met	9.70	0.4	Ptk2	9.51	1.7
Msh2	2.83	1.4	Rb1	11.00	0.7	Nfkb1	9.59	2.5
Nfkb1	2.90	0.6	Tlr4	11.43	4.0	Stat3	12.36	1.4
Socs1	3.29	0.4	Msh3	11.49	1.8	Rassf1	13.26	3.4
Hhip	4.92	0.7	Kdr	13.18	2.6	Nras	15.82	5.2
Xiap	8.94	1.5	Stat3	13.39	4.4	Myc	21.56	0.1
Tlr4	9.43	1.7	Nras	13.73	1.9	Socs1	22.18	8.2
E2f1	9.56	2.3	Rassf1	24.09	4.6	Tlr4	22.38	2.0
Rassf1	9.62	0.8	Itgb1	26.37	6.4	Xiap	32.57	1.3
Cxcr4	26.68	2.2	Xiap	47.84	0.2	E2f1	61.61	0.4
Wt1	45.26	0.6	Cxcr4	89.34	15.7	Cxcr4	69.98	30.4
Fzd7	46.26	8.3	Fzd7	310.04	40.9	Fzd7	355.07	26.1
Ctnnb1	224.14	82.6	Ctnnb1	622.81	12.2	Ctnnb1	387.38	101.3

Table 3.17: *Fold regulation of genes in mice liver tissue after treatment with* ***(A)*** *4 mg/Kg,* ***(B)*** *10 mg/Kg and* ***(C)*** *20 mg/Kg thorium injected intravenously after twelve months of treatment. Genes in red are upregulated and genes in blue are downregulated.*

These data of fold regulation of genes upon thorium treatment for one year was further analyzed and genes which are differentially expressed two or more folds were than plotted against their fold regulation at each thorium dose injected in mice. It was observed that at 4 mg/Kg, a total of 18 genes showed an upregulation of two or more than two folds and around 23 genes showed a downregulation of two or more than two folds. *Ccnd1, Nras, Flt1, Pin1, Fas, Pycard, Msh2, Nfkb1, Socs1, Hhip, Xiap, Tlr4, E2f1, Rassf1, Cxcr4, Wt1, Fzd7, Ctnnb1*

were upregulated by two or more folds and *Akt1, Adam17, Trp53, Angpt2, Runx3, Myc, Egfr, Msh3, Dab2ip, Rhoa, Bax, Fadd, Cdkn1b, Gstp1, Irs1, Pten, Bid, Smad4, Cdkn1a, Egf, Ccl5, Cflar, Tert* were the genes which were downregulated by two or more folds. Similarly, when expression of genes altered by 10 mg/Kg of thorium in mice after one year were analyzed, it was found that 51 genes were upregulated, and 05 genes were downregulated by two or more folds. *Cdkn2a, Socs3, Rhoa, Pten, Cdh1, Rac1, Ccnd1, Wt1, Fhit, Tnfsf10, Mcl1, Irs1, Dab2ip, Smad4, Vegfa, Tcf4, Cflar, Msh2, Yap1, Flt1, Smad7, Hgf, Runx3, Tert, Bax, Reln, Hhip, Ptk2, Pin1, Fas, Pycard, Pdgfra, Tgfb1, Cdkn1a, Bid, Nfkb1, Tgfa, Met, Rb1, Tlr4, Msh3, Kdr, Stat3, Nras, Rassf1, Itgb1, Socs1, Xiap, Cxcr4, Fzd7, Ctnnb1* were the genes upregulated and *Akt1, Adam17, Angpt2, Egf, Trp53* genes were downregulated by two or more folds. In case of 20 mg/Kg thorium treatment, it was found that 41 genes were upregulated two or more folds. *Rac1, Socs3, Smad4, Birc5, Fhit, Gstp1, Dlc1, Cdkn2a, Vegfa, Ccnd1, Msh2, Cflar, Smad7, Flt1, Bax, Tcf4, Wt1, Yap1, Pdgfra, Pycard, Tnfsf10, Tgfa, Bid, Rb1, Met, Tgfb1, Tert, Reln, Ptk2, Nfkb1, Stat3, Rassf1, Nras, Myc, Socs1, Tlr4, Xiap, E2f1, Cxcr4, Fzd7, Ctnnb1* had their expression upregulated while 11 genes i.e. *Egfr, Mcl1, Kdr, Fadd, Akt1, Ep300, Adam17, Trp53, Hras, Egf, Fas* were downregulated by two or more folds. The extent of the upregulation and downregulation of all these genes across all three doses were plotted against fold regulation and are shown in Figure 3.78 A-C.

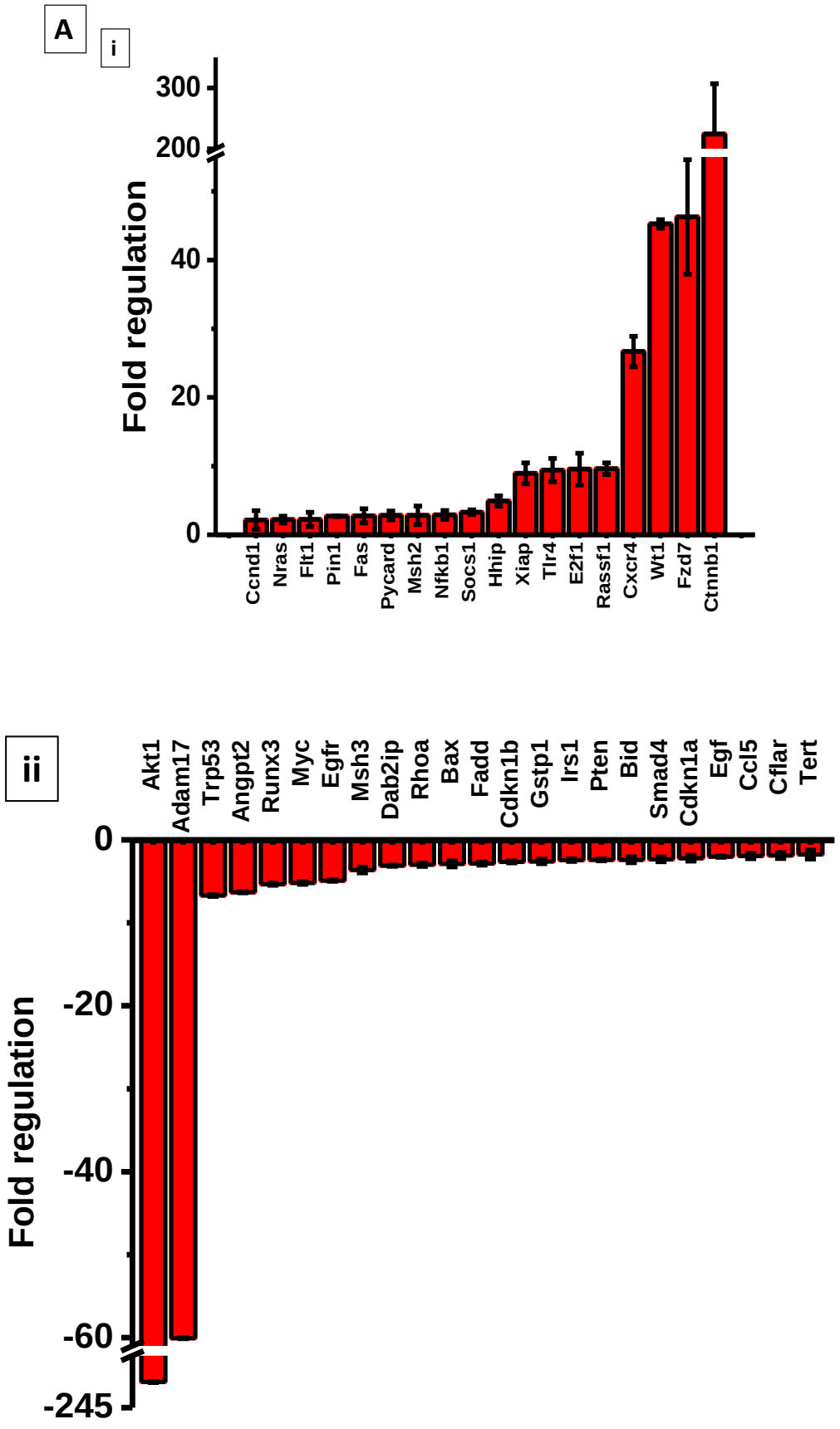
A
i
Fold regulation
300
200
40
20
0
Ccnd1
Nras
Flt1
Pin1
Fas
Pycard
Msh2
Nfkb1
Socs1
Hhip
Xiap
Tlr4
E2f1
Rassf1
Cxcr4
Wt1
Fzd7
Ctnnb1
ii
Fold regulation
0
-20
-40
-60
-245
Akt1
Adam17
Trp53
Angpt2
Runx3
Myc
Egfr
Msh3
Dab2ip
Rhoa
Bax
Fadd
Cdkn1b
Gstp1
Irs1
Pten
Bid
Smad4
Cdkn1a
Egf
Ccl5
Cflar
Tert

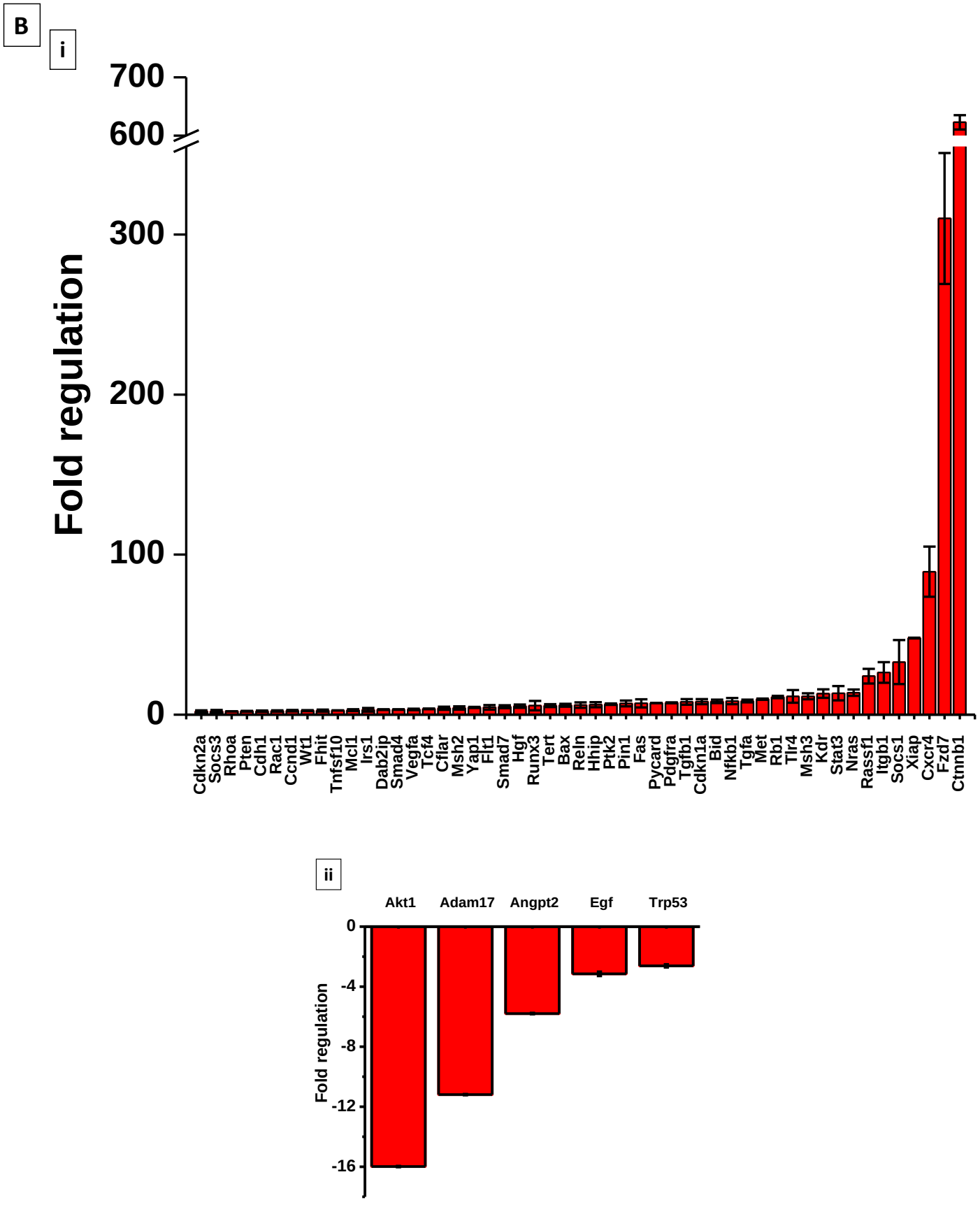
B
i
Fold regulation
700
600
300
200
100
0
Cdkn2a
Socs3
Rhoa
Pten
Cdh1
Rac1
Ccnd1
Wt1
Fhit
Tnfsf10
Mcl1
Irs1
Dab2ip
Smad4
Vegfa
Tcf4
Cflar
Msh2
Yap1
Flt1
Smad7
Hgf
Runx3
Tert
Bax
Reln
Hhip
Ptk2
Pin1
Fas
Pycard
Pdgfra
Tgfb1
Cdkn1a
Bid
Nfkb1
Tgfa
Met
Rb1
Tlr4
Msh3
Kdr
Stat3
Nras
Rassf1
Itgb1
Socs1
Xiap
Cxcr4
Fzd7
Ctnnb1
ii
Akt1
Adam17
Angpt2
Egf
Trp53
Fold regulation
0
-4
-8
-12
-16

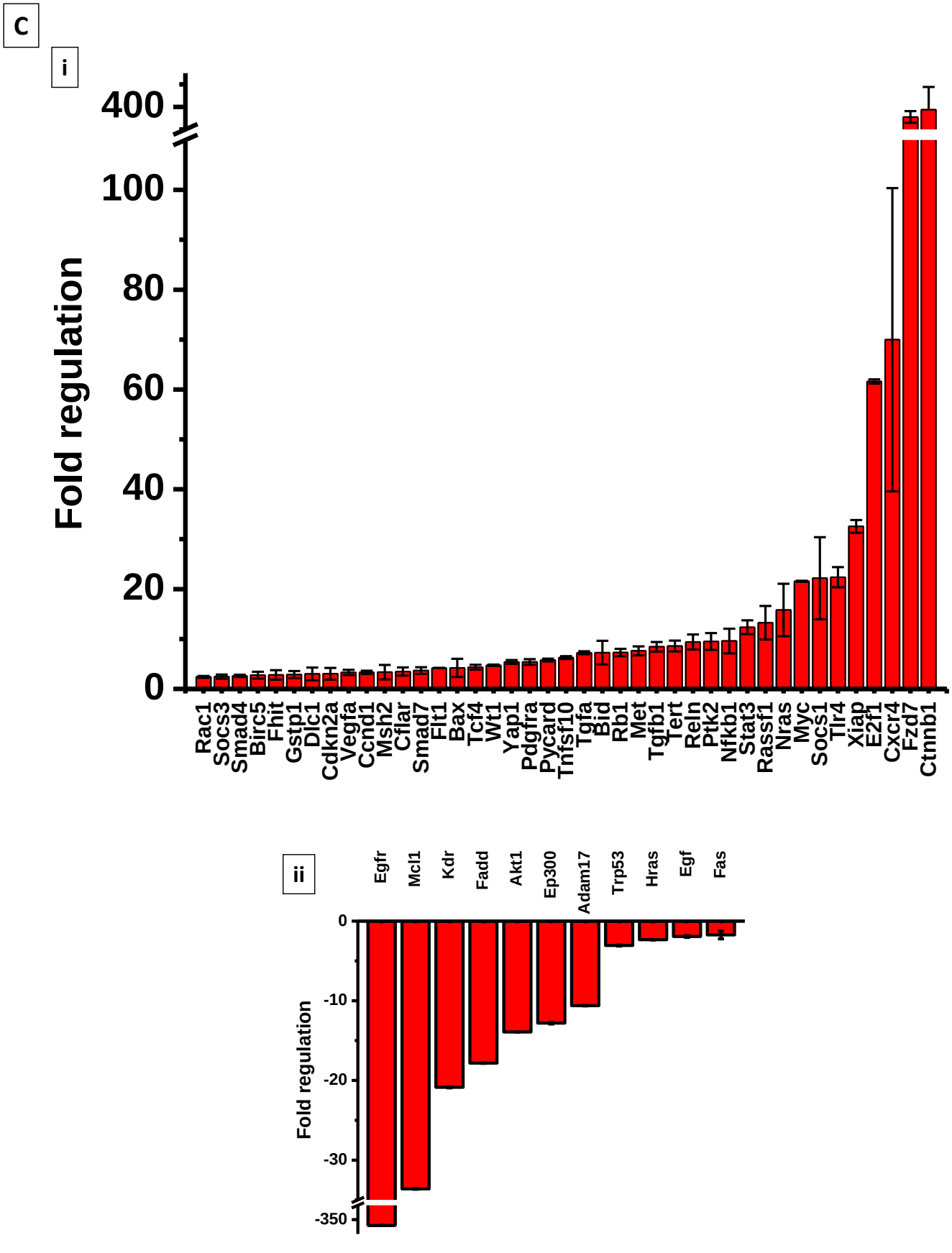
C
i
Fold regulation
400
100
80
60
40
20
0
Rac1
Socs3
Smad4
Birc5
Fhit
Gstp1
Dlc1
Cdkn2a
Vegfa
Ccnd1
Msh2
Cflar
Smad7
Flt1
Bax
Tcf4
Wt1
Yap1
Pdgfra
Pycard
Tnfsf10
Tgfa
Bid
Rb1
Met
Tgfb1
Tert
Reln
Ptk2
Nfkb1
Stat3
Rassf1
Nras
Myc
Socs1
Tlr4
Xiap
E2f1
Cxcr4
Fzd7
Ctnnb1
ii
Egfr
Mcl1
Kdr
Fadd
Akt1
Ep300
Adam17
Trp53
Hras
Egf
Fas
0
-10
-20
-30
-350
Fold regulation

Figure 3.73: *Expression profile of differentially expressed genes (DEGs) with more than two folds differential expression in mice liver tissue after treatment with,* ***(A)*** *4 mg/Kg* ***(i)*** *upregulated (18 genes) and* ***(ii)*** *downregulated (23 genes),* ***(B)*** *10 mg/Kg* ***(i)*** *upregulated (51 genes) and* ***(ii)*** *downregulated (05 genes), and* ***(C)*** *20 mg/Kg* ***(i)*** *upregulated (41 genes) and* ***(ii)*** *downregulated (11 genes), thorium for twelve months.*

The gene expression data was further analyzed and the top five most upregulated and downregulated genes in each treatment group were identified and are listed below in the Table 3.15.

Group	Upregulated genes	Downregulated genes
4 mg/Kg	*Ctnnb1 (224.14 ± 82.6), Fzd7 (46.23 ± 8.3), Wt1 (45.26 ± 0.6), Cxcr4 (26.68 ± 2.2), Rassf1 (9.62 ± 0.8)*	*Adam17 (-60.1 ± 0.01), Akt1 (-241.54 ± 0.001), Trp53 (-6.71 ± 0.1), Angpt2 (-6.31 ± 0.0), Runx3 (-5.34 ± 0.1)*
10 mg/Kg	*Ctnnb1 (622.81 ± 12.2), Fzd7 (310.04 ± 40.9), Cxcr4 (89.34 ± 15.7), Xiap (47.84 ± 0.2), Itgb1 (26.37 ± 6.4)*	*Akt1 (-15.98 ± 0.0), Adam17 (-11.19 ± 0.0), Angpt2 (-5.79 ± 0.0), Egf (-3.15 ± 0.1), Trp53 (-2.62 ± 0.1)*
20 mg/Kg	*Ctnnb1 (387.38 ± 101.3), Fzd7 (355.07 ± 26.1), Cxcr4 (69.98 ± 30.4), E2f1 (61.61 ± 0.4), Xiap1 (32.57 ± 1.3)*	*Egfr (-352.03 ± 0.0), Mcl1 (-33.61 ± 0.0), Kdr (-20.86 ± 0.1), Fadd (-17.81 ± 0.0), Akt1 (-13.91 ± 0.0)*

Table 3.18: *Top five upregulated and downregulated genes when mice were treated with 4, 10 and 20 mg/Kg of thorium for twelve months. The genes in red were upregulated while genes in blue were downregulated while the numbers in brackets indicate the fold regulation of each gene.*

Further studies were carried out using these DEGs with more than two folds differential expression. String Network Functional Enrichment Analysis was performed with these DEGs across all groups and various protein interactions were mapped (Figure 3.79 A-C)

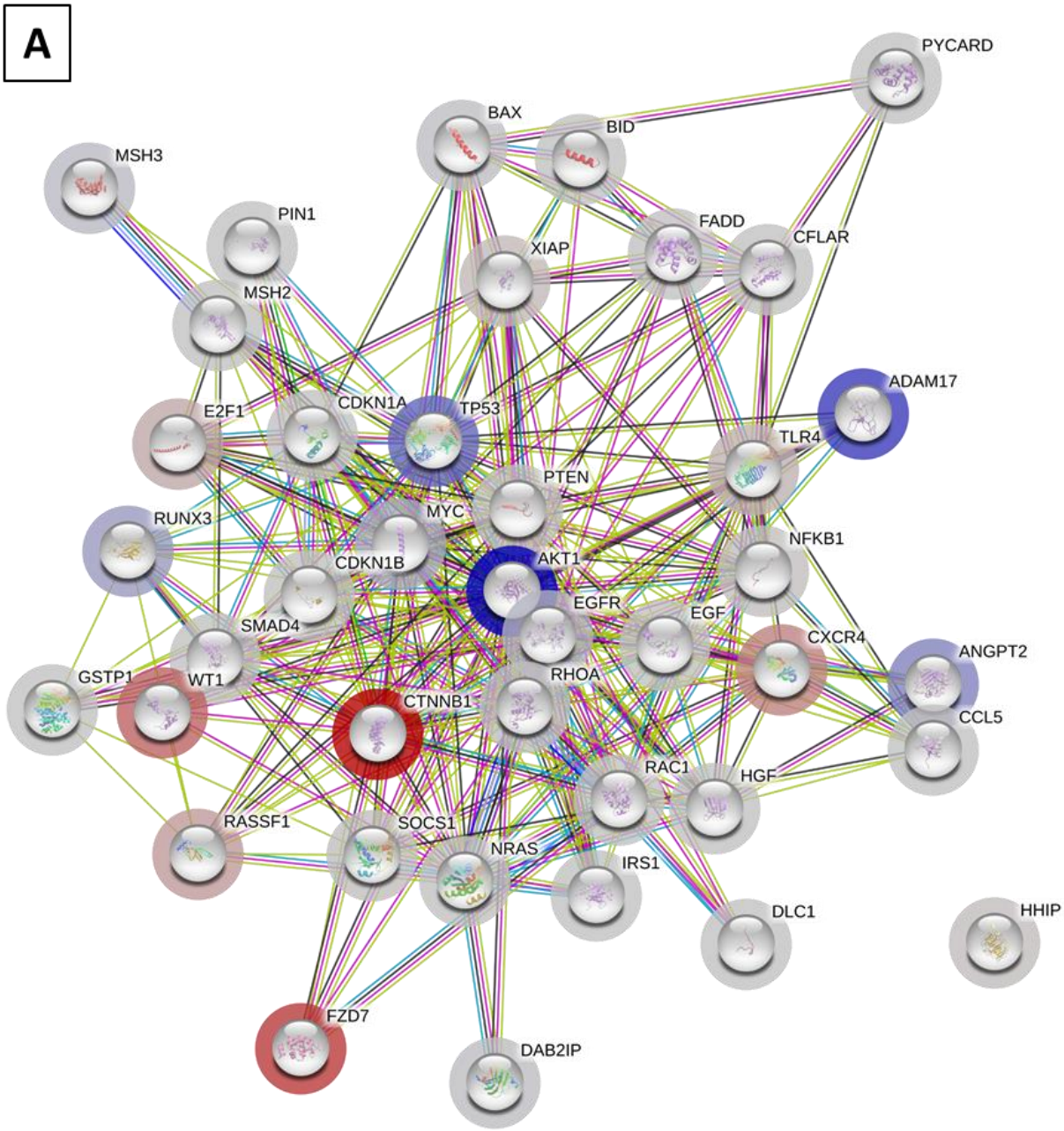

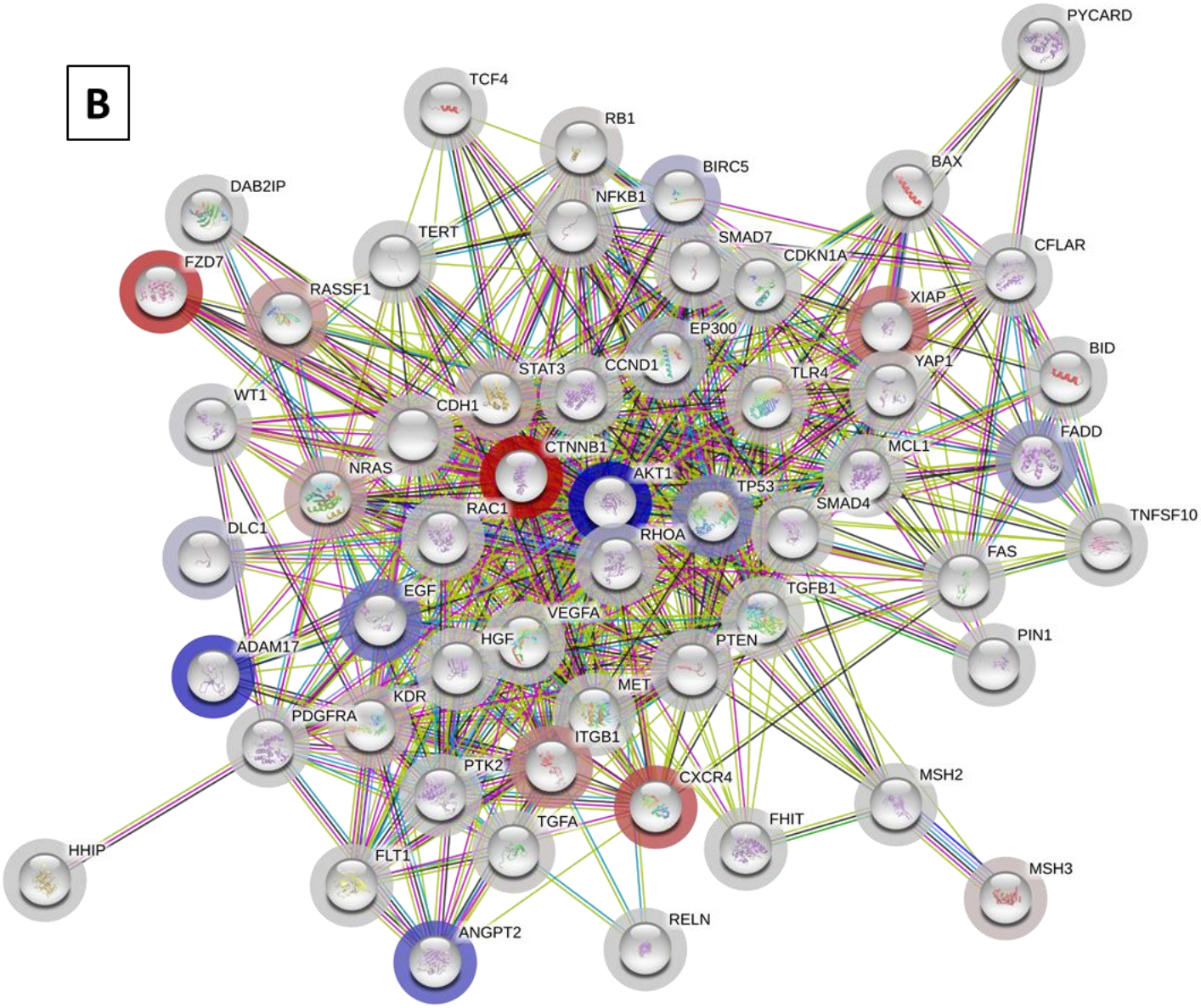
B
PYCARD
TCF4
RB1
BIRC5
BAX
DAB2IP
NFKB1
TERT
SMAD7
CDKN1A
CFLAR
FZD7
RASSF1
XIAP
EP300
BID
STAT3
CCND1
TLR4
YAP1
WT1
CDH1
FADD
CTNNB1
MCL1
NRAS
AKT1
TP53
SMAD4
TNFSF10
RAC1
DLC1
RHOA
FAS
EGF
TGFB1
VEGFA
PIN1
ADAM17
HGF
PTEN
MET
KDR
PDGFRA
ITGB1
PTK2
CXCR4
MSH2
TGFA
FHIT
HHIP
FLT1
MSH3
RELN
ANGPT2

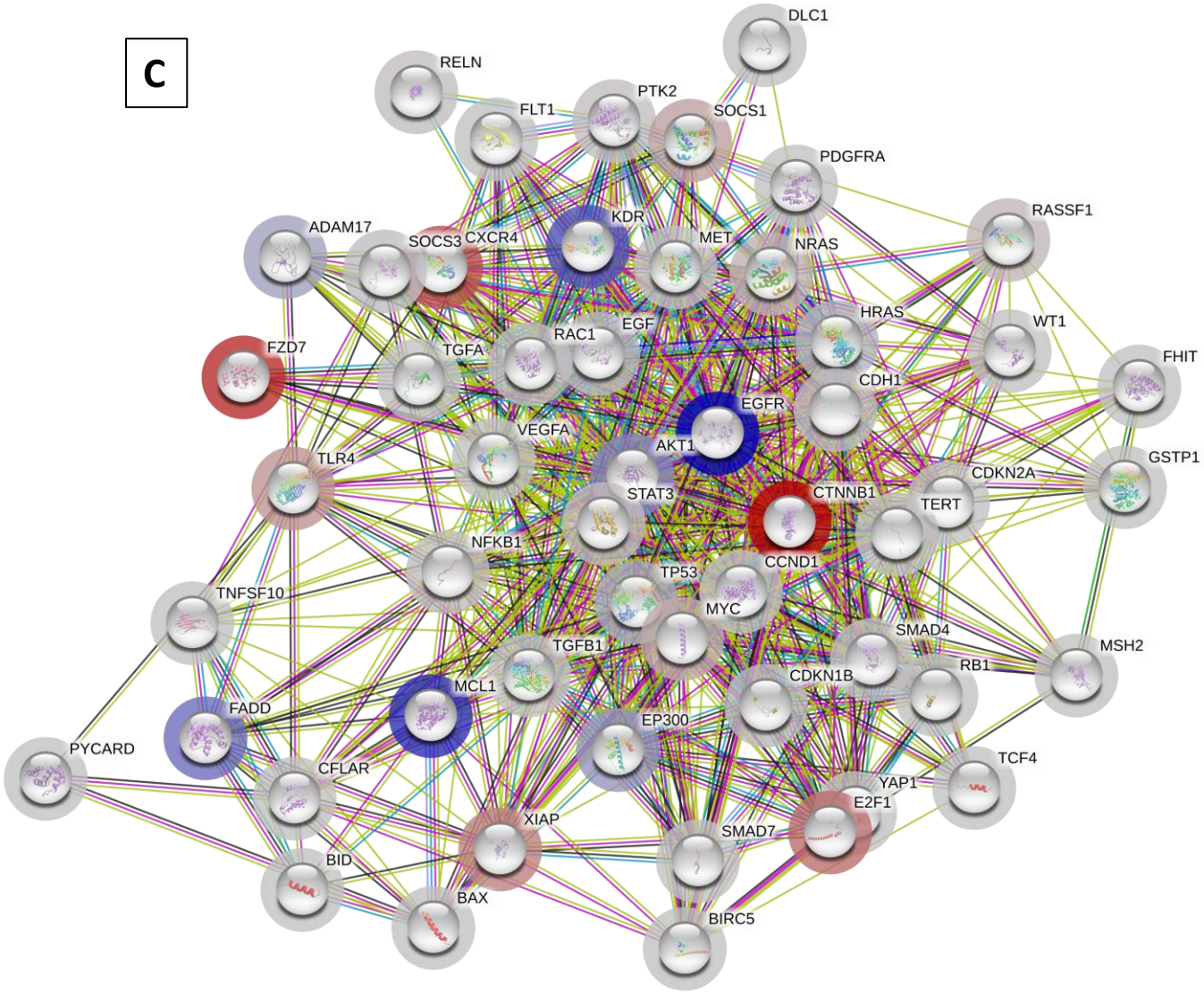

Figure 3.74: *Interaction among different proteins coded by DEGs with fold regulation more than two in mice liver tissue as was mapped by String Network Functional Enrichment Analysis after treatment with* ***(A)*** *4 mg/Kg* ***(B)*** *10 mg/Kg, and* ***(C)*** *20 mg/Kg thorium after twelve months. The proteins shown with red coloration showed maximum upregulation and in blue coloration showed maximum downregulation.*

Venn diagram was made in order to study the common genes which are upregulated and downregulated among these three treatment groups and is shown in Figure 3.80.

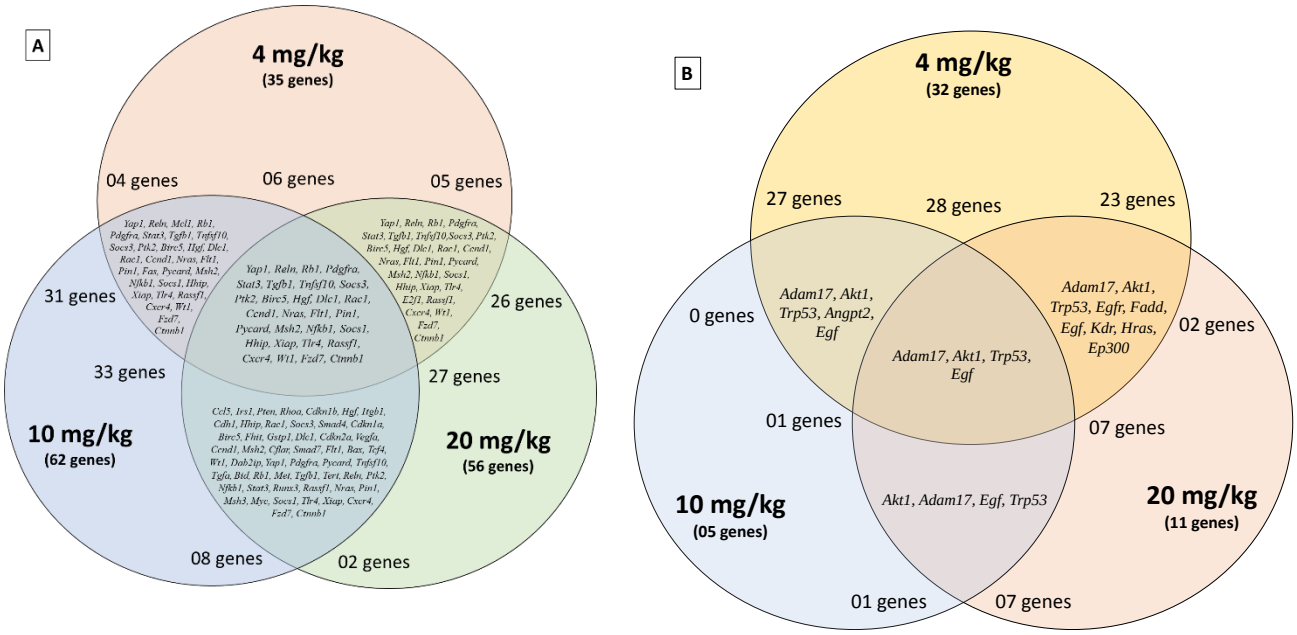

Figure 3.75: *Venn diagram showing genes commonly* ***(A)*** *upregulated and* ***(B)*** *downregulated after treating mice with 4,10 and 20 mg/Kg of thorium for twelve months. The total number of genes upregulated and downregulated are shown in brackets. Common genes are listed out and number of unique genes are written in numbers*

Additionally, KEGG pathway analysis software was used to study the different pathways in which these DEGs are known to play a role. The top 15 such pathways were chosen and presented below in a tabular form (Table 3.16 A-C):

No.	Altered pathways	Genes altered in each pathway (number of genes)
1	**Pathways in cancer**	*Ctnnb1, Cxcr4, E2f1, Fzd7, Hhip, Msh2, Nfkb1, Nras, Rassf1, Xiap, Akt1, Bax, Bid, Ccnd1, Cdkn1a, Cdkn1b, Egf, Egfr, Fadd, Fas, Gstp1, Msh3, Myc, Pten, Rhoa, Smad4, Trp53* **(27)**

2	**Human cytomegalovirus infection**	*Ctnnb1, Cxcr4, E2f1, Nras, Akt1, Bax, Bid, Ccl5, Ccnd1, Cdkn1a, Egfr, Fadd, Fas, Myc, Nfkb1, Rhoa, Trp53* **(17)**
3	**Human papillomavirus infection**	*Ctnnb1, E2f1, Fzd7, Nras, Akt1, Bax, Ccnd1, Cdkn1a, Cdkn1b, Egf, Egfr, Fadd, Fas, Nfkb1, Pten, Trp53* **(16)**
4	**Hepatitis C**	*Ctnnb1, E2f1, Nras, Akt1, Bax, Bid, Ccnd1, Cdkn1a, Egf, Egfr, Fadd, Fas, Myc, Nfkb1, Trp53* **(15)**
5	**PI3K-Akt signaling**	*Nras, Tlr4, Akt1, Angpt2, Ccnd1, Cdkn1a, Cdkn1b, Egf, Egfr, Flt1, Irs1, Myc, Nfkb1, Pten, Trp53* **(15)**
6	**Gastric cancer**	*Ctnnb1, E2f1, Fzd7, Nras, Akt1, Bax, Ccnd1, Cdkn1a, Cdkn1b, Egf, Egfr, Myc, Smad4, Trp53* **(14)**
7	**Kaposi sarcoma-associated herpesvirus infection**	*Ctnnb1, E2f1, Nras, Akt1, Angpt2, Bax, Bid, Ccnd1, Cdkn1a, Fadd, Fas, Myc, Nfkb1, Trp53* **(14)**
8	**Colorectal cancer**	*Ctnnb1, Msh2, Nras, Akt1, Bax, Ccnd1, Cdkn1a, Egf, Egfr, Msh3, Myc, Rhoa, Smad4, Trp53* **(14)**
9	**Hepatocellular carcinoma**	*Ctnnb1, E2f1, Fzd7, Nras, Akt1, Bax, Ccnd1, Cdkn1a, Egfr, Gstp1, Myc, Pten, Smad4, Trp53* **(14)**

10	**MicroRNAs in cancer**	*E2f1, Nras, Rassf1, Socs1, Ccnd1, Cdkn1a, Cdkn1b, Egfr, Irs1, Myc, Nfkb1, Pten, Rhoa, Trp53* **(14)**
11	**Epstein-Barr virus infection**	*E2f1, Akt1, Bax, Bid, Ccnd1, Cdkn1a, Cdkn1b, Fadd, Fas, Myc, Nfkb1, Runx3, Trp53* **(13)**
12	**Prostate cancer**	*Ctnnb1, E2f1, Nras, Akt1, Ccnd1, Cdkn1a, Cdkn1b, Egf, Egfr, Gstp1, Nfkb1, Pten, Trp53* **(13)**
13	**Breast cancer**	*Ctnnb1, E2f1, Fzd7, Nras, Akt1, Bax, Ccnd1, Cdkn1a, Egf, Egfr, Myc, Pten, Trp53* **(13)**
14	**Hepatitis B**	*E2f1, Nras, Tlr4, Akt1, Bax, Bid, Cdkn1a, Fadd, Fas, Myc, Nfkb1, Smad4, Trp53* **(13)**
15	**Human T-cell leukemia virus 1 infection**	*E2f1, Nras, Akt1, Bax, Ccnd1, Cdkn1a, Myc, Nfkb1, Pten, Smad4, Trp53, Xiap* **(12)**

A: 4 mg/Kg of thorium treatment for twelve months

No.	Altered pathways	Genes altered in each pathway (number of genes)
1	**Pathways in cancer**	*Bax, Bid, Birc5, Ccnd1, Cdh1, Cdkn1a, Cdkn2a, Ctnnb1, Cxcr4, Ep300, Fas, Fzd7, Hgf, Hhip, Itgb1, Met, Msh2, Msh3, Nfkb1, Nras, Pdgfra, Pten, Ptk2, Rac1, Rassf1, Rb1,*

		Rhoa, Smad4, Stat3, Tert, Tgfa, Tgfb1, Vegfa, Xiap, Akt1, Trp53, Egf ***(37)***
2	**PI3K-Akt signaling**	*Ccnd1, Cdkn1a, Flt1, Hgf, Itgb1, Kdr, Mcl1, Met, Nfkb1, Nras, Pdgfra, Pten, Ptk2, Rac1, Reln, Tgfa, Tlr4, Vegfa, Akt1, Angpt2, Egf, Trp53* ***(22)***
3	**Human papillomavirus infection**	*Bax, Ccnd1, Cdkn1a, Ctnnb1, Ep300, Fadd, Fas, Fzd7, Itgb1, Nfkb1, Nras, Pten, Ptk2, Rb1, Reln, Tert, Vegfa, Akt1, Egf, Trp53* ***(20)***
4	**Human cytomegalovirus infection**	*Bax, Bid, Ccnd1, Cdkn1a, Ctnnb1, Cxcr4, Fadd, Fas, Nfkb1, Nras, Pdgfra, Ptk2, Rac1, Rb1, Rhoa, Stat3, Vegfa, Akt1, Trp53* ***(19)***
5	**Proteoglycans in cancer**	*Ccnd1, Cdkn1a, Ctnnb1, Fas, Fzd7, Hgf, Itgb1, Kdr, Met, Nras, Ptk2, Rac1, Rhoa, Stat3, Tgfb1, Tlr4, Vegfa, Akt1, Trp53* ***(19)***
6	**Focal adhesion**	*Ccnd1, Ctnnb1, Flt1, Hgf, Itgb1, Kdr, Met, Pdgfra, Pten, Ptk2, Rac1, Reln, Rhoa, Vegfa, Xiap, Akt1, Egf* ***(17)***
7	**Kaposi sarcoma-associated herpesvirus infection**	*Bax, Bid, Ccnd1, Cdkn1a, Ctnnb1, Ep300, Fadd, Fas, Nfkb1, Nras, Rac1, Rb1, Stat3, Vegfa, Akt1, Angpt2, Trp53* ***(17)***

8	**MAPK signaling**	*Fas, Flt1, Hgf, Kdr, Met, Nfkb1, Nras, Pdgfra, Rac1, Tgfa, Tgfb1, Vegfa, Akt1, Angpt2, Egf, Trp53* ***(16)***
9	**Hepatocellular carcinoma**	*Bax, Ccnd1, Cdkn1a, Ctnnb1, Fzd7, Hgf, Met, Nras, Pten, Rb1, Smad4, Tert, Tgfa, Tgfb1, Akt1, Trp53* ***(16)***
10	**Hepatitis B**	*Bax, Bid, Birc5, Cdkn1a, Ep300, Fadd, Fas, Nfkb1, Nras, Rb1, Smad4, Stat3, Tgfb1, Tlr4, Akt1, Trp53* ***(16)***
11	**Gastric cancer**	*Bax, Ccnd1, Cdh1, Cdkn1a, Ctnnb1, Egf, Fzd7, Hgf, Met, Nras, Rb1, Smad4, Tert, Tgfb1, Akt1, Trp53* ***(16)***
12	**Colorectal cancer**	*Bax, Birc5, Ccnd1, Cdkn1a, Ctnnb1, Msh2, Msh3, Nras, Rac1, Rhoa, Smad4, Tgfa, Tgfb1, Akt1, Egf, Trp53* ***(16)***
13	**Rap1 signaling**	*Cdh1, Ctnnb1, Flt1, Hgf, Itgb1, Kdr, Met, Nras, Pdgfra, Rac1, Rhoa, Vegfa, Akt1, Angpt2, Egf* ***(15)***
14	**Hepatitis C**	*Bax, Bid, Ccnd1, Cdkn1a, Cflar, Ctnnb1, Fadd, Fas, Nfkb1, Nras, Rb1, Stat3, Akt1, Egf, Trp53* ***(15)***
15	**Ras signaling**	*Flt1, Hgf, Kdr, Met, Nfkb1, Nras, Pdgfra, Rac1, Rassf1, Rhoa, Tgfa, Vegfa, Akt1, Angpt2, Egf* ***(15)***

B: 10 mg/kg of thorium treatment for twelve months

No.	Altered pathways	Genes altered in each pathway (number of genes)
1	**Pathways in cancer**	*Bax, Bid, Birc5, Ccnd1, Cdh1, Cdkn1b, Cdkn2a, Ctnnb1, Cxcr4, E2f1, Fzd7, Gstp1, Met, Msh2, Myc, Nfkb1, Nras, Pdgfra, Ptk2, Rac1, Rassf1, Rb1, Smad4, Stat3, Tert, Tgfa, Tgfb1, Vegfa, Xiap, Akt1, Egf, Egfr, Ep300, Fadd, Hras, Trp53* ***(36)***
2	**Human cytomegalovirus infection**	*Bax, Bid, Ccnd1, Cdkn2a, Ctnnb1, Cxcr4, E2f1, Myc, Nfkb1, Nras, Pdgfra, Ptk2, Rac1, Rb1, Stat3, Vegfa, Akt1, Egfr, Fadd, Hras, Trp53* ***(23)***
3	**PI3K-Akt signaling**	*Ccnd1, Cdkn1b, Flt1, Met, Myc, Nfkb1, Nras, Pdgfra, Ptk2, Rac1, Reln, Tgfa, Tlr4, Vegfa, Akt1, Egf, Egfr, Hras, Kdr, Mcl1, Trp53* ***(21)***
4	**Human papillomavirus infection**	*Bax, Ccnd1, Cdkn1b, Ctnnb1, E2f1, Fzd7, Nfkb1, Nras, Ptk2, Rb1, Reln, Tert, Vegfa, Akt1, Egf, Egfr, Ep300, Fadd, Hras, Trp53* ***(20)***
5	**Hepatocellular carcinoma**	*Bax, Ccnd1, Cdkn2a, Ctnnb1, E2f1, Fzd7, Gstp1, Met, Myc, Nras, Rb1, Smad4, Tert, Tgfa, Tgfb1, Akt1, Egfr, Hras, Trp53* ***(19)***

6	**Gastric cancer**	*Bax, Ccnd1, Cdh1, Cdkn1b, Ctnnb1, E2f1, Fzd7, Met, Myc, Nras, Rb1, Smad4, Tert, Tgfb1, Akt1, Egf, Egfr, Hras, Trp53* ***(19)***
7	**Hepatitis C**	*Bax, Bid, Ccnd1, Cflar, Ctnnb1, E2f1, Myc, Nfkb1, Nras, Rb1, Socs3, Stat3, Akt1, Egf, Egfr, Fadd, Hras, Trp53* ***(18)***
8	**MicroRNAs in cancer**	*Ccnd1, Cdkn1b, Cdkn2a, E2f1, Met, Myc, Nfkb1, Nras, Pdgfra, Rassf1, Socs1, Stat3, Vegfa, Egfr, Ep300, Hras, Mcl1, Trp53* ***(18)***
9	**Hepatitis B**	*Bax, Bid, Birc5, E2f1, Myc, Nfkb1, Nras, Rb1, Smad4, Stat3, Tgfb1, Tlr4, Akt1, Ep300, Fadd, Hras, Trp53* ***(17)***
10	**Kaposi sarcoma-associated herpesvirus infection**	*Bax, Bid, Ccnd1, Ctnnb1, E2f1, Myc, Nfkb1, Nras, Rac1, Rb1, Stat3, Akt1, Ep300, Fadd, Hras, Trp53, Vegfa* ***(17)***
11	**Proteoglycans in cancer**	*Ccnd1, Ctnnb1, Fzd7, Met, Myc, Nras, Ptk2, Rac1, Stat3, Tgfb1, Tlr4, Vegfa, Akt1, Egfr, Hras, Kdr, Trp53* ***(17)***
12	**MAPK signaling**	*Flt1, Met, Myc, Nfkb1, Nras, Pdgfra, Rac1, Tgfa, Tgfb1, Vegfa, Akt1, Egf, Egfr, Hras, Kdr, Trp53* ***(16)***
13	**Non-small cell lung cancer**	*Bax, Ccnd1, Cdkn2a, E2f1, Fhit, Met, Nras, Rassf1, Rb1, Stat3, Tgfa, Akt1, Egf, Egfr, Hras, Trp53* ***(16)***

14	**Colorectal cancer**	*Bax, Birc5, Ccnd1, Ctnnb1, Msh2, Myc, Nras, Rac1, Smad4, Tgfa, Tgfb1, Akt1, Egf, Egfr, Hras, Trp53* ***(16)***
15	**Pancreatic cancer**	*Bax, Ccnd1, Cdkn2a, E2f1, Nfkb1, Rac1, Rb1, Smad4, Stat3, Tgfa, Tgfb1, Vegfa, Akt1, Egf, Egfr, Trp53* ***(16)***

C: 20 mg/kg of thorium treatment for twelve months

Table: 3.19. *List of pathways altered by more than two folds differentially expressed genes (DEGs) after treatment with* ***(A)*** *4 mg/Kg* ***(B) 1****0 mg/Kg, and* ***(C)*** *20 mg/Kg thorium after twelve months as mapped by KEGG pathway. Genes upregulated are represented in red color and downregulated genes are represented in blue color and the total number of DEGs expressed in brackets.*

It could be clearly observed that after twelve months, various pathways had been altered by thorium treatment under *in-vivo* conditions. When 4 mg/Kg thorium was used, it was found that in addition to genes involved in carcinogenic pathways, genes involved in pathways such as human cytomegalovirus infection pathway, human papillomavirus infection pathway, hepatitis C pathway, PI3K-Akt signaling pathway, genes involved in gastric cancer, hepatocellular carcinoma pathway, Kaposi sarcoma-associated herpesvirus infection etc. were also altered. Similarly, when 10 mg/Kg thorium dose was used, pathways such as PI3K-Akt signaling, human papillomavirus infection and human cytomegalovirus infection pathway, proteoglycans in cancer, focal adhesion, Kaposi sarcoma-associated herpesvirus infection pathway, MAPK signaling etc. were some of the top pathways, in addition to pathways in cancer, that were found to be activated due to alterations in gene expression. When a comparatively higher dose of 20 mg/Kg was used, genes for pathways such as human cytomegalovirus infection, PI3K-Akt signaling, Human papillomavirus infection,

hepatocellular carcinoma, gastric cancer, Hepatitis B and hepatitis C, genes involved in microRNAs in cancer etc. were found to be altered after one year of treatment. It is to be noted that at all three doses, after one year of treatment, genes involved in hepatocellular carcinoma development were the ones whose expression altered a lot by thorium treatment i.e., 14 genes in case of 4 mg/Kg, 16 genes in case of 10 mg/Kg and 19 genes when 20 mg/Kg of thorium was used.

Thorium exposure for long term under *in-vivo* conditions provides an important insight into the effects of thorium in human after many years of thorium exposure. It was observed that although, thorium treatment did not cause any effect on weight of mice, various morphological effects were observed such as loss of hair, change in eye-color, tail blackening and shedding off etc. Different histopathological and anatomical studies indicate that thorium accumulates mainly along the walls of blood vessels and its accumulation over a longer-period causes changes in tissue architecture in liver, spleen, and lungs. Serum biochemical studies showed an increase in proliferative and inflammatory cytokines and chemokines in mice.

Gene studies of mice liver after thorium treatment over longer duration showed upregulation and downregulation of various genes. After six months of exposure with 4 and 20 mg/Kg of thorium, genes such as *Hhip, Socs3, Tgfbr2, Rassf1, Msh2, Rb1, Bcl2, Reln, Tert, Cdkn2a, Ptgs2, Myc* were found to be upregulated while genes such as *Opcml, Igf2, Lef1* were downregulated. Different carcinogenic pathways were found to be activated following thorium treatment after six months at both thorium doses. Genes involved in different pathways such as hepatocellular carcinoma pathway, PI3K-Akt, human cytomegalovirus infection and papillomavirus infection, focal adhesion, gastric cancer, microRNAs in cancer, colorectal cancer, hepatitis C and Kaposi-sarcoma associated herpesvirus infection pathway etc. were found to have altered expression after thorium treatment.

Similarly, thorium treatment for twelve months at three different doses of thorium caused upregulation of *Yap1, Reln, Rb1, Pdgfra, Stat3, Tgfb1, Tnfsf10, Socs3, Ptk2, Birc5, Hgf, Dlc1, Rac1, Ccnd1, Nras, Flt1, Pin1, Pycard, Msh2, Nfkb1, Socs1, Hhip, Xiap, Tlr4, Rassf1, Cxcr4, Wt1, Fzd7, Ctnnb1* genes while genes such as *Adam17, Akt1, Trp53, Egf* were downregulated. Different pathways involved in carcinogenesis were found to have altered expression of gene following twelve months of thorium treatment. Genes involved in pathways such as hepatocellular carcinoma, PI3k-Akt signaling, human cytomegalovirus infection and papillomavirus infection, Hepatitis C, gastric cancer, Kaposi sarcoma-associated herpesvirus infection, colorectal cancer, hepatitis B were found to be altered followed twelve months of thorium treatment. Gene encoding proteoglycans involved in carcinogenesis were also found to altered.

At six months, upregulation of genes such as *Bcl2,* which is a member of anti-apoptotic family and *Ptgs2*, also known as *Cox2* are known to play a key role in hepatocarcinogenesis via various pathways (172,173). Overexpression of *Cox2* in HCC patients are generally associated to be higher in well-differentiated HCCs compared with less-differentiated HCCs. In non-cancerous cancer tissue, overexpression of *Cox2* has been found to have significant association with a short disease-free survival (173). Increased expression of various oncogenes such as *Myc* and *Tert* has also been documented in various cancer including HCCs (174,175). *c-Myc* was, in fact, the first oncogene found to be over-expressed in HCCs. According to genetic analyses, *c-Myc* overexpression is generally caused by genomic amplification at 8q24.1 and is present in up to 70% of alcohol and virus-related HCCs (174). In addition to *c-Myc*, overexpression of *Tert* due to mutation in its promoter region is also one of the most common genetic alterations found in HCCs (175). *Rassf1* is a tumor suppressor gene which suffers frequent inactivation due to promoter hypermethylation leading to loss of function. However,

Mansour et. al found that the level of hypermethylated *Rassf1* circulating in serum of HCC patients was significantly higher as compared to normal and/or patients with Hepatitis C Virus, (HCV) and can serve as a valuable diagnostic marker for screening population at risk of HCC development (176). Opioid binding protein/cell adhesion molecule-like (OPCML), is a glycosylphosphatidylinositol (GPI)-anchored cell adhesion-like molecule. This molecule is strongly associated with cell growth, invasion, and metastasis and tumorigenesis (177). *Opcml* is a tumor suppressor gene which is frequently downregulated in many cancers (178).

At twelve months, increased expression of genes such as *Birc5, Ctnnb1, Fzd7, Hgf* and *Ptk2* indicate the activation of Wnt/β-catenin pathway (179–183). Gene for cyclin D1, *Ccnd1*, when amplified and overexpressed has been reported in various human cancers including HCC. *Ccnd1* can lead to carcinogenesis by increasing angiogenesis and anchorage-independent growth via VEGF production (184). Overexpression of genes such as *Cxcr4, Pdgfra* are associated with tumor progression and metastasis. *Pdgfra* overexpression causes formation of various receptor-signaling protein complexes which in turn causes activation of different signaling pathways including PI3k-Akt, Ras-ERK, PLC-1 and Src pathway. The pathways ultimately cause cell proliferation and survival (185,186). Upregulation of other genes such as *NFkB1, Nras, Pin1, Rac1* etc. enhances the cell survival and invasion potential. *NFkB1* is the first responder to harmful stimuli and is overexpressed at all three thorium doses. It develops pro-inflammatory response in liver also causes cholesterol accumulation in liver cells via positive feedback loop (187,188). *Nras* overexpression is reported in many human cancers including HCC and is also responsible for hepatic lipid accumulation in mice. It regulates its function mainly by MAPK pathway (189). *Pin1* causes amplification of HCC tumorigenesis by interacting with key phosphoproteins involved in the process. It binds directly to E2F and strongly promotes RAS/MAPKs/CYCLIN/CDK cascade at multiple levels (190,191). When

Rac1 is overexpressed, it causes an increase in the modulation of anti-apoptotic and cell cycle machineries involved in cellular transformation. *Rac1* facilitates activation of PI3k-Akt pathway, thereby increasing survival of transformed cells (192). Similarly, genes such as *Tgfb1, Stat3, Tlr4, Xiap* when overexpressed causes increased survivability of cancer cells through various signaling cascades such as JAK-STAT signaling, ERK/MAPK signaling etc. The protein *Xiap* is the principal inhibitor of apoptosis and is found to be overexpressed in HCC (193). Similarly, downregulation of genes such as *Trp53* leads to development of hepatocellular carcinoma through MDM2-p53 pathway (194).

CHAPTER 4: GENERAL DISCUSSION

With the increased usage of thorium in nuclear and other industries, the risk of thorium exposure to nuclear workers as well as to public has increased. However, studies investigating molecular mechanism of thorium interaction with biological systems have not been well studied. Limited studies exist about effects of thorium on human exposure when thorotrast was used as radiographic contrast agent during 1950s (79). Later on, cohort studies of thorotrast administered patients demonstrated significantly increased risks (36–129 times) for primary liver cancer, which are significantly correlated with the volume of thorotrast injected (150,195). Despite this, studies to establish the mechanism of thorium induced carcinogenesis is not well reported in the literature.

In the present thesis, mechanism of cellular uptake/internalization of thorium was studied, which was extended to investigate the gene expression changes in human liver cells in combination of alpha radiation and in Swiss mice after long term exposure with thorium. But, while initiating the *in-vitro* experiments, it was realized that existing techniques (like ICP-MS, TXRF) for thorium estimation in biological samples face multiple limitations like availability of costly facilities, requirement of high volume of samples and requirement of expertise for data acquisition/analysis. Over and above these techniques cause a delay in acquiring results which, in most of the routine biological experiments, is required instantly for designing next set of experiments. To overcome these limitations, a colorimetric method using arsenazo dye for thorium estimation was developed. In this assay conditions were optimized (i.e., 2.3 N HCl and 50 µM arsenazo), which makes the assay specific for thorium in its detection as compared to other chemically similar and biologically relevant metals such as La (III), Ce (IV), U(VI), Fe (III), Zn (II), Ca (II), Cu (II) and Mn (II). Arsenazo has been used for detection of thorium and other rare earth elements from the natural samples (107). However, these methods were quite tedious and suitable for enough thorium in natural samples. In one

of the seminal studies, arsenazo method has been used for spectrophotometric determination of bone ash samples in bulk quantity (in grams) (196). Compared to these studies, the assay developed requires small volume (~0.2 ml) of sample and can estimate the thorium concentration as low as 2.5 µM and as high as 40 µM. This range of thorium is suitable for most of the routine *in-vitro* and *in-vivo* biological experiments. In all these experiments, the assay showed specificity for thorium estimation as compared to other metals ions. The reason for observed specificity of arsenazo for thorium could be that thorium hydrolyzes under strong acidic conditions to form thorium ions which then react with arsenazo to form a colored complex having absorption maxima at 660 nm. The conditions developed in the current assay uses 2.3 N HCl and a pH of ~-0.4 providing an appropriate condition for thorium hydrolysis (116,117). Other metal ions are known to hydrolyze under mild acidic or neutral conditions. Because of this, they could not combine with arsenazo to give a colored complex thus, making the assay thorium specific (116). La (III), UO_2^{2+}, Ce (IV), Ca (II), Fe (III) and Cu (II) have already been reported in literature to undergo hydrolysis and form colored complex with arsenazo at higher pH (pH > 2-3) (116). Interestingly, the assay was found to correlate with thorium estimation by standard techniques like TXRF. Also, the assay is easy to conduct, less time consuming and high throughput.

Thorium, being a heavy metal ion, cannot enter cells easily. Previous studies from our laboratory showed that proliferation response of low concentration of thorium (0.1-10 µM) in HepG2 cells, which was found to be associated with insulin-like growth factor 1 receptor and activation of downstream activate PI3k and MAPK signaling pathways (61). Other unpublished studies from our lab also showed that thorium treatment results in alterations in shape of mitochondria and cytoskeletal (actin filaments) organization. These results indicated for the cellular internalization of thorium, which however, was not well investigated in

literature. Thorium being similar to iron, the role of transferrin (an iron carrier protein) in cellular internalization of thorium was studied. Surprisingly, thorium uptake was not affected significantly in presence or absence of transferrin. Although, these results could not establish the role of transferrin in cellular uptake of thorium, further studies are required using primary cell lines over-expressing transferrin receptors. It would also be important to know whether interaction of thorium with transferrin has caused any conformational changes in receptor protein, which affected its uptake. These results also suggest possibility of non-transferrin mediated mechanism of thorium internalization to liver cells, which has been reported for iron uptake (197,198). Different metals are known to exert their toxicity through various cellular mechanisms. Affecting the calcium cellular homeostasis has been suggested for metal like Cd and Pb, which mimic Ca and Zn at their specific sites and bind calmodulin (199,200), protein kinase C (201–203). However, such information is not available for thorium. Cellular internalization results showed that majority of the thorium is internalized by a mechanism which is independent of receptor mediated transport, role of various ion channels present on plasma membrane and endoplasmic reticulum membrane were studied. Various ion channels such as calcium (both voltage-dependent and voltage-independent), potassium, water ion channel (on plasma membrane) and calcium ion channel (on endoplasmic reticulum membrane) were studied for their possible role in thorium uptake by using their respective inhibitors. Out of different ion channels studied, thorium uptake was significantly inhibited in the presence of thapsigargin (ER Ca2+ mobilizer), while other calcium ion channel inhibitors showed an increase in thorium uptake. These studies suggested modulation of thorium uptake by intracellular level of cytoplasmic calcium. These results are in agreement for some studies showing role of voltage dependent calcium channels, which are known to affect the cellular entry of Pb and Cd (204). Although majority of thorium was internalized by non-receptor

mediated pathway, it was observed that a small amount (~15%) of thorium was still internalized by receptor mediated pathway and hence, it would be interesting to study the role of different receptors and their pathways in thorium uptake along with the interplay of different calcium ion channels and thorium in detail.

Upon its internalization, thorium was found to interact mostly with cytoskeletal proteins followed by cytoplasmic and nuclear proteins. Thorium binds to both soluble-nuclear as well as chromatin-bound proteins. A small amount of thorium was also bound to membrane proteins which could also be visualized as small, granules-like aggregates in transmission electron microscopic images. These granules are tightly attached to cell membrane and appear to be small thorium-containing particles excluded by cells into the extracellular matrix. It could also be seen that thorium binding leads to several alterations in cellular architecture like shrinkage of nucleus followed by its disintegration, reduction in shape and number of mitochondria and arrangement of various cellular organelles from peri-nuclear to towards one pole of nucleus. Even though studies pertaining to localization of heavy metal radio-nuclides are not well investigated, the results obtained in the present thesis showing cytoskeleton proteins as the major sub-cellular target of thorium is in agreement with previous study where morphometric studies by image analysis of isolated glomeruli and mesangial cultured cells showed that cadmium and uranium induced a dose- and time-dependent glomerular contraction accompanied by disorganization of the cytoskeleton (205). It would be of great interest to study the binding and interaction of thorium to various soluble-nuclear and chromatin-bound proteins, especially DNA.

Heavy metal radio nuclides such as thorium induced health effects would involve its chemical and radiobiological interaction with biological systems. However, only limited studies exist investigating the gene expression alterations after treatment of these heavy metal

radionuclides. In one such study, PTEN gene expression was significantly increased in endometrial tumors of patients living in the areas of high-risk depleted uranium exposure, in comparison to patient tumors from low-risk areas (206). Effect of depleted uranium has been studied using transcriptomics approach in adult and embryo of zebrafish which indicated an impact of parental exposure upon the total RNAs transmitted from the mother to eggs, and the up-regulated genes were those associated with post-translational protein modification and trafficking and cellular signaling pathways, whereas the down-regulated genes concerned the translational process, cell cycle regulation and several cell signaling pathways (207). In another transcriptomics study pertaining to uranium toxicity, human renal cells showed that 25% of the genes modulated were concerned with signal transduction and trafficking. The study also showed that the toxicity caused heavy disturbances in calcium pathway and that genes related to nephroblastoma were involved (208).

Compared to these studies, in the present study a different approach has been followed to study the alterations in gene expression after thorium treatment in human liver cells. Here to simulate human exposure conditions, cells were treated continuously with thorium and intermittent doses (three) of external alpha irradiation. A panel of 84 genes pertaining to human liver carcinogenesis was studied. It was found that after 5 passages, genes such as *TP53, BCL2, TLR4, CASP8, TCF4, CFLAR, GSTP1, PTEN, TGFB1, RHOA, MTDH, EGFR, IRS1, TNFRSF10B, CDKN1A, TNFSF10, BAX, SMAD4, STAT3, PTK2, XIAP, CCND1, FZD7, MET, TGFBR2, FAS, BID, CDKN1B, TGFA, IGFBP1, E2F1, HRAS, SMAD7, FADD, ANGPT2,PTGS2, ADAM17, EP300, RELN, BIRC2, IGF2, CCL5, CCND2, RB1, FHIT, RASSF1* etc. were found to be overexpressed in all treatment groups and genes such as *KDR, PYCARD, SOCS3, PDGFRA, MYC* were downregulated in all groups. Various pathways where these 84 genes played a key role were altered because of the altered expression of these genes.

Pathways such as PI3k-Akt signaling, Human papillomavirus infection, Human cytomegalovirus infection, Kaposi sarcoma-associated herpesvirus infection, microRNAs in cancer, Hepatocellular carcinoma, Prostate cancer, Focal adhesion, Gastric cancer pathways were the topmost carcinogenic pathways whose genes were found to have altered expression upon treatment across all groups. When the same treatment was continued till passage 15, it was found that genes such as *BAX, MYC, CDKN1A, TNFRSF10B, PTEN, MSH2, CCND1, MET, BIRC5, BIRC2, HHIP, CXCR4, SMAD7, EGF, SFRP2, TGFBR2, ADAM17, CCL5, DLC1, AKT1, KDR, TERT* were upregulated and genes such as *CDH1, OPCML, NFKB1, CDKN1B, STAT3, RAC1, RASSF1, TP53, NRAS, SMAD4, E2F1, CTNNB1, GADD45B, CFLAR, PTGS2* were downregulated across all treatment groups. Pathway analysis using KEGG pathway mapper showed carcinogenic pathways such as PI3k-Akt signaling, gastric cancer, human papillomavirus infection, colorectal cancer, hepatocellular carcinoma, Epstein-Barr virus infection, hippo signaling were found to have altered gene expression in all three groups. Various pathways such as PI3k-Akt, Wnt/β-catenin etc. have been implicated as the key pathway involved in causing thorium induced injury based on the gene expression profile however, further studies are required to confirm their role.

Thorium toxicity was also studied under in-vivo conditions as well using Swiss mice as the model organism. Thorium bio-distribution studies found that thorium mainly accumulated in liver of mice after all treatment times i.e., 1, 6 and 12 months followed by spleen and bone. However, when specific thorium was considered, it was found that the concentration of thorium was highest in spleen followed by liver and bone. Spleen being most thorium dense organ indicated presence of some high affinity binding sites which requires further exploration. Thorium was found to get cleared from liver after its initial deposit and accumulate in spleen. The movement of thorium could be facilitated by macrophages which

has been shown to interact with thorium (209). However, further experiments are required to confirm this hypothesis.

Further imaging of these organs using X-ray phase contrast imaging using Synchrotron showed blood vessels to be the major sites of thorium deposition in liver and spleen. The same was also confirmed by immunohistochemistry. H&E staining of the thorium treated tissues showed injury in liver where spleen and lungs showed developed of cancer in various stages. Brain and bone, however, did not show any structural alterations due to thorium deposition. Development of lung cancer through inhalation of thorium dust particles in a known phenomenon (86), however, in this thesis, we report the development of lung cancer through intra-venous injection of thorium under *in-vivo* conditions for the first time. Plutonium being similar to thorium in its alpha emitting property could be looked up to understand the mechanism involved in causing lung cancer by thorium. Some of the key findings of mechanism of lung cancer due to plutonium exposure shows molecular and genetic alterations of Ki-ras in preneoplastic foci and neoplasms in the lungs of rats after inhalation of $^{239}PuO_2$ aerosols. Specific Ki-ras point mutations were present in 46% of the radiation-induced malignant neoplasms (210). Lung tumors from beagle dogs exposed to $^{239}PuO_2$, which showed altered expression of the p53 tumor suppressor gene and proto-oncogene erbB-2 proteins (211). The mechanism of lung cancer following intravenous injection of thorium needs further investigation in detail.

Study of biochemical parameters also showed an increase in the level of glucose in serum while a decrease in the amount of urea and creatinine was observed. Further studies of cytokine and chemokine profile analysis showed an increase in the expression of proliferative and inflammatory cytokines in serum suggesting an environment conducive of excessive cellular growth and division. Similar to *in-vitro* model, Swiss mice were also subjected to long-

term exposure of different doses of thorium (6 and 12 months) and their effect on alterations of gene expression were studied using the same panel of 84 genes which are known to play a role in hepatocarcinogenesis. It was found that after 6 months of treatment, genes such as *Hhip, Socs3, Tgfbr2, Rassf1, Msh2, Rb1, Bcl2, Reln, Tert, Cdkn2a, Ptgs2, Myc* were upregulated while genes such as *Opcml, Igf2 and Lef1* were downregulated across all treatment groups. Pathway's analysis using KEGG mapper showed alteration of various carcinogenic pathways such as PI3k-Akt pathway, hepatocellular carcinoma pathway, pathways involved in human cytomegalovirus and papillomavirus infection along with pathways for focal adhesion, gastric cancer, microRNAs in cancer, colorectal cancer pathway and hepatitis C pathways to have altered expression in all treatment groups. Similarly, at 12 months, it was found that genes such as *Yap1, Reln, Rb1, Pdgfra, Stat3, Tgfb1, Tnfsf10, Socs3, Ptk2, Birc5, Hgf, Dlc1, Rac1, Ccnd1, Nras, Flt1, Pin1, Pycard, Msh2, Nfkb1, Socs1, Hhip, Xiap, Tlr4, Rassf1, Cxcr4, Wt1, Fzd7, Ctnnb1* were upregulated and genes such as *Adam17, Akt1, Trp53, Egf* were downregulated across all treatment groups. Pathway analysis showed various carcinogenic pathways such as PI3k-Akt pathway, hepatitis C pathway, gastric cancer, colorectal cancer, hepatocellular cancer, human cytomegalovirus and papillomavirus infection pathway and hepatitis B are some of the key pathways which showed altered gene expression across all treatment groups. Based on the upregulation and downregulation of various genes, PI3k-Akt, Wnt/β-catenin were the main pathways involved in hepatocarcinogenesis.

Both *in-vitro* and *in-vivo* studies showed the involvement of same pathways for carcinogenesis. These pathways should be studied in detail to understand the key roles played by them and develop a molecular model of hepatocellular carcinoma caused by thorium accumulation in liver.

CHAPTER 5:
CONCLUSIONS AND FUTURE DIRECTIONS

Even if thorium is being seen as an attractive replacement of uranium for the nuclear energy production and in many industrial applications, the cellular and molecular targets of thorium are still not well established. Moreover, the effect of thorium on intracellular organelles and the molecular pathways through which may exert its carcinogenic effect is also required to be studied. To address the unanswered questions in the literature, in the present study a range of *in vitro* and *in vivo* studies were carried using cellular and molecular techniques. Based on these experiments, the major conclusions of the thesis are as following:

a. Commonly used methods (ICP-MS, ICP-AES, TXRF) for thorium estimation are limited for their day-to-day use for biological samples due to costly instrumentation and requirement of extensive sample preparation, large sample volume and technical expertise for acquisition/analysis. To overcome these limitations, in the preset thesis for the first time a colorimetric method based on arsenazo dye was established to estimate thorium in biological samples.

b. The arsenazo based method was found to an easy, high throughput and convenient spectrophotometry-based arsenazo assay for routine thorium estimation in biological samples. The technique was also found to be specific to thorium, and not to monazite's common contaminants [La (III), Ce (IV) and U(VI)] and other biologically relevant metals (such as Ca, Fe, Mn, Zn, Cu).

c. Thorium uptake in human normal liver cells was found to be unaffected by transferrin but partially governed by endocytosis.

d. Out of different ion channels studied, thorium uptake was significantly inhibited in the presence of thapsigargin (ER Ca^{2+} mobilizer), while other calcium ion channel

inhibitors increased the thorium uptake. Based on the inhibitor study, it is hypothesized that cellular uptake of thorium is being governed by the level of cytoplasmic calcium.

e. The order of thorium binding to different sub-cellular protein fractions was found to be cytoskeletal > cytoplasmic > extracellular > chromatin > nuclear > membrane. TEM studies showed that thorium internalization leads to a significant increase in the number of extracellular membranous vesicle-like extensions, nucleus distortion and nucleolus disintegration, altered mitochondrial structure from oval to flat disc-shaped.

f. Expression a panel of 84 genes involved in hepatocarcinogenesis studied after thorium treatment and without alpha particle irradiation showed pronounced magnitude of alteration in their expression for the late passage (P15) than the cells obtained at the early passage (P5). At P5, genes such as *ADAM17, ANGPT2, BAX, BCL2, BID, BIRC2, CASP8, CCL5, CCND1, CCND2, CDKN1A, CDKN1B, CFLAR, E2F1, EGFR, EP300, FADD, FAS, FHIT, FZD7, GSTP1, HRAS, IGF2, IGFBP1, IRS1, MET, MTDH, PTEN, PTGS2, PTK2, RASSF1, RB1, RELN, RHOA, SMAD4, SMAD7, STAT3, TCF4, TGFA, TGFB1, TGFBR2, TLR4, TNFRSF10B, TNFSF10, TP53, XIAP* were over-expressed whereas genes such as *KDR, PYCARD, SOCS3, PDGFRA, MYC* were downregulated in all the treatment groups. Whereas at P15, genes such as *BAX, MYC, CDKN1A, TNFRSF10B, PTEN, MSH2, CCND1, MET, BIRC5, BIRC2, HHIP, CXCR4, SMAD7, EGF, SFRP2, TGFBR2, ADAM17, CCL5, DLC1, AKT1, KDR, TERT* were over-expressed whereas genes such as *CDH1, OPCML, NFKB1, CDKN1B, STAT3, RAC1, RASSF1, TP53, NRAS, SMAD4, E2F1, CTNNB1, GADD45B, CFLAR, PTGS2* are downregulated in all the treatment groups.

f. Thorium bio-distribution studies in male Swiss mice intravenously injected with thorium showed total thorium highest in the liver followed by spleen > skeleton > kidney

> lungs whereas thorium concentration per gram of tissue was highest in spleen followed by liver > skeleton > kidney > lungs.

g. Synchrotron imaging performed to study the anatomical changes of liver of mice treated with thorium showed shortening of the blood vessels in a dose-dependent manner while thorium seems to be accumulated along the blood vessel of the spleen.

h. Histopathological studies performed after six and twelve months of thorium treatment showed normal liver histopathology at 4 and 10 mg/Kg dose, whereas protein deposition was observed in the hepatocytes at 20 mg/Kg. Spleen at 10 mg/Kg showed an increased extramedullary hematopoiesis at the red pulp. Thorium at high concentration (20 mg/Kg) showed amyloid deposition at 6 months and increased megakaryocytosis at 12 months.

i. Histopathology of bone and brain showed normal tissue architecture with no visible abnormality. Histopathology of lungs did not show any abnormality in the tissue architecture at 6 months. Interestingly at 12 months, the highest dose of thorium (20 mg/Kg) caused papillary adenoma neoplasia in lungs.

j. An increase in the level of glucose in the blood was observed at 1 month, 6 and 12 months.

k. Analysis of serum cytokine and chemokine profiles showed an increase in the levels of proliferative, inflammatory cytokines/chemokines after 12 months of thorium treatment.

l. Gene expression studies in liver tissue showed that at low dose (i.e., at 4 mg/Kg) the number of genes with altered expression was decreased at higher time point i.e., 12 months compared to 6 months. However, at higher dose i.e., at 20 mg/Kg, the number

of genes with altered expression showed a marked increase at 12 months as compared to 6 months.

M. After 6 months, *Hhip, Tgfbr2, Rassf1, Msh2, Bcl2, Tert, Cdkn2a, Ptgs2, Myc* are some of the oncogenes which showed an increase while genes like *Opcml,* showed downregulation. Similarly, after 12 months, *Pdgfra, Stat3, Tgfb1, Ptk2, Birc5, Hgf, Nras, Flt1, Pin1, Msh2, Nfkb1, Hhip, Xiap, Tlr4, Rassf1, Cxcr4, Wt1, Fzd7, Ctnnb1* were the common genes with increased expression and tumor suppressor gene *Trp53* was downregulated in thorium treated groups.

At one hand, the thesis provides deeper mechanistic insights about cellular and molecular effects of thorium-induced toxicity and carcinogenesis. On the other hand, it opens many new avenues for research in thorium biology. Some of the future directions of the thesis are as following:

a. Thesis showed that cellular uptake of thorium to be governed by the level of cytoplasmic calcium. Further studies are needed to understand the role of calcium ion/store-operated channels and associated proteins in thorium uptake.

b. Spleen was found to be one of the major target organs. Moreover, the histopathological studies of spleen showed an increased extramedullary hematopoiesis at the red pulp, amyloid deposition and megakaryocytosis after thorium treatment. Spleen plays major role in immune system and hence in the process of toxicity as well as in carcinogenesis. Hence, it would be interesting to study the effect of thorium on immune parameters and its contribution in toxicity/carcinogenesis.

c. Incidence of thorium induced liver and bone cancer has been established. In the thesis, for the first-time lung cancer incidence after intravenous injection of thorium was observed. However, detail mechanism of lung carcinogenesis caused by thorium treatment is further warranted.

d. In the present thesis effect of thorium nitrate after intravenous administration was studied. Effects of other chemical forms of thorium with other routes of administration (inhalation, wound) should also be studied. It would be interesting to study different dust sizes of chemical forms of thorium after different routes of administration especially after inhalation.

e. The magnitude of health effects of thorium may get affected by many confounding factors associated with thorium workers as well as to the public. Hence, role of factors (like smoking, hepatitis virus infection) in the process of thorium-induced lung/liver carcinogenesis can be envisaged.

CHAPTER 6:

BIBLIOGRAPHY

REFERENCES

1. Iryna P. Toxicity of Radionuclides in Determining Harmful Effects on Humans and Environment. Journal of Environmental Science and Public Health. 2017;01(02):115–9.

2. Plutonium and nuclear power [Internet]. 2015. p. 1–8. Available from: https://www.world-nuclear.org/information-library/nuclear-fuel-cycle/fuel-recycling/plutonium.aspx#:~:text=Plutonium%2C both that routinely made,million kilowatt-hours of electricity.

3. Wikipedia contributors. Plutonium [Internet]. Wikipedia,The Free Encyclopedia; 2021. Available from: https://en.wikipedia.org/w/index.php?title=Plutonium&oldid=998333721

4. W. G. Sutcliffe and T.J. Trapp. Reactor-Grade and Weapons-Grade Plutonium in Nuclear Explosives [Internet]. US Department of Energy. 1997. p. 37–9. Available from: http://www.ccnr.org/plute.html

5. Plutonium in Use From single atoms to multiton amounts. Los Alamos Science. 2000. p. 10–5.

6. Morss L. Uranium [Internet]. Encyclopædia Britannica. p. 4–8. Available from: https://www.britannica.com/science/uranium

7. Kale AB, Bandela NN, Kulkarni JA. Radiological and Chemo-Toxicological Risk Assessment of Naturally Occurred Uranium in Ground Water from Aurangabad District of Maharashtra. International Journal of Environmental Science. 2018;3:49–55.

8. Wikipedia contributors. Uranium [Internet]. Wikipedia, The Free Encyclopedia; 2020. Available from: https://en.wikipedia.org/w/index.php?title=Uranium&oldid=996520506

9. Association WN. What is Uranium? How Does it Work? [Internet]. 2014. Available from: http://www.world-nuclear.org/information-library/nuclear-fuel-cycle/introduction/what-is-uranium-how-does-it-work.aspx

10. Lenntech. Thorium - Th Chemical properties of thorium - Health effects of thorium - Environmental effects of thorium. 2021. p. 1–2.

11. René M. Nature, Sources, Resources, and Production of Thorium. In: Descriptive Inorganic Chemistry Researches of Metal Compounds. InTech; 2017.

12. Hutton JH. Nature and Sources of Folk-Belief. Folklore. 1942 Jun;53(2):82–94.

13. Wikipedia contributors. Thorium [Internet]. Wikipedia, The Free Encyclopedia; 2020. Available from: https://en.wikipedia.org/w/index.php?title=Thorium&oldid=995021663

14. Vijayan PK, Shivakumar V, Basu S, Sinha RK. Role of thorium in the Indian nuclear power programme. Progress in Nuclear Energy. 2017 Nov;101:43–52.

15. Contributors W. Occurrence of thorium [Internet]. Wikipedia, The Free Encyclopedia. 2001. p. 1–6. Available from: https://en.wikipedia.org/w/index.php?title=Occurrence_of_thorium&oldid=995583065

16. Dubey N, Singh R. UNTAPPED URANIUM/THORIUM RESERVES. Department of Atomic Energy. 2012. p. 1–2.

17. Schulz WW. Thorium processing. Encyclopædia Britannica.

18. Kelly GN. A Review of Worldwide Occupational Exposures. Radiation Protection Dosimetry. 1994 May 1;53(1–4):1–12.

19. Kumar A, Ali M, Pandey BN. Understanding The Biological Effects of Thorium and Developing Efficient Strategies for Its Decorporation and Mitigation. BARC Newsletter. 2013;(335):55–60.

20. Yadav R, Ali M, Kumar A, Pandey B. Mechanism of carcinogenesis after exposure of actinide radionuclides: Emerging concepts and missing links. Journal of Radiation and Cancer Research. 2017;8(1):20.

21. Division of Toxicology and Environmental Medicine. Public Health Statement: Plutonium. Agency For Toxic Substances And Disease Registry. 2010.

22. Division of Toxicology and Human Health Sciences. Public Health Statement: Uranium [Internet]. Agency For Toxic Substances And Disease Registry. 2013. Available from: https://www.atsdr.cdc.gov/ToxProfiles/tp150-c1-b.pdf%0Ahttp://www.atsdr.cdc.gov

23. Pandey BN, Kumar A, Tiwari P, Mishra KP. Radiobiological basis in management of accidental radiation exposure. International Journal of Radiation Biology. 2010 Aug;86(8):613–35.

24. Gehle K. Case Study in Environmental Medicine - Uranium Toxicity [Internet]. Vol. 66, ATSDR. 2009. p. 37–9. Available from: https://www.fairportlibrary.org/images/files/RenovationProject/Concept_cost_estimate_accepted_031914.pdf

25. Benarie M. Handbook on the toxicology of metals. Science of The Total Environment.

1982 Aug;24(3):293–4.

26. Steinckwich N, Frippiat J-P, Stasia M-J, Erard M, Boxio R, Tankosic C, et al. Potent inhibition of store-operated Ca 2+ influx and superoxide production in HL60 cells and polymorphonuclear neutrophils by the pyrazole derivative BTP2. Journal of Leukocyte Biology. 2007 Apr;81(4):1054–64.

27. Keith S, Wohlers DW, Ingerman L. Toxicological Profile for Thorium [Internet]. ATSDR's Toxicological Profiles. CRC Press; 2002. Available from: http://www.crcnetbase.com/doi/10.1201/9781420061888_ch150

28. Fay M, Brattin WJ, Donohue JM. Public Health Statement [Internet]. Vol. 15, Toxicology and Industrial Health. 1999. p. 652–4. Available from: http://journals.sagepub.com/doi/10.1177/074823379901500802

29. Bhattacharyya MH, Larsen RP, Cohen N, Ralston LG, Moretti ES, Oldham RD, et al. Gastrointestinal Absorption of Plutonium and Uranium in Fed and Fasted Adult Baboons and Mice: Application to Humans. Radiation Protection Dosimetry. 1989 Jan 1;26(1–4):159–65.

30. Council NR. Health Risks of Radon and Other Internally Deposited Alpha-Emitters. Washington, D.C.: National Academies Press; 1988.

31. Voelz GL, Buican IG. Plutonium and Health: How great is the risk? Vol. 26, Los Alamos Science. 2000. p. 74–89.

32. Burns C. Overview of Plutonium and Its Health Effects [Internet]. 2002. p. 1–16. Available from: http://www.clarku.edu/departments/marsh/projects/community/plutonium.pdf

33. Kumar A, Mishra P, Ghosh S, Sharma P, Ali M, Pandey BN, et al. Thorium-induced oxidative stress mediated toxicity in mice and its abrogation by diethylenetriamine pentaacetate. International journal of radiation biology. 2008 Apr 3;84(4):337–49.

34. Upton AC, Shore RE, Harley NH. The health effects of low-level ionizing radiation. Annual review of public health. 1992 May;13(1):127–50.

35. FRIEBEN, E. Demonstration eines cancroids des rechten handruckens, das sich nach langdauerner einwirkung von roentgenstrahlen entwickelt hatte. Forsch Roentgenstr. 1902;6:106–11.

36. Benner S. Book Review: Protection in Diagnostic Radiology. Acta Radiologica. 1959 Dec 1;Original S(6):496–496.

37. Kumar C, Shetake N, Desai S, Kumar A, Samuel G, Pandey BN. Relevance of radiobiological concepts in radionuclide therapy of cancer. International Journal of Radiation Biology. 2016 Apr 2;92(4):173–86.

38. Department of Health, Education, and Welfare, Washington D (USA). O of the S. Interagency task force on the health effects of ionizing radiation: report of the work group on public information [Internet]. 1979. Available from: https://www.osti.gov/biblio/6422265

39. Boice JDJ, Fraumeni JFJ. Radiation Carcinogenesis: Epidemiology and Biological Significance. American Journal of Clinical Oncology. 1984;7(6):p746.

40. Ullrich RL. Radiation Carcinogenesis. In: Radiation Biology. CRC Press; 2020. p. 111–28.

41. Goodhead DT. Initial Events in the Cellular Effects of Ionizing Radiations: Clustered

Damage in DNA. International Journal of Radiation Biology. 1994 Jan 3;65(1):7–17.

42. Ward JF. Radiation Mutagenesis: The Initial DNA Lesions Responsible. Radiation Research. 1995 Jun 1;142(3):362.

43. Zdzienicka MZ. Mammalian mutants defective in the response to ionizing radiation-induced DNA damage. Mutation Research/DNA Repair. 1995 May;336(3):203–13.

44. Petrini JHJ, Bressan DA, Yao MS. TheRAD52epistasis group in mammalian double strand break repair. Seminars in Immunology. 1997 Jun;9(3):181–8.

45. Davis AJ, Chen DJ. DNA double strand break repair via non-homologous end-joining. Translational cancer research. 2013 Jun;2(3):130–43.

46. Yandell DW, Dryja TP, Little JB. Somatic mutations at a heterozygous autosomal locus in human cells occur more frequently by allele loss than by intragenic structural alterations. Somatic Cell and Molecular Genetics. 1986 May;12(3):255–63.

47. Li C-Y, Yandell DW, Little JB. Molecular mechanisms of spontaneous and induced loss of heterozygosity in human cells in vitro. Somatic Cell and Molecular Genetics. 1992 Jan;18(1):77–87.

48. Amundson SA, Xia F, Wolfson K, Liber HL. Different cytotoxic and mutagenic responses induced by X-rays in two human lymphoblastoid cell lines derived from a single donor. Mutation Research/Fundamental and Molecular Mechanisms of Mutagenesis. 1993 Apr;286(2):233–41.

49. Lomax ME, Folkes LK, O'Neill P. Biological Consequences of Radiation-induced DNA Damage: Relevance to Radiotherapy. Clinical Oncology. 2013 Oct;25(10):578–85.

50. Cadet J, Douki T, Ravanat J-L. Oxidatively Generated Damage to the Guanine Moiety of DNA: Mechanistic Aspects and Formation in Cells. Accounts of Chemical Research. 2008 Aug;41(8):1075–83.

51. Milligan JR, Aguilera JA, Paglinawan RA, Ward JF, Limoli CL. DNA strand break yields after post-high LET irradiation incubation with endonuclease-III and evidence for hydroxyl radical clustering. International Journal of Radiation Biology. 2001 Jan 3;77(2):155–64.

52. Nikitaki Z, Nikolov V, Mavragani I V., Mladenov E, Mangelis A, Laskaratou DA, et al. Measurement of complex DNA damage induction and repair in human cellular systems after exposure to ionizing radiations of varying linear energy transfer (LET). Free Radical Research. 2016 Nov 1;50(sup1):S64–78.

53. Ansoborlo É, Amekraz B, Moulin C, Moulin V, Taran F, Bailly T, et al. Review of actinide decorporation with chelating agents. Comptes Rendus Chimie. 2007 Oct;10(10–11):1010–9.

54. Fouillit M, Grillon G, Fritsch P, Rateau G, Pavé D, Delforge J, et al. Comparative tissue uptake and cellular deposition of three different plutonium chemical forms in rats. International Journal of Radiation Biology. 2004 Sep 3;80(9):683–9.

55. Weber W, Doyle-Eisele M, Melo DR, Guilmette RA. Whole-body distribution of plutonium in rats for different routes of exposure. International Journal of Radiation Biology. 2014 Nov 12;90(11):1011–8.

56. Taylor DM. The Metabolism of Plutonium and Related Elements: ICRP Publication 48. Radiation Protection Dosimetry. 1989 Jan 1;26(1–4):137–40.

57. Van der Meeren A, Moureau A, Laurent D, Laroche P, Angulo JF. In vitro assessment of plutonium uptake and release using the human macrophage-like THP-1 cells. Toxicology in Vitro. 2016 Dec;37:25–33.

58. Wada I, Horiuchi H, Mori M, Ishikawa Y, Fukumoto M, Mori T, et al. High Rate of Small TP53 Mutations and Infrequent Loss of Heterozygosity in Malignant Liver Tumors Associated with Thorotrast: Implications for Alpha-Particle Carcinogenesis. Radiation Research. 1999 Dec;152(6):S125.

59. Lizon C, Fritsch P. Chemical toxicity of some actinides and lanthanides towards alveolar macrophages: an in vitro study. International journal of radiation biology. 1999 Nov 3;75(11):1459–71.

60. Kumar A, Ali M, Pandey BN, Hassan PA, Mishra KP. Role of membrane sialic acid and glycophorin protein in thorium induced aggregation and hemolysis of human erythrocytes. Biochimie. 2010 Jul;92(7):869–79.

61. Ali M, Kumar A, Pandey BN. Thorium induced cytoproliferative effect in human liver cell HepG2: Role of insulin-like growth factor 1 receptor and downstream signaling. Chemico-Biological Interactions. 2014 Mar;211(1):29–35.

62. Kumar A, Ali M, Ningthoujam RS, Gaikwad P, Kumar M, Nath BB, et al. The interaction of actinide and lanthanide ions with hemoglobin and its relevance to human and environmental toxicology. Journal of Hazardous Materials. 2016 Apr;307:281–93.

63. Ali M, Sadhu B, Boda A, Tiwari N, Das A, Musharaf Ali SK, et al. Thorium decorporation efficacy of rationally-selected biocompatible compounds with relevance to human application. Journal of Hazardous Materials. 2019 Mar;365(November):952–61.

64. Oliveira MS, Duarte IM, Paiva A V., Yunes SN, Almeida CE, Mattos RC, et al. The Role of Chemical Interactions Between Thorium, Cerium, and Lanthanum in Lymphocyte Toxicity. Archives of Environmental & Occupational Health. 2014 Jan 9;69(1):40–5.

65. da F. Iwahara LK, de Oliveira MS, de Alencar MAV. Evaluation of the effect of three constituent metals of monazita on the radiosensibility of human osteoblasts. Journal of Environmental Radioactivity. 2019 Nov;208–209(June):106011.

66. Szefer P, Falandysz J. Uranium and thorium content in long-tailed ducks (Clangula hyemalis L.). Science of The Total Environment. 1983 Aug;29(3):277–80.

67. Karbe L, Schnier C, Siewers HO. Trace elements in mussels (Mytilus Edulis) from coastal areas of the North Sea and the Baltic. Multielement analyses using instrumental neutron activation analysis. Journal of Radioanalytical Chemistry. 1977 Sep;37(2):927–43.

68. Kochhann D, Pavanato MA, Llesuy SF, Correa LM, Konzen Riffel AP, Loro VL, et al. Bioaccumulation and oxidative stress parameters in silver catfish (Rhamdia quelen) exposed to different thorium concentrations. Chemosphere. 2009 Oct;77(3):384–91.

69. Jadon A, Mathur R. Gametogenic count and histopathological effect of thorium nitrate and uranyl nitrate on mice testes. Andrologia. 2009 Apr 24;15(1):40–3.

70. Likhachev IP. Pathological anatomy, etiology and pathogenesis of remote sequelae of radiation dust exposure. Arkhiv patologii. 1976 Apr;38(4):18–26.

71. Easton TW. The role of macrophage movements in the transport and elimination of intravenous thorium dioxide in mice. American Journal of Anatomy. 1952

Jan;90(1):1–33.

72. Peter E, Lehmann M. Interaction of Thorium with Blood Serum Proteins in Vivo. International Journal of Radiation Biology and Related Studies in Physics, Chemistry and Medicine. 1981 Jan 3;40(4):445–50.

73. Peter-Witt E, Volf V. Comparison of Ca-DTPA and Zn-DTPA in Removing 234Th from the Rat. Health Physics. 1985 Sep;49(3):395–403.

74. Kumar A, Sharma P, Ali M, Pandey BN, Mishra KP. Decorporation and therapeutic efficacy of liposomal-DTPA against thorium-induced toxicity in the Wistar rat. International Journal of Radiation Biology. 2012 Mar 23;88(3):223–9.

75. Kumar A, Ali M, Mishra P, Pandey BN, Sharma P, Mishra KP. Thorium-induced neurobehavioural and neurochemical alterations in Swiss mice. International Journal of Radiation Biology. 2009 Jan 3;85(4):338–47.

76. Rezk MM. A Neuro-Comparative Study between Single/Successive Thorium Dose Intoxication and Alginate Treatment. Biological Trace Element Research. 2018 Oct 29;185(2):414–23.

77. Abdel-Rahman M, Rezk MM, Abdel Moneim AE, Ahmed-Farid OA, Essam S. Thorium exerts hazardous effects on some neurotransmitters and thyroid hormones in adult male rats. Naunyn-Schmiedeberg's Archives of Pharmacology. 2020 Feb 3;393(2):167–76.

78. Rezk MM, Mohamed AA, Ammar AA. Thorium Harmful Impacts on the Physiological Parameters of the Adult Male Albino Rats and Their Mitigation Using the Alginate. Toxicology and Environmental Health Sciences. 2018 Dec

11;10(5):253–60.

79. Goto A, Takebayashi Y, Liu D, Li L, Saiga T, Mori T, et al. Microdistribution of alpha particles in pathological sections of tissues from thorotrast patients detected by imaging plate autoradiography. Radiation research. 2002 Jul;158(1):54–60.

80. Muramatsu Y, Ishikawa Y, Yoshida S, Mori T. Determination of Thorium in Organs from Thorotrast Patients by Inductively Coupled Plasma Mass Spectroscopy and X-Ray Fluorescence. Radiation Research. 1999 Dec;152(6):S97.

81. Stehney AF. Organ Distribution of Thorium in Thorium Workers: Good Agreement with New Models of the International Commission on Radiological Protection. Radiation Research. 1999 Dec;152(6):S110.

82. Stehney AF, Lucas HF. Thorium Isotopes in Autopsy Samples from Thorium Workers. Health Physics. 2000 Jan;78(1):8–14.

83. Warnakulasuriya T, Williams S, Dabarera M, Rodrigo K, Weerakkody T, Wickremasinghe R. Frequency of micronuclei among persons resident in the vicinity of a mineral sand processing factory in Pulmoddai, Sri Lanka. Mutagenesis. 2017 Oct 17;32(5):511–6.

84. Dang HS, Jaiswal DD, Sunta CM. Daily intake of thorium by an Indian Urban population. Science of The Total Environment. 1986 Dec;57:73–7.

85. Ludwig T, Schwa D, Seitz G, Siekmann H. Intakes of Thorium While Using Thoriated Tungsten Electrodes for TIG Welding. Health Physics. 1999 Oct;77(4):462–9.

86. Chen X-A, Cheng Y-E, Rong Z. Recent results from a study of thorium lung burdens and health effects among miners in China. Journal of Radiological Protection. 2005

Dec 1;25(4):451–60.

87. Valiathan MS, Kartha CC, Eapen JT, Dang HS, Sunta CM. A geochemical basis for endomyocardial fibrosis. Cardiovascular research. 1989 Jul 1;23(7):647–8.

88. Iyengar GV, Kawamura H, Dang HS, Parr RM, Wang JW, Akhter P, et al. Estimation of internal radiation dose to the adult Asian population from the dietary intakes of two long-lived radionuclides. Journal of Environmental Radioactivity. 2004 Jan;77(3):221–32.

89. Namil Um, Masao Miyake and TH. Zero-Carbon Energy Kyoto 2010. Yao T, editor. Green Energy and Technology. Tokyo: Springer Japan; 2011. 165–170 p. (Green Energy and Technology; vol. 66).

90. Ali M, Kumar A, Kumar M, Pandey BN. The interaction of human serum albumin with selected lanthanide and actinide ions: Binding affinities, protein unfolding and conformational changes. Biochimie. 2016 Apr;123:117–29.

91. Kuntz ID, Gasparro FP, Johnston MD, Taylor RP. Molecular interactions and the Benesi-Hildebrand equation. Journal of the American Chemical Society. 1968 Aug 1;90(18):4778–81.

92. Misra NL, Dhara S, Aggarwal SK. Total Reflection X-ray Fluorescence Spectrometry for Characterization of Nuclear Materials. BARC Newsletter. 2014. p. 1–8.

93. Yadav R, Pandey BN, Kumar A. Estimation and in-situ detection of thorium in human liver cell culture by arsenazo-III based colorimetric assay. BioMetals. 2020 Feb 2;33(1):75–85.

94. M V JB, Shinde SG, S SK, Ali M, Vasumathy R, Kumar A, et al. Dosimetry and

Radiobiological Studies of Automated Alpha-Particle Irradiator. Journal of Environmental Pathology, Toxicology and Oncology. 2013;32(3):263–73.

95. Karthik K, Rajan V, Pandey BN, Sivasubramanian K, Paul SFD, Venkatachalam P. Direct and bystander effects in human blood lymphocytes exposed to 241 Am alpha particles and the relative biological effectiveness using chromosomal aberration and micronucleus assay. International Journal of Radiation Biology. 2019 Jun 3;95(6):725–36.

96. Franken NAP, Rodermond HM, Stap J, Haveman J, van Bree C. Clonogenic assay of cells in vitro. Nature protocols. 2006;1(5):2315–9.

97. Agrawal AK, Singh B, Kashyap YS, Shukla M, Sarkar PS, Sinha A. Design, development and first experiments on the X-ray imaging beamline at Indus-2 synchrotron source RRCAT, India. Journal of Synchrotron Radiation. 2015 Nov 1;22(6):1531–9.

98. Snigirev A, Snigireva I, Kohn V, Kuznetsov S, Schelokov I. On the possibilities of x-ray phase contrast microimaging by coherent high-energy synchrotron radiation. Review of Scientific Instruments. 1995 Dec;66(12):5486–92.

99. Hoheisel M. Review of medical imaging with emphasis on X-ray detectors. Nuclear Instruments and Methods in Physics Research Section A: Accelerators, Spectrometers, Detectors and Associated Equipment. 2006 Jul;563(1):215–24.

100. Sun Z. The Promise of Synchrotron Radiation in Medical Science. Australasian medical journal. 2009 May 30;1(5):1–5.

101. Kak AC, Slaney M. Principles of Computerized Tomographic Imaging. Society for

Industrial and Applied Mathematics; 2001.

102. Limaye A. Drishti: a volume exploration and presentation tool. In: Stock SR, editor. Developments in X-Ray Tomography VIII. SPIE; 2012. p. 85060X.

103. Yadav R, Agrawal AK, Ali M, Kumar A, Singh B, Kashyap Y, et al. Thorium-induced Anatomical and Histopathological Changes in Liver of Swiss Mice. Toxicology and Environmental Health Sciences. 2018 Jun 11;10(2):97–106.

104. Kim SW, Roh J, Park CS. Immunohistochemistry for pathologists: Protocols, pitfalls, and tips. Journal of Pathology and Translational Medicine. 2016;50(6):411–8.

105. Livak KJ, Schmittgen TD. Analysis of relative gene expression data using real-time quantitative PCR and the 2-ΔΔCT method. Methods. 2001;25(4):402–8.

106. Veyseh S, Niazi A. A novel aeration-assisted homogenous liquid–liquid microextration for determination of thorium and uranium in water and hair samples by inductively coupled plasma-mass spectroscopy. Talanta. 2016 Jan;147:117–23.

107. Rožmarić M, Ivšić AG, Grahek Ž. Determination of uranium and thorium in complex samples using chromatographic separation, ICP-MS and spectrophotometric detection. Talanta. 2009 Nov 15;80(1):352–62.

108. Losno M, Pellé J, Marie M, Ferrante I, Brennetot R, Descroix S, et al. Separation and preconcentration of actinides from concentrated nitric acid by extraction chromatography in microsystems. Talanta. 2018 Aug;185:586–91.

109. Bártová H, Kučera J, Musílek L, Trojek T, Gregorová E. Determination of U, Th and K in bricks by gamma-ray spectrometry, X-ray fluorescence analysis and neutron activation analysis. Radiation Physics and Chemistry. 2017 Nov;140(January):161–6.

110. Savvin S. Analytical use of arsenazo III Determination of thorium, zirconium, uranium and rare earth elements. Talanta. 1961 Sep;8(9):673–85.

111. Rohwer H, Hosten E. pH dependence of the reactions of arsenazo III with the lanthanides. Analytica Chimica Acta. 1997 Mar;339(3):271–7.

112. Choi S, Lee J-Y, Yun J-I. Stability Constants and Spectroscopic Properties of Thorium(IV)–Arsenazo III Complexes in Aqueous Hydrochloric Medium. Journal of Solution Chemistry. 2017 Jun 13;46(6):1272–83.

113. Hosten E, E. Rohwer H. Complexation reactions of uranyl with arsenazo III. Analytica Chimica Acta. 1997 Nov;355(1):95–100.

114. Ashry HA, Khazbak AE, Soliman FAS, Ibrahim MA. Determination of uranium and thorium content in the various stages of monazite upgrading. Applied Radiation and Isotopes. 1995 Aug;46(8):735–9.

115. Lal M, Choudhury RK, Joseph D, Bajpai HN, Tyer CSP. Elemental analysis of selected Indian monazite ores by energy dispersive X-ray fluorescence /EDXRF/ spectroscopy. Journal of Radioanalytical and Nuclear Chemistry Letters. 1989 Sep;137(2):127–33.

116. Savvin SB. Analytical applications of arsenazo III—IIDetermination of thorium, uranium, protactinium, neptunium, hafnium and scandium. Talanta. 1964 Jan;11(1):1–6.

117. Torapava N, Persson I, Eriksson L, Lundberg D. Hydration and Hydrolysis of Thorium(IV) in Aqueous Solution and the Structures of Two Crystalline Thorium(IV) Hydrates. Inorganic Chemistry. 2009 Dec 21;48(24):11712–23.

118. Dhara S, Prabhat P, Misra NL. Direct Compositional Characterization of (U,Th)O 2 Powders, Microspheres, and Pellets Using TXRF. Analytical Chemistry. 2015 Oct 20;87(20):10262–7.

119. Beauchemin D. Inductively Coupled Plasma Mass Spectrometry Methods. In: Encyclopedia of Spectroscopy and Spectrometry. 3rd ed. Elsevier; 2017. p. 236–45.

120. Gorden AE V., Xu J, Raymond KN, Durbin P. Rational Design of Sequestering Agents for Plutonium and Other Actinides. Chemical Reviews. 2003 Nov;103(11):4207–82.

121. Mashayekhi M, Amanlou M, Sadeghi K, Mosayebniya M, Ardestani MS, Mehravi B. Diethylentriaminepentaacetic Acid-deoxyglucoseamine (DTPA-DG): Novel Nanosized Anti-Wilson s Disease Cell Model. American Journal of Biomedical Sciences. 2013 Jan;5(1):34–46.

122. Harris WR, Carrano CJ, Pecoraro VL, Raymond KN. Siderophilin metal coordination. 1. Complexation of thorium by transferrin: structure-function implications. Journal of the American Chemical Society. 1981 May;103(9):2231–7.

123. Morgan EH. Factors affecting the synthesis of transferrin by rat tissue slices. The Journal of biological chemistry. 1969 Aug 10;244(15):4193–9.

124. Wikipedia F. Ionic radius. Wiki. 1000. p. 1–10.

125. McKnight GS, Lee DC, Hemmaplardh D, Finch CA, Palmiter RD. Transferrin gene expression. Effects of nutritional iron deficiency. The Journal of biological chemistry. 1980 Jan 10;255(1):144–7.

126. Durmaz Y, Donato M, Monteiro M, Gouveia L, Nunes ML, Gama Pereira T, et al.

Effect of temperature on α-tocopherol, fatty acid profile, and pigments of Diacronema vlkianum (Haptophyceae). Aquaculture International. 2009 Aug 16;17(4):391–9.

127. Clarkson DT, Earnshaw MJ, White PJ, Cooper HD. Temperature dependent factors influencing nutrient uptake: an analysis of responses at different levels of organization. Symposia of the Society for Experimental Biology. 1988;42(42):281–309.

128. Terrar DA. Structure and function of calcium channels and the actions of anaesthetics. British journal of anaesthesia. 1993 Jul;71(1):39–46.

129. Bean BP. Classes of Calcium Channels in Vertebrate Cells. Annual Review of Physiology. 1989 Mar;51(1):367–84.

130. Yu AS. Calcium channels. Current opinion in nephrology and hypertension. 1994 Sep;3(5):497–503.

131. Feng T, Kalyaanamoorthy S, Barakat K. L-Type Calcium Channels: Structure and Functions. In: Ion Channels in Health and Sickness. InTech; 2018.

132. Rahman S, Rahman T. Unveiling some FDA-approved drugs as inhibitors of the store-operated Ca2+ entry pathway. Scientific Reports. 2017 Dec 16;7(1):12881.

133. Guo D-Q, Zhang H, Tan S-J, Gu Y-C. Nifedipine Promotes the Proliferation and Migration of Breast Cancer Cells. Liu X, editor. PLoS ONE. 2014 Dec 1;9(12):e113649.

134. Bastioli G, Piccirillo S, Castaldo P, Magi S, Tozzi A, Amoroso S, et al. Selective inhibition of mitochondrial sodium-calcium exchanger protects striatal neurons from α-synuclein plus rotenone induced toxicity. Cell Death & Disease. 2019 Feb 28;10(2):80.

135. Li X-T, Li X-Q, Hu X-M, Qiu X-Y. The Inhibitory Effects of Ca2+ Channel Blocker Nifedipine on Rat Kv2.1 Potassium Channels. Barnes S, editor. PLOS ONE. 2015 Apr 20;10(4):e0124602.

136. Hirasawa M, Pittman QJ. Nifedipine facilitates neurotransmitter release independently of calcium channels. Proceedings of the National Academy of Sciences. 2003 May 13;100(10):6139–44.

137. Garcia ML, Slaughter RS, King VF, Kaczorowski GJ. Inhibition of sodium-calcium exchange in cardiac sarcolemmal membrane vesicles. 2. Mechanism of inhibition by bepridil. Biochemistry. 1988 Apr 5;27(7):2410–5.

138. Baudet S, Shaoulian R, Bers DM. Effects of thapsigargin and cyclopiazonic acid on twitch force and sarcoplasmic reticulum Ca2+ content of rabbit ventricular muscle. Circulation Research. 1993 Nov;73(5):813–9.

139. Lückhoff A, Clapham DE. Calcium channels activated by depletion of internal calcium stores in A431 cells. Biophysical Journal. 1994 Jul;67(1):177–82.

140. Omelchenko A, Shrirao AB, Bhattiprolu AK, Zahn JD, Schloss RS, Dickson S, et al. Dynamin and reverse-mode sodium calcium exchanger blockade confers neuroprotection from diffuse axonal injury. Cell Death & Disease. 2019 Oct 27;10(10):727.

141. Watanabe Y, Kimura J. Blocking Effect of Bepridil on Na+/Ca2+ Exchange Current in Guinea Pig Cardiac Ventricular Myocytes. Japanese Journal of Pharmacology. 2001 Apr;85(4):370–5.

142. Wictome M, Henderson I, Lee AG, East JM. Mechanism of inhibition of the calcium

pump of sarcoplasmic reticulum by thapsigargin. Biochemical Journal. 1992 Apr 15;283(2):525–9.

143. Thastrup O, Cullen PJ, Drobak BK, Hanley MR, Dawson AP. Thapsigargin, a tumor promoter, discharges intracellular Ca2+ stores by specific inhibition of the endoplasmic reticulum Ca2(+)-ATPase. Proceedings of the National Academy of Sciences. 1990 Apr 1;87(7):2466–70.

144. Sehgal P, Szalai P, Olesen C, Praetorius HA, Nissen P, Christensen SB, et al. Inhibition of the sarco/endoplasmic reticulum (ER) Ca2+-ATPase by thapsigargin analogs induces cell death via ER Ca2+ depletion and the unfolded protein response. Journal of Biological Chemistry. 2017 Dec;292(48):19656–73.

145. Parekh AB, Putney JW. Store-Operated Calcium Channels. Physiological Reviews. 2005 Apr;85(2):757–810.

146. Flourakis M, Lehen'kyi V, Beck B, Raphaël M, Vandenberghe M, Abeele F V., et al. Orai1 contributes to the establishment of an apoptosis-resistant phenotype in prostate cancer cells. Cell Death & Disease. 2010 Sep 16;1(9):e75–e75.

147. Deng X, Wang Y, Zhou Y, Soboloff J, Gill DL. STIM and Orai: Dynamic Intermembrane Coupling to Control Cellular Calcium Signals. Journal of Biological Chemistry. 2009 Aug;284(34):22501–5.

148. Fukumoto M, Kuwahara Y, Ohkubo Y, Wang L. Analysis of carcinogenic mechanisms of liver cancers induced by chronic exposure to alpha-particles from internally deposited Thorotrast. Radiation Measurements. 2006 Oct;41(9–10):1186–90.

149. van Kampen RJW, Erdkamp FLG, Peters FPJ. Thorium dioxide-related haemangiosarcoma of the liver. The Netherlands journal of medicine. 2007 Sep;65(8):279–82.

150. Akira K, Mori T, Seki M, Kato Y. The risk of thorium-induced liver cancer estimated from the results of the sixth epidemiological survey (1983). 1987.

151. Wang X, Feng C, Li M. ADAM17 mediates hypoxia-induced drug resistance in hepatocellular carcinoma cells through activation of EGFR/PI3K/Akt pathway. Molecular and Cellular Biochemistry. 2013 Aug 28;380(1–2):57–66.

152. Shang N, Wang H, Bank T, Perera A, Joyce C, Kuffel G, et al. Focal Adhesion Kinase and β-Catenin Cooperate to Induce Hepatocellular Carcinoma. Hepatology. 2019 Nov 22;70(5):1631–45.

153. Dziadziuszko R, Camidge DR, Hirsch FR. The Insulin-Like Growth Factor Pathway in Lung Cancer. Journal of Thoracic Oncology. 2008 Aug;3(8):815–8.

154. Plati J, Bucur O, Khosravi-Far R. Dysregulation of apoptotic signaling in cancer: Molecular mechanisms and therapeutic opportunities. Journal of Cellular Biochemistry. 2008 Jul 1;104(4):1124–49.

155. Aldinucci D, Colombatti A. The Inflammatory Chemokine CCL5 and Cancer Progression. Mediators of Inflammation. 2014;2014:1–12.

156. Yao W, Wang T, Huang F. p300/CBP as a Key Nutritional Sensor for Hepatic Energy Homeostasis and Liver Fibrosis. BioMed Research International. 2018;2018:1–14.

157. Xie J, Wei J, Lv L, Han Q, Yang W, Li G, et al. Angiopoietin-2 induces angiogenesis via exosomes in human hepatocellular carcinoma. Cell Communication and Signaling.

2020 Dec 17;18(1):46.

158. DACTARI. Thorium Physico-chemical properties Thorium Acute toxicity DACTARI [Internet]. A database for chemical toxicity and radiotoxicity assesement of radionuclides. CEA, France. 2018. Available from: http://www.dactari.toxcea.org

159. Papadimitropoulos A, Friess S, Beckmann F, Salmon P, Riboldi S, Hutmacher D, et al. Comparative study of desktop- and synchrotron radiation-based micro computed tomography analyzing cell-seeded scaffolds in tissue engineering of bone. In: Stock SR, editor. Developments in X-Ray Tomography VI. SPIE; 2008. p. 70780T.

160. Bilderback DH, Elleaume P, Weckert E. Review of third and next generation synchrotron light sources. Journal of Physics B: Atomic, Molecular and Optical Physics. 2005 May 14;38(9):S773–97.

161. Bravin A, Coan P, Suortti P. X-ray phase-contrast imaging: from pre-clinical applications towards clinics. Physics in Medicine and Biology. 2013 Jan 7;58(1):R1–35.

162. Desai S, Srambikkal N, Yadav HD, Shetake N, Balla MMS, Kumar A, et al. Molecular Understanding of Growth Inhibitory Effect from Irradiated to Bystander Tumor Cells in Mouse Fibrosarcoma Tumor Model. Roberts DD, editor. PLOS ONE. 2016 Aug 25;11(8):e0161662.

163. Baratta JL, Ngo A, Lopez B, Kasabwalla N, Longmuir KJ, Robertson RT. Cellular organization of normal mouse liver: a histological, quantitative immunocytochemical, and fine structural analysis. Histochemistry and Cell Biology. 2009 Jun 3;131(6):713–26.

164. Herman GT. Filtered Backprojection for Parallel Beams [Internet]. 2009. p. 135–58. Available from: http://link.springer.com/10.1007/978-1-84628-723-7_8

165. Limaye A. Drishti: a volume exploration and presentation tool. In: Stock SR, editor. Developments in X-Ray Tomography VIII. 2012. p. 85060X.

166. Lu H, Yuan G, Yin Z, Dai S, Jia R, Xu J, et al. Effects of subchronic exposure to lead acetate and cadmium chloride on rat's bone: Ca and Pi contents, bone density, and histopathological evaluation. International journal of clinical and experimental pathology. 2014;7(2):640–7.

167. CPCSEA, Committee for the Purpose of Control And Supervision of Experiments on Animals [Internet]. 2018. p. 1–213. Available from: http://cpcsea.nic.in/WriteReadData/userfiles/file/Compendium of CPCSEA.pdf

168. Rivadeneyra-Domínguez E, Becerra-Contreras Y, Vázquez-Luna A, Díaz-Sobac R, Rodríguez-Landa JF. Alterations of blood chemistry, hepatic and renal function, and blood cytometry in acrylamide-treated rats. Toxicology Reports. 2018;5(May):1124–8.

169. Williams JL. The Significance of Blood Chemistry. The American Journal of Nursing. 1925 Jan;25(1):2.

170. Miles J. Health risks of radon and other internally deposited alpha-emitters. Endeavour. 1988 Jan;12(4):197.

171. Zhang J-M, An J. Cytokines, inflammation, and pain. International anesthesiology clinics. 2007;45(2):27–37.

172. Shimizu S, Takehara T, Hikita H, Kodama T, Miyagi T, Hosui A, et al. The let-7 family of microRNAs inhibits Bcl-xL expression and potentiates sorafenib-induced

apoptosis in human hepatocellular carcinoma. Journal of Hepatology. 2010 May;52(5):698–704.

173. Cervello M, Montalto G. Cyclooxygenases in hepatocellular carcinoma. World Journal of Gastroenterology. 2006;12(32):5113.

174. Zheng K, Cubero F, Nevzorova Y. c-MYC—Making Liver Sick: Role of c-MYC in Hepatic Cell Function, Homeostasis and Disease. Genes. 2017 Apr 19;8(4):123.

175. Amisaki M, Tsuchiya H, Sakabe T, Fujiwara Y, Shiota G. Identification of genes involved in the regulation of TERT in hepatocellular carcinoma. Cancer Science. 2019 Feb 4;110(2):550–60.

176. Mansour LA, El Raziky M, Mohamed AA, Mahmoud EH, Hamdy S, El Sayed EH. Circulating Hypermethylated RASSF1A as a Molecular Biomarker for Diagnosis of Hepatocellular Carcinoma. Asian Pacific journal of cancer prevention : APJCP. 2017;18(6):1637–43.

177. Li C, Tang L, Zhao L, Li L, Xiao Q, Luo X, et al. OPCML is frequently methylated in human colorectal cancer and its restored expression reverses EMT via downregulation of smad signaling. American journal of cancer research. 2015;5(5):1635–48.

178. Zhang N, Xu J, Wang Y, Heng X, Yang L, Xing X. Loss of opioid binding protein/cell adhesion molecule-like gene expression in gastric cancer. Oncology Letters. 2018 Apr 24;15(6):9973–7.

179. Chen X, Duan N, Zhang C, Zhang W. Survivin and Tumorigenesis: Molecular Mechanisms and Therapeutic Strategies. Journal of Cancer. 2016;7(3):314–23.

180. Tanabe S, Kawabata T, Aoyagi K, Yokozaki H, Sasaki H. Gene expression and

pathway analysis of CTNNB1 in cancer and stem cells. World Journal of Stem Cells. 2016;8(11):384.

181. Monga SPS, Mars WM, Pediaditakis P, Bell A, Mulé K, Bowen WC, et al. Hepatocyte growth factor induces Wnt-independent nuclear translocation of beta-catenin after Met-beta-catenin dissociation in hepatocytes. Cancer research. 2002 Apr 1;62(7):2064–71.

182. Fan Z, Duan J, Wang L, Xiao S, Li L, Yan X, et al. PTK2 promotes cancer stem cell traits in hepatocellular carcinoma by activating Wnt/β-catenin signaling. Cancer Letters. 2019 May 28;450(February):132–43.

183. Chan K, Lo R. Deregulation of Frizzled Receptors in Hepatocellular Carcinoma. International Journal of Molecular Sciences. 2018 Jan 21;19(1):313.

184. Tashiro E, Tsuchiya A, Imoto M. Functions of cyclin D1 as an oncogene and regulation of cyclin D1 expression. Cancer science. 2007 May;98(5):629–35.

185. Wang Y, Pennock SD, Chen X, Kazlauskas A, Wang Z. Platelet-derived Growth Factor Receptor-mediated Signal Transduction from Endosomes. Journal of Biological Chemistry. 2004 Feb;279(9):8038–46.

186. Teicher BA, Fricker SP. CXCL12 (SDF-1)/CXCR4 Pathway in Cancer. Clinical Cancer Research. 2010 Jun 1;16(11):2927–31.

187. He M, Zhang W, Dong Y, Wang L, Fang T, Tang W, et al. Pro-inflammation NF-κB signaling triggers a positive feedback via enhancing cholesterol accumulation in liver cancer cells. Journal of Experimental & Clinical Cancer Research. 2017 Dec 18;36(1):15.

188. Luedde T, Schwabe RF. NF-κB in the liver--linking injury, fibrosis and hepatocellular carcinoma. Nature reviews Gastroenterology & hepatology. 2011 Feb;8(2):108–18.

189. Gao M, Liu D. CRISPR/Cas9-based Pten knock-out and Sleeping Beauty Transposon-mediated Nras knock-in induces hepatocellular carcinoma and hepatic lipid accumulation in mice. Cancer Biology & Therapy. 2017 Jul 3;18(7):505–12.

190. Cheng C-W, Leong K-W, Tse E. Understanding the role of PIN1 in hepatocellular carcinoma. World Journal of Gastroenterology. 2016;22(45):9921.

191. Cheng C-W, Chow AKM, Pang R, Fok EWS, Kwong Y-L, Tse E. PIN1 Inhibits Apoptosis in Hepatocellular Carcinoma through Modulation of the Antiapoptotic Function of Survivin. The American Journal of Pathology. 2013 Mar;182(3):765–75.

192. Bosco EE, Mulloy JC, Zheng Y. Rac1 GTPase: a "Rac" of all trades. Cellular and molecular life sciences : CMLS. 2009 Feb;66(3):370–4.

193. Shiraki K, Sugimoto K, Yamanaka Y, Yamaguchi Y, Saitou Y, Ito K, et al. Overexpression of X-linked inhibitor of apoptosis in human hepatocellular carcinoma. International Journal of Molecular Medicine. 2003 Nov 1;12(5):705–8.

194. Meng X, Franklin DA, Dong J, Zhang Y. MDM2–p53 Pathway in Hepatocellular Carcinoma. Cancer Research. 2014 Dec 15;74(24):7161–7.

195. Lipshutz GS, Brennan T V., Warren RS. Thorotrast-induced liver neoplasia: a collective review. Journal of the American College of Surgeons. 2002 Nov;195(5):713–8.

196. Petrow HG, Strehlow CD. Spectrophotometric determination of thorium in bone ash using Arsenazo III. Analytical Chemistry. 1967 Feb 1;39(2):265–7.

197. Scheiber-Mojdehkar B, Zimmermann I, Dresow B, Goldenberg H. Differential response of non-transferrin bound iron uptake in rat liver cells on long-term and short-term treatment with iron. Journal of Hepatology. 1999;31(1):61–70.

198. Parkes JG, Randell EW, Olivieri NF, Templeton DM. Modulation by iron loading and chelation of the uptake of non-transferrin-bound iron by human liver cells. BBA - General Subjects. 1995;1243(3):373–80.

199. Ouyang H, Vogel HJ. Metal ion binding to calmodulin: NMR and fluorescence studies. BioMetals. 1998;11(3):213–22.

200. Kern M, Wisniewski M, Cabell L, Audesirk G. Inorganic lead and calcium interact positively in activation of calmodulin. Neurotoxicology. 2000 Jun;21(3):353–63.

201. Tomsig JL, Suszkiw JB. Multisite interactions between Pb2+ and protein kinase C and its role in norepinephrine release from bovine adrenal chromaffin cells. Journal of neurochemistry. 1995 Jun;64(6):2667–73.

202. Sun X, Tian X, Tomsig JL, Suszkiw JB. Analysis of differential effects of Pb2+ on protein kinase C isozymes. Toxicology and Applied Pharmacology. 1999;156(1):40–5.

203. Markovac J, Goldstein GW. Picomolar concentrations of lead stimulate brain protein kinase C. Nature. 1988 Jul;334(6177):71–3.

204. Marchetti C. Role of Calcium Channels in Heavy Metal Toxicity. ISRN Toxicology. 2013 Jan 30;2013:1–9.

205. L'Azou B, Henge-Napoli MH, Minaro L, Mirto H, Barrouillet MP, Cambar J. Effects of cadmium and uranium on some in vitro renal targets. Cell biology and toxicology. 2002;18(5):329–40.

206. Jumaah AS, Al-Haddad HS, Mahdi LH, Hatem E, Al-Janabi AAH, McAllister K, et al. Increased PTEN gene expression in patients with endometrial carcinoma from areas of high risk depleted uranium exposure. BMC Research Notes. 2019 Dec 29;12(1):708.

207. Gombeau K, Bourdineaud J-P, Ravanat J-L, Armant O, Camilleri V, Cavalie I, et al. Epigenetic, histopathological and transcriptomic effects following exposure to depleted uranium in adult zebrafish and their progeny. Aquatic Toxicology. 2017 Mar;184:14–25.

208. Prat O, Berenguer F, Malard V, Tavan E, Sage N, Steinmetz G, et al. Transcriptomic and proteomic responses of human renal HEK293 cells to uranium toxicity. Proteomics. 2005 Jan;5(1):297–306.

209. Jones TC, Hirsch JG. The interaction between toxoplasma gondii and mammalian cells: II. The absence of lysosomal fusion with phagocytic vacuoles containing living parasites. Journal of Experimental Medicine. 1972;136(5):1173–94.

210. Stegelmeier BL, Gillett NA, Rebar AH, Kelly G. The molecular progression of plutonium-239–induced rat lung carcinogenesis: Ki-ras expression and activation. Molecular Carcinogenesis. 1991;4(1):43–51.

211. Tierney LA, Hahn FF, Lechner JF. p53, erbB-2 and K-ras gene alterations are rare in spontaneous and plutonium-239-induced canine lung neoplasia. Radiation research. 1996 Feb;145(2):181–7.

LIST OF SCHEMES

Thesis Highlight

Name of the Student: Rakhee Yadav
Name of the CI/OCC: Bhabha Atomic Research Centre, Mumbai
Enrolment No.: LIFE01201304007
Thesis Title: Cellular and Molecular Basis of Thorium-induced Cytotoxicity and Carcinogenesis
Discipline: Life Sciences **Sub-Area of Discipline:** Metal Carcinogenesis (Thorium)
Date of viva voce: 14.05.2021

Thorium utilization in nuclear industry has increased drastically which in turn enhanced the risk of its exposure to occupational workers/public. Thorium toxicity is reported in literature; however, its mechanism of toxicity and carcinogenesis remains elusive. Present thesis attempts to elucidate the mechanism of thorium toxicity and carcinogenesis in humans using both in-vitro and in-vivo model. A colorimetric method is first standardised for estimation of thorium in biological samples as the standard techniques for thorium estimation (such as ICP-MS, ICP-AES, TXRF) are tedious, require lot of sample preparation, expensive and not high throughput. Studies under in vitro model showed that thorium is mainly intracellularized using Ca^{2+} ion channels present on plasma membrane and is deposited mainly on cytoskeletal proteins. Thorium bio-distribution studies on mice showed liver, spleen and skeleton to be the major target organs of thorium deposition where thorium deposits mainly around blood vessels. Histopathological evaluation indicated hepatocyte hypertrophy in liver, megacytokaryosis in spleen and deposition of an amorphous proteinaceous material in liver and spleen. Papillary adenoma was also observed in lungs. Evaluation of serum biochemical changes suggested an increase in glucose, ALT and ALP concentration. Elevated levels of inflammatory and proliferative cytokine and chemokine were also observed. Long term thorium exposure under both in vitro and in vivo conditions causes alterations in the expressions of various genes involved in various pathways of cell survival (TGF-β, MAPK, PI3k, RAS and cell cycle/apoptosis), cell fate (transcriptional regulation) and genomic maintenance (DNA damage control). However, further experiments need to be performed to establish these pathways as the key pathways involved in thorium-induced hepatocarcinogenesis.

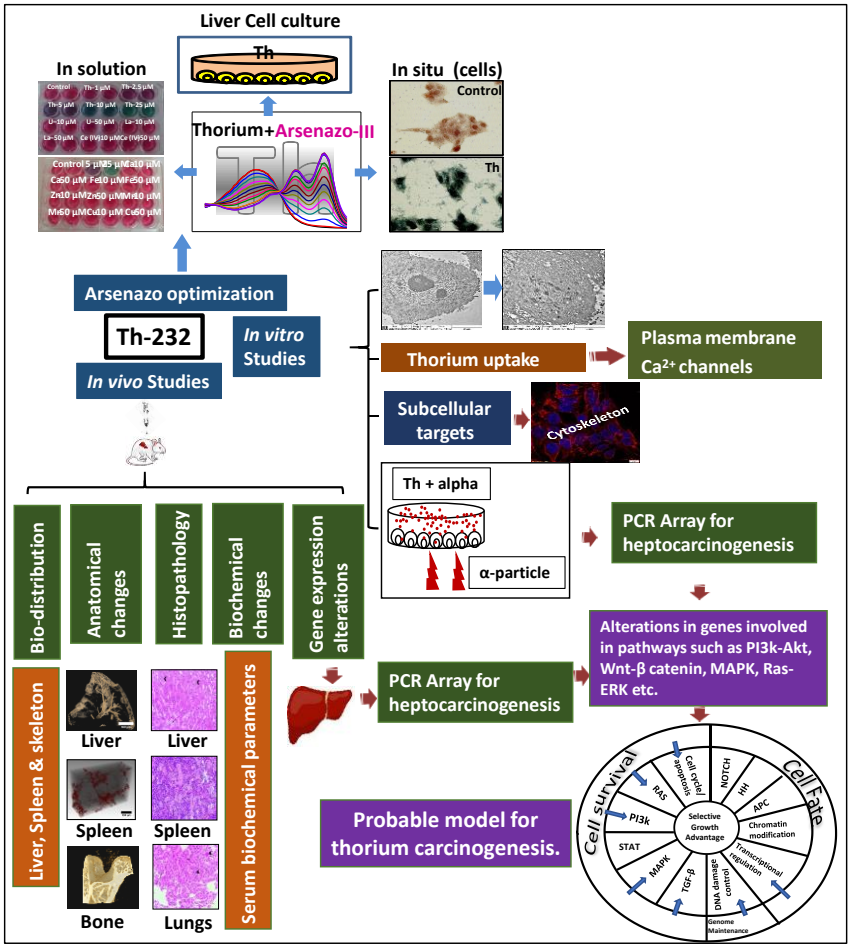

Fig: Thorium Cytotoxicity and Carcinogenesis under in-vitro & in-vivo conditions